THE UNIVERSITY
of EDINBURGH

NOVEL CLOSED-LOOP FRP REINFORCEMENT FOR CONCRETE TO ENHANCE FIRE PERFORMANCE

Mohamed Ahmed Kiari

A thesis submitted for the degree of

Doctor of Philosophy

2016

Declaration

The work in this thesis has been completed solely by Mohamed A. Kiari at the University of Edinburgh under the supervision of Dr. Tim J. Stratford and Prof. Luke A. Bisby. Full reference is given where other sources are used. This work has not been submitted for any other degree or professional qualification.

Mohamed A. Kiari

October 2016

Abstract

The use of fibre-reinforced polymer (FRP) as an internal reinforcement for concrete has many advantages over steel, most notably lack of corrosion which is considered to be a major problem for structures incorporating steel. In Europe alone, it is estimated that the annual repairing and maintenance costs associated with steel corrosion in infrastructure are around £20 billion (Nadjai et al., 2005). Despite of its corrosion resistance, the widespread use of FRP as an internal reinforcement for concrete was hindered due to its relatively weak performance at elevated temperatures, such as in the event of fire. Under heating, the polymer matrix in FRP softens, which causes bond degrading between reinforcement and concrete. The softening of polymer matrices occurs around their glass transition temperatures, which is typically in the range of 65–150 °C. The sensitivity of FRP bond to temperature is recognised in design guidelines, therefore many advise against utilising FRP as an internal reinforcement for concrete in structures where fire performance is critical. On the other hand, fibres, the other component of FRP, can tolerate temperatures much higher than polymer matrices.

This research investigates a new design for FRP internal reinforcement, which exploits the fact that the FRP fibres in general and carbon fibres in particular are capable of sustaining a large proportion of their original strength at high temperatures. Instead of the traditional way of using separate bars, FRP reinforcement was made as closed loops produced through the continuous winding of carbon fibre tows. When the surface bond degrades at elevated temperatures, interaction with concrete can still be provided through bearing at loop ends.

The concept of FRP loops was investigated through a series of experimental work. Firstly, the performance of carbon FRP (CFRP) loops was evaluated through a series of push-off tests in which specimens consisting of CFRP loops bridging two concrete cubes were tested in pull-out using hydraulic jacks. Specimens with straight and hooked reinforcement were produced as well for comparison. A total number of 18 specimens were tested at ambient temperature, glass transition temperature (T_g), and above T_g. Results showed that while at ambient temperature there was no distinction in performance. At elevated temperatures, CFRP loops developed strength about three

times higher than specimens with straight or hooked bars. Also, while failure mode occurred due to de-bond in the case of straight and hooked reinforcement, rupture failure occurred with CFRP loops.

For better demonstration of the concept in more realistic conditions, four-point bending tests were conducted upon 28 beam specimens reinforced either with CFRP loops or straight bars as flexural reinforcement. Beams were tested under monotonic loading at ambient temperature, or under sustained loads with localised heating over the midspan region that contained the reinforcement overlaps. The benefit of CFRP loops became evident in the elevated temperature tests. Beam specimens with spliced straight bars failed due to debonding after a short period (up to 15 minutes) of fire exposure. Conversely, the fire endurance increased four to five times when CFRP loop reinforcement was used. Unlike straight bars, debonding failure was avoided as failure occurred due to reinforcement rupture. The overlap length of the CFRP loops was found to be important in the order for the loop to develop full capacity. Premature failure can occur with short overlap length due to shear off concrete within the overlap zone. The presence of transverse reinforcement increases confinement levels for reinforcement, so the bond failure of straight bars at ambient temperature testing was eliminated when stirrups were provided. However, at elevated temperatures straight bars failed by pull-out even in presence of transverse reinforcement.

To facilitate design with CFRP loops, a numerical analysis tool was developed to calculate the bond stress-slip response of reinforcement at ambient and elevated temperatures. A Matlab programme was designed based on a one-dimensional analytical model for steel. The bond law was modified to be used for CFRP reinforcement. Other analytical models from the literature to account for bond degradation with temperature and tensile strength of curved FRP were also utilised. The developed Matlab code has the capability of producing slip, axial stress, and bond stress distribution along reinforcement.

The novel FRP loop reinforcement was demonstrated to be a promising solution for enhancing the fire performance of CFRP internal reinforcement at elevated temperatures. It contributes to removing a major obstacle preventing widespread use

of FRP-reinforced concrete, and paves the way for CFRP reinforcement to be used in situations where fire performance is critical.

Lay Summary

Traditionally steel is used as concrete reinforcement in structures. A major problem associated with using steel as reinforcement is corrosion. Steel corrosion causes a reduction in the reinforcement cross-section and consequently reduces its ability to carry loads. There is a high cost associated with infrastructure maintenance and repair in connection with steel corrosion. In Europe alone, the estimated annual cost is £20 billion.

Fibre reinforcement polymer (FRP), a non-corrosive material, which has been used for decades in the aerospace and automotive industries, has emerged as an effective alternative of steel reinforcement. However, the widespread use of FRP as a reinforcement for concrete was hindered due to relatively weak performance at elevated temperatures, as in the case of fire. Under heating, the polymer matrix used in FRP manufacturing softens, which causes bond degrading between the FRP reinforcement and concrete, which can lead to failure. The fibres in FRP, on the other hand, can tolerate temperatures much higher than polymer matrices.

This research investigates a new design of FRP internal reinforcement in which FRP reinforcement is made as closed loops that can maintain interaction with concrete even after the polymer softens. The experimental results demonstrated that FRP loop reinforcement can be a promising solution for enhancing the fire performance of FRP internal reinforcement at elevated temperatures. Therefore, it can contribute in removing a major obstacle in the way of widespread use of FRP reinforced concrete.

Acknowledgements

I would like to thank my supervisors Dr. Tim Stratford and Prof. Luke Bisby for their mentor and massive support throughout this phase of my life. Also I would like to extend my gratitude to Prof. Emilio Nigro and Dr. Antoni Bilotta for hosting my visit to the University of Naples Federico II and for their helpful guidance.

I gratefully acknowledge the financial support from the Libyan Minister of Higher Education which has been crucial for this work to be done.

I'm also grateful for the financial support from COST Action (TU1207) to fund my research visit to University of Naples Federico II.

The experimental part of this work was very physically demanding due to the involvement of casting, handling, and testing of heavy concrete beams. I owe a lot to Zaid Al-Azzawi, Emma McIntyre, and Daryan Othman who provided me with help in the process. Eleni Triantafyllidou are Silvian Grosu also are thanked for their help with the early stage of experimental work.

I'm also grateful to the lab technicians Derek Jardine and Jim Hutcheson for the support they provided. Also I would like to thank my friends and colleagues at the University of Edinburgh, and particularly at John Muir building, for their friendship and encouragement along the way.

Finally, but by no means least, I owe a lot of what achieved in my life to the unlimited and unconditional support of my parents and siblings. You are the most important people in my life and I dedicate this work to you.

Contents

List of Figures

List of Tables

Chapter 1 – Introduction

1.1 FRP in Civil Engineering Applications

The repair and maintenance of deteriorated and substandard infrastructure are a challenge that is being faced globally. This challenge is more acute in developed countries, as most of the infrastructure was built in the middle of last century (Firmo, 2015). Traditionally steel and concrete have been the main construction materials that have been exploited in construction. One major cause for infrastructure deterioration is steel corrosion. For example, in European Union countries alone, it is estimated that the annual repair and maintenance cost associated with steel corrosion in infrastructure is around £20 billion (Nadjai et al., 2005).

Fibre reinforcement polymer (FRP), a non-corrosive material has been used for decades in the aerospace and automotive industries, and has emerged as an effective alternative for steel reinforcement. The high durability of FRP can extend to the whole life span of structure and consequently significantly reduce repair and maintenance costs associated with steel reinforcement (Imjai et al., 2009). The utilisation of FRP in civil engineering applications dates back to the 1950s; however, it was not until the 1970s when FRP was considered as a material for structural applications (ISIS, 2007). FRP properties such as a high strength-to-weight ratio, and its electrochemical corrosion resistance make it a valuable structural material. Advances in FRP manufacturing technologies led to reduced cost and improved performance (Nigro et al., 2013). The most common types of FRP used in civil engineering applications are carbon (CFRP), glass (GFRP), basalt (BFRP), and aramid (AFRP). Among these

types, CFRP provides the highest strength, stiffness and fatigue resistance (Firmo, 2015; GangaRao et al., 2007). The interest and research in utilising FRP as an internal reinforcement material emerged in various design guidelines in many countries.

Wider use of FRP has, however, been hindered due to the difficulties in meeting design codes and fire endurance criteria (Firmo, 2015; Bisby et al., 2002; Green et al., 2007). The comparatively low fire resistance of FRPs is mainly due to its bond performance (McIntyre et al., 2014). The deterioration in FRP bond occurs around the glass transition temperature of polymer (T_g), which is typically in the range of 65 to 150 °C depending on the composition and production process of the resins, fibre type, fibre fraction volume, and modulus of elasticity (Saafi, 2002; Bisby et al., 2002; Al-Zahrani, 1995). A few studies have proposed solutions to improve the fire performance of FRP, such as providing fire protection systems for whole structural elements to providing anchorage of FRP bars in areas protected from fire (Kodur et al., 2005; Nigro et al., 2011a; Nigro et al., 2011b). Enhancing the fire performance of FRP reinforcement is recognised as a critical need in the research community to enable these materials to be used in structures with more confidence.

1.2 Research Significance

This research proposes and investigates a new design of FRP internal reinforcement intended to enhance the fire performance of FRP-reinforced concrete, which has hampered wider spread of FRP in civil engineering applications. Instead of the traditional use of straight separate FRP bars, the longitudinal reinforcement is made in closed FRP loops. The loops were made by winding long continuous carbon fibre tows. This design exploits the fact that the FRP fibres in general, and carbon fibres in particular, are capable of sustaining a large proportion of their original strength at high temperatures. Unlike the case of straight bars, CFRP loops interaction with concrete does not rely only upon surface bond for load transfer, as load can still be resisted through bearing at the loop ends even after the resin softens. The idea of FRP loop and the loop manufacturing procedure, that are used in this work, were generated by the

author, in conjunction with Dr. Tim J. Stratford and Prof. Luke A. Bisby who supervised this Ph.D. thesis.

The research presents experimental evidence through of a series of tension, push-off, and beam tests, that demonstrate the capability of CFRP loops at elevated temperatures. A numerical tool was developed for analysis and design of FRP internal reinforcement for fire performance. A Matlab code was developed to calculate the bond-slip response of both FRP straight bars and loops at ambient and elevated temperatures.

The research carried out in this thesis contributes to the following domains:

1. Bond behaviour of CFRP internal reinforcement at elevated temperature.

2. Fire behaviour of RC beams reinforced internally with new CFRP loops.

3. Analysis of bond at ambient and elevated temperatures for FRP internal reinforcement.

1.3 Aims, Objectives and Methodology

This Ph.D. thesis has two main aims:

1. to investigate the performance of a new design of CFRP loop reinforcement in concrete at ambient and elevated temperatures and compare it with traditional straight bar reinforcement; and
2. to develop an analysis tool that can be used for the design of FRP loop reinforced concrete for elevated temperature performance.

To meet the aims of the research the following objectives were defined:

• to design a mechanism for producing continuous closed CFRP loop;

• to prepare and test small scale proof of concept samples that compare the performance of the proposed design of CFRP loop against CFRP straight and hooked bars at ambient and elevated temperatures;

• to design, prepare and test beam specimens reinforced with either CFRP loops or straight bars at ambient and elevated temperatures;

• to obtain and analyse data describing the flexural strength, deflection, and fire resistance time of tested specimens;

• to reform analytical model used for steel reinforcement to be used for bond stress-slip analysis of FRP bars and loops; and

• to integrate the temperature dependency of FRP bond strength in an analysis process utilising pre-existing models.

To achieve these objectives, samples of CFRP loops were first produced by winding continuous carbon tows around custom-built moulds. As proof of concept the produced reinforcement was tested in tension and push-off test setups at ambient and elevated temperatures. Loop performance was compared to samples with either straight or hooked bars. The tension and push-off tests allowed a quick assessment of CFRP loop fire performance.

The tension and push-off tests were followed by two phases of beam tests to investigate CFRP loop performance as flexural reinforcement. The first phase consisted of beams reinforced either with overlapped loops, spliced bars, or continuous straight bars. The flexural capacity of beams with different reinforcement arrangements was first assessed through a four-point bending test. Then specimens were heated at the mid-span (where loop overlap and bar splices are located) by gas radiant panels while beams were being held under a sustained load. To investigate the influence of some parameters, loop overlap length, transverse reinforcement, and size of heated zones were changed in the beams in the second phase. The beam tests provided crucial details in terms of load bearing capacity, deflection and fire resistance between beams with different reinforcement types and highlighted the merit of the proposed design.

A numerical analysis tool is also needed to provide a preliminary methodology for the design of beams with CFRP loops for fire performance, and so pre-existing analytical models of steel and FRP reinforcement were evaluated. A one-dimensional finite element model for steel from the literature was modified to be used for the case of both FRP bars and loops. That was done through changing the model bond law. The model was used alongside other models to describe the influence of temperature on bond strength and tensile capacity of the curved part of loop based on its geometry. The three models were combined and used to assess the load bearing capacity of embedded reinforcement, and can be used in the design process to calculate the required embedded length and curved part geometry that is needed to sustain a certain amount of stress at specified temperatures.

1.4 Thesis Outline

The present thesis is organized into eight chapters:

Chapter 1: This chapter contains a background about FRP applications in civil engineering. It also describes the research significance along with the thesis aims, objectives, and methodology.

Chapter 2: Provides a literature review that covers FRP composition, applications in civil engineering, advantages and drawbacks, mechanical and thermal properties, bond behaviour of FRP bars in concrete and their behaviour at elevated temperatures.

Chapter 3: This chapter contains a description of the CFRP loop production procedure. It also contains the first sets of experimental work carried out in the form of tension and push-off tests. The tension and push-off tests were intended to provide an initial assessment of the capability of CFRP loops. In push-off test specimens with either straight or hooked bars with the same mechanical properties were also tested for comparison. As performance at elevated temperatures is the main purpose, in addition to ambient, specimens were tested at glass transition temperature and 50 °C above that temperature. Details of the tension and push-off tests methodologies and the results obtained are discussed within the chapter.

Chapter 4: This chapter covers the ambient beam tests. The first part of the chapter provides a description of specimens designs and the test methodology of four-point bending tests conducted upon beams reinforced with either CFRP loops or straight bars. This is followed by details of specimen preparation and the equipment used for loading. The final part of the chapter contains the obtained results and discussion which cover flexural capacity, load-deflection response, failure modes, fire resistance time and crack patterns of the specimens tested.

Chapter 5: The heated beam tests are discussed in this chapter. The first part of the chapter provides a brief description of the experimental programme and test methodology in which beam specimens tested under sustained monotonic and transient localised heating over the mid-span region. The results obtained are placed at the end of the chapter along with the discussion.

Chapter 6: This chapter establishes an analysis framework for FRP bond response at ambient and elevated temperatures, which paves the way for the design of CFRP loops for fire performance. The chapter contains details of a Matlab code that was developed based on modifying bond law in one-dimensional finite element model for steel reinforcement. The chapter also includes a description of temperature effects on bond stress distribution and development length of FRP reinforcement. A comparison between the numerical model predictions and experimental results of beam tests is also provided within Chapter 7.

Chapter 7: Draws the conclusions of this experimental research and numerical work and presents recommendations for future developments.

Chapter 2 – Literature Review

2.1 Introduction

Fibre-reinforced polymer (FRP) have many advantages over traditional steel reinforcement, such as the lack of corrosion and lightweight. A substantial obstacle to their widespread use, however, is the poor performance of an FRP-reinforced concrete member in fire. The bond between the FRP reinforcement and the concrete degrades due to polymer matrix softening at temperatures around its glass transition temperature. As a consequence of this bond degradation, all means of force transfer between FRP bar and concrete are severely damaged, the reinforced concrete member can then become unable to carry the required load, and a brittle failure results from the loss of the tension reinforcement. This chapter provides a brief review of the literature regard the composition and mechanical properties of FRP reinforcement. It also discusses the degradation of FRP bond strength and mechanical properties at elevated temperatures and the related effect on flexural concrete members incorporating FRP reinforcement.

2.2 Fibre Reinforced Polymer (FRP)

Fibre Reinforced Polymer (FRP) is a composite of two main components: high strength fibres and a polymer matrix (Figure 2.1). Other FRP constituents used in small quantities are coatings and fillers. As with any composite, the constituent materials are combined to achieve properties superior to individual components alone. FRP and sub components are produced with a variety of properties to suit different applications and

this makes it difficult to make a generalisation about FRP characteristics (ISIS, 2007; GangaRao et al., 2007).

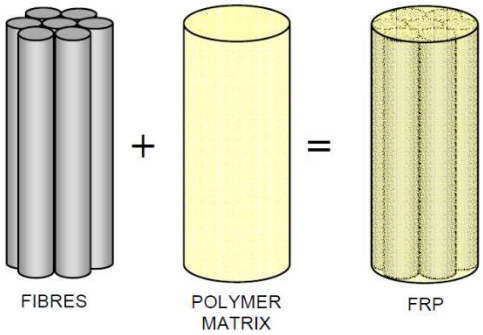

Figure 2.1 FRP constituent components (ISIS, 2003).

Fibres have high strength and provide the tensile capacity and stiffness of the composites. The polymer matrix's function, on the other hand, is to provide load sharing between individual fibres through shear stress developed at the interface with the fibres (Nadjai et al., 2005; GangaRao et al., 2007). The polymer matrix also provides environmental protection for fibres. For concrete application, carbon and glass fibres are typical, and the common matrix types are epoxy and vinyl esters (GangaRao et al., 2007; ISIS, 2003; ACI, 2012).

FRP material was originally developed for use in the aerospace and automobile industries, but was later utilised as reinforcement for concrete structures from the 1950s (ISIS, 2007). Since then, the usage of FRP for civil engineering application has been growing noticeable mainly due to reduction in materials cost. FRP can be found in different types and shapes. As tension reinforcement FRP can be found as unidirectional bars made of fibres orientated along bar longitudinal axis. FRP is also used as unidirectional or orthogonal sheets for repairing and strengthening applications, but these are outside the scope of the current work. Despite the higher cost, FRP was utilised for structural purposes due to high strength-to-weight ratio and resistance to de-icing chemicals in comparison to metals (GangaRao et al., 2007, ISIS, 2003). FRP does, however, have some characteristics which can negatively impact their structural performance with concrete, such as lack of ductility, low transverse strength, and high coefficient of thermal expansion (ACI, 2015; CEB-FIP, 2007).

2.3 Fibres

As was mentioned in the previous section fibres are used in FRP to provide strength and stiffness (ISIS, 2003; ACI, 2015). In structural applications, the fibres within FRP are continuous and orientated in specific directions to optimise the composite strength. The selection of fibres is mainly based on the characteristic of stiffness and strength. Fibres are also characterised by a very large ratio of length-diameter and very small diameter of about 5-10 microns (Figure 2.2). Because of their small diameter, a section of FRP bar typically contains thousands of fibres. This makes FRP less affected by any flaw in individual fibres. When any individual fibres is broken, force within will be transferred to surrounding fibres through the polymer matrix (ISIS, 2003).

For civil engineering applications, the most common types of fibres used are glass and carbon (graphite). The selection among fibres types is influenced by many considerations such as the required strength, stiffness, durability, and cost (ISIS, 2003; CSA, 2012).

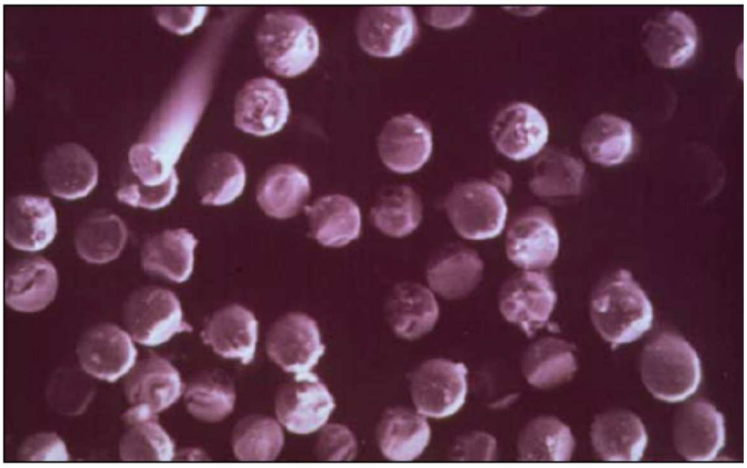

Figure 2.2 Scanning electron micrograph of carbon fibres (ISIS, 2003).

2.3.1 Glass Fibres

Glass fibres are typically produced in a process called direct melt where fibres are made by fast (200 mph) and continuous drawing from glass melt (ISIS, 2003; GangaRao et al., 2007). The glass filaments are then cooled rapidly within 10^{-5}

second. A protective coat (sizing) is applied to reduce static friction between fibres and enhances bond with matrix (GangaRao et al., 2007). The chemical composition of glass fibres includes silica, calcium, alumina, and borosilicate (GangaRao et al., 2007; ACI, 2015; CSA, 2012). Group of glass filaments are combined to produce a strand, then group of strands make roving which is the form of the most commonly available glass fibres in the market. Glass fibres are characterised by high strength and high chemical properties when compared with steel, and their cost is lower than carbon fibres. The drawbacks, however, are low modulus of elasticity, sensitivity of abrasion in comparison to steel. Typical mechanical properties of glass fibres are shown in Table 2.1. The mechanical properties of glass fibres deteriorate under elevated temperature which is discussed in more details in section 2.10.2

2.3.2 Carbon Fibres

Carbon fibres were used in the current research. They are produced by a process called 'controlled pyrolysis', in which raw materials are subjected to complex heating treatments: carbonizing and graphitization (GangaRao et al., 2007; ISIS, 2003). Typical mechanical properties of carbon fibres are shown in Table 2.1. The most common precursors used in carbon fibres productions are Polyacrylonitrile (PAN) and pitch (CSA, 2012; ACI, 2015; Walsh and Corporation, 2001). PAN are synthetic fibres, while pitch are petroleum or coal based (GangaRao et al., 2007). In the manufacturing process, the precursor materials are initially heated at 200 – 400 °C in a process to cross-link carbon chain so they don't break in subsequent higher temperature treatments. This is followed by carbonization where fibres are heated in oxygen absence at temperature of 800 – 2000 °C to remove any non-carbon impurities. In graphitization treatment, fibres are stretched between 50–100% and heated between 1100 and 3000 °C (CEB-FIP, 2007; GangaRao et al., 2007). The stretching results in an orientated crystalline structure that gives higher modulus of elasticity to the fibres. The effect of carbonisation temperature upon the carbon fibre modulus of elasticity is shown in Table 2.2. The manufacturing process is then finished with epoxy sizing for fibres surface treatment to improve bonding between fibre and epoxy matrix in composites (GangaRao et al., 2007; CEB-FIP, 2007). Commercial carbon fibres are

available in form of bundles of 1,000 to 160,000 parallel filaments (CEB-FIP, 2007). The effect of elevated temperatures on carbon fibres properties is discussed in section 2.10.2.

Table 2.1 Typical mechanical properties of fibres (ISIS, 2007).

Fibre Type		Tensile Strength (MPa)	Young's Modulus (GPa)	Elongation (%)	Coefficient of Thermal Expansion (10^{-6})	Poisson's Ratio
Carbon						
PAN	High Strength	3500	200 – 240	1.3 – 1.8	-1.2 to -0.1	-0.2
	High Modulus	2500 – 4000	350 – 650	0.4 – 0.8	7 to 12	
Pitch	Ordinary	780 – 1000	38 – 40	2.1 – 2.5	-1.6 to -0.9	N/A
	High Modulus	3000 – 3500	400 – 800	0.4 – 1.5		
Glass						
E-Glass		3500-3600	74 – 75	4.8	5.0	0.2
R-Glass		4900	87	5.6	2.9	0.22

Table 2.2 Effect of temperature of modulus of carbon fibres (GangaRao et al., 2007).

Carbon Fibres Grade	Low modulus	Standard modulus	Intermediate modulus	High modulus
Carbonisation temperature (°C)	up to 1000	1000 – 1500	1500 – 2000	2000+
Young's Modulus (GPa)	up to 200	200 – 250	250 – 325	325+

Carbon fibres have been utilised in structural engineering applications due to their several advantages over glass fibres such as high tensile strength and high ratio of modulus-to-weight, low coefficient of linear thermal expansion and high fatigue strength (GangaRao et al., 2007; ISIS, 2003; Walsh and Corporation, 2001). On the other hand, the main disadvantages of carbon fibres include cost and lack of ductiliy when compared to steel (GangaRao et al., 2007; ACI, 2015).

2.4 Polymeric Matrices

The matrix is the binder between the fibres in FRP composites. The matrix serves two main functions; it protects fibres from environmental degradation, and it provides load sharing between individual fibres (Bisby et al., 2005; ACI, 2015; ISIS, 2003; ISIS, 2007). In general, the polymer is called a resin in its wet state and the matrix after curing (CEB-FIP, 2007). Within FRP composites, the fibres provide strength and stiffness, whilst the matrices transfer force between the fibres through shear stress developed within the matrix. Therefore, good bond between fibres and matrix is essential for the strength of an FRP (ISIS, 2003; GangaRao et al., 2007).

A polymer matrix is an organic compound which consists of a long chain of molecules (GangaRao et al., 2007; ISIS, 2003). There is a great variety of matrix types, but the focus here is mainly upon the types commonly used in structural engineering applications, in which matrix is divided into two broad categories: thermoplastic and thermosetting (ISIS, 2007; ACI, 2015; GangaRao et al., 2007).

Thermoplastic matrices consist of long chains of molecules with weak connections between each other, but with strong bond between molecules themselves. This enables thermoplastic matrices to be repeatedly softened and hardened under heating without any significant changes to their molecules structure.

Thermosetting polymers, on the other hand, consist of long chain of molecules which are cross-linked. Therefore, these polymers deteriorate under repeated softening and hardening at elevated temperatures. In most structural engineering applications, thermoset polymers are used because of their better properties of chemical resistance, creep, and relaxation compared to thermoplastics (CEB-FIP, 2007; ISIS, 2007; ISIS, 2003). Thermosetting polymers also have low viscosity, which is useful to achieve higher fibres fracture volume and good wet-up of fibres. These polymers are also characterised with low coefficient of thermal expansions and good resistance to solvents (CEB-FIP, 2007). The drawbacks with thermosetting is irreversibly softened, which prevents from bending FRP reinforcement on site, as this has to be done during manufacturing process. There are three common types of thermosetting polymers used

in structural engineering applications: polyesters, vinyl esters, and epoxies (ISIS, 2003; GangaRao et al., 2007). Typical mechanical properties of thermosetting matrices are shown in Table 2.3.

Table 2.3 Typical properties of thermosetting matrices (CEB-FIP, 2007).

Properties	Matrix		
	Polyester	**Epoxy**	**Vinyl ester**
Density (kg/m^3)	1200 – 1400	1200 – 1400	1150 –1350
Tensile Strength (MPa)	34.5 – 104	55 – 130	73 – 81
Longitudinal Young's Modulus (GPa)	2.1 – 3.45	2.75–4.10	3.0 – 3.5
Poisson's Ratio	0.35 – 0.39	0.38–0.40	0.36 – 0.39
Thermal Expansion Coefficient (10^{-6})	55 – 100	45 – 65	50 – 75
Moisture Content (%)	0.15 – 0.60	0.08 – 0.15	0.14 – 0.30

2.4.1 Polyesters

Polyester resin is made of constituents components of organic acids and glycols (CEB-FIP, 2007; GangaRao et al., 2007). The low cost of precursors materials make polyester resin represents high portion of thermosetting polymer resin used in composites industry (GangaRao et al., 2007).

2.4.2 Vinyl Esters

Vinylester polymers are characterised with good resistance to strong acids and alkali (ISIS, 2003; GangaRao et al., 2007). Therefore, vinylester are used as matrix of FRP reinforcement for concrete (ISIS, 2003). They also have less tendency to moisture absorption and shrinkage compared to polyesters. The drawback with vinylester is that their cost are marginally higher than polyester (ISIS, 2003). Vinylester also have high volume shrinkage about 5% – 10% and moderate adhesive strength (GangaRao et al., 2007).

2.4.3 Epoxies

In comparison to other types of resin, epoxies are more commonly used for FRP wet lay-up applications because of their ability to cure at ambient temperature and also due to their strong adhesion characteristics (ISIS, 2003). In the current research FRP reinforcement is made by wet lay-up process therefore epoxy resin was used. Epoxy resins have low volume shrinkage and good resistance to chemicals apart from acid.

The disadvantage of them is that they cost significantly more than vinyl esters and polyesters resins (ISIS, 2003; GangaRao et al., 2007). The properties of polymer matrix are temperature dependant which is discussed later in section 2.10.1.

2.5 Bond Behaviour of FRP Bars to Concrete

Bond is the means of force transfer between reinforcement and concrete. Bond is characterised by horizontal shear forces occur on the outer surface of the bar (Figure 2.3). Bond stress has nonlinear distribution along bar and it is a function of the bending moment, pull-out force or any other forces acting on the member (Baena et al., 2009; Nigro et al., 2012a; Al-Zahrani et al., 1999; Katz, 1999; ACI, 2015; GangaRao et al., 2007). In order to achieve the full capacity of a section, the concrete and reinforcement should deform together without any slippage between them. In reality, this is hard to achieve, as the rupture strain of FRP bars ranges from 0.015 to 0.025, which is several times higher than the failure strain of concrete (0.003 – 0.0045). Good confinement of concrete, however, can minimise the negative impacts and provide warnings to eliminate chances of catastrophic failure (GangaRao et al., 2007).

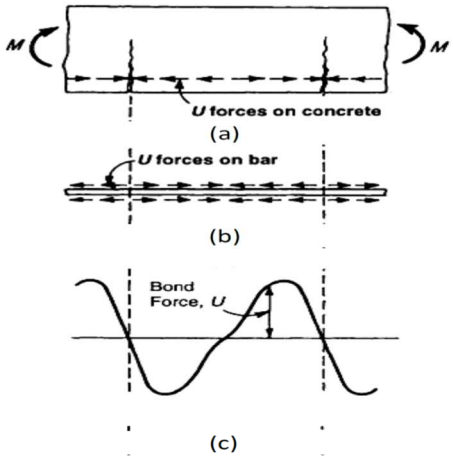

Figure 2.3 Nonlinear variation of bond force along FRP bar: (a) cracked concrete section; (b) bond forces on bar; (c) variation of bond stress (Ametrano, 2011).

FRP bars are made with various different surface configurations, including: sand-coated, ribbed, or helically wrapped (Figure 2.4); and from all of these, the polymer

matrix is the key component (Green et al., 2007; ACI, 2015; ISIS, 2007). Bar surface configuration significantly affects bond mechanism, however, for now there is no standardisation for FRP reinforcement surface configuration (ISIS, 2007; ACI, 2015; Bakis et al., 1998; Baena et al., 2009). Forces are transferred between the reinforcement (whether steel or FRP) and the concrete, which happened through three different mechanisms: (1) chemical adhesion, (2) friction forces generated due to the roughness of interface, (3) mechanical interlock between concrete and rebar surface (Figure 2.5). Ehsani et al. (1995) conducted beam and pull-out tests and concluded that main bond mechanisms are friction and chemical adhesion. GangaRao et al. (2007), however, stated that mechanical interlock is the primary mechanism of bond while chemical adhesion has a low influence.

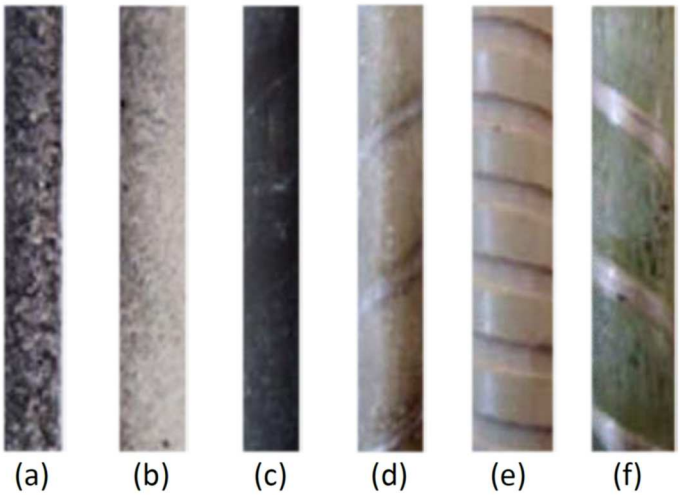

Figure 2.4 Surface configuration of commercially FRP bars: (a) sand coated CFRP bars; (b) sand coated GFRP bar; (c) surface textured CFRP bar, (d) helically wrapped-sand coated GFRP bar, (e) grooved GFRP bar; (f) helically wrapped GFRP bar (Ametrano, 2011).

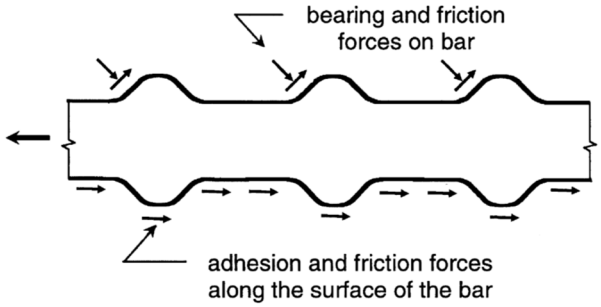

Figure 2.5 Bond force transfer mechanisms (ACI, 2003).

The bond behaviour of FRP bars differs from their traditional steel counterparts in terms of the force transfer mechanisms and failure modes, which is due to the major differences in material properties. Whilst steel is an homogeneous elasto-plastic material, FRP is anisotropic and linear-elastic to failure (Quayyum, 2010). The properties of the FRP control the bond with concrete, unlike with steel reinforcement where concrete strength is the control factor (Bakis et al., 1998). The value of bond stress developed at failure with steel is generally higher than with FRP reinforcement, and the magnitude of slip with FRP bars is bigger (Ehsani et al., 1995). This implies that longer development length is needed for FRP bars.

2.5.1 Bond Failure Modes

To avoid bond failure and allow bars to develop their full tensile capacity, bars should be anchored adequately and/or concrete surrounding the bar should be well-confined by means of concrete cover and/or transverse reinforcement. When such conditions are provided, concrete will be able to resist the radial splitting stresses generated on rebar surface. Failure then will occur as concrete crushing, bar rupture failure, or shear failure. However, if anchoring conditions were not provided adequately, failure can occur due to slippage of bar or splitting of concrete (Quayyum, 2010; GangaRao et al., 2007; Harajli and Abouniaj, 2010).

Splitting Failure

This type of failure occurs when the splitting forces generated around the reinforcement overcome the level of confinement of concrete surrounding the bars (Aly et al., 2006). This failure is initiated with cracks occur in perpendicular direction and parallel to reinforcement, then propagate toward concrete surface (Figure 2.6) (Ametrano, 2011; Cosenza et al., 2002).

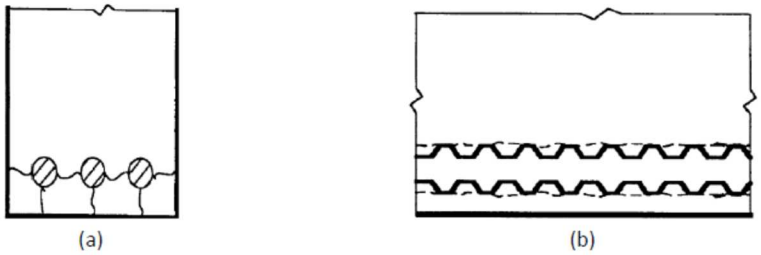

Figure 2.6 Bond failure modes: (a) End view showing splitting cracks between bar and concrete (b) Side view of member showing shear crack and/or concrete crushing due to pull-out (ACI, 2003).

Pull-out Failure

This failure occurs when bars are pulled-out of concrete without rupture or concrete splitting. This happens when concrete is well-confined so interfacial failure occurs in terms of bar rips are sheared off by concrete (Figure 2.6) (Ametrano, 2011, Okelo and Yuan, 2005, Cosenza et al., 2002).

2.5.2 Development Length and Splicing of FRP Reinforcement

The development length is defined as the shortest embedded length required for bar to develop its full tensile capacity (ISIS, 2007, Thamrin and Kaku, 2005, Cosenza et al., 2002).

Development Length of Straight Bars

The design guidelines ISIS (2007) and (FIP, 2007) provide an expression, Equation 2.1, to calculate the required development length (or anchorage) of straight FRP which includes modification factors to account for the effects of different parameters as shown below. The design guidelines (ACI, 2015) also include expression for development length (Equation 2.2), but they do not account for transverse reinforcement effect and it yields a higher value of development length.

$$l_d = 0.45 \frac{k_1 k_4}{\left(d_{cs} + k_{tr} \frac{E_{frp}}{E_s} \right)} \left(\frac{f_{frp}}{f_{cp}} \right) A \qquad (2.1)$$

Where: l_d development length; k_1 bar location factor; k_4 is bar surface factor; d_{cs} concrete cover factor; k_{tr} transverse reinforcement index; E_{frp} longitudinal Young's modulus of the FRP bar (MPa); E_s is Young's modulus of steel (MPa); f_F tensile strength of FRP bar (MPa); f_{cr} is concrete cracking strength; *A* bar cross-section area.

$$l_d = \frac{\propto \frac{f_{fr}}{0.083\sqrt{f_c'}} - 340}{13.6 + \frac{C}{d_b}} d_b \qquad (2.2)$$

Where: l_d development length; f_{fr} is stress level in bar; α is bar location modification factor and should be used as 1 because less 305 mm of concrete is cast below the reinforcement; f_c' concrete compressive strength (MPa); *C* is the lesser of the cover to the centre of the bar or one-half of the centre-on-centre spacing of the bars being developed; d_b bar diameter (mm).

Tension Lap Splice

Lap splice is used when continuity of reinforcement is required. In the current research overlapped reinforcement was used to assess the bond quality of different reinforcement arrangements. Design guidelines ISIS (2007) distinguish between two types of tension splice based on stress level in reinforcement and fraction of bar spliced with given length as seen in Table 2.4. For reinforcement with class A, splice length is $1.0\,l_d$; while splice length of Class B is $1.3\,l_d$. Hence, when all reinforcement are spliced within same area and full reinforcement strength is required, splice length of Class B ($1.3\,l_d$) is used.

Table 2.4 Type of required tension lap splice

$\frac{A_{frp,\text{provided}}}{A_{frp,\text{required}}}$	$\frac{f_{frp}}{f_{frpu}}$	Maximum percentage of A_{frp} spliced within required lap length	
		50%	100%
2 or more	0.5 or less	Class A	Class B
Less than 2	More than 0.5	Class B	Class B

Where: l_d is development length (mm), A_{frp} is area of FRP bar (mm^2), f_{frp} is stress in FRP bar (MPa), f_{frpu} is ultimate tensile strength of FRP bar (MPa).

2.5.3 Factors Affect FRP Bond

The bond stress developed by FRP bars is influenced by several factors which are described below.

Transverse Reinforcement

Transverse reinforcement (such as shear stirrups) enhances bond strength, as it increases the confinement around FRP bars, which in turn increases the resistance against the propagation of splitting cracks (Orangun et al., 1977; Aly et al., 2006). Transverse reinforcement also leads to a more even distribution of bond stress along a bar (Orangun et al., 1977). However, in case of pull-out failure, transverse reinforcement provide no extra capacity because concrete is strong enough to resist radial cracking; therefore, failure occurs as shearing off of bar lugs (Orangun et al., 1977; Aly et al., 2006; Quayyum, 2010).

Bar Diameter

The effect of bar diameter on bond strength is similar to steel. When bar size increases, bond strength is decreased. That can be attributed to several factors, such as the effect of Poisson's ratio, or shear lag through the diameter of the reinforcement. Furthermore, as the bar diameter increases there will be more chance of water being trapped beneath the bar when the concrete is cast, which causes formation of voids and reduces contact surface which results in weaker bond between the bar and the surrounding concrete (Aly et al., 2006; Achillides and Pilakoutas, 2004; Okelo and Yuan, 2005; Quayyum, 2010; Tighiouart et al., 1999).

Embedment Length

The influence of embedment length on bond strength has been investigated by many researchers and FRP bond strength was found to be inversely proportional to the embedment length. The nonlinear distribution of bond stress is highest at the loaded

end, and decreases toward the free end, and consequently a longer embedment length produces less average bond stress along the bar (Achillides and Pilakoutas, 2004; Aly et al., 2006). Similar trends for hooked FRP reinforcement were observed by Ehsani et al. (1995) when they conducted pull-out test on hooked FRP bar. Results showed that embedment length also has a significant influence on the slip value at failure and initial stiffness. If adequate embedment length was provided, FRP bar will develop more (or full) capacity (Achillides and Pilakoutas, 2004; Aly et al., 2006; Ehsani et al., 1995).

Bar Position

The ACI design guidelines (ACI 440.1R-15) define 'top bars' as horizontal bars that have more than 305 mm of concrete beneath at the time of embedment. Top bars develop less bond strength because air, water, and fine particles migrate toward upper part of concrete while casting concrete. This results in lower quality of concrete surrounding 'top bars' and reduces bonding. In calculations of development length from both ACI 440.1R-15 and CSA s806-12, the values of modification factor for 'top bar' are found to be 1.5 and 1.3, respectively (ACI, 15; CSA, 2012).

Concrete Cover

Concrete cover affects bond of reinforcement as it influences the level of confinement. Research has shown a significant correlation between bond failure modes (pull-out or concrete splitting) and concrete cover (Okelo and Yuan, 2005; GangaRao et al., 2007). Splitting failure is initiated with radial cracks propagating toward the outer surface of concrete; therefore, concrete cover is an important factor of bond capacity (GangaRao et al., 2007). Ehsani et al. (1996) conducted a series of beam and pull-out tests and observed that bond failure occurred as pull-out when concrete cover equals bar diameter or less while splitting failure took a place when concrete cover increased. Harajli and Abouniaj (2010) conducted beam tests of spliced FRP reinforcement, and reported that when pull-out failure occurred, increasing concrete cover has minor effect on bond strength. The side concrete cover was also found to be important as splitting cracks propagate toward the thinnest concrete cover whether it is at the bottom or side (Aly et al., 2006). Canadian guideline (CAN/CSA, 2012) recommends

minimum concrete cover of $3.5\,d_b$ or 40 mm to account for the effect of temperature as well, and this limit could be relaxed if transverse reinforcement is provided. The design guideline ISIS (2007) considers the environmental effect for minimum concrete cover as it distinguishes between internal and external structural elements (Table 2.5).

Table 2.5 Concrete cover of flexural reinforcement (ISIS, 2007).

Type of Exposure	Beam	Slab
Internal	max ($2.5\,d_b$ or 40 mm)	max ($2.5\,d_b$ or 20 mm)
External	max ($2.5\,d_b$ or 50 mm)	max ($2.5\,d_b$ or 30 mm)

* d_b = bar diameter

2.6 Curved FRP Reinforcement

Curved reinforcing bars are used for anchorages, element connections, and stirrups. In the current research curved FRP reinforcement was utilised as tension reinforcement for concrete elements. Producing curved FRP bars is not straightforward because FRP is not ductile. Unlike steel reinforcement, FRP bars cannot be bent on site. Cold bending for mild steel, for example, with a ratio of bend radius-to-bar diameter of 2 would induce a plastic strain of 20%. FRP bars cannot tolerate such a high value of strain because either fibres at the outer part will rupture in tension or buckle at the inner side while being not ductile. Typically, ultimate strain varies between 1% and 2.5% for FRP. Therefore, cold bending of FRP requires high ratio of bend radius-to-bar diameter, which might not be practical (Figure 2.7) (Imjai et al., 2009).

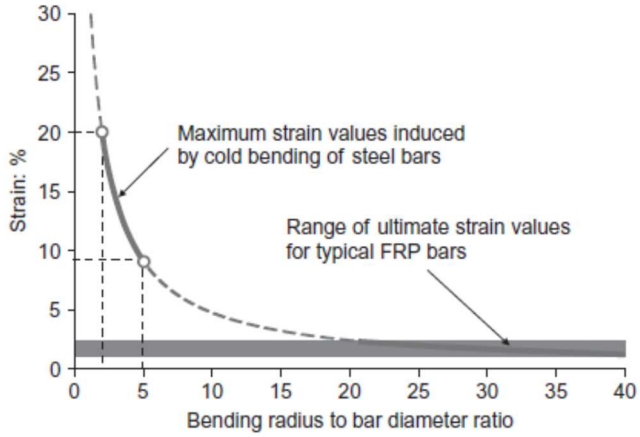

Figure 2.7 Strain induced in cold bent bar (Imjai et al., 2009).

Bending under heat is not recommended, as most of FRP bars used in civil engineering field are made using thermosetting resin which is if heated to near glass transition temperature (T_g) (see section 2.10.1), permanent damage will be caused and the strength of bar will be reduced significantly (Guadagnini et al., 2006; Ahmed et al., 2010; GangaRao et al., 2007). As a consequence, curved FRP reinforcement must be pre-formed. Pre-formed bent bars are made before the cure of the resin during the manufacturing process.

The bent portion of bar experiences conditions of multiaxial loading, lateral loading due to bearing against concrete, and longitudinal loading due to friction, adhesion, and bearing forces (Figure 2.8). The bent portion has less capacity than the straight segment of a FRP bar, because of stress concentration due to the curvature and the multiaxial stress status generated caused by axial forces and transverse (normal) forces due to bearing against concrete. In addition to the weakness of FRP in the transverse direction compared to longitudinal direction (Guadagnini et al., 2006; Ahmed et al., 2010). Experimental work has shown that the tensile capacity of curved FRP is proportional to the ratio of curvature radius-to-reinforcement thickness r/t (Lees and Winistörfer, 2011; Guadagnini et al., 2006; Ehsani et al., 1995). In addition, Winistorfer (2001) conducted experimental tension tests on curved FRP straps and found that the tensile capacity of the curved part is limited to 60% of the composite unidirectional tensile strength. An analytical model by Winistorfer (2001) suggested a

severe stress concentration occur at contact surface between FRP strip and concrete. The researcher proposed that replacing the solid and relatively thick straps by straps made of number of non-laminated layers to reduce this stress concentration (CEB-FIP, 2001). The proposed design is supposed to enhance the tensile strength of curved part through reducing the interlamina shear stress within the composite to allow more uniform strain distribution within the composite (CEB-FIP, 2001).

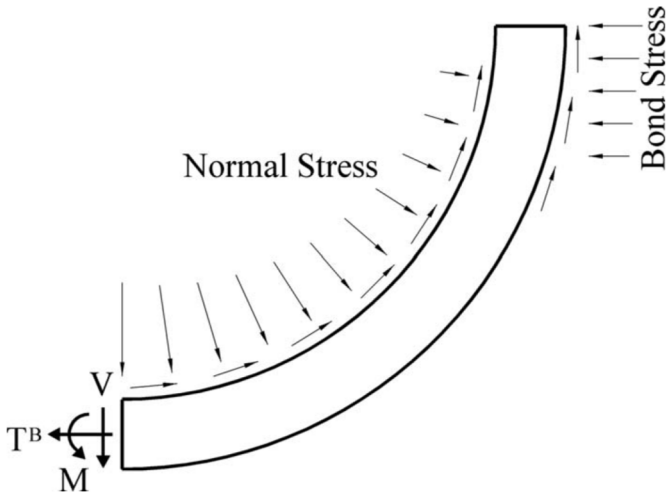

Figure 2.8 Stresses status at bend (Ahmed et al., 2010).

American Concrete Institute guidelines (ACI440.1R-15) provide an equation to estimate the reduction in tensile capacity of bar at bends (ACI, 2015):

$$f_{fb} = \left(0.05\frac{r_b}{d_b} + 0.3 \right) f_{fu} \leq f_{fu} \qquad (2.3)$$

Where: f_{fb} is design tensile strength of the bend of FRP bar (MPa), r_b is radius of the bend (mm), d_b is diameter of reinforcing bar (mm), f_{fu} is design tensile strength of FRP considering reductions for service environment (MPa).

As can be seen in equation (2.3), the strength of curved reinforcement is a function of bend radius (r_b) and bar diameter (d_b). Ehsani et al. (1995), however, conducted research on thirty-six 90-degrees GFRP hooks and found that not only r_b/d_b determines the capacity of the bend, but also the tail length and embedment length.

Concrete strength was found to have less influence. A minimum value of 3.0 for r_b/d_b was recommended by the authors (Ehsani et al., 1995).

Imjai et al. (2009) conducted pull-out tests on curved thermoplastic FRP strips and found that the capacity of the bend is mainly a function of the bent geometry. The researchers found that the use of minimum of bend radius-to-strip thickness *r/t* of 4 will guarantee that the bent capacity will not be less than 40% of composite ultimate strength. The researchers also observed that the ACI (2015) equation (2.3) overestimates the capacity of the bend. Also in contrast to what the equation suggests, results showed that bend capacity does not vary linearly with *r/t* ratio, and failure is not solely controlled by bend geometry but bond status along the embedded portion influences failure load as well (Imjai et al., 2009).

2.6.1 Development Length for Bent Bars

Providing hook at bar end enhances bond performance with concrete (Ehsani et al., 1995). Therefore, the Canadian guidelines (CAN/CSA, 2012) provide the following expressions to calculate the development length of bent bars:

$$l_d = 165k_2\frac{d_b}{\sqrt{f_c'}} \text{ for } f_t \leq 520\ MPa \tag{2.4}$$

$$l_d = \frac{f_t}{3.1}k_2\frac{d_b}{\sqrt{f_c'}} \text{ for } \ < f_t < 1040\ MPa \tag{2.5}$$

$$l_d = 300k_2\frac{d_b}{\sqrt{f_c'}} \text{ for } f_t \geq 1040\ MPa \tag{2.6}$$

Where: k_2 is concrete density factor (1.3 for structural low-density concrete, 1.2 for semi low-density concrete, 1.0 for normal density concrete), f_c' is compressive strength of concrete (MPa), d_b is bar diameter (mm), f_t is bar tensile strength (MPa).

Provided that the development length is not less than $12d_b$ or 230 mm, the tail length of a bent bar (l_t) should not be less than $12d_b$. The bend radius (r_b) should not be less than $3d_b$.

2.7 Tensile Tests for FRP Straight and Bent Bars

Both design codes CSA s806-12 and ACI 440.3R-04 provide testing methods to measure the ultimate capacity of FRP straight bars, bent bars, and stirrups under tensile force in the direction of fibres. Straight bars are tested under axial tensile load, while the bent portion in bent reinforcement is put under bi-axial loading status (longitudinal loading through pull-out of straight portion in additional to transverse stress generated at the bend due bond stresses). For bent reinforcement, there are two test methods: push-off test and tension test (ACI, 2004; CAN/CSA, 2012). Modified versions of both tests were utilised in the current research (Chapter 3) to assess the tensile and bond performance of the proposed design of FRP loops.

2.7.1 Tensile Test of Straight Bars

Tensile test on straight bars are conducted to determine the ultimate tensile capacity, Young's modulus, and elongation of FRP reinforcement. Specimens should be anchored within sleeves filled with epoxy or expansive cement grout to avoid damage to the FRP which is weak in the transverse direction, and to be able to transfer large loads into the FRP (CAN/CSA, 2012).

2.7.2 Push-off Test for Curved Bars

Push-off tests involving two blocks of concrete pushed apart using a hydraulic jack. The reinforcement bridges between the two blocks (Figure 2.9), and consequently is placed in tension as the blocks are pushed apart. This test configuration can be used to investigate stirrups and curved reinforcement.

The dimensions of the concrete block can be adjusted to suit different sizes of stirrups or bend but the dimensions are recommended not to be less than 200 mm and the tail length (l_t) not to exceed 150 mm (ACI, 2004). To avoid concrete splitting before the rupture of FRP bars, steel stirrups can be provided along the concrete blocks. The straight portion of bar before the bend is de-bonded, so that tensile force is transferred directly to the bend. A tube can be used to prevent surface contact between bar and concrete, but it should be ensured that the sides of tube are sealed, so concrete will not get inside while casting. If a sample fails by splitting, an additional sample should be

tested to replace the failed sample. If failure occurs as bars pull-out, it means that the bend radius and tail length are not sufficient. These parameters have to be adjusted, in addition to concrete block dimensions if needed, and then test should be repeated. A load cell can be used to measure the applied load by the hydraulic jack. The bend capacity and reduction factor can be calculated as written in (2.7) and (2.8), respectively (CAN/CSA, 2012; ACI, 2004).

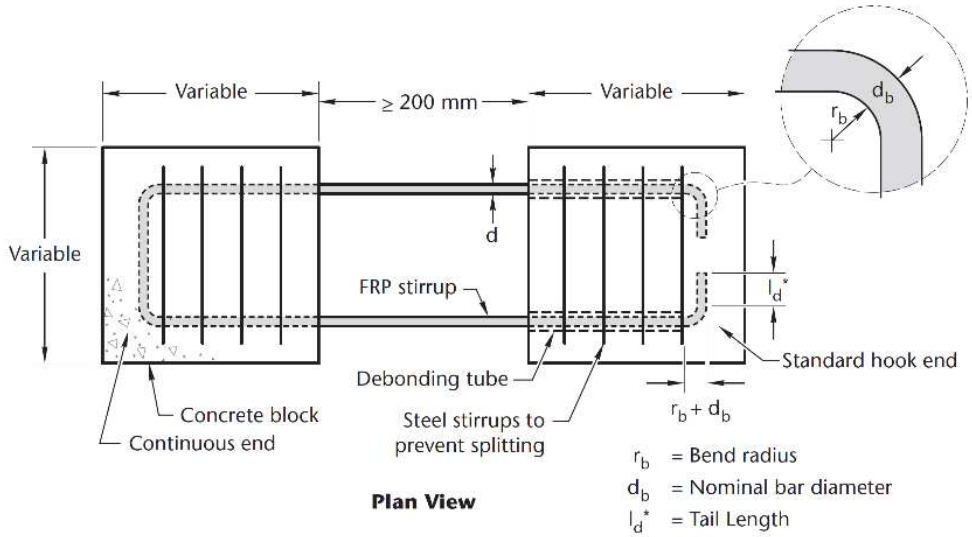

Figure 2.9 Configuration of push-off test method (CAN/CSA, 2012)

$$f_{ub} = \frac{F_{ub}}{A} \tag{2.7}$$

Where: f_{ub} is bend capacity of the FRP stirrups (MPa), F_{ub} is ultimate load capacity from bend test (N), A is cross-sectional area of one leg of FRP stirrup (mm^2).

$$X = \frac{f_{ub}}{f_u} \tag{2.8}$$

Where: X is strength reduction factor due to bend and f_u is bar ultimate tensile strength (MPa).

2.7.3 Tension Test for Curved Bars

This tension test aims to determine bend capacity and investigate the effect of corner radius on tensile strength of FRP reinforcement. This test method is suggested by ACI (2012) and designated with name B.12 test method. This test is conducted using a

special setup, as shown in the test configuration in Figure 2.10. Testing frame consists of separate upper and lower parts which specimen is fit between. The FRP sample in U–shape is placed into a groove within the upper part while the ends are anchored in the lower part of test frame. A suitable anchorage system should be used to ensure that failure occurs at bent and not at the grips. The testing machine for this test should have the ability to apply tension forces on the sample until failure. The loading speed can vary according to the material used; the recommended rate is 1.0 – 2.0 mm/min. If the strain distribution along the bend is required, strain gauges can be mounted at the corners. The reduced tensile strength can be calculated according to Equation (2.9) (ACI, 2004).

$$S = \frac{P}{2A} \tag{2.9}$$

Where: S is reduced tensile strength of specimen corresponding to specific bend radius (MPa), P is failure load (N), A is cross-sectional area of tested bar (mm^2).

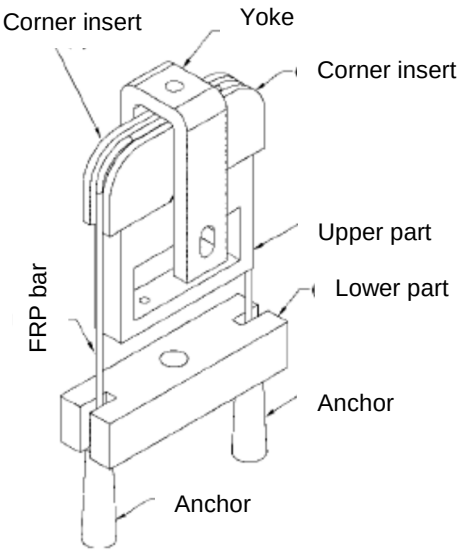

Figure 2.10 Configuration of bent FRP reinforcement tension test (ACI, 2012).

Ahmed et al. (2010) conducted an experimental work on sixty FRP bar specimens (24 straight bar, 16 C–shape bar, and 20 U–shape bars) in order to compare and check the reliability of results obtained by using B.12 and push-off tests. The obtained results confirmed the reduction of reinforcement capacity at bends. It was also observed that

the bend capacity measured using B.12 test method was consistently lower by 30% – 40% than push-off test method. This is mainly due to the fact that surface indentations on bar will increase stress concentration, while the embedded bar in concrete as in push-off test method allows better distribution of stress along the bent. Therefore, push-off test method is considered to be more representative to case in reality, where hooked FRP bars or stirrup will be in contact with concrete.

2.8 Bond Strength Test Methods for FRP Bars

There are two types of bond tests: the beam test and the pull-out test. Each test gives different values of bond strength (ACI, 2004) due to different loading configurations as explained below.

2.8.1 Pull-out Test

According to the Canadian standard CSA (2012), a pull-out test is conducted by embedding bar in concrete cubes of size 150 mm. The embedment length can be taken as $5d_b$ as defined in ACI (2012) or $4d_b$ as defined in CSA (2012), where d_b is bar diameter (Figure 2.11). Concrete can be either cast perpendicular to the rebar to simulate the case of a beam or slab, or cast parallel to the bar to simulate the case of columns. Bond strength (τ) using a direct pull-out test is measured by dividing maximum pull-out load by bonded area as shown in equation (2.10) (CAN/CSA; 2012, ACI, 2004). This method provides an average value of bond strength. Therefore, it is possible to find two bars with same bond strength, but with different slip values and elongation (Al-Zahrani, 1995).

$$\tau = \frac{P}{u\,l} \tag{2.10}$$

Where: τ is average bond stress, P is tensile load, u is the perimeter length of the FRP rod, l is embedded length.

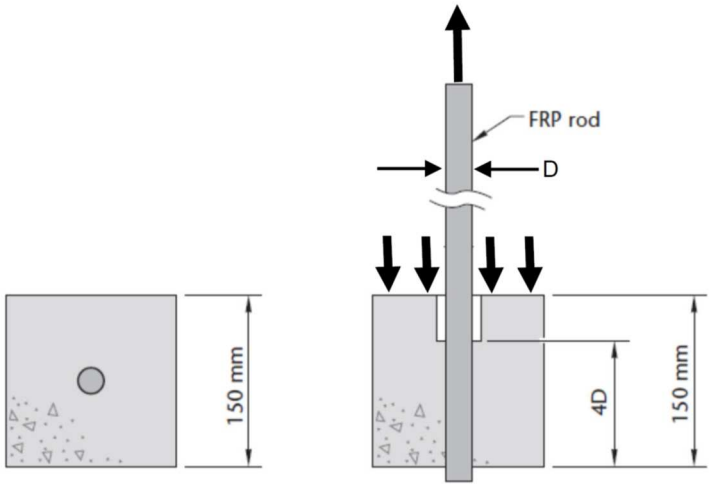

Figure 2.11 Pull-out test specimen (CAN/CSA, 2012).

Pull-out force is applied to the FRP bar through specific designed gripping systems as used in tensile test (CAN/CSA, 2012;ACI, 2015).

The value of displacement measured from different types of bond tests does not only present the slip of reinforcement relative to concrete, but also includes the elastic elongation of the bar (Baena et al., 2009; Ehsani et al., 1995). In bond test of steel, the second value is ignored because the elastic modulus of steel is high. In contrast, FRP has a relatively low modulus of elasticity therefore the elastic elongation is extracted from the measured displacement to obtain the actual slip of reinforcement (Ehsani et al., 1995).

2.8.2 Beam Test

Bond performance of reinforcing bars can also be assessed within concrete beam specimens. The values of bond strength obtained by beam test are typically less compared to pull-out. The reason for that is in pull-out test the chance of concrete splitting is omitted as concrete surrounding the bar is under pressure which restricts cracks formation. This status of compressive stresses surrounding bars does not present the situation in reality. In this sense, beam test is more realistic, but the pull-out test is more commonly used because it is much simpler to conduct. In addition, there is lack of standards and sufficient experiments data about beam tests (Tighiouart et al., 1998). Both ACI (2012) and CSA (2012) only mention beam test, but they do not provide

detailed information about test samples or procedure. Among beam test types, (b) and (d) in (Figure 2.12) are more commonly used in the literature (e.g. (Abbasi and Hogg, 2006; Harajli and Abouniaj, 2010; Rafi and Nadjai, 2011; McIntyre et al., 2015)). In these test rebar bond quality can be assessed through specimen failure mode, crack patterns, and flexural member stiffness. In the current research bond performance of the proposed CFRP loop against straight reinforcement were assessed by beam test types (b) and (d) as discussed in Chapters 4, 5, and 6.

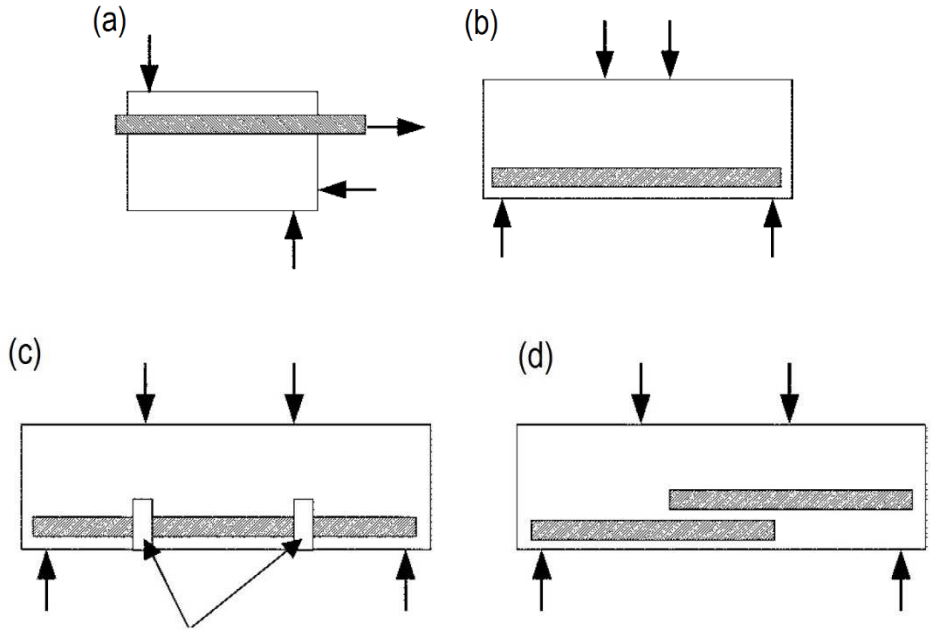

Figure 2.12 Types of beam bond test: (a) beam-end specimen (b) simple beam specimen (c) hinged beam-end specimen (d) splice specimen **(ACI, 2012)**.

2.9 Bond Stress-Slip Laws

The bond stress-slip relation is important for the design process to calculate the development length of FRP bars. While many experimental works were carried out to characterise the bond of FRP bars, very little analytical work has been done to produce analytical models (FIP, 2007). For steel reinforcement there are well known bond stress-slip models, such as B.E.P. (named after researchers Bertero, V, Eligehausen,

R., and Popov, E. P.), (Figure 2.13), that have been developed for deformed steel reinforcement and which effectively capture the bond response. However, some experimental studies demonstrated that these models can not directly put in use for FRP reinforcement due to the differences in materials properties (Cosenza, 1997; Baena, 2009). There have been many attempts to produce a generalised model for bond stress-slip for FRP reinforcement, however, this is hard to achieve due to the lack of standardisation of FRP reinforcement surface configuration (Cosenza et al., 1997).

Malvar (1994) carried out an extensive experimental work to evaluate bond behaviour of GFRP bar with four different surface configurations (deformed and indented surfaces). Based on the obtained data Malvar (1994) proposed a model for bond stress-slip, equation (2.11).

$$\frac{\tau}{\tau_m} = \frac{F\left(\frac{S}{S_m}\right) + (G-1)\left(\frac{S}{S_m}\right)^2}{1 + (F-2)\left(\frac{S}{S_m}\right) + G\left(\frac{S}{S_m}\right)^2} \tag{2.11}$$

Where τ_m Peak bond stress, s_m slip at peak bond stress, F and G are empirical constants determined experimentally by curve fitting of data.

Cosenza (1995) proposed a refinement for the ascending branch of B.E.P. model to enhance the model predictions within the serviceability state limit. The resulted model was denoted as C.M.R. (named after researchers Cosenza, E., Manfredi, G., and Realfonzo, R.). The expression for the ascending branch is provided in Equation 2.12. The authors justified their use of B.F.P. model instead of Malvar's that the latter is less accurate in capturing the initial bond response (Baena Munoz, 2010).

$$\frac{\tau}{\tau_m} = \left(1 - e^{\frac{-s}{s_r}}\right)^{\beta} \tag{2.12}$$

Where τ_m peak bond stress, s_r and β parameters based on curve-fitting of the actual data.

Tighiouart et al. (1998) suggested values for C.M.R. bond model parameters s_r and β as 0.25 and 0.5 respectively based on experimental investigation conducted on GFRP rebars with varying bar diameter and embedment length.

Cosenza (1997) experimentally evaluated the bond stress-slip relation of GFRP bars and observed that the response lacks the second constant branch of B.E.P. model for steel therefore suggested not to consider it, Figure 2.13. The constant second branch is caused by concrete sheared off by lugs of steel bars (Eligehausen et al., 1983), such trend is not observed in FRP bars due to the much lower transverse strength. While same law of for ascending branch of original B.E.P model (equation 2.12) was used, a new expression was proposed for the descending branch (equation 2.13). The resulted model is known as Double Branch Model (D.B.M.) and it is expressed by Equations (2.13-2.15).

$$\frac{\tau}{\tau_1} = \left(\frac{s}{s_1}\right)^{\alpha} \qquad s < s_1 \qquad (2.13)$$

$$\frac{\tau}{\tau_1} = 1 - p\left(\frac{s}{s_m} - 1\right) \qquad s_1 < s < s_3 \qquad (2.14)$$

$$\tau = \tau_3 \qquad s > s_3 \qquad (2.15)$$

Where τ and s are bond stress and slip respectively, τ_1 is the maximum bond stress, s_1 is slip corresponds with maximum bond stress, α and p are parameters to be determined based of curve fitting experimental results, s_3 slip at the end of descending branch.

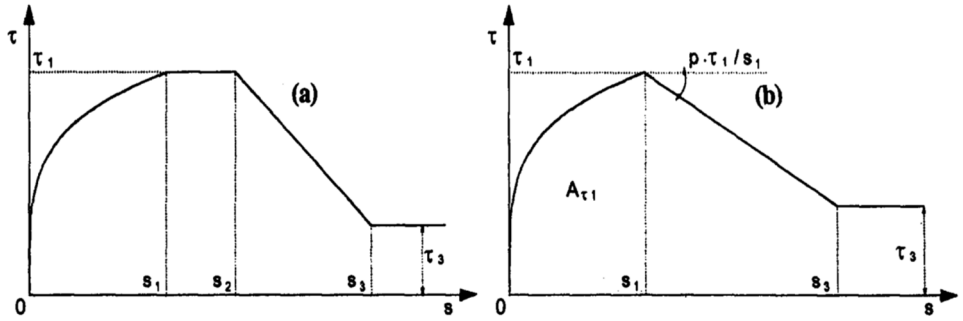

Figure 2.13 (a) B.E.P. Model; (b) D.B.M. Model (Cosenza et al., 1996).

A comparison between the bond models of Malvar, D.BM., and C.M.R. and experimental data from the literature showed that the bond performance of FRP bars is influenced by bar surface configuration. Indented and grain covered bars developed higher bond strength and some values of bond strength were higher than steel (FIP, 2007). Factors that affect FRP bond (transverse reinforcement, bar diameter, embedment length, bar position, and concrete cover) are discussed in details in section 2.5.3, while elevated temperatures effect on FRP bond strength is discussed in 2.11.

The D.B.M. model was used within the numerical analysis of the current research (Chapter 6) because it is more commonly used in the literature and the model parameters are reported for FRP bars with different surface configurations.

2.10 Behavior of FRP Reinforcement at Elevated Temperatures

The main constituents of concrete structural elements incorporating FRP are concrete, FRP, and sometimes steel as well. The response of each of these materials are profoundly different at elevated temperatures. Under heating, concrete undergoes a change of its properties which is mainly attributed to water evaporation, altering of concrete chemical composition, and physical integrity. The influence of elevated temperatures on concrete mechanical and thermal properties has been reported extensively in the literature (ACI, 1989, Arioz, 2007, Khoury, 2000). Figure (2.14) illustrates the degradation of some concrete mechanical properties under elevated temperature based on parameters from Eurocode 2 (Firmo, 2015, British Standard Institution, 1987). Under heating failure may occur as concrete spalling resulted of water vapour pressure inside concrete pores and bond loss between the cement paste and aggregate (Firmo, 2015).

The mechanical properties of steel also reduce as temperatures increases, Figure (2.14). The yield strength of steel reinforcement decreased by 50% at about 600 °C (Firmo, 2015). An extensive review on behavior of reinforcing steel at elevated temperatures can be found in (Lie, 1992; Khoury, 2000).

FRP reinforcement is more sensitive to temperature than concrete and steel (Bisby et al., 2005). A reduction in FRP mechanical properties occurs around FRP glass transition temperature (Firmo, 2015; Bisby et al., 2005). The constituent components of FRP (matrix and fibers) respond differently to elevated temperatures (Bisby et al., 2005; Blontrock et al., 1999). The response of each of FRP constituents (matrix and fibres) are discussed in the following section.

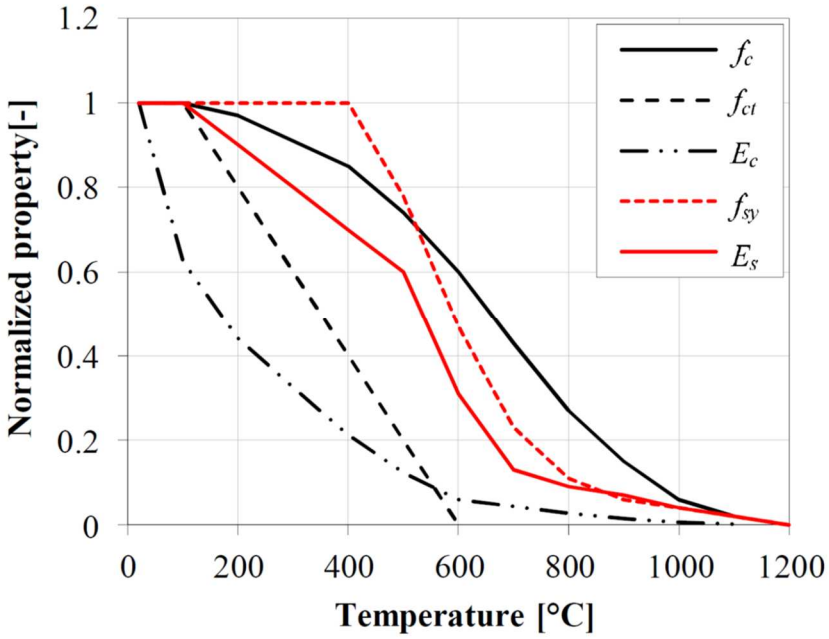

Figure 2.14 Typical mechanical properties of concrete (compressive strength, f_c, tensile strength, f_{ct}, and elastic modulus, E_c) and steel (yielding stress, f_{sy}, and elastic modulus, E_s) as a function of temperature, according to Eurocode 2 Part 1-2 (Firmo, 2015).

2.10.1 Matrix

There is a great variety of polymer matrices produced by industry. Therefore, a generalisation about their response at elevated temperatures can be difficult to find. The focus here is on the commonly used polymer matrices in manufacturing of internal FRP reinforcement. The polymer matrix is much more sensitive to increased temperature than fibres. A mild increase in temperature can cause polymer matrix to undergo a gradual softening up to a point where matrix behaviour changes from glassy to rubbery, the temperature at which this transition happens is called glass transition temperature T_g (GangaRao et al., 2007; ACI, 2015; CAN/CSA, 2012). Around glass transition temperature (T_g), the molecular structures of polymer matrix undergo changes which lead the elastic modulus of matrix to reduce significantly (CAN/CSA, 2012; ACI, 2015). Figure (2.15) shows an example of glass transition temperature response of FRP sample produced by dynamic mechanical analysis test (DMA) (McIntyre et al., 2014). With DMA test the glass transition temperature can be determined in three ways, Tg_{Onset} which is defined by the intersect of tangent lines of initial and maximum negative slopes of storage modulus curve (Figure 2.15) while *Tg*

Midpoint is defined as the temperature at maximum negative slope. *Tg Tan δ* is defined as the temperature corresponds to the peak of Tan Delta curve. In essence, all three definitions are arbitrary but they are used as an indication of polymer matrix softening temperature (McIntyre et al., 2014). Glass transition temperature can vary extensively but usually in range of 65°– 150°C depending on composition and production process of resins, fibre type, fibre fraction volume, and modulus of elasticity (Saafi, 2002; Bisby et al., 2002; Al-Zahrani, 1995). The value of T_g may also vary by the testing method used to measure it (McIntyre et al., 2014). As polymer matrix is softened under heating, it loses the ability to transfer load between fibres, which results in reducing tensile strength of FRP reinforcement which can cause a premature failure (Nadjai et al., 2005; McIntyre et al., 2015; Bisby et al., 2005; Kodur et al., 2005; Katz et al., 1999; Nigro et al., 2011b; ACI, 2015). Softening of the polymer matrix also causes a significant degradation of bond between FRP bars and concrete which is discussed in section 2.11.

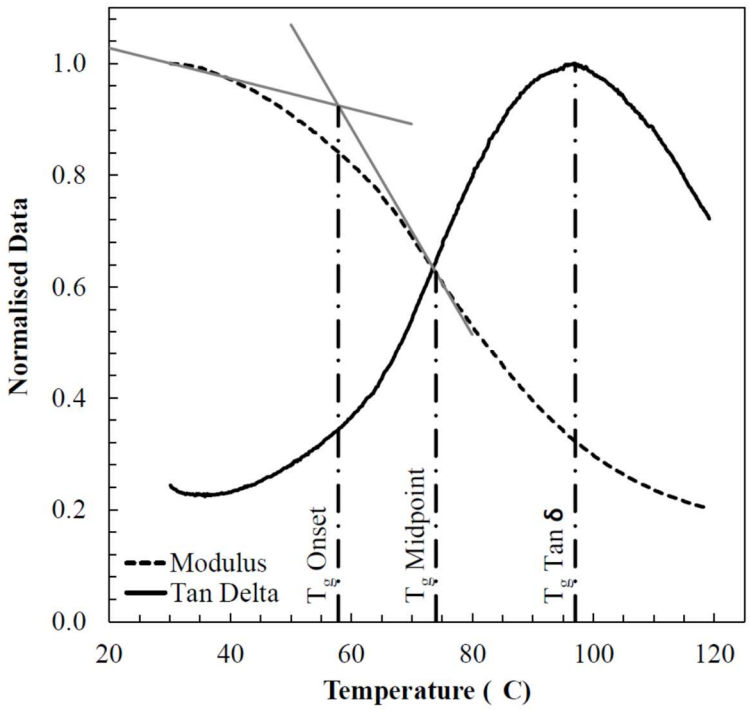

Figure 2.15 Glass transition temperature response of FRP sample produced by dynamic mechanical analysis test (McIntyre et al., 2014)

Testing Methods for Evaluation of FRP T_g

The most common testing methods used to characterise T_g of FRP are DMA (Dynamic Mechanical Analysis), TGA (Thermogravimetric Analysis), Light and SE (Scanning Electron) Microscopy, and DSC (Differential Scanning Calorimetry) (FIP, 2007). In dynamic mechanical analysis (DMA) test method, coupon of tested material is subjected to a mechanical oscillation at a user specified frequency and over a specified range of temperatures. Data of load-deformation response are measured, and they are function of temperature, time and frequency. For FRP a main application is determining the glass transition temperature (T_g) of composite, which is a useful indication of FRP stiffness and bond strength deterioration with temperature. Thermogravimetric analysis (TGA) and differential scanning calorimetry (DSC) tests methods are used to measure the mass and the energy changes of the materials as a function of temperature and time. As in DMA specimens are also tested over a range of temperatures increases at a constant rate (Gomes et al., 2012).

In the current research DMA test method was used to determine the glass transition temperature of the produce FRP. With DMA test changes in material stiffness and damping can be measured and these are expressed as modulus and tan delta. Two types of modulus can be measured through the test (Menard, 2008):

- Storage modulus *E'* is an indicator of material elastic response and is used to measure stored energy.
- Loss modulus *E''* is an indicator of material viscose response and it measures the dissipated energy in form of heat

Tan delta is the ratio of loss of storage and is one of the methods to indicated *Tg* (Menard, 2008) which is used in the current study.

2.10.2 Fibres

The carbon and glass fibres can tolerate higher temperatures than polymer matrix. Temperature threshold for glass and carbon fibres are 880 °C and 1600 °C, respectively. At elevated temperatures, the presence of oxygen can cause oxidation of carbon fibres. There is no clear limit of safe temperature but a value of 500 °C is

recommended to use (ACI, 2006). Sauder et al. (2004) conducted a series of tensile tests on carbon fibre of different types and found mild reduction in tensile strength and modulus of elasticity up to temperature of 1600 °C. Unlike matrix, fibres are non-combustible which is beneficial as it reduces the fuel available in fire event (Bisby et al., 2005). Figure 2.16 shows reduction of tensile strength of carbon, glass, and aramid fibres at elevated temperatures based on experimental data gathered from the literature.

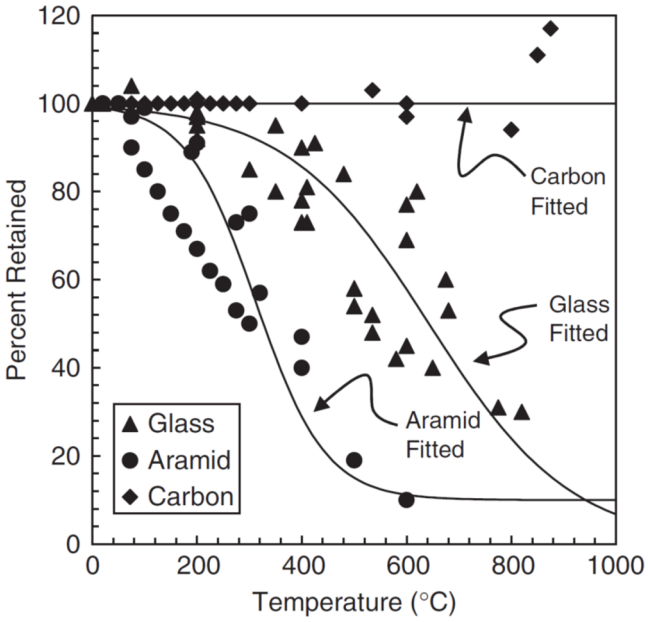

Figure 2.16 Reduction of fibres tensile strength at elevated temperatures. (Bisby et al., 2005).

2.10.3 FRP reinforcement

As discussed in the previous sections (2.10.1 and 2.10.2) the constituent compounds of FRP undergoes deterioration at elevated temperatures. Consequently, the mechanical properties of the composite as all reduce when exposed to heating. Nigro et al. (2008) gathered data from the literature of experimental tests conducted to measure the influence of temperature on FRP reinforcement integrity. The data then was used to generate equations describes reduction in FRP tensile strength and Young's modulus with temperature (equations 2.14 and 2.15). The study considered different types of FRP (carbon, glass, and aramid). The obtained results showed good agreement with similar work done by Bisby et al. (2005), Figure 2.17. Figure 2.17

shows high scatter of data which is expected and attributed to the wide range of matrices and fibres mechanical properties, fibres fracture volumes, and manufacturing techniques that are used in the industry. Therefore, graphs in Figure 2.17 only suggest a general trend for FRP tensile strength and Young's modules deterioration behaviour with temperature. Consequently, results obtained from Equations 2.14-2.15 will contain undefined errors. More accurate results can be obtained through conducting tensile tests at different temperatures.

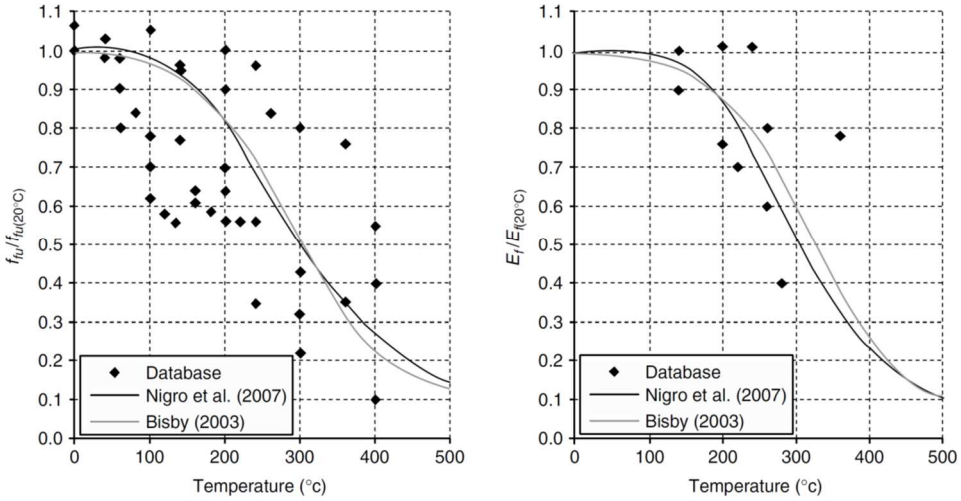

Figure 2.17 Deterioration behavioural of FRP tensile strength and Young's modules with temperature (Nigro et al., 2012b).

$$\rho_f(T) = \frac{f_{fu}(T)}{f_{fu}} = \frac{0.05}{0.05 + 8.0\times10^{-11}\times T^{3.55}} \quad (2.16)$$

$$\rho_E(T) = \frac{E_f(T)}{E_f} = \frac{0.28}{0.28 + 6.0\times10^{-12}\times T^{4.3}} \quad (2.17)$$

Where ρ_f *(T)* and ρ_E*(T)* are reduction factors for tensile strength and the Young modulus of the bars, respectively, based on the temperature, *T,* in the bar.

2.11 Bond of FRP Bars at Elevated Temperatures

It has been discussed in previous sections that bond between reinforcement and concrete is important for force transfer which happens mainly through bar surface. It was also established that the polymer matrix is an essential component in the formation

for bar surface and its mechanical performance is dependent on temperature. This makes the interaction (bond) between FRP reinforcement and concrete is highly dependent on temperature.

The topic of bond of FRP reinforcement has been investigated by many researchers and sensitivity of FRP reinforcement to elevated temperature has been reported. Bisby et al. (2005) gathered experimental data about performance of internal FRP reinforcement at elevated temperatures. Collected data showed that in the range of 100 – 220 °C, the bond strength can degrade to about just 10% of its value at ambient temperature (Figure 2.18). Katz et al. (1999) conducted pull-out tests on various types of FRP bars at different temperatures up to 250°C. Results showed that elevated temperature can cause a reduction of bond strength up to 90%. It was also observed that bond modulus (slope of ascending part of load-slip curve) tends to decrease as temperatures increases. Katz et al. (1998) also noticed that bond strength of pull-out test specimens reduced by 50% at temperature of 125°C, at which the temperature coincides with glass transition temperature of the matrix. Figure 2.19 shows the effect of temperature on load-slip response by pull-out test for FRP bars with different surface configuration.

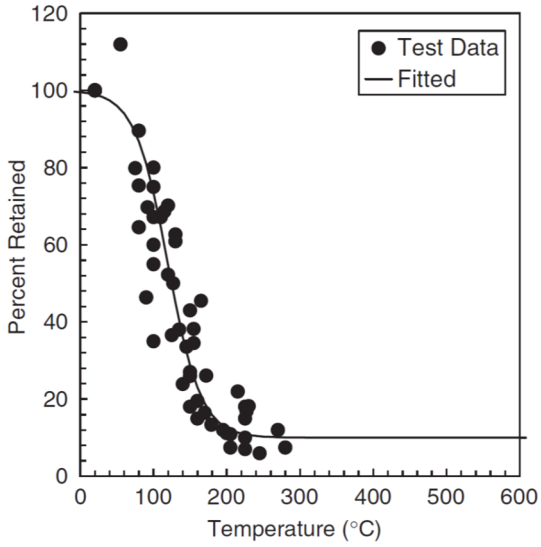

Figure 2.18 Variation in bond strength with temperature for various types of FRP bars (Bisby et al., 2005).

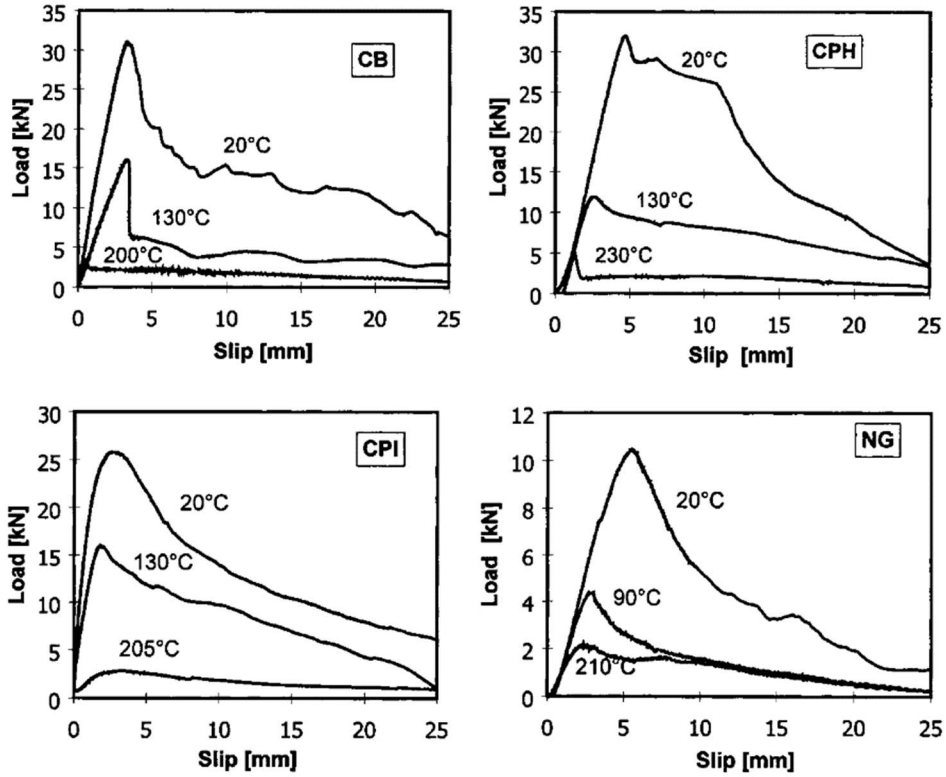

Figure 2.19 Effect of temperature of load-slip response of FRP bars with different surface configurations: (CB) large deformation, (CPH) helix-sand coating, (CPI) helix-resin roughening, (NG) helix-sand coating with deformations (Katz et al., 1999).

2.11.1 Effect of Transverse Thermal Expansion of FRP

Damage can occur in structural element reinforced with FRP reinforcement due to mismatch between transverse coefficient of thermal expansion (CTE) of FRP and concrete. The transverse CTE of FRP composite is controlled by matrix (resin) and it is three to six times higher than concrete. When temperature changes, this thermal incompatibility changes the state of stress that FRP bar works under from axial state to multi-axial state of stress (Masmoudi et al., 2011; Al-Zahrani, 1995). The resultant radial stresses have a negative effect as well on concrete surrounding bars. A relative small increase in temperature can induce/widen existing cracks in concrete adjacent to rebar which in turn reduce confinement of concrete surrounding rebar and facilitate de-bonding (Gentry and Husain, 1999; GangaRao et al., 2007). Longitudinal strains under effect of loading help in alleviating thermal swelling. Analytically, Gentry and Husain (1999) estimated that if a glass/vinyl ester bar is operated at 40% of its ultimate

strength (assumed to be 600 MPa), the swelling resulted by an increase of temperature by 40°C will be diminished by the transverse shrinkage caused by the axial tensile strain. However, in regions having low bending moment and high shear stress (typical anchorage zones near supports) where bond stress is maximum, thermal swelling is expected to overwhelm any shrinkage due to axial strain. Experimentally, it was shown that the bar with helical wrapping as surface configuration had significantly lower transverse expanding (up to 50% less) compared with other bars with different surfaces (Gentry and Husain, 1999). Higher temperatures surpassing the matrix glass transition temperature (see section 2.10.1) can introduce another sort of damage, degrading surface bond with concrete, due to resin softening (Bisby et al., 2005; McIntyre et al., 2015; Blontrock et al., 2011). The effect of low temperature (freezing temperature and below) on FRP mechanical properties is less severe than that of elevated temperatures. Low temperature causes reduction of FRP elongation fracture toughness and impact strength (GangaRao et al., 2007).

2.11.2 Modelling the Effect of Temperature on FRP Bond Strength

To account for the effect of temperature on bond strength, a semi-empirical model was developed by Katz and Berman (2000), equation 2.18. The model uses three parameters: glass transition temperature and degree of crosslinking of polymer matrix at reinforcement surface, in addition to residual bond stress. The model was designed to capture the typical trends in FRP bond strength with temperature (such shown in Figure 2.18) where severe reduction in bond strength occurs beyond T_g .The glass transition temperature used in the model was measured using differential scanning calorimeter (DSC), see section 2.10.1 for more details. The residual bond strength is defined as the residual bond strength at a high temperature (<350 °C) where no further reduction occurs (Katz and Berman, 2000).

$$\tau^* = 0.5(1-\tau_r^*)tanh\left\{-\frac{0.02}{C_r}\left[T - k_1\left(T_g + \frac{k_1}{0.02}C_r\right)\right]\right\} + 0.5(1+\tau_r^*) \quad (2.18)$$

$$k_1 = \begin{cases} 1, & T_g \leq 80, \\ 1 - 0.025(T_g - 80), & 80 < T_g < 120, \\ 0, & T_g \geq 120 \end{cases}$$

Where τ^* normalized residual bond strength, C_r degree of cross linking for polymeric matrix (relates to the number of polymer chains that interconnect together), T_g is the glass transition temperature in °C.

2.11.3 Analytical Calculations of FRP Development Length in Fire

To determine the development length of FRP internal reinforcement at elevated temperature Nigro et al. (2012a) developed an iterative finite difference procedure. The procedure is based on discretised bar into element small enough to assume slip (s) and shear stress (τ) can be presented at mid of element. Then with an iterative procedure slip is changed at load point and calculated at the consecutive nodes through bond law. The development length is measured as the length at which the assumed slip value at loaded end causes slip, axial stress, and bond stress diminishes to zero. When combined with Katz and Berman (2000) model for bond stress reduction with temperature, the Nigro et al. (2012a) model can be used to calculate the development length at different temperatures.

2.12 Fire Behaviour of Flexural Elements Incorporating FRP Reinforcement

The performance of internal FRP reinforcement was investigated through testing of concrete beams and slabs at elevated temperatures. Weber (2008) tested concrete beams reinforced with spliced GFRP bars in heated region and thick concrete cover of 60 mm was used. The splice length corresponded to 66 times bar diameter and beams were able to withstand fire exposure for 90 minutes before they failed by pull-out. McIntyre et al. (2015) tested concrete beams reinforced with spliced CFRP and GFRP

bars along the heated region. Bond failure occurred as pull-out at early stage of heating (around 7–11 minutes).

Anchoring FRP reinforcement in areas not directly exposed to fire (cold anchorage) is a technique that was found to improve the fire performance of structural elements incorporating FRP reinforcement. Rafi et al. (2007) conducted a series of four-point bending tests at elevated temperature upon beams with CFRP tension reinforcement. A sustained load corresponded with 35% of ambient strength was applied on beams during heating. Length of 250 mm at each end of beams were kept out of furnace (cold anchorage). FRP reinforcement at unexposed zones was found to maintain interaction with concrete and failure occurred due to concrete crushing. Kodur et al. (2005) tested concrete slabs reinforced with CFRP bars at elevated temperatures and only under self-weight and found that heat transfer was similar to specimens reinforced with steel bars. At elevated temperature, the polymer matrix was burnt off and only fibres were left behind. Concrete cover was found to have a significant influence as slabs with thicker concrete cover were able to achieve longer fire resistance time. Slabs thickness and aggregates types, on the other hand, were found to have a minor effect on fire resistance.

The influence of reinforcement geometry was assessed by Abbasi and Hogg (2006). Fire resistance time exceeding 90 minutes was achieved with beams reinforced with GFRP bars hooked at ends and bars ends anchored in areas not directly exposed to fire. In (Nigro et al., 2011a; Nigro et al., 2011b) concrete slabs reinforced with GFRP bars anchored out of heated zone with different configuration of reinforcement shape and concrete cover were tested in flexural under heating. Results showed failure occurred as pull-out when straight bars used with cold anchorage length of 250 mm. Using hooks at bars ends or increasing cold anchor length to 500 mm led that failure mode changed to bar rupture and enhanced fire resistance time and load bearing capacity.

Concrete cover was also found to profoundly influence the heat transfer, as thicker concrete cover delayed heat progress into the beam. Results from heated tests of beam

with cold anchorage technique showed that after resin softening, fibres can continue resisting load as long as anchorage at bars end was maintained.

Chapter 3 Tension and Push-off Tests

3.1 Introduction

Two experimental tests are discussed within this chapter to characterise the proposed design of CFRP loops. Tension tests were used to examine the tensile capacity of CFRP loops at ambient and elevated temperature. It was also used to evaluate different designs of CFRP loop. The other test is push-off test which investigates the bond performance of CFRP loop against straight and hooked reinforcement at ambient and elevated temperatures. The two sets of tests are intended as an elementary assessment of the efficiency of CFRP loop concept. Further experimental work in form of beam test is discussed within Chapters 4, 5, and 6.

The design concept of CFRP loop and manufacture procedure are explained first in this chapter. This is followed by description of tension test set-up, specimens, results and discussion. Details of push-off test come after. The chapter is then concluded with a summary of experimental results and discussion.

Results of the experimental results showed that CFRP loops are able to sustain higher loads under heating in comparison to traditional methods of reinforcement.

3.2 Design of FRP Loop Reinforced Concrete

The previous chapter (section 2.11) highlighted the severe degradation of FRP reinforcement bond strength at elevated temperatures which is attributed to the softening of polymeric matrix. To overcome the sensitivity of FRP reinforcement to elevated temperatures, this study proposes utilising closed FRP loops, which are made

from filament wound of long continuous fibres as an internal reinforcement for concrete beams. The proposed design takes advantage of the fact that fibres, especially carbon, can tolerate temperatures much higher than the glass transition temperature of resins. Making reinforcement into a closed loop shape adds another mechanism of interaction between FRP reinforcement and concrete. When the chemical, interlock, and friction bond mechanisms of force transfer are lost or severely deteriorated due to resin softening, tensile forces in the reinforcement (FRP fibres) can still be transferred to concrete at loop ends (Figure 3.1). Beam tests that compare the performance of CFRP loop reinforcements against straight bars are discussed in Chapters 4, 5, and 6.

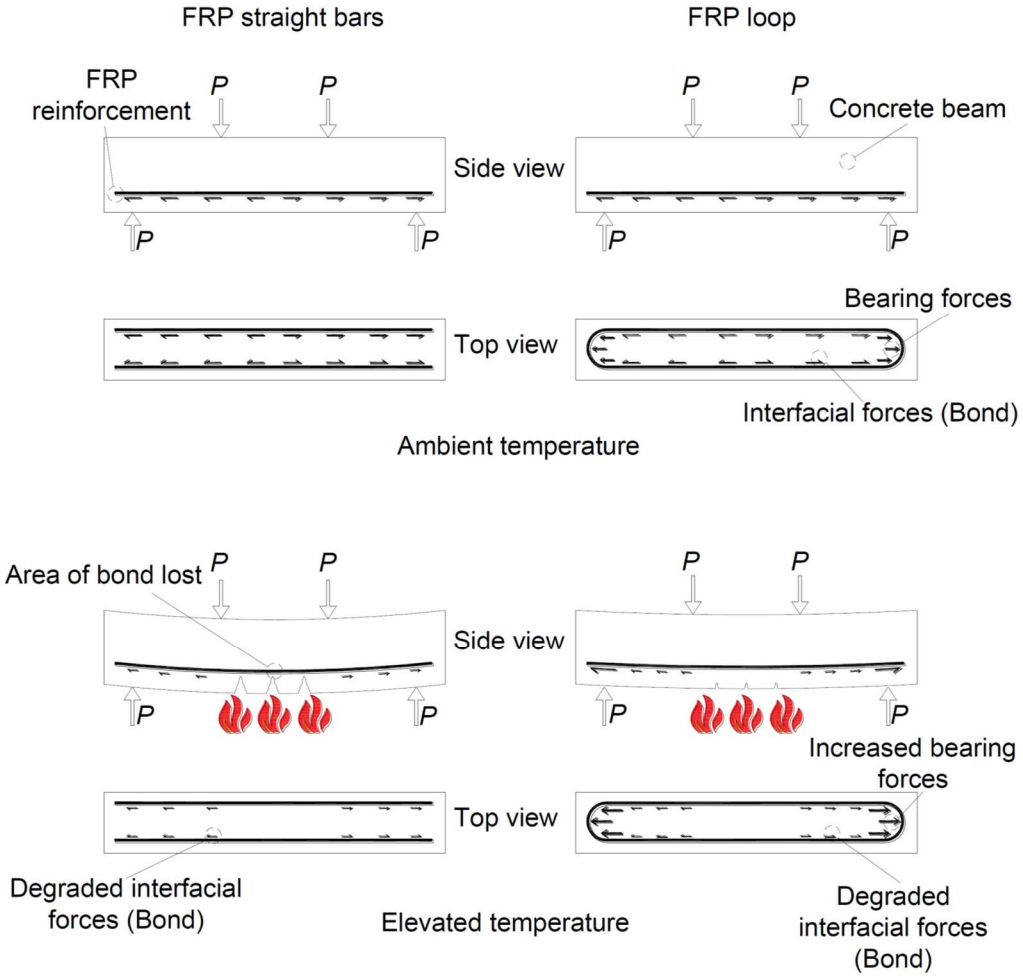

Figure 3.1 Performance of FRP reinforcement at elevated temperature within a beam, straight bars vs. loops. (Beam tests are discussed within chapters 4, 5, and 6).

3.3 Manufacturing process of the FRP loops

For the proposed design to be able to maintain interaction with concrete at elevated temperatures, it has to be made as a closed loop. Traditionally FRP bars are made in a pultrusion process where fibres are passed through a sink of resin and pulled under pressure into straight bars. Using a single continuous fibre tow to form the loop is necessary because (as discussed in section 2.6), straight FRP bars cannot be bent to shape due to the high strains that result, and because it is not possible to join FRP bar to form a closed loop without relying upon polymer matrix at the connection, which will fail at elevated temperatures.

As part of the current work, closed loops of FRP were produced by winding fibres around a mould that works like a mandrel (Figure 3.2). The closed FRP loops were made by winding a continuous fibre filament within a groove in the mould. The groove shape controls the cross section shape of the produced FRP loops. In order for the loops to be taken out of the mould after hardening, the mould was built of stacked PVC sheets of varying sizes to create grooves between them with the desired shape and size. In this research, it was decided to make FRP loops as a cross-section of a square section of 5 mm size and mould grooves were made accordingly. Before the winding process, the grooves in the mould were coated with a coating of demoulding agent, PVA, to prevent resin from adhering to the mould. The mould was provided with a manual rotating mechanism to facilitate the winding process (Figure 3.3). Moulds were made with different length to produce different sizes of loops. The grooves of moulds were also used to produce straight FRP bars used in beam tests as will be discussed in Chapter 4.

The resin was applied between the layer of carbon fibres tows by a brush (Figure 3.3). Once the fibre winding process around the mould was finished, the loop samples were left in the mould for 24 hours for an ambient temperature cure. Afterwards, the mould was disassembled and the loops were taken out.

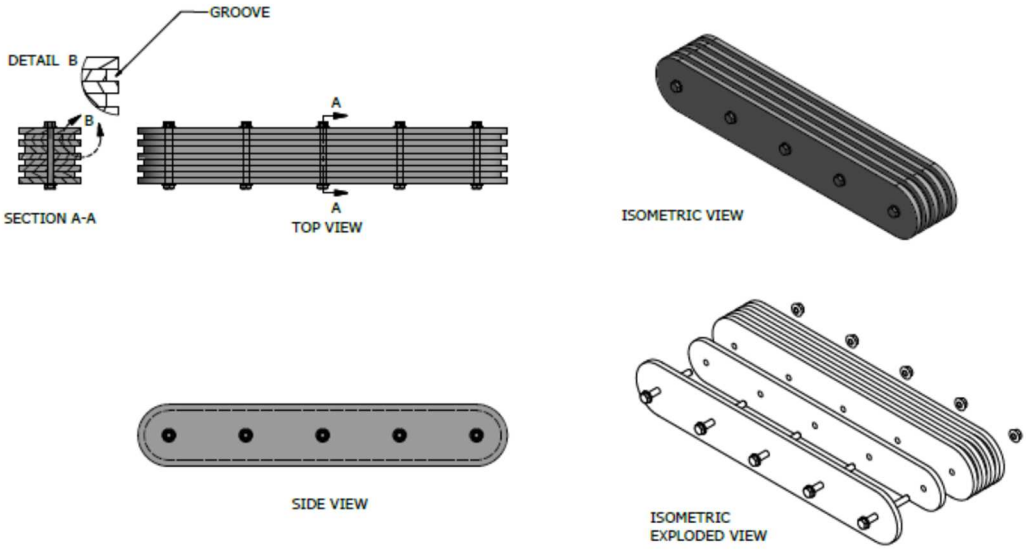

Figure 3.2 PVC mould used to produce closed FRP loops.

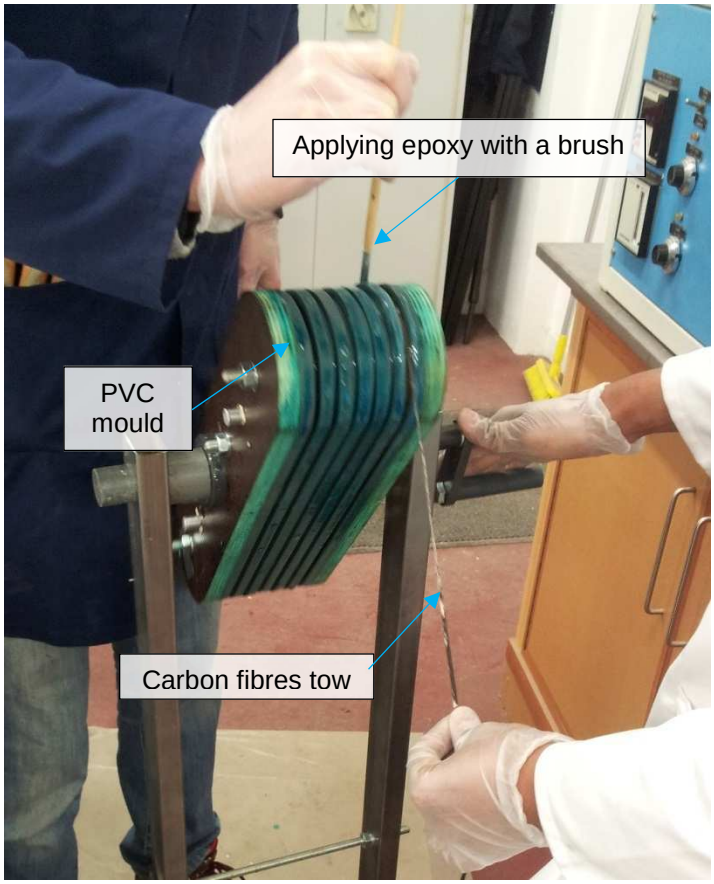

Figure 3.3 Filament winding of CFRP loops around a mould.

To improve the surface bond properties and make it better resemble what is used in reality, the surface of the CFRP loops were sand coated. This has been done by applying resin to the reinforcement surface, then applying a fine glass sand by hand, as shown in Figure 3.4.

Figure 3.4 Sand coating of CFRP loop through bonding sand to reinforcement surface by epoxy.

The final stage of the manufacturing process was to post-cure the samples to enhance the polymer matrix mechanical and thermal properties. For the resin used, the curing temperature recommended by the manufacturer was 60 °C. The FRP reinforcements were therefore post-cured in a drying oven for 12 hours at 60 °C.

3.3.1 Properties of Constitute Materials

In terms of fibre types, both carbon and glass fibres can be used to produce FRP loops. In this research, however, only carbon fibres tows were used. That was mainly because they have higher tolerance to elevated tempratures and are available in the local market as finer filament than glass. This allows more filaments to be laid in mould grooves which increases the mechanical interlock between fibres**.** Grafil 34-700 high strength continuous carbon fibers (Figure 3.5) were utilised throughtout this research to make the FRP reinforcement . The mechnical and thermal properties of carbon fibre tows as provided by the manufacterer in the product datasheet are listed in Tables 3.1-3.3.

Table 3.1 Mechanical properties of carbon fibre tows (Mitsubishi Rayon Carbon Fiber and Composites, 2014).

Fibre type	Number of Filaments	Tensile Strength (MPa)	Young's modulus (GPa)	Cross-sectional area (mm^2)	Elongation (%)	Filament diameter µm
Grafil 34-700WD	12000	4830	234	0.444	2.0	7

Table 3.2 Mechanical properties normalized to 60% of fibre volume of carbon tows (Mitsubishi Rayon Carbon Fiber and Composites, 2014). (Values for 44% fraction volume were calculated by the researcher through interpolation)

		Fibre volume	60%	44%
Tensile Properties	0◦	Strength	2572 MPa	1860 MPa
		Modulus	137 GPa	100 GPa
	90◦	Strength	81 MPa	59 MPa
		Modulus	9.2 GPa	6.7 GPa
Compressive Properties	0°	Strength	1365 MPa	996 MPa
		Modulus	127 GPa	93 GPa
	90°	Strength	196 MPa	143 MPa
		Modulus	10.2 GPa	7.4 GPa
Flexural Properties	0°	Strength	253 MPa	185 MPa
		Modulus	132 GPa	96 GPa
	90°	Strength	102 MPa	74 MPa
		Modulus	8.8 GPa	6.4 GPa

Table 3.3 Thermal properties of carbon fibre tows (Mitsubishi Rayon Carbon Fiber and Composites, 2014).

Coefficient Thermal Expansion	0.5 (10-6 m/m/K)
Specific Heat	0.74 (J/gK)
Thermal Conductivity	7 (W/mK)

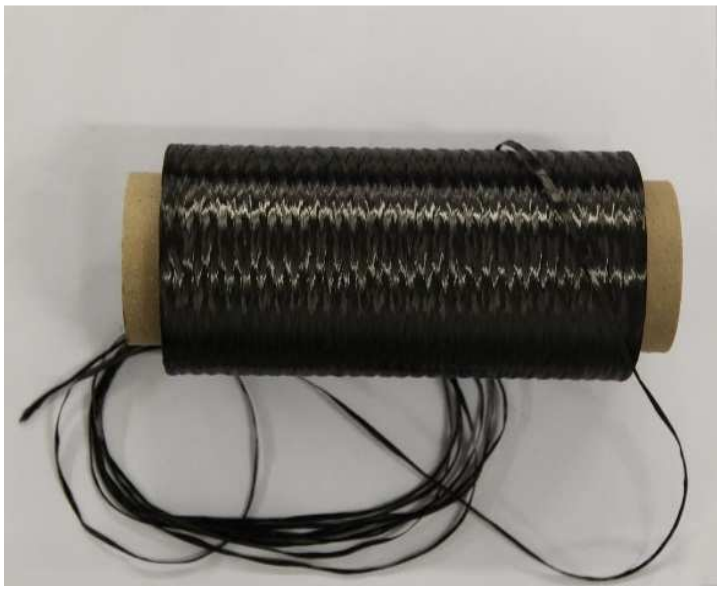

Figure 3.5 Carbon fibre tows used in making CFRP loops.

Tyfo-S and H-EL2 epoxy resins were used as resins. These two-part epoxies are compatible with carbon fibres and designed for wet-layup and structural strengthening applications. H-EL2 epoxy is suitable for high temperature applications. The mechanical properties of both epoxy resins as provided in the products datasheets are listed in Table 3.4.

Table 3.4 Mechanical properties of Tyfo-S and H-EL2 epoxy resins (FYFE Tyfo-S, Easy Composites).

Property	Tyfo-S	H-EL2
Tensile Strength	72.4 MPa	58 – 68 MPa
Compressive Strength	68.2 MPa	107 – 117 MPa
Flexural Strength	123.4 MPa	58 – 68 MPa

3.3.2 Dynamic Mechanical Analysis Test

Dynamic mechanical analysis (DMA), see section 2.10.1, was used to determine the glass transition temperature of the produced CFRP reinforcement. Two samples of size 15×5×2.5 mm were cut out from region of reinforcement where H-EL2 high temperature resin was used (Figure 3.17). Other two samples of same size were cut off of CFRP loops patch prepared for push-off test (section 3.5) where Tyfo-S rein was used. The reinforcement used in push-off test was manufactured in same process of

tensile test control specimen except the number of carbon fibre tows rounds were increased from 24 to 25. This difference was considered not to have a significant effect of the measured T_g therefore same value of T_g was assumed for tension test specimens. The test configuration of DMA was three-point bending which was operated at frequency of 1 Hz and strain level 0.05. The samples were tested for temperature range was from about 20 to 150 °C for samples with Tyfo-S and because higher T_g was expected for H-EL2 resin higher range (-25 to 200 °C) was used. The heating rate was constant at 2 °C/min.

The measured values glass transition temperature of the tested samples of CFRP loops with two different types of epoxy matrices using tan δ are listed in Table 3.5 along values of Tg_{Onset} and $Tg_{Midpoint}$ (see section 2.10.1). Figure 3.6 shows the storage modulus change with temperature obtained from DMA test of a sample with Tyfo-S matrix. Figures showing the response of the other tested specimens are placed within Appendix A.

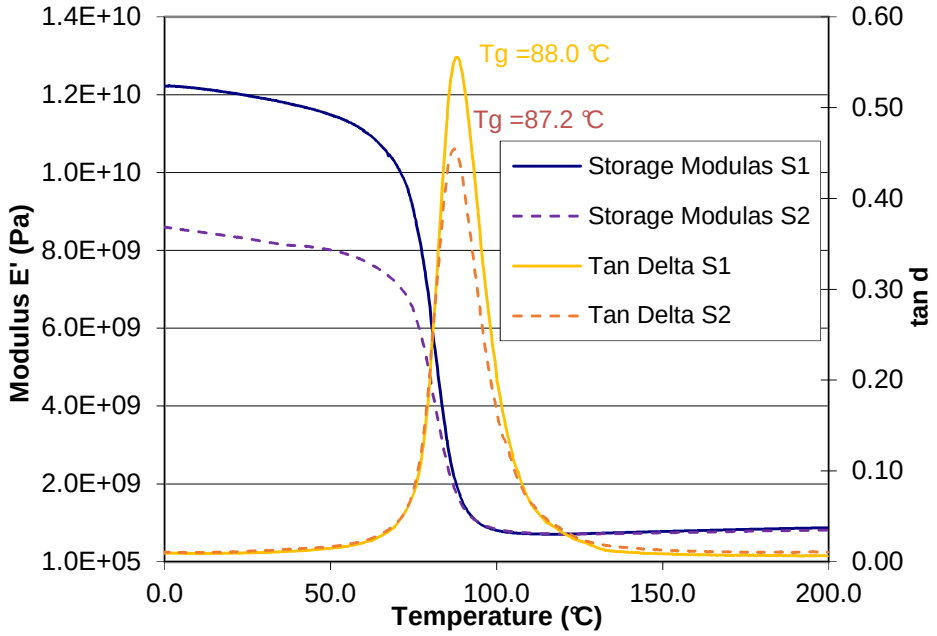

Figure 3.6 DMA results for samples S1 and S2 with Tyfo-S resin type.

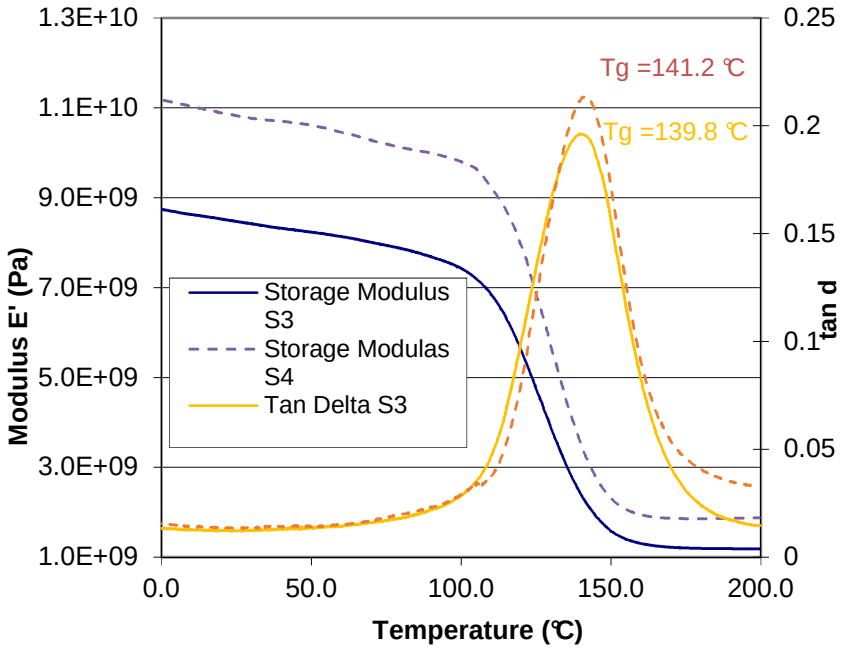

Figure 3.7 DMA results for sample for samples S3 and S4 with H-EL2 high temperature resin.

Table 3.5 Results of Dynamic Mechanical Analysis.

Resin Type	Sample	T_g Onset [°C]	T_g Midpoint [°C]	T_g Tan δ [°C]	Average T_g Tan δ [°C]
Tyfo-S	S1	69	72	85.0	84.9
	S2	73	79	84.7	
H-EL2	S3	110	119	139.8	140.5
	S4	112	122	141.2	

3.4 Tension Tests

3.4.1 Overview

Tension test are the first set of tests that characterised the bare CFRP loops, without embedding them in concrete. The aims of these tests were to:

- determine the tensile strength of the reinforcement, which would usually be governed by the strength of the curved portion of the loop;
- characterise the strength of the reinforcement at elevated temperature; and

- investigate different configurations of the FRP loops to understand whether the tensile strength of the curved part could be improved.

A universal testing machine was used to test the loop in tension and a purposely built heating system was used to locally heat one end of the looped specimens to 100 °C.

3.4.2 Tension Test Configuration

The tension test was designed to provide a quick assessment of CFRP loop tensile capacity at ambient and elevated temperatures. The test setup is a modified version of test method B.12 specified by ACI (2012) to determine effect or bend radius on FRP bar tensile strength (see section 2.7.3). The test method was modified to allow the loop to be tested as a whole rather than having the curved part only on one side as in the ACI (2012) test setup. The test was conducted using an Avery 7104 universal test machine in which the loop ends were anchored between a fixed part and a moving crosshead of the machine (Figure 3.8 and 3.9). The curved part of the loops were anchored against the testing machine frame using reinforced concrete inserts which have the same curvature at the loose ends. Tensile force was applied to the loops by moving the testing machine crosshead upward. The recommended loading rate by ACI (2012) for tensile test is 1 – 2mm/min. However because the used testing machine does not have the capability to produce displacement control loading, the tensile test was done in load control at rate of 13 kN/min until failure. The value 13 kN/min was chosen to produce loading rate of ≈ 2 mm/min taking in consideration the length of straight portion of the loop 745 mm (Figure 3.15), cross-section size (5 mm for each leg of loop) and Young's Modulus 103.21 GPa (Appendix C).

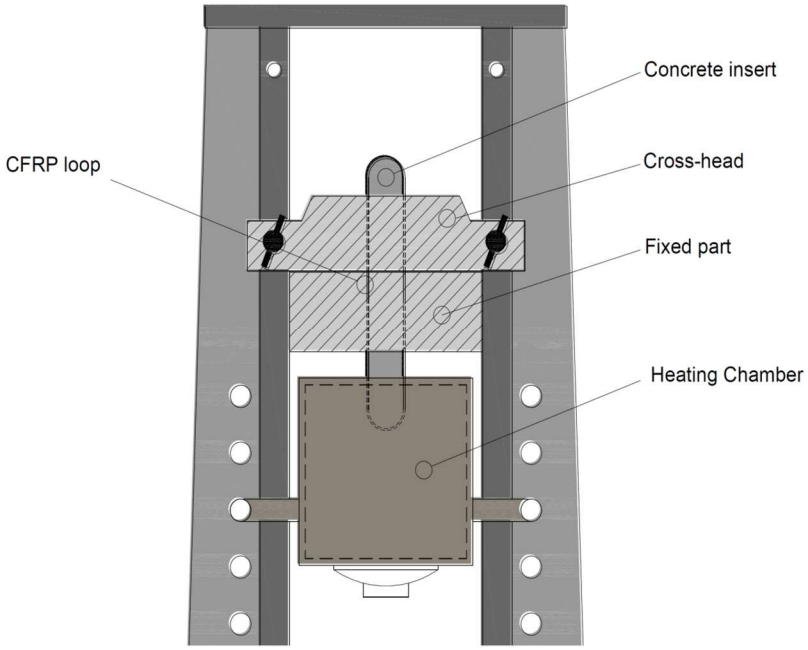

Figure 3.8 Schematic of CFRP loop tensile test setup.

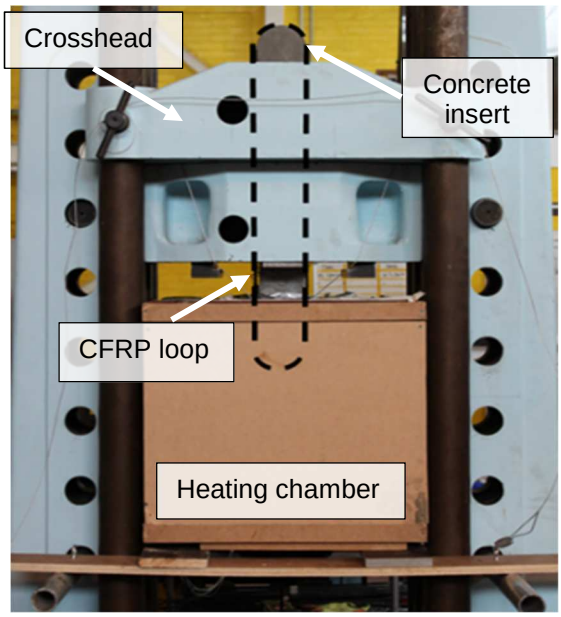

Figure 3.9 Testing apparatus for CFRP loop tension test.

To test specimens at elevated temperatures a purpose-built heating chamber was used to heat one end of the loop by convection to the desired testing temperature. The heating chamber was built using an 18 mm thick plywood frame, insulated on the inside with 50 mm thick polyisocyanurate (PIR) boards. A halogen heating unit with

heating capability up to 250 °C was installed at the bottom of chamber. To ensure uniform heating inside the chamber, the radiation from the halogen lamp was blocked with plywood board and two electrical fans were installed on the block board, and the air was circulated using the fan of the halogen heating system, so that the specimen was heated by convection (Figures 3.10-3.11). An opening was made at the top of the chamber to allow the loop ends and a concrete insert to be placed inside the chamber. The chamber has two doors open to glass sheets to observe the specimens inside (Figures 3.10-3.11).

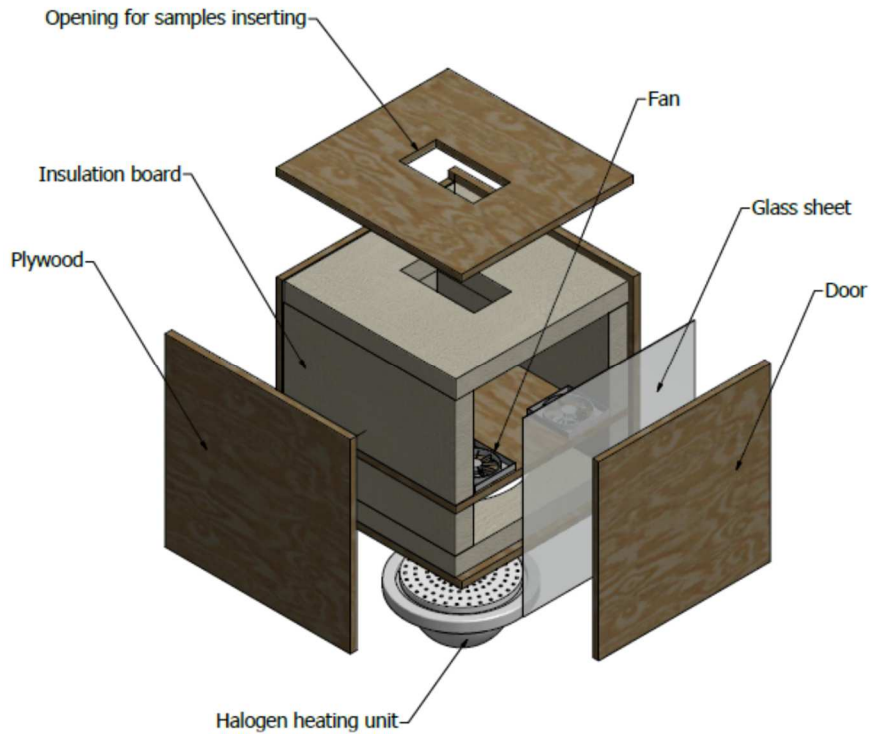

Figure 3.10 Purposely-built heating chamber for heated tension test of CFRP loop.

.

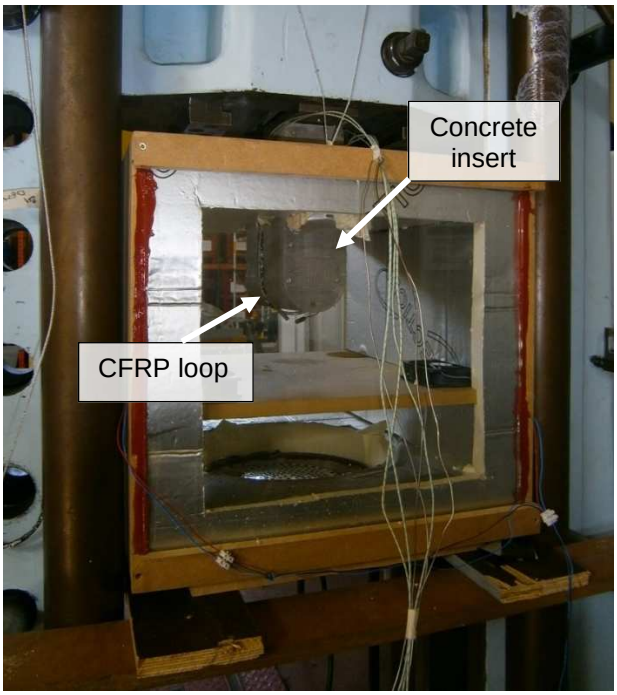

Figure 3.11 Heating chamber used in tension tests.

The aim was to test at a temperature higher than the glass transient temperature of the Tyfo-S matrix, such that softening of the matrix would cause a reduction in CFRP loop tensile strength. Dynamic mechanical analysis (Table 3.5) gave a glass transition temperature [T_g] of 84.9 °C for the Tyfo-S resin, and 140.5 °C for H-EL2. The testing temperature in tension test was limited to 100 °C because it is the maximum working temperature for the fans used inside the heating chamber. The heated length of loop was 140 mm to include the curved part and straight legs part of the loop (Figure 3.12).

To ensure that the CFRP loop reinforcement reached the target temperature, thermocouples were placed inside additional pieces of CFRP within the chamber. The CFRP bits were made by cutting some CFRP loop reinforcements to a size of 5×5×25 mm (i.e. the same geometry and thermal properties as the loops being tested). One end of the CFRP piece was drilled to a diameter of 2 mm and 12 mm depth (Figure 3.13), and a type K thermocouple (TC) was inserted to measure the temperature at the centre of the CFRP, with the hole sealed with epoxy resin (Figures 3.13-3.14). Temperature was recorded at a rate of 0.5Hz. The CFRP loops were heated until thermocouples

inside the CFRP bits showed a temperature of 100 °C, and then the load was applied until failure. The gas temperature inside the oven was also monitored by two K type thermocouples placed adjacent to the tested specimen as shown in Figure 3.12.

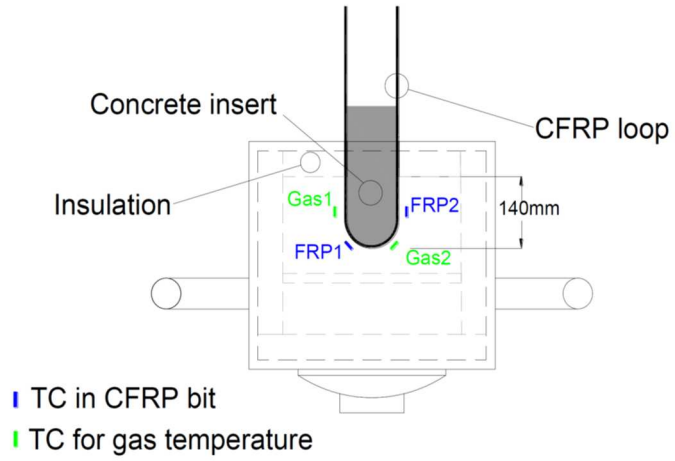

Figure 3.12 Schematic of CFRP loop inside heating chamber.

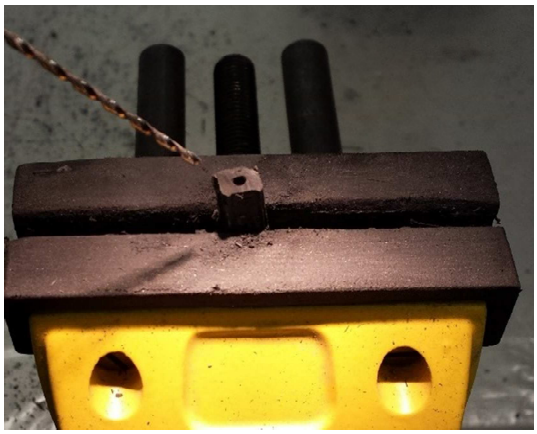

Figure 3.13 Drilling CFRP piece to insert a thermocouple.

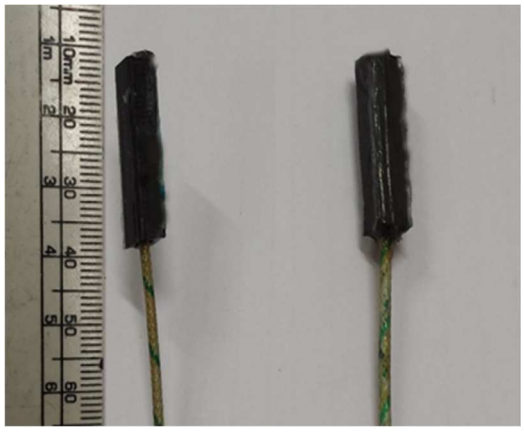

Figure 3.14 CFRP pieces containing thermocouples.

3.4.3 Specimens Design

The CFRP loops were made with an outer length of 845 mm (Figure 3.15), to fit within a universal testing machine frame. All of the tension test loops were made with a total of 24 rounds of carbon fibre tows and a 50 mm inner radius of curved part. The number

of rounds 24 is divisible by 2 and 3 which the number of concentric loops used in some samples as explained below. Tyso-S resin was used in the production of all tension specimens, however, high temperature resin H-EL2 was used in one loop type which is denoted as 'loop with high temperature resin'.

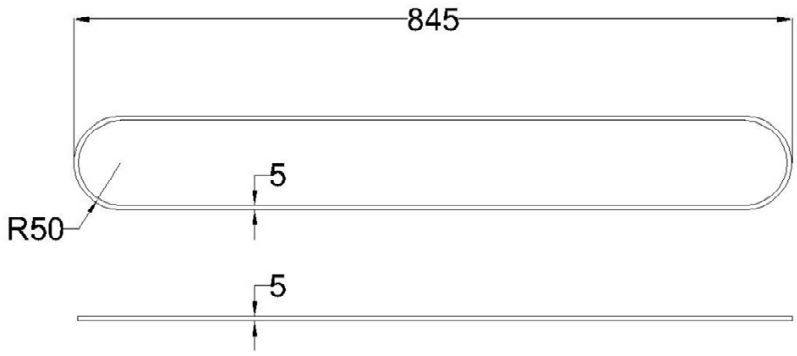

Figure 3.15 Dimensions of CFRP loop specimens for tensile test.

For optimisation purposes and to investigate the effect of section geometry and matrix glass transition temperature (T_g), six types of CFRP loops were prepared:

1. Continuously Wound Loops: specimens of this type were made by winding a single epoxy-saturated carbon fibre tow. This type is the simplest in terms of production and it was used as benchmark (control specimen) to compare the performance of other types against. The cross section of the loop produced was a square of 5 mm size (Figure 3.15).

2. Two Concentric Loops: Instead of making one loop with a 5 mm square section, specimens of this type were made as two concentric loops. Each of the concentric loops has a thickness of 2.5 mm and a width of 5 mm (Figure 3.16). The specimens of this type were intended to investigate the effect of interlamina shear stress, which is a matrix-dependent property and is affected by composite section geometry (see section 2.6). Each of the loops were made by continuous winding a single carbon fibre tow, with 12 rounds of carbon fibre tow in each of the concentric loops. The inner loop was made first and left to ambient cure for 24 hours. Afterwards, PVA demoulding agent was applied on the inner loop surface before the sequent outer loop was winded on

top in same process of the inner loop. The demould agent prevented the epoxy resin from adhering the two concentric loops to each other. This design enabled both loops to share tensile forces while allowing them to have differential elongation, which could reduce interlamina shear stress.

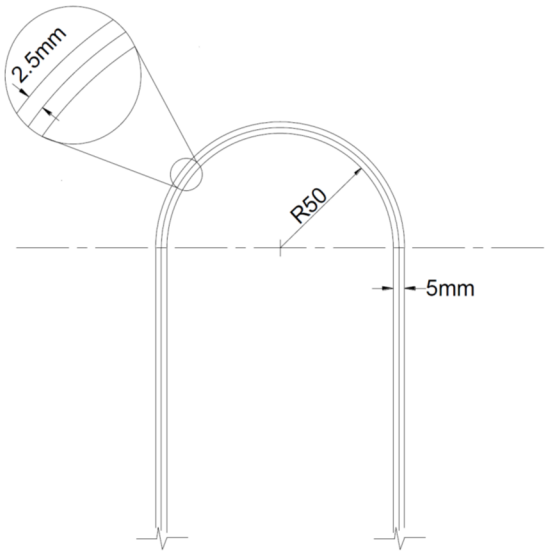

Figure 3.16 Geometry of two concentric CFRP loops.

3. Three Concentric Loops: As with two concentric loops, this loop type was intended to be used to evaluate the influence of interlamina shear stress on loop failure load. Loops of this type are made in similar steps to two concentric loops, but with three concentric loops each with eight tow rounds (Figure 3.17).

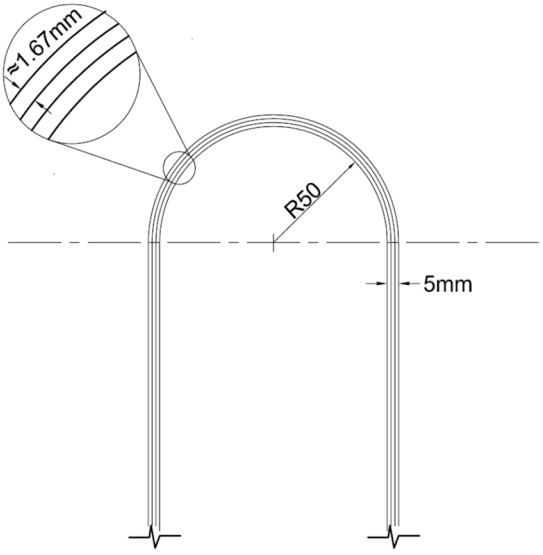

Figure 3.17 Geometry of three concentric CFRP loops.

4. Loops with High Temperature Resin: In this type epoxy resin with a higher glass transition temperature performance was used at the loop ends. High temperature resin was only used within the critical areas of loop reinforcement where matrix softening has a higher impact. The curved part of loop reinforcement is the critical segement of reinforcement where reinforcement is under a combination of axial and transverse forces (see section 2.6). High temperature epoxy resin (H-EL2), (Table 3.4), was used at the loop ends, while normal Tyfo-S resin was used in the rest of the loop (Figure 3.18). This arrangement exploited the benefit of better thermal properties without the associated high cost of the more expesive resin.

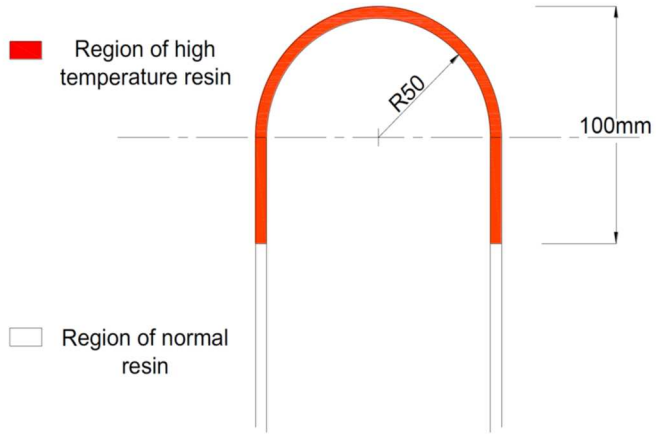

Figure 3.18 CFRP with high temperature at the ends.

As mentioned above in the production of these loops two types of resin were used instead of one. As the epoxy resins were applied to the fibres by brushes, it was possible to control which type of resin to apply in which areas. The curing process was carried out in two stages, because the high temperature resin (H-EL2) requires higher curing temperatures than normal resin (Tyfo-S). Exposing normal resin to temperature higher than its T_g can cause it to degrade. Therefore, in the first curing stage the whole loops were cured at 60 °C in a drying oven. Afterwards, only parts with high temperature resin were post cured at a higher temperature using heating tape (Figure 3.19). The temperature curing cycle recommended by the manufacturer for high

temperature resin is one hour for each 20 °C of temperature increment. After the initial curing of whole loops at 60 °C (curing temperature for normal resin), post curing to the regions with H-EL2 was done with the heating tape at temperatures cycles of 80, 100, 120 and 140°C. Temperature was monitored by means of K-type thermocouples which were fit between the heating tape and FRP (Figure 3.19).

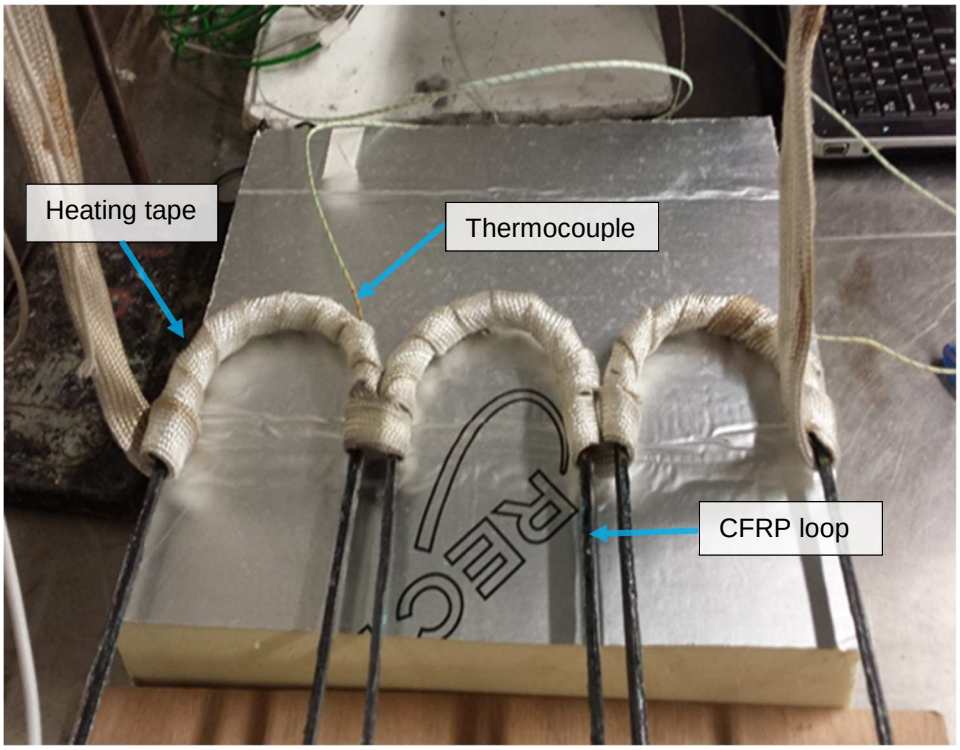

Figure 3.19 Regional curing of loops with heating tape with high temperature resin at the ends.

5. CFRP Loops with Reinforced Ends: As discussed previously in section 2.6 the curved part of the FRP is an area of stress concentration and has less strength than the straight portion of reinforcement. Providing extra reinforcement at the curved part of the loop could potentially enhance its capacity under axial and transverse forces. The extra reinforcement was provided in the form of CFRP tape wrapped around the loop ends (Figure 3.20).

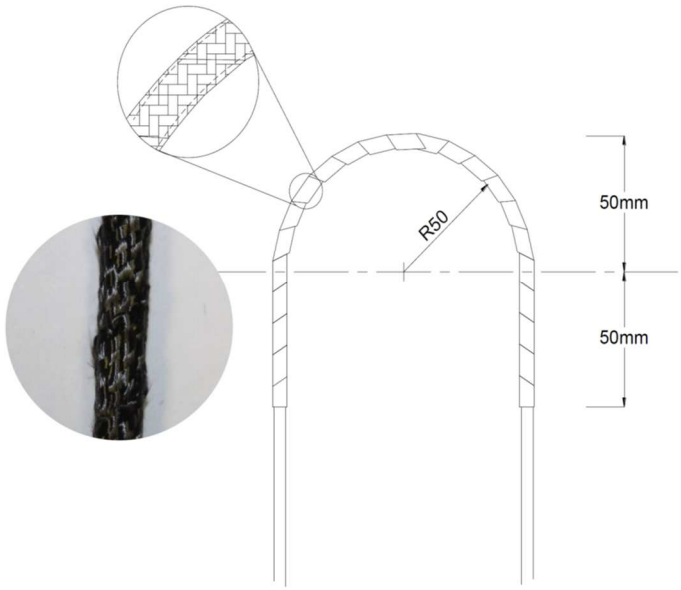

Figure 3.20 Schematic drawing of CFRP loop reinforced with CFRP tape at the ends.

The preparation of the sample was by wrapping CFRP tape saturated with Tyfo-S epoxy resin around ambient cured loop ends. The loop was made by winding 24 rounds of continuous fibre tows as in the control specimen. The CFRP tape texture was a plain 90° weave of 3k carbon tow (Figure 3.21). The tape has a thickness of 0.3 mm and a width of 12.5 mm. Wrapping was at an angle of 45° along the loop to optimise in-plane shear resistance. The mechanical properties of the CFRP tape as provided by the manufacturer in the product datasheet and is listed in Table 3.6.

Table 3.6 Mechanical properties of carbon tows used in CFRP tape.

Number of filaments	3000
Filament diameter	7 μm
Tensile strength	4120 MPa
Tensile modulus of elasticity	234 GPa
Density	1.79 g/cm^3
Elongation	1.8%

Figure 3.21 Plain wave carbon fibre tape.

- **6. CFRP loops with flat ends:** Many researchers report the dependency of curved FRP tensile capacity in the reinforcement section geometry. The tensile capacity of curved FRP was found to be proportional to the ratio of curvature radius to reinforcement thickness *r/t* (Lees and Winistörfer, 2011; Imjai et al., 2007b; Ehsani et al., 1995; Guadagnini et al., 2006). To investigate to what extent the section geometry can affect the reinforcement strength, loop specimens were made with flat ends, but the legs of the loops were kept with square cross-section of 5×5 mm. The thickness at the ends was reduced to 2 mm and the width increased to 12.5 mm to keep the same area of cross-section area as other loops types. This makes the radius to thickness (*r/t*) ratio = 25, which is increased by 2.5 in comparison to other groups. The loops were produced in same manner as other loop specimens by continuous winding of 24 rounds of carbon tows, however, the grooves of the mould was modified at both ends to allow for a wider section at the loops ends (Figure 3.22).

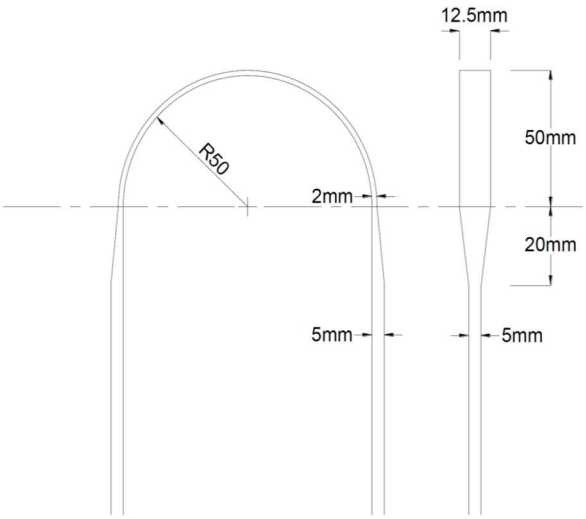

Figure 3.22 Geometry of CFRP loops with flat ends.

3.5 Tension Test Results

3.5.1 Heating of the Tension Test Specimens

Figure 3.23 below shows temperature progression during tension test of a continuous loop sample (AS3). The figure shows thermocouples data of gas temperature gas and CFRP pieces which were used to indicate the temperature at the centre of the CFRP loops. Figures showing the temperature progression during the tests of other samples are placed within Appendix B.

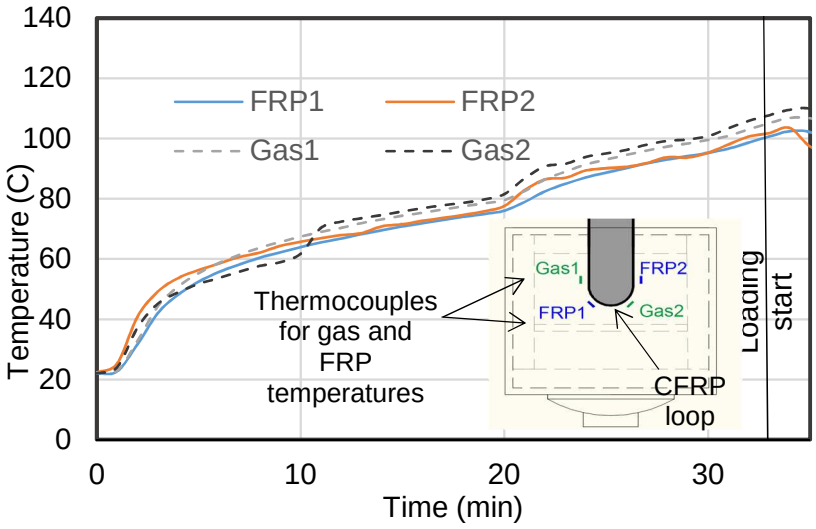

Figure 3.23 Temperature propagation for CFRP and gas in tension test of specimens AS3 (continuous loop).

3.5.2 Failure Loads and Mechanisms

All specimens failed by rupture at the end the curved part (Figures 3.25-3.28). Table 3.7 lists the failure loads of each specimen. Figure 3.24 is a bar chart shows the difference in failure load between different samples at ambient temperature and when heated.

Table 3.7 Failure load of loops in tension test at ambient and 100 °C.

Specimens Type	Sample No.	Failure load (kN)	Average failure load (kN)	Sample No.	Failure load (kN)	Average failure load (kN)	CFRP Temperature at failure (°C)	Strength difference (%)
	Ambient temperature			Loading started at 100 °C				
Control	AS1	42.3	42.6	AS3	35.4	34.1	100	-20
	AS2	42.8		AS4	32.8		103	
Two concentric	BS1	39.6	42.4	BS3	28.5	26.8	105	-37
	BS2	45.2		BS4	25.1		101	
Three concentric	CS1	28.6	35.4	CS3	28.3	27.9	102	-21
	CS2	42.2		CS4	27.4		103	
With high temp. resin	DS1	45.2	46.7	DS3	39.6	39.0	104	-16
	DS2	48.2		DS4	38.4		105	
With CFRP tape	ES1	40.6	41.4	ES3	35.1	34.5	102	-17
	ES2	42.1		ES4	33.8		102	
With flat end	FS1	35.8	34.3	FS3	41.8	38.6	103	+13
	FS2	32.7		FS4	35.4		107	

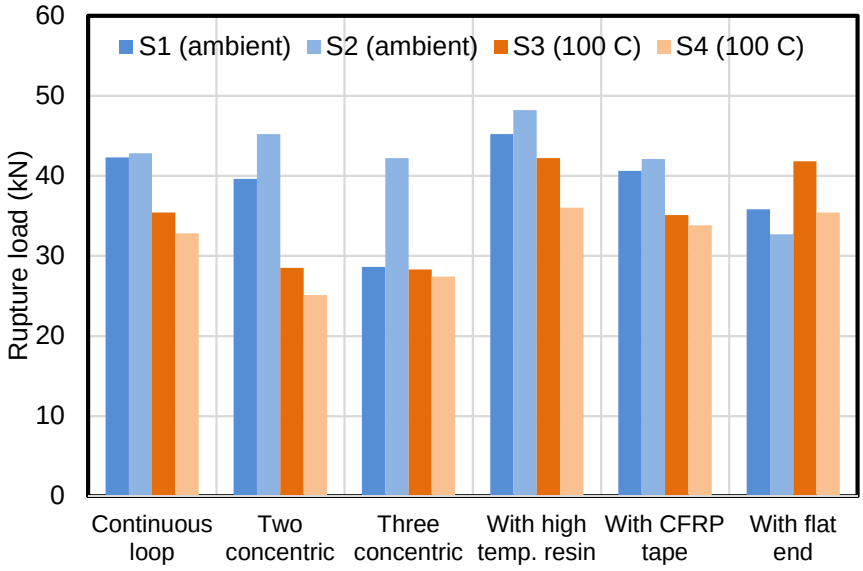

Figure 3.24 Rupture load of different types of loops at ambient temperature and 100 °C.

Figure 3.25 Rupture failure within the bend of a flat-end specimen (FS2).

Figure 3.26 Rupture failure and splitting cracks occur in the bend of innermost fibres for a continuous-loop specimen (AS1).

Figure 3.27 Rupture failure in the inner loop of a three-concentric loop specimen at 100°C (CS3).

Figure 3.28 Rupture and splitting cracks at the inside of bend of high temp. resin specimen (DS1).

3.5.3 Discussion of Tension Tests Results

Tension Capacity at Ambient Temperature

1. Tension test provided a mechanism to evaluate the performance of CFRP loops under tension forces. The control specimens (made from continuous winding) achieved average ultimate load of ≈43 kN. Failure load varied between specimens of different types but all specimen failed by rupture. The variation in tension strength occurred within specimen of same type could be attributed to variability emerged from manual manufacture process of CFRP reinforcement and/or due to experimental uncertainties.

2. Specimens made of concentric loops (two and three) had fluctuating results and no improvement in failure load was achieved in comparison to loops made from continuous winding (control specimens). This can be an indication that either interlamina shear stress does not have a significant effect for the section size used or the used technique is not effective. Also because interlamina strength is a matrix dominant property enhancing mechanical properties of polymer could be more effective and result in higher strength of loop curved part.
3. There was a slight improvement, ≈ 10%, in the strength samples with high temperature resin (H-EL2) despite the tensile strength of H-EL2 resin is marginally lower than Tyfo-S as suggested by the products datasheets (Table 3.5). The enhanced strength achieved with H-EL2 resin could be attributed to strength improvement due to curing at higher temperature.
4. Specimens strengthened with CFRP tape achieved similar failure load to control specimens as can be seen in Table 3.7 and Figure 3.24. This indicates that the tape strengthen technique is not efficient as no significant enhancement of ultimate tensile strength was achieved.
5. Despite the fact that loops with flat ends have a higher *r/t* ratio which is supposed to increase the tensile strength of the bend (Ehsani et al., 1996; ACI, 2015, Imjai et al., 2009; Imjai et al., 2007a), specimens of this type developed a failure load ≈ 20% less than control specimen. The effect of *r/t* ratio on bend strength might be more evident at lower values of *r/t*, as in cases of FRP flat sheets and strips, where most of the related research is carried out.
6. All specimens shared the same failure mode as they all failed by rupture. Failure occurred as expected within the curved part of reinforcement due to the multiaxial stress status generated by axial tension forces and transverse forces by bearing against concrete. The effect is exaggerated due to the fact that fibres are weaker in a transverse direction (see section 2.6 for more details). It was also noticed that failure location always occurred at the end of curved part which indicates that higher stress concentration exists there. Even in the case of loop with flat ends rupture did not occur within the area where section geometry changes, but within the flat curved section (Figure 3.25). This eliminates the

possibility that failure initiated due to stress concentration caused by section geometry change.

When examining failure mechanism, some trends can be observed. The rupture is initiated from the innermost fibres (Figures 3.25-3.28), which indicates they are under higher stresses. This is consistent with other researchers' observations about curved FRP reinforcement (Ahmed et al., 2010; Meier and Winstörfer, 2007; Winistorfer and Mottram, 2001). Splitting cracks were also observed (Figure 3.26 and Figure 3.28) which could be resulted by interlamina stresses.

The Effect of Elevated Temperature

1. When the CFRP loops were heated locally (over 140 mm at one end) to 100 °C, a reduction in failure load was observed in all of the specimens except loops with flat ends. The control specimens experienced a reduction in tension strength by 20%. Reduction in the strength under heating is expected due to matrix softening which reduces its ability of load sharing between fibre filaments (see section 2.10.1 for more details).

2. As at ambient temperature, the concentric loops specimens developed the lowest failure load, ≈ 27 kN with strength reduction between 21-37% in comparison with ambient results. Because they are the most complex in production and provide no improvement strength, concentric loops are not recommended as a design option of CFRP loops.

3. The localised usage of high temperature resin at the curved part appeared not be very effective. Despite the fact the testing temperature was 40 °C below the T_g of the high temperature resin, strength reduction of about 16% occurred which not significantly far from 20% reduction occurred in control specimen where T_g is less than test temperature. However, more effect on tensile strength could be evident at higher temperatures.

4. As in ambient temperature, strengthening the curved part of loops with CFRP tape was found to be ineffective as no improvement to loop tension capacity was achieved.

5. The loops with the flat ends was an exception as there was a some improvement, 13%, in strength under heating conditions (Table 3.7); however, this result is inconclusive and could have been due to experimental uncertainties.

6. Failure mode was maintained the same as in ambient temperature. All specimens failed at the heated end due to rupture at the end of the curved part.

The tension tests provided an evaluation of the capability of different configurations of CFRP loops to resist tension forces at ambient and 100 °C. It has been concluded that the basic continuous winding loop type is preferred as it achieved strength either comparable or exceed more complex designs. Hence the tension test was intended as a quick assessment method. It did not include preparing concrete specimens reinforced with CFRP loops. However, after specific design was chosen based on tensile test results, push-off test series was planned to demonstrate the performance of CFRP loops in concrete which is discussed in the following sections.

3.6 Push-off Tests

3.6.1 Overview

The second test series is push-off which involved testing CFRP loops embedded in concrete as shown in test arrangements Figure (3.29). The performance of the loops at both ambient and elevated temperatures was contrasted with straight and hooked bars. The aim of these tests was to provide a quick evaluation of loops bond performance which can aid in the design of more of complex configuration of beam test.

3.6.2 Push-off specimen design

The push-off test method for FRP bent bars and stirrups is specified by guidelines (ACI, 2012) and (CSA, 2012). The test involves FRP reinforcement bridging two

concrete blocks which are pushed apart by a hydraulic jack which put the reinforcement under tension. This test configuration is intended to investigate stirrups and curved reinforcement tensile strength (refer to section 2.7.2 for more details). The dimension of specimens was chosen to allow them to fit inside the available oven. The concrete cube dimensions were 180 mm and total length of the whole specimen was 500 mm. To avoid the effect on bond from the loaded surface, bond breaks were made by wrapping four layers of 0.5 mm thick electrical insulation tape on a 25 mm length of CFRP reinforcement at loading surface (Figure 3.30).

The purpose of a push-off test as specified by ACI (2012) and CSA (2012) is to evaluate the capacity of the curved part of reinforcement; therefore, the straight part of the reinforcement is debonded from concrete so all applied forces are carried by the curved part (Figure 2.10). However, in the current research the straight parts of reinforcement were embedded so that comparisons between CFRP loop and traditional methods of straight and hooked reinforcement can be made (Figure 3.30). The embedded length of reinforcement in all specimens was made the same, 266 mm in each concrete block. The radius of the bend was kept 50 mm as used in tensile tests specimens. This makes the ratio between bend radius to bar size equal to 10. Four conventional Φ6 steel bars were cast between the pair of concrete blocks near the corners. Their purpose is preventing damage of the CFRP reinforcement when handling specimens, especially when taking them out of the oven. The steel rebars were cut just before applying the load. To monitor the temperature of reinforcement, thermocouples were tied to the CFRP reinforcement at midpoint of the curved part (Figure 3.29-3.30).

When push-off forces are applied to two concrete cubes, they are resisted by circumferential stress (bond) around the embedded part of reinforcement. Therefore, the modified push-off test can be used to assess bond performance of different reinforcement arrangements. At elevated temperatures the load transfer at reinforcement surface was expected to reduce due to the softening of polymeric matrix, and consequently bond degradation could be assessed through the change in the pull-out force and reinforcement slip response due to heating.

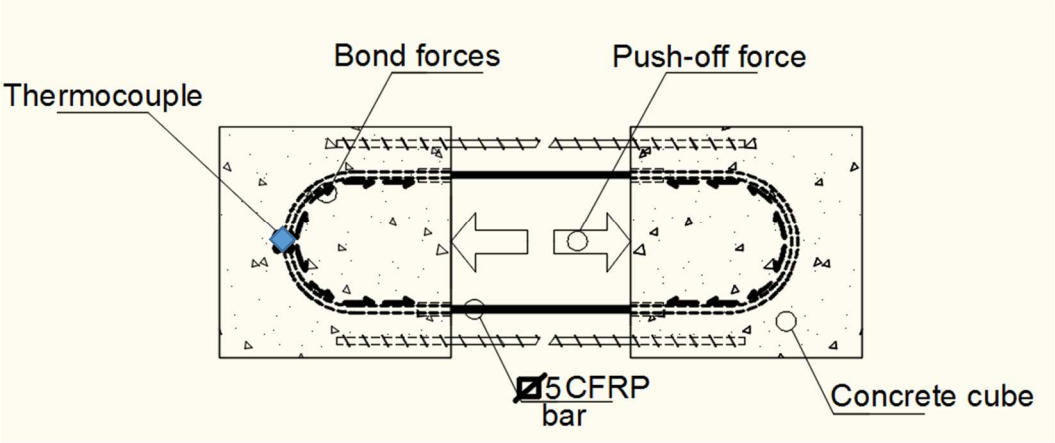

Figure 3.29 CFRP loop in push-off test.

3.6.3 Specimens Types

To compare the performance of CFRP loops with traditional methods of hooked and straight CFRP reinforcement, three different types of test specimens were designed (Figure 3.30).

- Type L (loop) specimens contained a filament wound loop of CFRP.
- Type H (hook) specimens contained the same closed loop, except that the reinforcement was cut at one end, making the loop within one of the blocks into two hooked bars.
- Type S (straight) has a conventional reinforcement arrangement of two straight bars at one end and closed curved part at the other end.

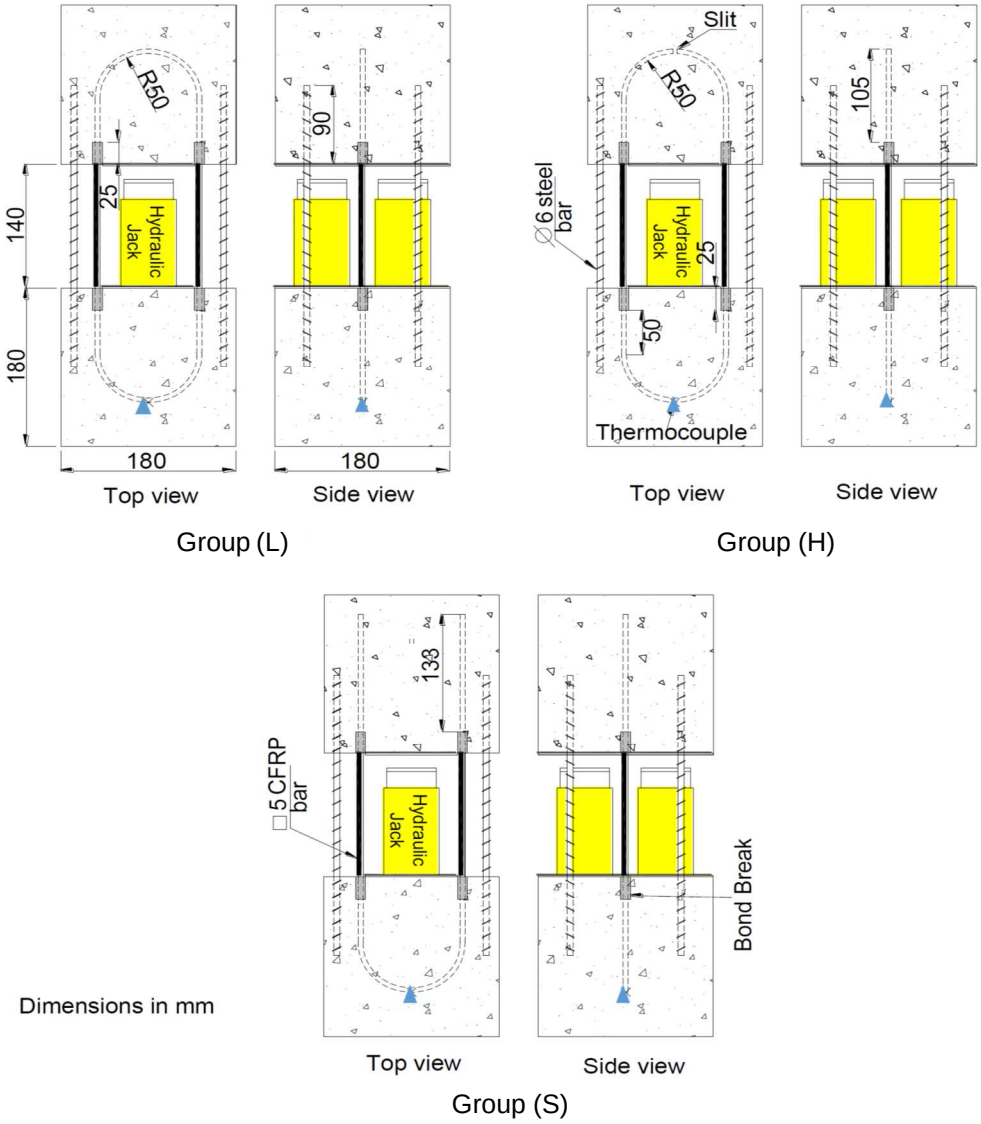

Figure 3.30 Push-off test specimens.

The CFRP loop reinforcement was manufactured by the same process of tension test control specimen previously mentioned in section 3.3 except that the number of carbon fibre tow rounds were increased from 24 to 25, and only the parts of reinforcement to be embedded inside the concrete were sand-coated. The reinforcement with straight bars at one end (type S) was initially made as a longer loop then the curved part at one end was cut off.

3.6.4 Push-off Specimen Preparation

Plywood formwork was designed and built to produce the required samples (Figure 3.31-3.32). The formwork design was made in such a way that the concrete cast direction is perpendicular to the CFRP reinforcement, as is the case for beams (Figure 3.31). The specimen preparation before casting the concrete is shown in Figures 3.31-3.32. Slits were made in the formwork to secure the reinforcement in place, and additional support was provided through wooden strips. Figure 3.33 shows the formwork after the concrete was cast.

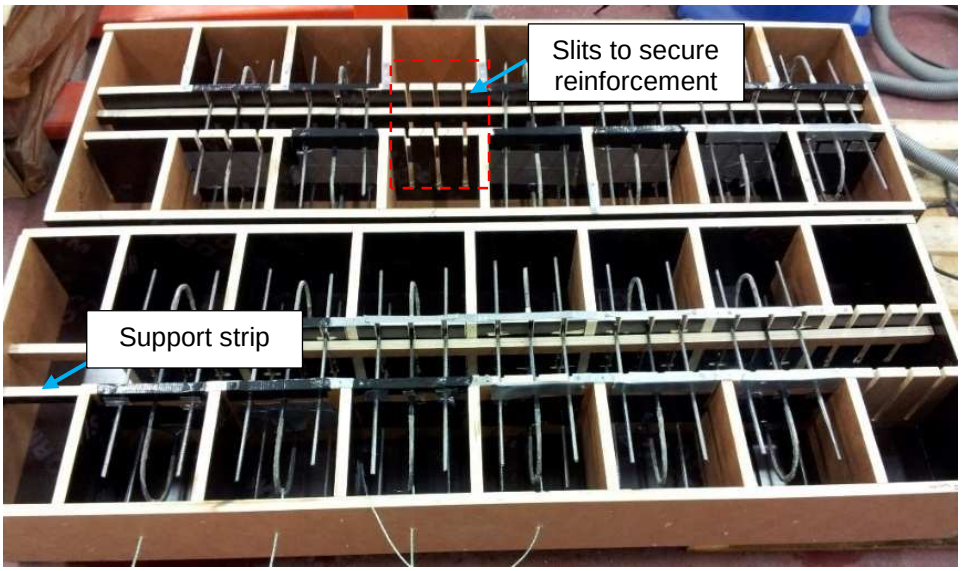

Figure 3.31 Plywood formwork to produce push-off test specimens.

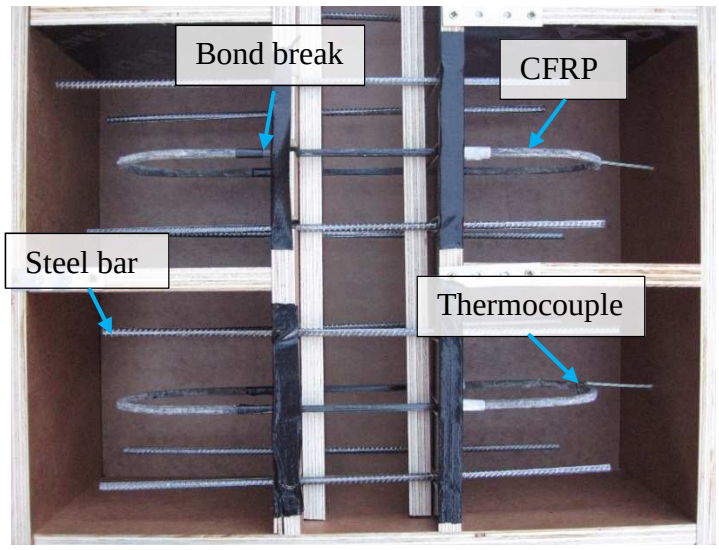

Figure 3.32 Part of the formwork specimen of Group H prior to casting.

A ready-mix concrete with basalt aggregate and glass sand aggregate was used. The concrete properties based on the mean value of three cube compressive tests and three cylinder split tests are listed in Table 3.8.

Table 3.8 Ready-mix concrete properties.

28-day compressive strength (MPa)	Tensile strength (MPa)	Maximum aggregate size (mm)	Slump value (mm)
34.4[1]	3.2[2]	10	82

[1]*standard deviation = 0.62,* [2]*standard deviation = 15.8*

Figure 3.33 Formwork after casting the concrete for the push-off test specimens.

The mechanical and thermal properties of the carbon fibre tows are listed in Tables 3.1-3.3 as provided by the manufacturer. The tensile and compressive properties in Table 3.2 are normalised for a fibre volume of 60% (Mitsubishi Rayon Carbon Fiber and Composites, 2014).

3.6.5 Experimental Programme

To compare the performance of the looped reinforcement against straight CFRP reinforcement, specimens from all groups were tested at three temperatures:

- Unheated (ambient temperature);
- Heated to the glass transition temperature of the FRP, T_g = 85 °C, at which the resin is partially softened; or
- Heated to well above the glass transition temperature, T = 130 °C, at which the resin mechanical properties were severely deteriorated.

The glass transition temperature of the produced CFRP reinforcement was measured using DMA test which is discussed in section 3.2.2. Cao (2009) conducted tensile tests upon CFRP and GFRP coupons, of which tan δ T_g = 85 °C and found that tensile strength is stable in close range beyond T_g up to 200 °C. Therefore, in the current study the performance of specimens tested at temperature of 130 °C might be a presentative of performance at even higher temperatures.

A total of eighteen specimens, six in each group, were prepared. Two specimens of each group were tested at an ambient temperature, two at T_g (85 °C) and two at 130 °C (Table 3.9).

Table 3.9 Beam specimens annotations and descriptions

Reinforcement type	**Testing temperature**		
	Ambient	**T_g = 85** °C	130 °C
Loops	L1	L3	L5
	L2	L4	L6
Hooked	H1	H3	H5
	H2	H4	H6
Straight bars	S1	S3	S5
	S2	S4	S6
Number of specimens	6	6	6
Total	18		

3.6.6 Test Configuration and Instrumentation

Two 10 tonne hydraulic jacks were fitted between the concrete cubes as shown in Figures 3.34 and 3.35. The two jacks were fixed at the bottom together with a 5 mm steel bearing plate so they could be inserted and positioned quickly, which is needed in heating tests. Another 5 mm steel bearing plate was used on the top of the jacks. A third 10 tonne hydraulic jack was positioned to act against a load cell. All three jacks were connected in parallel to a manual hydraulic pump (Figure 3.35). This arrangement makes the value of load as measured by the load cell, to be half the load value applied on the specimen.

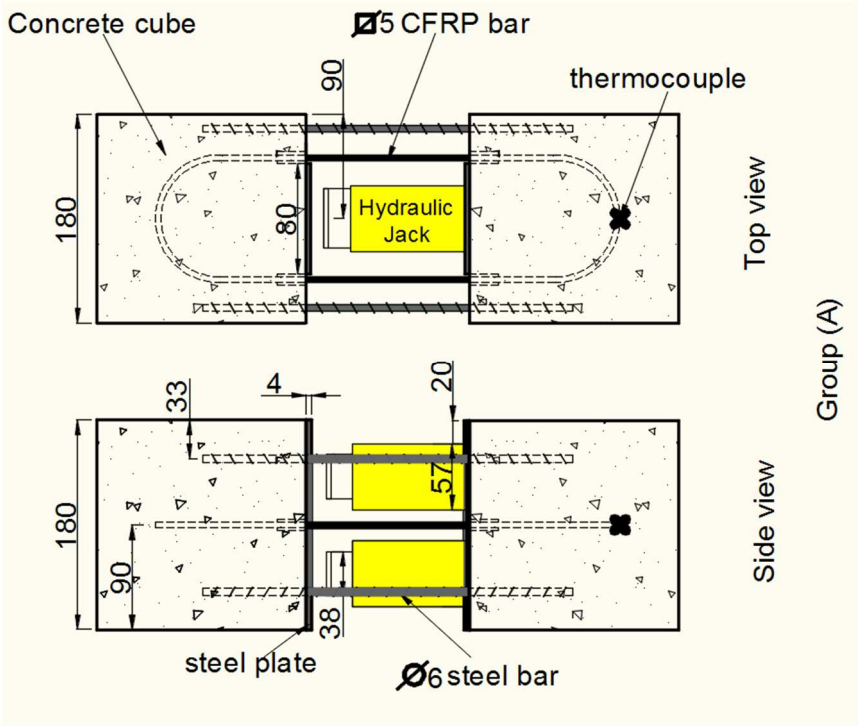

Figure 3.34 Using hydraulic jacks to perform push-off test.

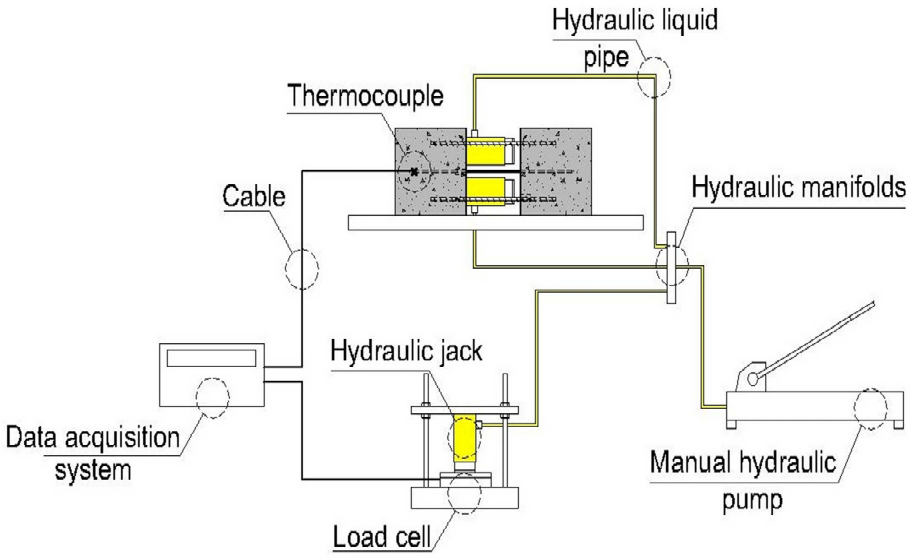

Figure 3.35 Layout of testing equipment used in push-off test.

For the heated tests, the specimens were heated in a radiation oven (Figure 3.36). A test bench was placed in front of the oven to allow the specimen to be slid out of the oven and tested quickly (Figure 3.36), before the temperature of the specimen had reduced significantly. The steel reinforcement bars were cut with an angle grinder once the hydraulic jacks were inserted into place and before applying the load. In the heated specimens lateral support was provided by means of a roller as shown in Figure 3.36. This aimed to help reduce rotation of the cubes that occur as a results of high bond degradation and under the effect of any eccentricity.

A type K thermocouple was placed on the reinforcement at the middle of the curved part of the reinforcement (Figures 3.30 and 3.34). This was connected to the data acquisition system and used to monitor and record the CFRP reinforcement temperature. One thermocouple was used in each heated specimen. The number and location of thermocouples was chosen to not affect the reinforcement surface bond.

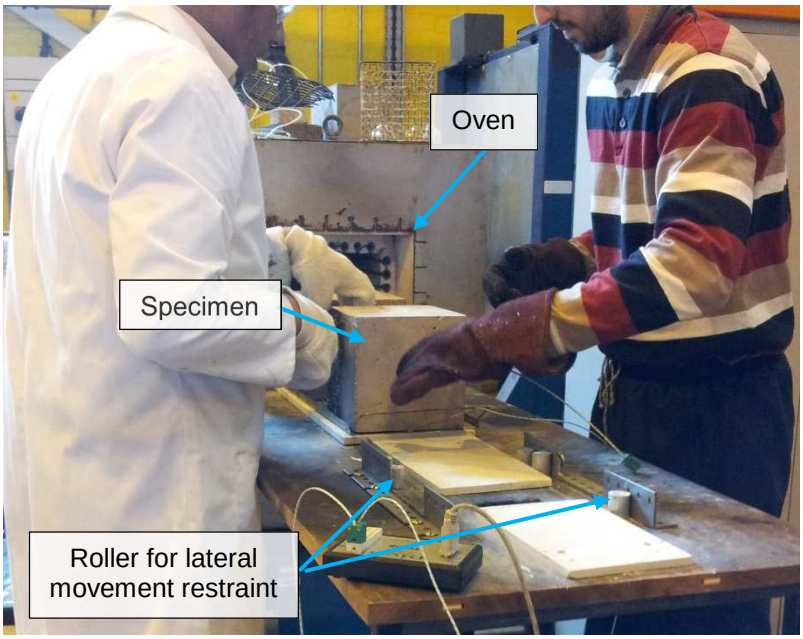

Figure 3.36 Push-off specimen slid out of oven for testing.

The relative displacement of the two concrete blocks and the pull-out of the CFRP reinforcement from the concrete was measured using digital image correlation (DIC) technique, the specimens were painted with a high-contrast pattern before being placed in the oven and a series of images was captured at 0.2 Hz using two high-resolution cameras, placed on either side of the specimen (Figure 3.37). A bespoke DIC algorithm (White et al., 2003) was used to track the movement of four pixel patches in these images placed on the concrete and CFRP reinforcement on either side of the specimen (Figure 3.38). These patches allow the FRP extension and slip to be determined. Patches 2 and 3 were placed on the FRP reinforcement as close as possible to the concrete. The relative movement of patches 2 and 3 were used to determine strain in the FRP. Patches 1 and 4 were placed on the concrete cubes to track their movement, which is used to determine the slip of reinforcement. A particular advantage of DIC for these tests was that it could be quickly applied to heated specimens without any need for contact.

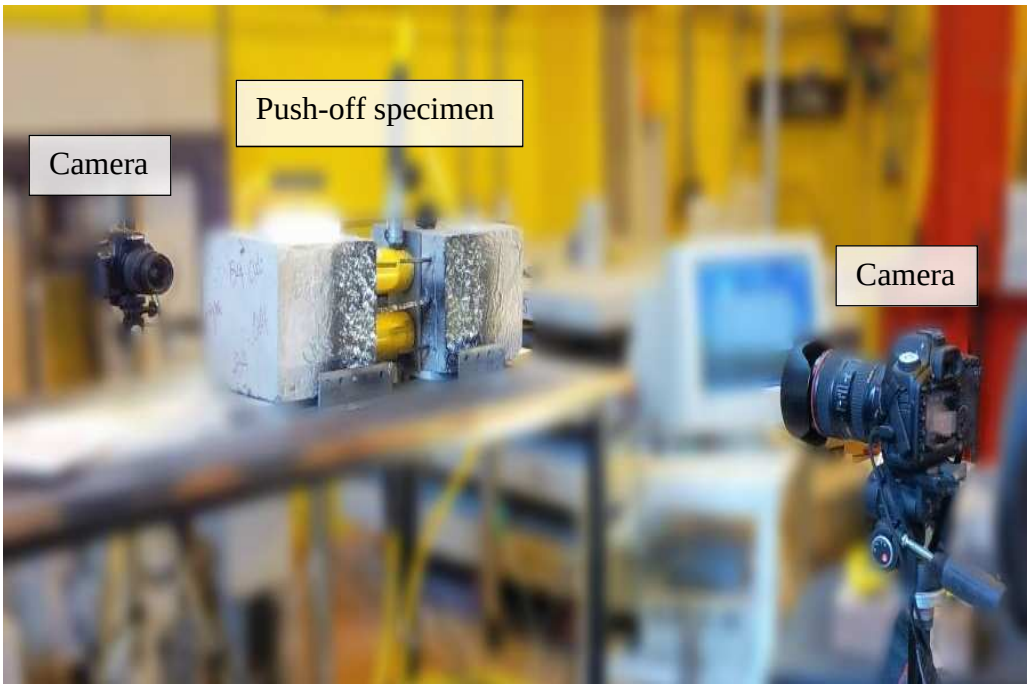

Figure 3.37 High resolutions cameras used for DIC to measure specimen displacement.

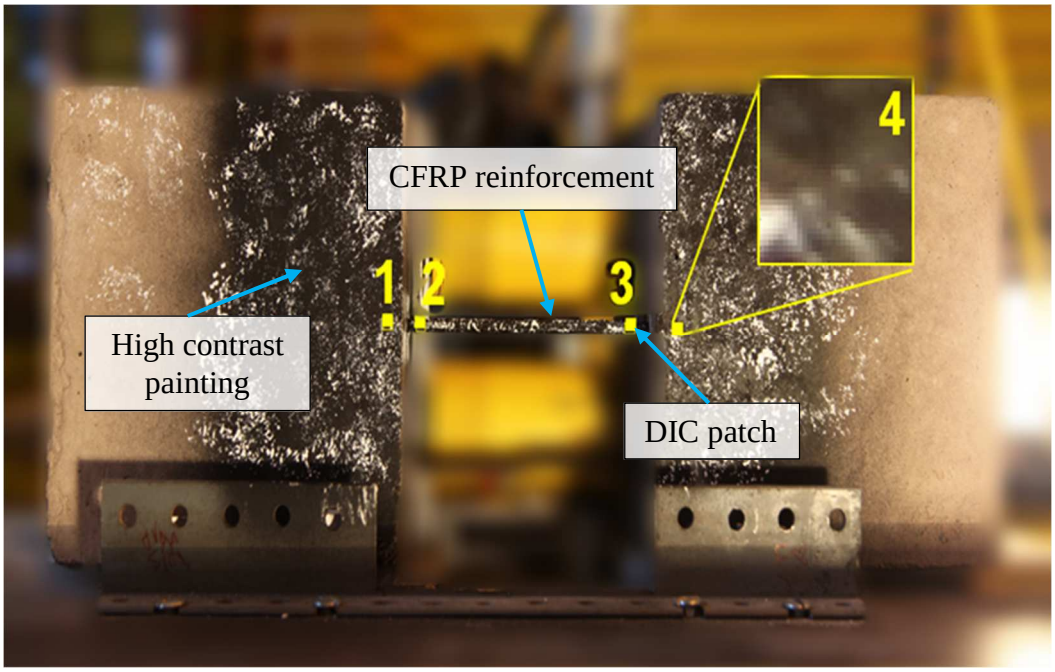

Figure 3.38 DIC patches used for CFRP reinforcement strain and slip measurements.

3.6.7 Results and Analysis of Push-off Tests at Ambient Temperature

Results showed that at ambient temperature there was no clear distinction in performance between different types of reinforcement. Detailed results are presented below.

Failure Loads and Mechanisms

Table 3.10 lists failure loads and mechanisms of specimens of different types. The dominant failure mode at ambient is rupture. Figures 2.39-2.43 show failure mode of specimens at ambient temperature. Two unsynchronised data-loggers were used to record temperature and load data. To synchronise temperature and load data, the time between reaching testing temperature and start of loading was needed to be assumed. This time was assumed to be 5 minutes as an estimation for the duration to slide specimens out of the oven and inserting hydraulic jacks for testing. The values of temperature at failure in Table 3.10 are taken from the logged temperature data based on the assumed period of 5 minutes between reaching testing temperature and start of loading.

Table 3.10 Failure loads and modes of push-off tests

Test type	Specimen Type	Test	Failure load (kN)	Average failure load (kN)	Temperature at Failure[(1)]	Failure mode
Ambient	L	L1	66.98	61.50	Ambient	Rupture – in free length
		L2	56.20		Ambient	Rupture – in free length
	H	H1	58.88	55.31	Ambient	Rupture – in free length
		H2	51.74		Ambient	Rupture – in free length
	S	S1	45.36	47.67	Ambient	Pull-out
		S2	49.98		Ambient	Rupture – in free length
T_g (85°C)	L	L3	35.16	38.96	91°C	Rupture – within bond area
		L4	42.77		85°C	Rupture – within bond area
	H	H3	12.81	14.01	85°C	Pull-out
		H4	15.20		87°C	Pull-out
	S	S3	15.09	16.27	87°C	Pull-out
		S4	17.44		-[(2)]	Pull-out
130°C	L	L5	32.77	32.47	131°C	Rupture – within bond area
		L6	32.17		131°C	Rupture – within bond area
	H	H5	8.63	10.26	130°C	Pull-out
		H6	11.89		130°C	Pull-out
	S	S5	9.42	9.05	130°C	Pull-out
		S6	8.68		130°C	Pull-out

[(1)]Estimated values, [(2)]Data for this specimen are not available.

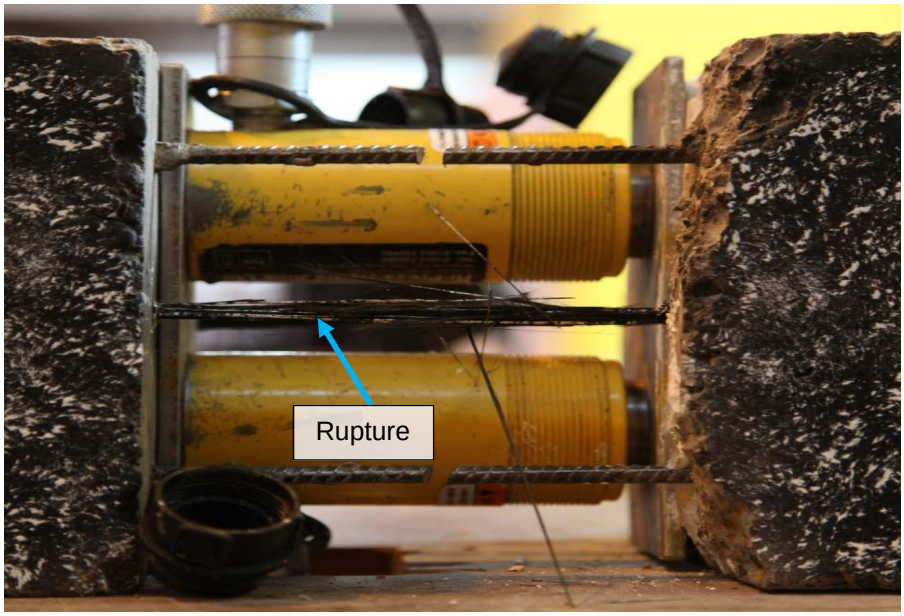

Figure 3.39 FRP rupture within the free length, CFRP loop specimen L2 (ambient).

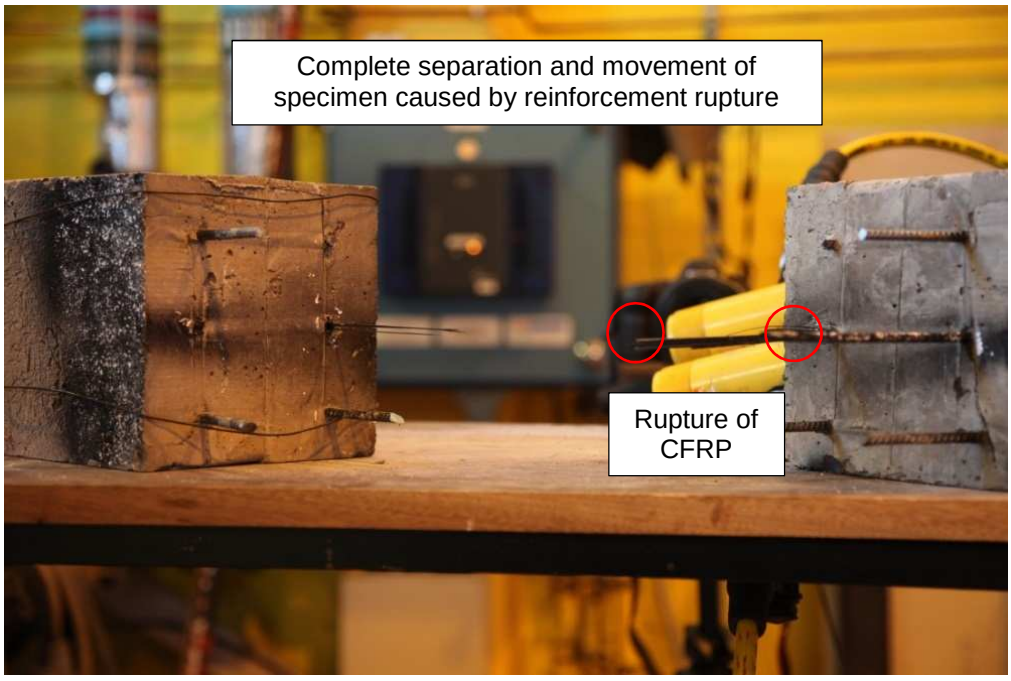

Figure 3.40 Rupture of FRP reinforcemetn and seperation of concrete cubes, hooked reinforceement specimen H1 (ambient).

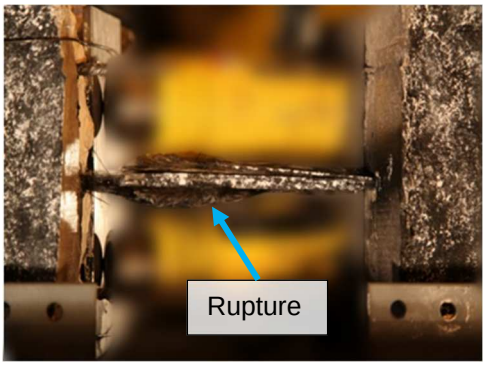

Figure 3.41 FRP rupture within the free length, S2 (ambient).

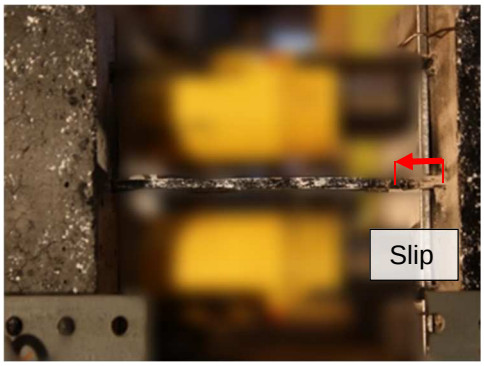

Figure 3.42 CFRP reinforcement pull-out of specimen S1 (ambient).

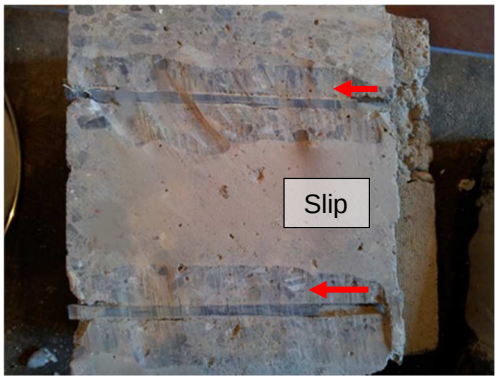

Figure 3.43 Pull-out of straight FRP reinforcement, S1 (ambient).

Stress-Strain Response

The displacement data generated by DIC technique was used to obtain stress-strain response of CFRP loops as shown in Figure 3.44 below.

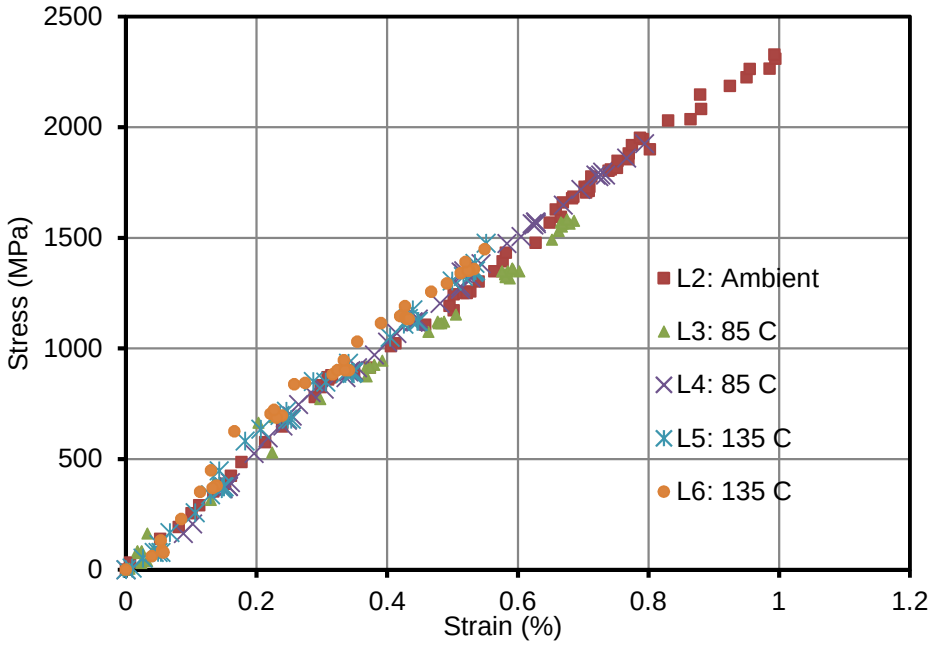

Figure 3.44 Stress-strain response of CFRP closed loops (Group L) based on fibres cross-section area only (The response for L1 was not captured due to an equipment failure)

Load-Slip Response

Figures (3.45-3.47) below shows load-slip response of push-off specimens with different types.

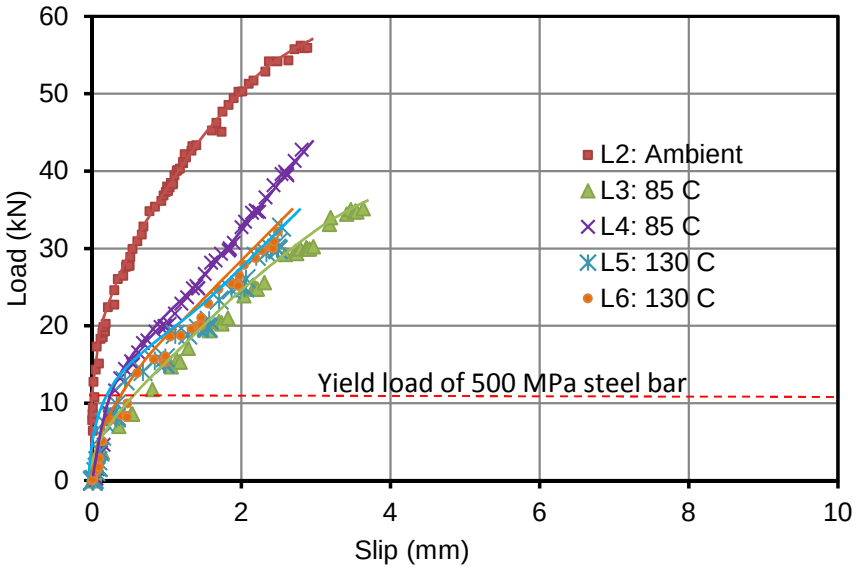

Figure 3.45 Load-slip response for Group A specimens,
(The response for L1 was not captured due to an equipment failure).

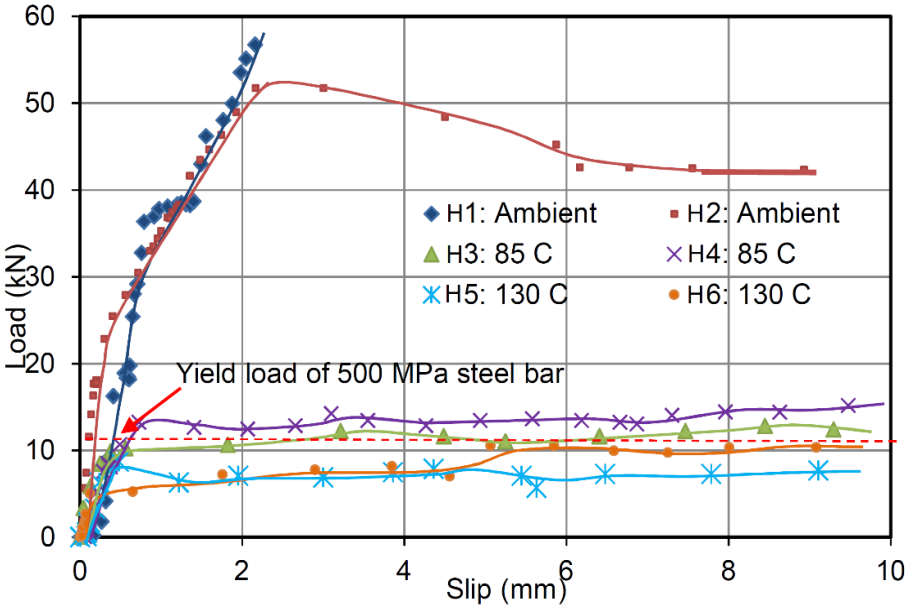

Figure 3.46 Load-slip response for Type H specimens.

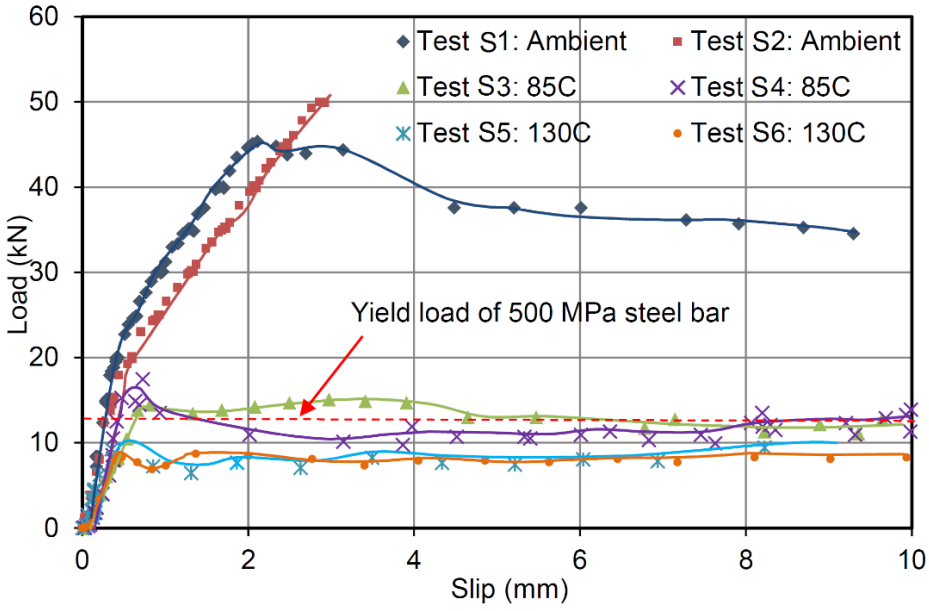

Figure 3.47 Load-slip response for Type S specimens.

3.6.8 Discussion of Push-off Ambient Temperature Results

Failure Loads and Mechanisms

At ambient temperature all specimens failed by reinforcement rupture within the free length between cubes (Figures 3.39-3.41), except one specimen of straight bars (S1), which failed by pull-out (Figures 3.42-3.43). Rupture within the free length of the reinforcement indicates that the reinforcement was sufficiently bonded to the concrete for it to reach its ultimate capacity. Although they have the same failure mode, the failure load of the specimen failed by rupture varied with a standard deviation of 6.7. This could be attributed to variability emerged from manual manufacture process of CFRP reinforcement, and/or any eccentricity in load applying. The only specimen that failed by pull-out failure at ambient is specimen of straight bar (specimen S1), (Figures 3.42-3.43). This could be an indication that the reinforcement development length is close to the embedded length of 133 mm used or can be a result of material variability.

Stress-Strain Response (Reinforcement Stiffness)

The change in distance between DIC patches 2 and 3 (Figure 3.38) on the free length of loop reinforcement was used to determine strain in CFRP reinforcements between concrete cubes. For stress calculation, it was opted to use the actual areas of carbon fibres rather than total area of reinforcement cross-section because the cross-sectional area of fibres tows and their mechanical properties are defined. Another reason is that although the produced reinforcement section was intended to be 5 mm square, the process of wet lay-up and winding fibres into grooves in the mould caused the produced reinforcement to have variation in section height as it was in the range of 4.9 to 6 mm. It is thinner at the curved part, where more tension is built up during winding process and thicker at middle of the straight portion. The area of carbon fibre tows used in reinforcement can be calculated as 25 rounds of carbon tows were used and cross-section of each tow are provided by the manufacturer as 0.444 mm^2 (Table 3.1).

The resulting stress-strain curve of Type L (loop reinforcement) is shown in (Figure 4.44). The slope of data is 231.2 GPa represents Young's modulus of carbon fibres, which is very close to the value provided by manufacturer 234 GPa (Table 3.1). The

lateral (out of plane) movement occurred in specimens with hooked and straight reinforcement induced error in deformation measured with DIC and therefore stress-strain response could not be generated. As a limitation of DIC it was found that the response just before failure might not be captured due to occurrence of deformation such as local rupture of fibres or splitting cracks within the tracked patches.

Load-Slip Response

The recorded load and DIC data was used to produce a load-slip response for the three groups of specimens, Figures 3.45 to 3.47. The obtained data of slip through DIC have some uncertain level of error due to some out of plane movement (rotation of concrete cubes) of specimens especially those with straight and hooked reinforcement. The lateral movement increases with slip, in Figure 3.43 unequal slip of bar can be seen. The provided lateral roller support on each side was found not to fully restrain cube rotation.

The slip was calculated as the difference in displacement between patches (1, 2) and (3, 4) in (Figure 3.38). The actual slip then was corrected by subtracting the elastic elongation in free length of the CFRP reinforcement using equation (3.1). The free length of CFRP is considered to be the length between the concrete blocks in addition to the length within the bond break area, i.e.190 mm, (Figure 3.30). The slip was also calculated as the average value of readings from both cameras on each side of the specimen (which should reduce error induced by lateral movement). The load-slip figures are marked with an 11.1kN reference load, which is the yield load of a 500 MPa steel bar with the same cross-sectional area of the fibres used in the reinforcement, 22.2 mm^2. It can be seen from Figures 3.45-3.47 all reinforcement types were able to develop failure load exceeds yield stress steel. As a general trend all specimens show a reduction in stiffness as load increases. This typical behaviour is attributed to the shearing off sand particles (Soong et al., 2011).

$$S_c = S_{1,4} - L\,\varepsilon_{2,3} \tag{3.1}$$

Where S_c = the corrected slip; $S_{1,4}$ = slip between patches 1 and 4; L = CFRP free length (190 mm); $\varepsilon_{2,3}$ = The strain in CFRP between patches 2 and 3; The term [$L\ \varepsilon_{2,3}$] = The elastic elongation.

3.6.9 Results of Push-off Heated Tests

Specimens Heating

A typical temperature progress curve of CFRP reinforcement and gas temperature inside the oven is shown in Figure 3.48. The graph shows the temperature recorded from two thermocouples, one placed on CFRP reinforcement (Figure 3.30), and the other measuring gas temperature inside the oven. Temperature was recorded at a rate of 1 Hz. The reinforcement temperature within the concrete lagged behind the gas phase temperature. It took 105 minutes to reach a T_g temperature 85 °C and almost 6 hours to reach 130 °C. The process of taking the samples out of oven and testing them took up to 7 minutes on average and during that time, CFRP temperature dropped by about 3 °C.

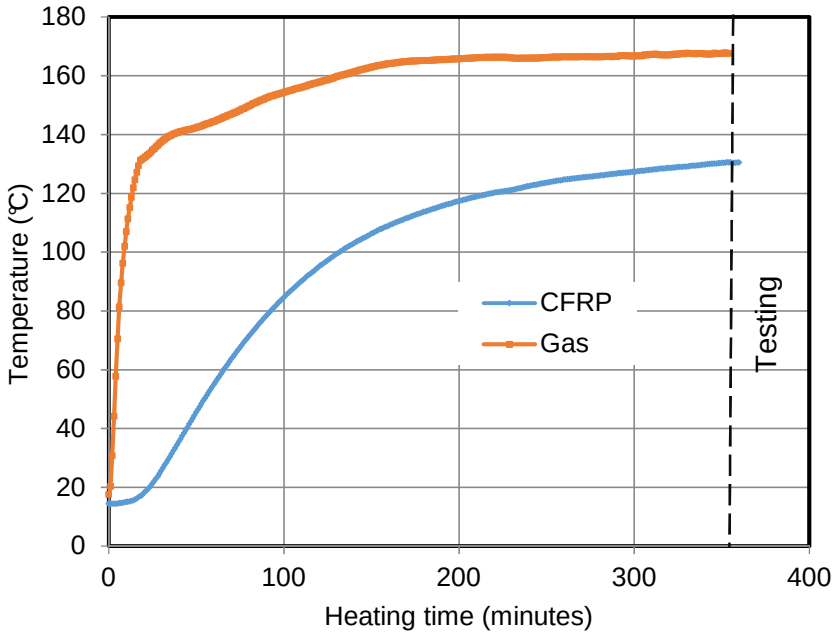

Figure 3.48 Temperature propagation during heating and testing of hooked reinforcement specimen B6.

Failure Load and Mechanisms

Table 3.10 shows failure load and mechanisms of push-off specimens in heated test. Figures 3.49-3.54 show failure modes of specimens from different types.

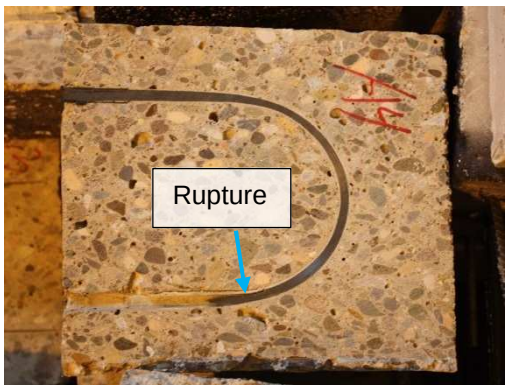

Figure 3.49 FRP rupture within the bonded area, L4 (85°C).

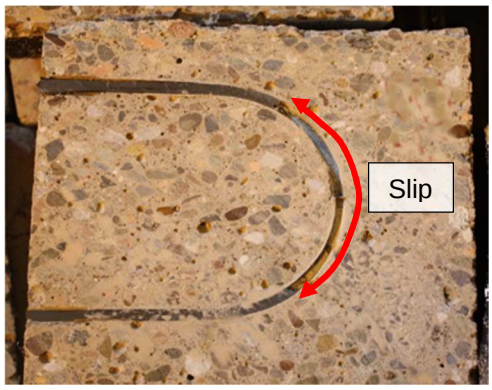

Figure 3.50 Pull-out of hooked FRP reinforcement, H4 (85°C).

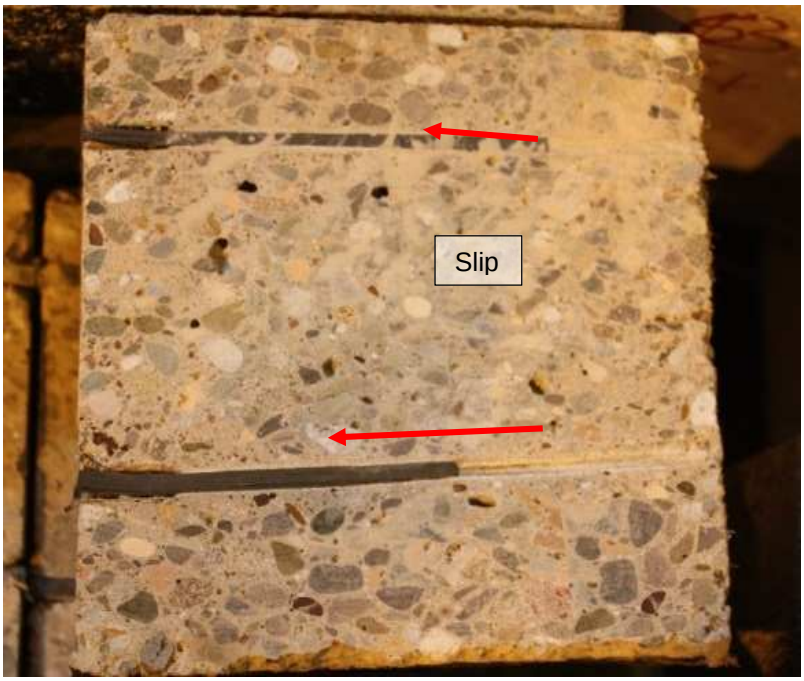

Figure 3.51 Pull-out of straight FRP reinforcement, S4 (85°C).

Figure 3.52 CFRP rupture at curved part, specimen with CFRP loop L6 (130°C)

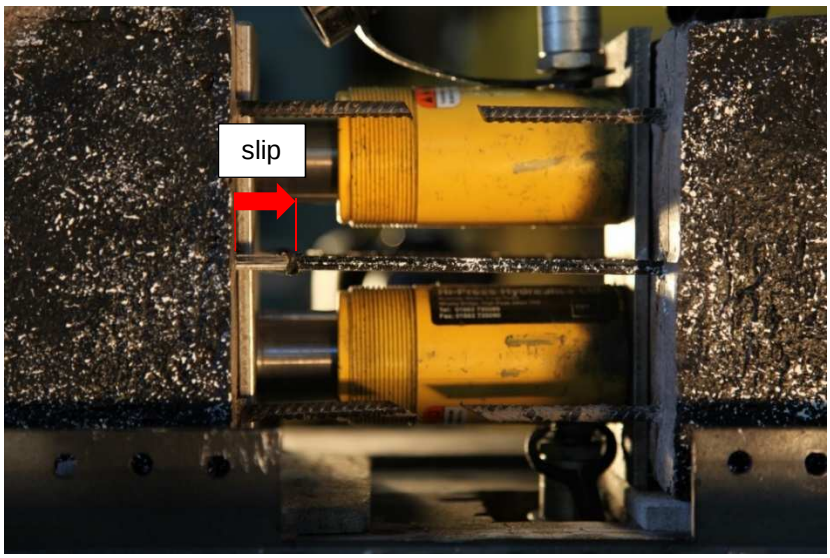

Figure 3.53 Pull-out failure of specimen with hooked reinforcement (specimen H6 at 130°C).

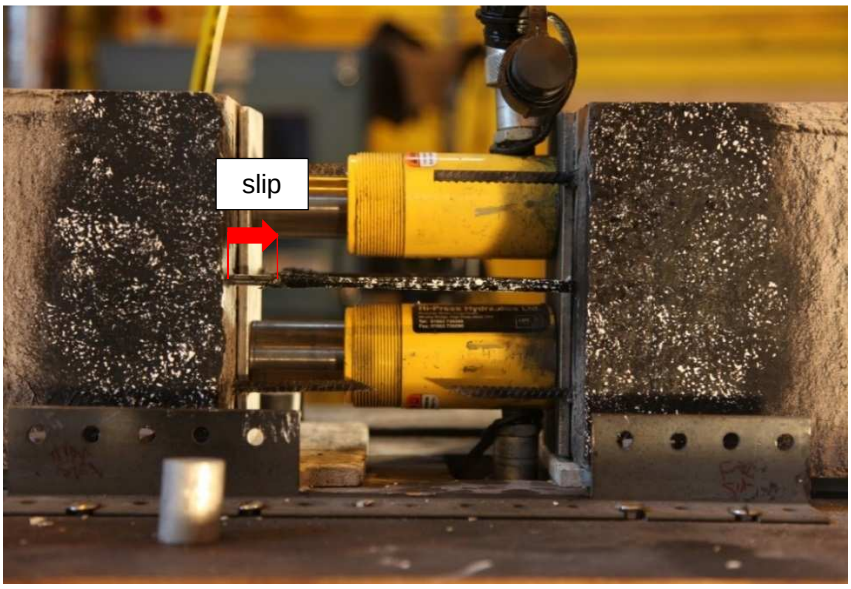

Figure 3.54 Pull-out failure of specimen with straight reinforcement (specimen S6 at 130°C)

Load-Slip Response

Figures 3.45-3.47 show load-slip response of specimens of different types in heated tests.

3.6.10 Discussion of Push-off Heated Tests Results

Failure Load and Mechanisms

Under heating, there was a clear difference in the responses between specimens reinforced with loops and those of straight and hooked reinforcement in term of failure load and mode. While all specimens of different types experienced strength reduction under heating, it was more severe for specimens with straight and hooked reinforcement.

At the glass transition temperature, resin softening caused a dramatic decrease of bond with concrete. For specimens with CFRP loops a reduction of about 37% occurred when specimens were heated until the reinforcement reached T_g (85 °C). Failure mode was maintained as rupture which indicates that the reinforcement was sufficiently anchored to concrete. CFRP loop reinforcement was able to maintain interaction with

concrete after resin softening, because the reinforcement is mechanically locked, with the closed loop embedded in concrete. Under heating, the rupture location of the loops changed from free length to curved part within the embedded region (Figure 3.52). The curved part of CFRP reinforcement has less strength than the straight portion due to stress concentration resulting from longitudinal stress and lateral stress from bearing with concrete. The effect of stress concentration is exaggerated due to the weakness of fibres in transverse directions (Ahmed et al., 2010; Shehata et al., 2000; Imjai et al., 2009). Rupture failure occurred within the free length at ambient temperatures because fewer forces (if any) were transferred to the curved part due to the bond with the concrete along the embedded length. However, surface bond degrades due to resin softening when heating the strength of the curved part determines the strength of the loop reinforcement.

The design guideline ACI (2015) includes an equation to calculate the reduced strength of FRP bars at bends (equation 3.2).

$$f_{fb} = (0.05\frac{r}{d} + 0.3)\, f_{fu} \leq f_{fu} \qquad (3.2)$$

Where f_{fb} = strength at bent up portion, f_{fu} = ultimate tensile strength, r = bend radius, d = bar diameter.

For r/d = 10, as used in this study, this equation predicts that the bent portion of the CFRP loop will be 20% weaker than the straight portion of the loop. However, a reduction of 31% was found when compares the average rupture load of loop straight portion at ambient in push-off test (Table 3.10), 61.5 kN, with average tensile capacity of curved part from tensile tests (Table 3.10) 42.6 kN. This agrees with Imjai (2009) observation that the ACI equation (3.2) can overestimate the bend capacity.

When hooked and straight bars reinforcement **were** heated to T_g the developed strength was reduced to only 25 to 35% of ambient strength and failure mode changed from rupture to pull-out. Slip of reinforcement can be observed from the sectioned off specimens (Figure 3.50-3.51). The severe reduction of bond strength at T_g demonstrates the poor performance of traditional FRP reinforcement at elevated

temperatures. Such severe strength reduction of CFRP bond strength under heating is reported by other researchers (Bisby et al., 2005; Katz et al., 1999; Saafi, 2002).

Further strength reduction occurred in specimens where reinforcement temperature increased to 130 °C (45 °C above T_g). CFRP loops developed strength about 52% of ambient temperature in contract to only 20% for specimens reinforced with straight and hooked bars. There was no significant advantage of hooked reinforced over straight bar as similar strength was achieved. Failure mechanism were the same as at T_g, CFRP loop failed due to rupture at curved portion (Figure 3.52), while both straight and hooked reinforced failed in debond by pull-out (Figure 4.53-4.54). It can be seen from **Figures** 3.45-3.47 while all reinforcement types were able to develop failure load exceeds yield stress steel at ambient temperature, at elevated temperature only CFRP loop achieved higher failure stress than streel counterpart.

Stress-Strain Response (Reinforcement Stiffness)

The slope of stress-strain data (Young's modulus) of CFRP loop did not change with temperature (Figure 4.44). The measured stiffness 231.2 GPa is very close to the value provided by manufacturer 234 GPa (Table 3.1). This provides a check upon the test method and also shows that the stiffness of carbon fibres is not affected by temperature within the tested range 85-130 °C.

Load-Slip Response

Under heating the stiffness is reduced as sand coating particles are sheared at lower loads when the binder resin softens. CFRP loops have no post-peak response, as they do not pull out, but fail by rupture. Softening occurred post to the peak in case of straight and hooked reinforcements followed by pull-out at a constant load due to abrasion between the bar and the concrete (Soong et al., 2011).

3.7 Summary

- The performance of the CFRP loops was assessed through tension tests and push-off tests at ambient and elevated temperatures. Specimens reinforced with straight and hooked reinforcement were also tested for comparison.

- Tension tests were used to evaluate the performance of loop in tension and to compare the performance of different loop designs. Results showed that no significant enhancement of tensile capacity was achieved with more complex designs over loop produced from continuous winding of carbon tows and with constant cross section. Therefore, this design is used in the rest of tests in the current study.

- The curved part is the critical segment CFRP loop where brittle rupture failure always occurs. Rupture failure occurred within the curved part of reinforcement due to the multiaxial stress status generated by axial tension forces and transverse forces by bearing against concrete.

- Push-off tests were used to demonstrate the performance of CFRP loop within concrete against straight or hooked reinforcement. At ambient temperature there was no clear distinction in performance. However, at elevated temperatures the benefit of CFRP became evident as three times higher strength was achieved in comparison to specimens with straight and hooked bars. In addition, CFRP loops under heating were able to develop rupture stresses exceeding a comparable yield stress of 500 MPa for steel reinforcement.

Chapter 4 – Ambient Four-Point Bending Test

4.1 Overview

In the previous chapter, the performance of CFRP loops compared to straight and hooked reinforcement was assessed through a series of tensile and push-off tests. Results showed that CFRP loops were able to develop higher failure load than specimens with straight and hooked CFRP bars at elevated temperatures. Tension and push-off tests provided a quick assessment but the tests configurations did not provide a good representation of reinforcement in beams. In the tension tests, the loops were tested bare (without being cast into concrete), while in the push-off tests splitting failure was minimised due to the thick concrete cover and the confinement pressure generated by the hydraulic jacks.

In this chapter, phase I and II of the bending tests upon beam specimens reinforced with either CFRP loops or straight bars at ambient temperature are presented. The concrete beams reinforced with CFRP loops were loaded in four-point bending, and beam specimens with straight CFRP bars were also tested for comparison. Phase I and II beam specimens differs in terms of concrete strength, transverse reinforcement, and length of heated region in heated tests.

In addition to the ambient temperature tests, in next the following chapter (5) heated tests were also carried out in which a gas radiant panel was used to heat the mid-span section of the beams while beams were held under a sustained load.

In the phase I beam tests at ambient temperature, the specimens with CFRP loops failed prematurely in concrete shear along loops overlap length. This failure mechanism indicated that a longer overlap length and/or transverse reinforcement is required. This failure mode was avoided in phase II by using a longer overlap length and transverse reinforcement.

4.2 Test Specimens and Nomenclature

In the beam specimens, CFRP loops were used as tension reinforcement. Four-point bending tests were carried out to demonstrate the loops' performance as flexural reinforcement. By comparing the performance at ambient and elevated temperatures of beam incorporating CFRP loops and others with CFRP straight bars, the effectiveness of the CFRP loops could be evaluated.

The CFRP reinforced beam specimens for the four-point bending test were designed in accordance with the design guidelines ACI (2015) and ISIS (2007), see Appendix C. The chosen cross-section for beams was 160×150 mm (Figures 4.1-4.2). Beams had length of 1610 mm and span of 1470 mm. Beams were either reinforced in tension with CFRP loops or straight CFRP rebars. Steel reinforcement was used as shear and compression reinforcement.

To compare the performance of beams reinforced with loops against straight bars at ambient and elevated temperatures, four types of specimens were produced for phase I (Figure 4.1), and three types for phase II (Figure 4.2). All specimens had the same reinforcement properties, but differed in reinforcement arrangements as detailed below:

Phase I specimens (Figure 4.1):

A. Beams reinforced with three overlapping CFRP loops. The loop in the middle is entirely within the heated region.
B. Beams reinforced with two loops overlapped within the heated region, while the other ends are positioned in region not directly exposed to fire.
C. Beams reinforced with straight bars spliced within the heated region

D. Beams reinforced with continued bars bridges the heated region.

Phase II specimens (Figure 4.2):

E. Beams reinforced with two CFRP loops overlapped along the heated region, while the other ends of loops were positioned in regions not directly exposed to fire.
F. The same as the type E specimens, but with transverse reinforcement was provided along the overlap region.
G. Beams reinforced with straight bars spliced along the heated region. Transverse reinforcement was provided along the overlap region.

Type A specimens were intended to represent the case where the whole loop was exposed to fire. Type B and C specimens represent the case where one end of reinforcement falls within heated region, while the other end is anchored in a region not directly exposed to fire. The reinforcement in these specimens overlapped within the heated mid-span, the effect of temperature on reinforcement interaction with concrete could be assessed through fire resistance time, deflection, cracks formation and failure mechanism.

Type D specimens had continuous reinforcement that bridges the heated region and was anchored in the ends of the beams that were not directly exposed to fire. The performance of specimen of type D will be used as a bench mark (control specimen) to assess the effectiveness of other reinforcement arrangement (types A, B and C) against.

In Phase II of the beam tests (E, F, and G) the design of the overlap or and bars splice regions was revised by providing transverse steel reinforcement (to provide confinement) and/or increased overlap length Figure 4.2.

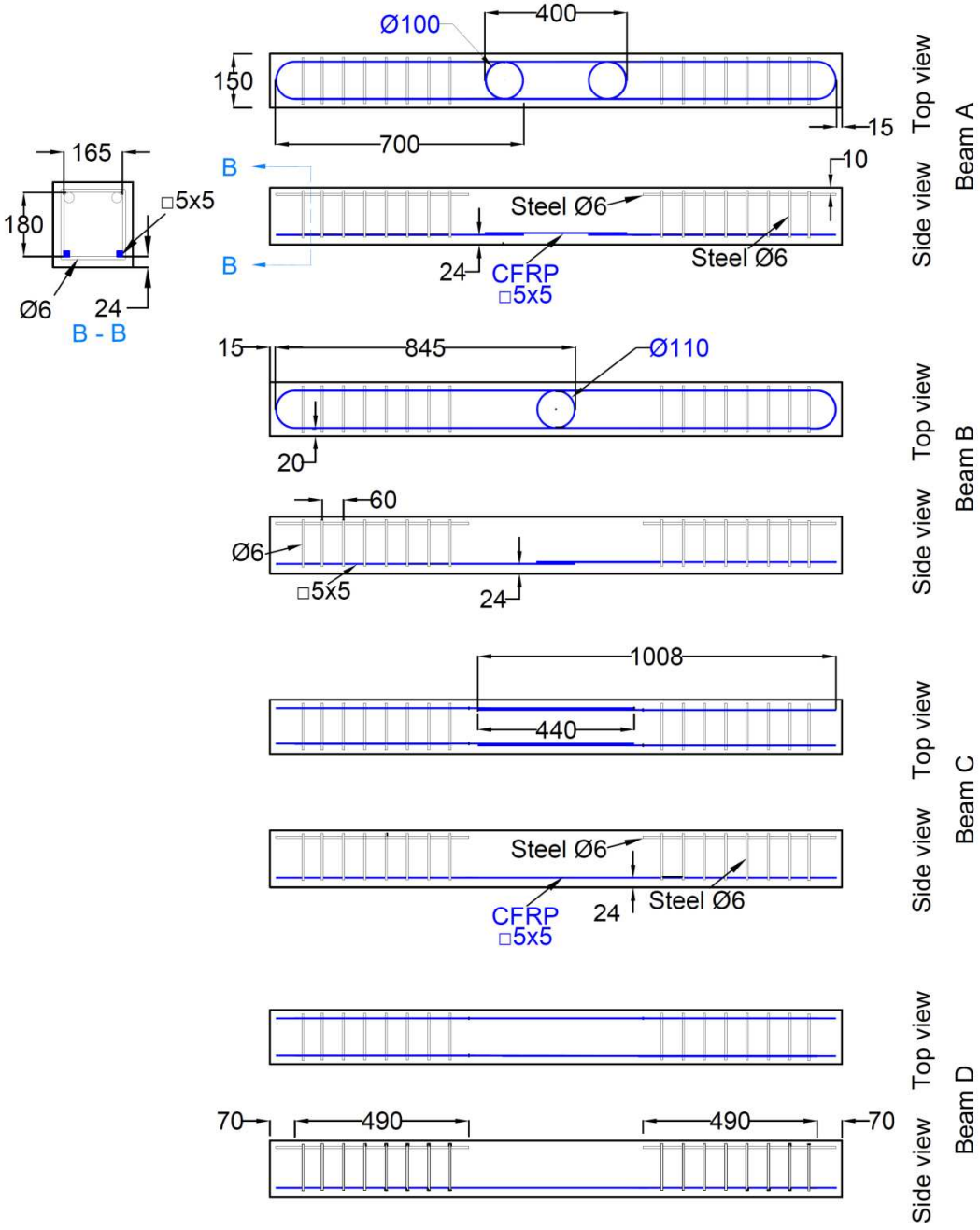

Steel compression bars omitted from beams top view

Dimensions in mm

Figure 4.1 Test specimens and reinforcement arrangement of phase I specimens.

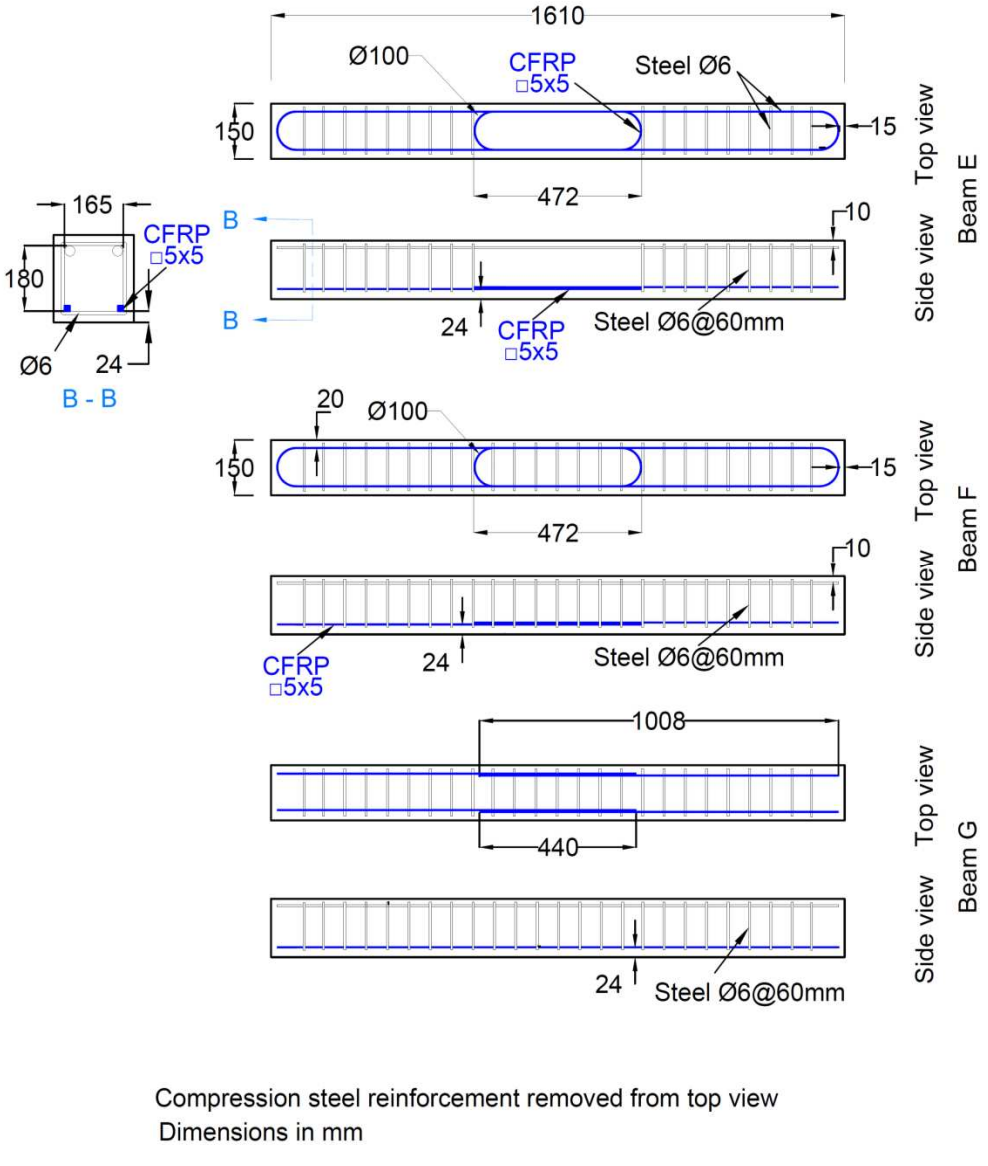

Figure 4.2 Test specimens and reinforcement arrangement of phase II specimens.

Strain compatibility analysis and the design equations of ACI (2015) and ISIS (2007) guidelines were used to obtain estimated values of the section flexural capacity, the required shear steel reinforcement, and CFRP bars development length. As the main aim is to assess the performance of FRP tension reinforcement, the beams were designed to be under-reinforced with reinforcement ratio 0.0011 (the balanced reinforcement ratio is 0.0025). The ultimate tensile strength of CFRP reinforcement was assumed the average value of the rupture stresses obtained from the push-off tests at ambient temperature; 56.76 kN (see Table 3.10). Based on this, the estimated flexural capacity of section was 7.1 kN-m which corresponds to a failure load of 30.0 kN (see Appendix C.1). Shear force and bending moment diagrams at the design failure load are shown in Figure 4.3.

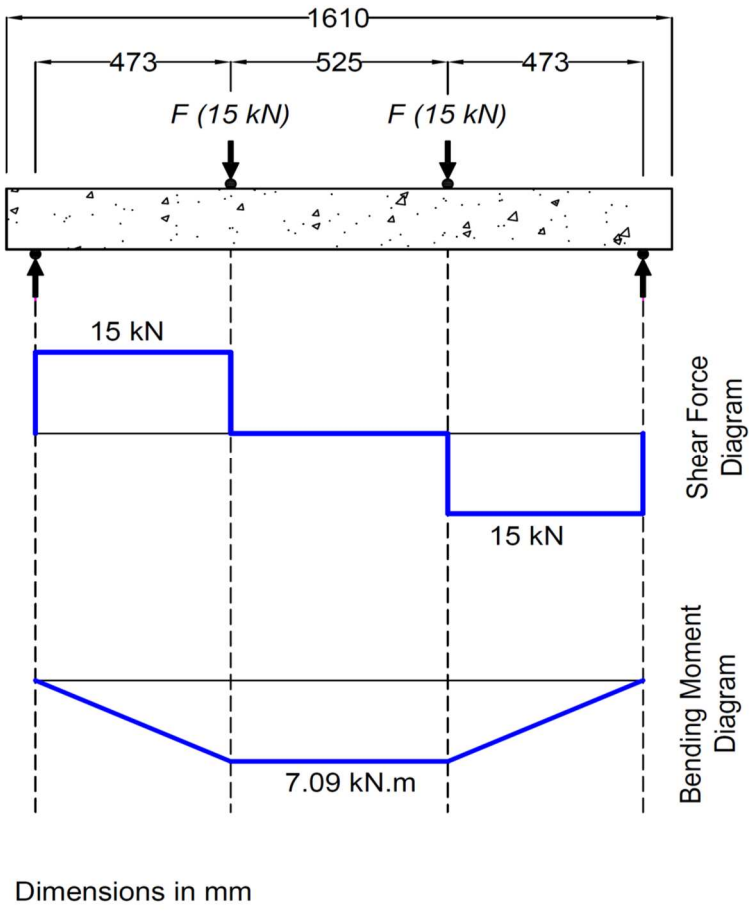

Figure 4.3 Shear force and bending moment diagrams of beam under four-point bending test.

4.2.1 Failure Criteria

The failure criteria for the beam specimens at both ambient and elevated temperatures was defined as one of the following conditions: rupture of CFRP reinforcement, crushing of concrete in compression area, bond failure, or when deflection exceeds L/30 as defined by BS 476: Part 20 (British Standard Institution, 1987).

4.3 Experimental Programme

By comparing the performance of beams reinforced with CFRP loops and straight bars, the effectiveness of the proposed design of CFRP loops could be evaluated. A total of twenty-eight specimens, four in each type, were included in the testing programme, as shown completely in Tables 4.1 for phases I and II. Two specimens from each type (A, B, C, D, E, F and G) were tested under these two following conditions:

- Unheated (at ambient temperature).
- Heated at the mid-span using a gas radiant panel.

Beam specimens at ambient temperature were loaded under displacement control at 2 mm/min until the specimens reached failure. In the heated tests, all of the specimens were held under a sustained load and localised heating was applied using a gas radiant panel over the central region of the beams. Heated tests are discussed in the chapter 5.

Table 4.1 Beam specimens nomenclature and descriptions for ambient tests

Beam Type	Reinforcement	Ambient Test (static monotonic loading of 2 mm/min)
Phase I		
A	Spliced CFRP loops (two loops)	A1
		A2
B	Spliced CFRP loops (three loops)	B1
		B2
C	Spliced straight CFRP bars	C1
		C2
D	Continuous straight CFRP bars	D1
		D2
Phase II		
E	Spliced CFRP loops	E1
		E2
F	Spliced CFRP loops with mid span stirrups	F1
		F2
G	Spliced straight CFRP bars	G1
		G2
Total Number of specimens		**14**

4.4 Mechanical Properties of Constitutive Materials

4.4.1 CFRP Reinforcement

The CFRP reinforcement was made of the same carbon fibres tows that were used in the previous tension and push-off test series (Chapter 3). The mechanical and thermal properties of carbon fibre tows are listed in Tables 3.1-3.3. A different type of two component epoxy resin (EL2) was used to impregnated the carbon fibres tows in the

beam tests. The mechanical properties of the epoxy as provided in the product datasheet are listed in Table 4.2.

Table 4.2 Mechanical properties of EL2 epoxy resin.

Property	Typical Test Value	ASTM Method
Tensile Strength	72.4 MPa	D638 Type[1]
Tensile Modulus	3.18 GPa	D638 Type[1]
Elongation	5.0%	D638 Type[1]
Compressive Strength	86.2 MPa	D695
Flexural Modulus	3.2 GPa	D695
Flexural Strength	123.4 MPa	D790
Flexural Modulus	3.12 GPa	D790

[1]Testing temperature 21℃ Crosshead speed 13mm/min.

4.4.2 Concrete

Ready-mix concrete of class C25/30, consistency S2, and 10 mm aggregate were used to produce the beam specimens. Cube samples size of 100 mm and cylinders samples size of 100×200 mm were used for compression and tensile tests. The cubes and cylinders were prepared and stored with beam specimens, then tested at 28 days. Tables 4.3 and 4.4 show the compression test results of phase I and II cube specimens. The mean cube compressive strength was found to be 42.37 MPa for phase I while was found to be 23.7 MPa for phase II. The difference of concrete strength between the two phases was not intentional, but it occurred due to a delivery of under-strength ready mix concrete. The concrete tensile strength was measured by the indirect split-cylinder test method, and the Eurocode 2 (BS EN 12390-6, 2009) empirical formula was used to calculate tensile strength f_{ct} from the failure load F of the split-cylinder test, equation (4.1). Results of tensile split test are listed in Tables 4.5 and 4.6 for phase I and II respectively.

$$f_{ct} = \frac{2F}{\pi LD} \tag{4.1}$$

Where: f_{ct} is the concrete tensile strength, F is the failure load, L is the cylinder height, D is the cylinder diameter.

Table 4.3 Results of cube tests at 28-day age (Phase I specimens).

Sample Label	Compressive Strength f_c' (MPa)
C1	39.4
C2	44.5
C3	43.2
Mean Value	42.4

Table 4.4 Results of cylinder tensile splitting test at 28-day age (Phase I specimens).

Sample Label	Failure Load F (kN)	Split tensile strength f_{ct} (MPa)
S1	83.30	2.65
S2	93.70	2.98
S3	90.60	2.88
Mean Value	89.20	2.84

Table 4.5 Results of cube tests at 28-day age (Phase II specimens).

Sample Label	Compressive Strength f_c' (MPa)
C1	23.4
C2	23.5
C3	24.3
Mean Value	23.7

Table 4.6 Results of cylinder tensile splitting test at 28-day age (Phase II specimens).

Sample Label	Failure Load *F* (kN)	Split tensile strength f_{ct} (MPa)
S1	40.1	1.28
S2	48.3	1.54
S3	49.1	1.56
Mean Value	45.8	1.46

4.4.3 Steel Reinforcement

The steel reinforcing bars used as compression and shear reinforcement were 6 mm ribbed steel with a measured yield stress of 550 MPa (Batson, 2013).

4.5 Beam Specimens Preparation

4.5.1 Manufacture of CFRP Reinforcement

The CFRP reinforcement loops were made by the same manufacturing process as the reinforcement used in the tension and push-off tests in the previous chapter (section 3.3), except that the length of reinforcement was changed according to the dimensions shown in Figures 4.1 and 4.2. The same PVC moulds (Figures 3.3) as were used to produce loops for push-off test were used to produce the short loops in the beam specimens of group A (Figure 4.1). Moulds of a longer length were manufactured to produce the longer loops (Figure 4.4).

Figure 4.4 Producing CFRP loops for specimens Beam A and B by winding carbon filaments around a PVC mould.

The straight bars for specimen type D were 1580 mm long, and these were difficult to form as a loop from which the straight bars could be cut (as was the case for the straight bars in the push-off test). Instead, the PVC moulds which were used to produce the loops for beam specimens type A and B were aligned and then carbon fibres tows were pulled inside the grooves of the moulds (Figures 4.5-4.6). For each bar, the carbon fibres were pulled back and forth within the mould grooves in 25 layers and were anchored at both ends to keep some tension force in fibres similar to the case when winding around a mould for loops producing (Figures 4.7-4.8). Epoxy resin was applied to each layer of the carbon fibres tows by a brush. The shorter straight bars of

beam specimens type C were made in the same way as the longer bars of beam specimens type D, and then were chopped off using a cutting disk.

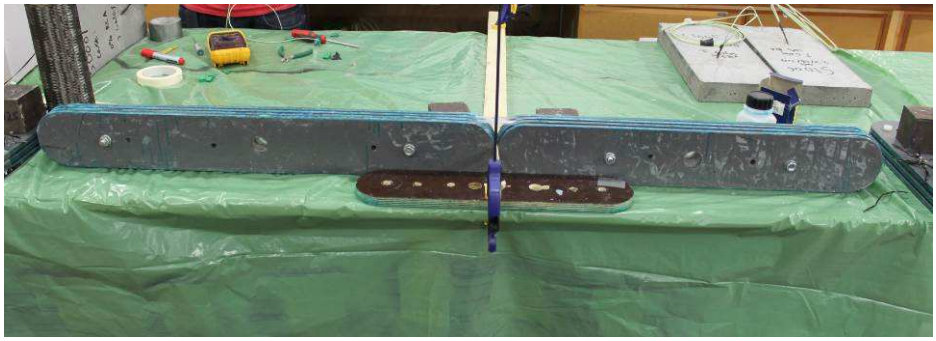

Figure 4.5 Two CFRP PVC moulds are aligned to produce straight bars

Figure 4.6 Epoxy saturated carbon fibre tows laid into mould grooves to produce CFRP straight bar.

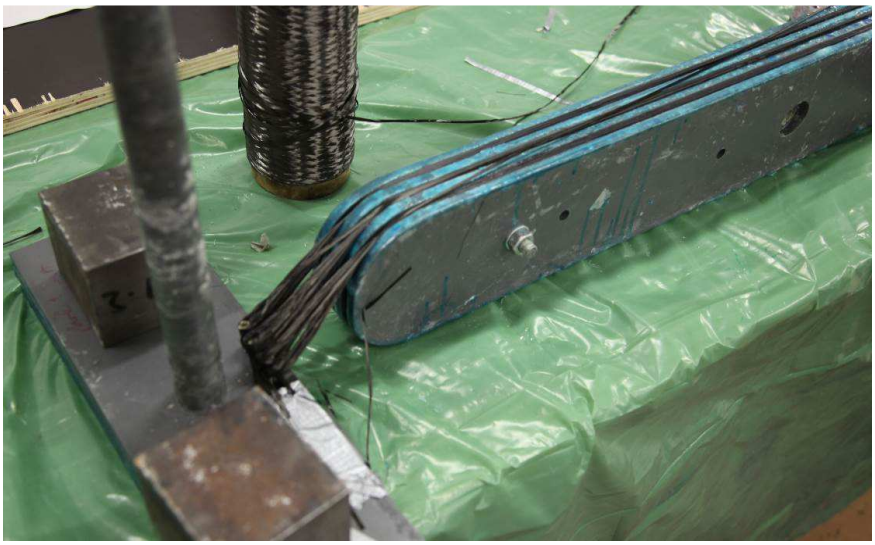

Figure 4.7 Carbon fibre tows anchored at each side of mould.

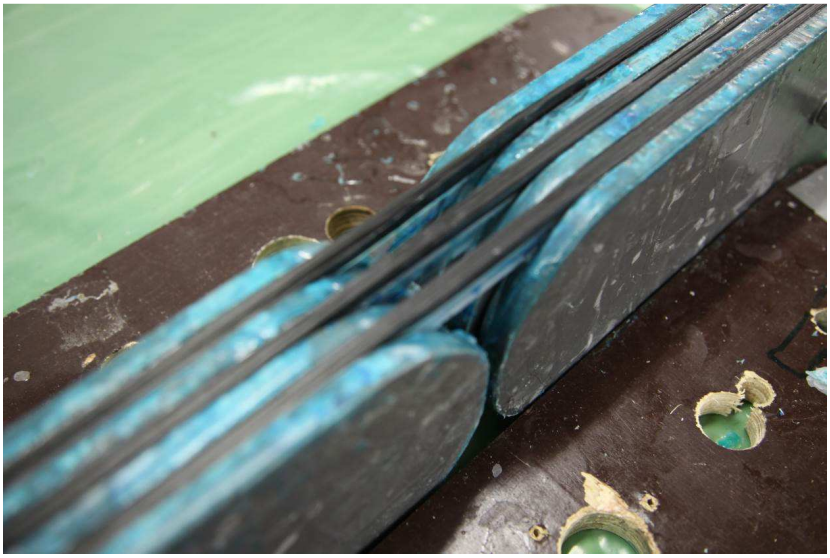

Figure 4.8 Straight CFRP bars inside mould.

After ambient cure for 24 hours, the specimens were sand coated using fine glass sand and epoxy resin as a binder. After 24 hours, all of the CFRP reinforcement was post-cured at 60 °C for 12 hours. The CFRP reinforcement of beam specimens A, B, C and D after curing and coating are shown in Figures 4.9-4.11. Two sample for dynamic mechanical analysis were prepared and tested as previously discussed in section 3.2.2. Results of DMA test are provided in Appendix A. The glass transition temperature, T_g, was found to be 87.6 °C.

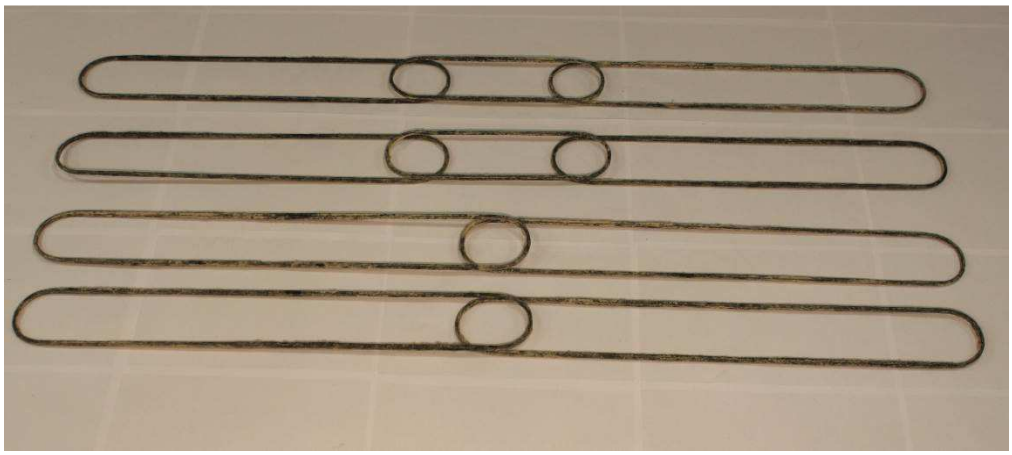

Figure 4.9 Sand coated CFRP loops reinforcement for beam specimens A and B

Figure 4.10 Sand coating of CFRP loop reinforcement.

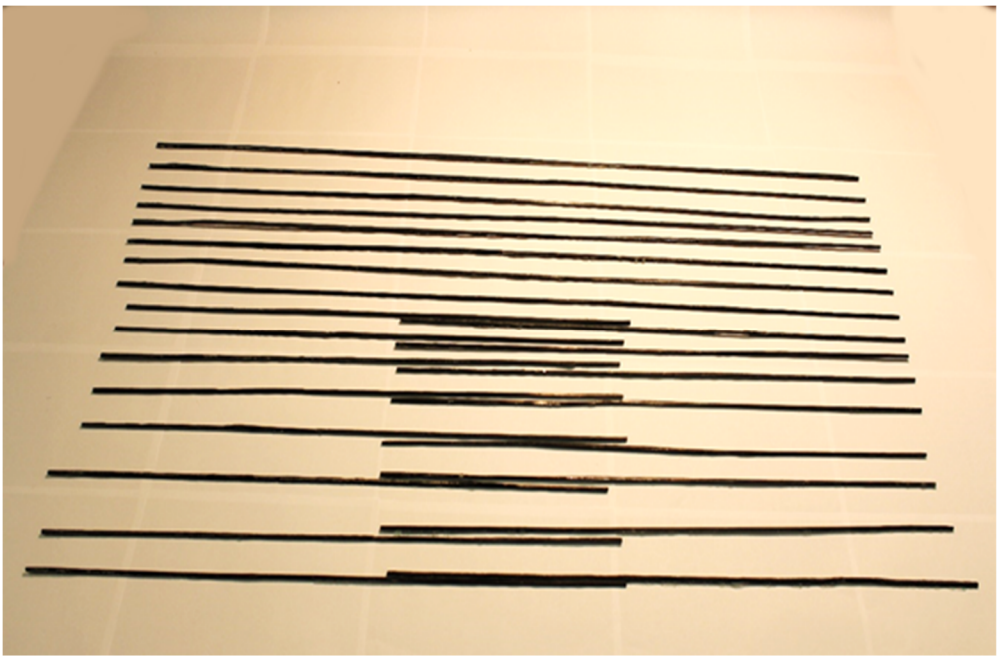

Figure 4.11 Uncoated CFRP straight bars for beam specimens C and D.

4.5.2 Installing Strain Gauges

For phase II beam specimens strain gauges were glued to CFRP reinforcement surface directly (not on the sand coating) with epoxy resin to monitor strain development of CFRP reinforcement (Figure 4.12). In case of overlapped loops, they were stacked above each other and therefore the stain gauges were installed on top surface of the upper loop (Figure 4.13). Spliced straight bars were placed at the same level with stain gauges glued to the upper surface. After being glued to the reinforcement, the strain gauges were coated with silicone rubber to protect them from moisture (Figure 4.13).

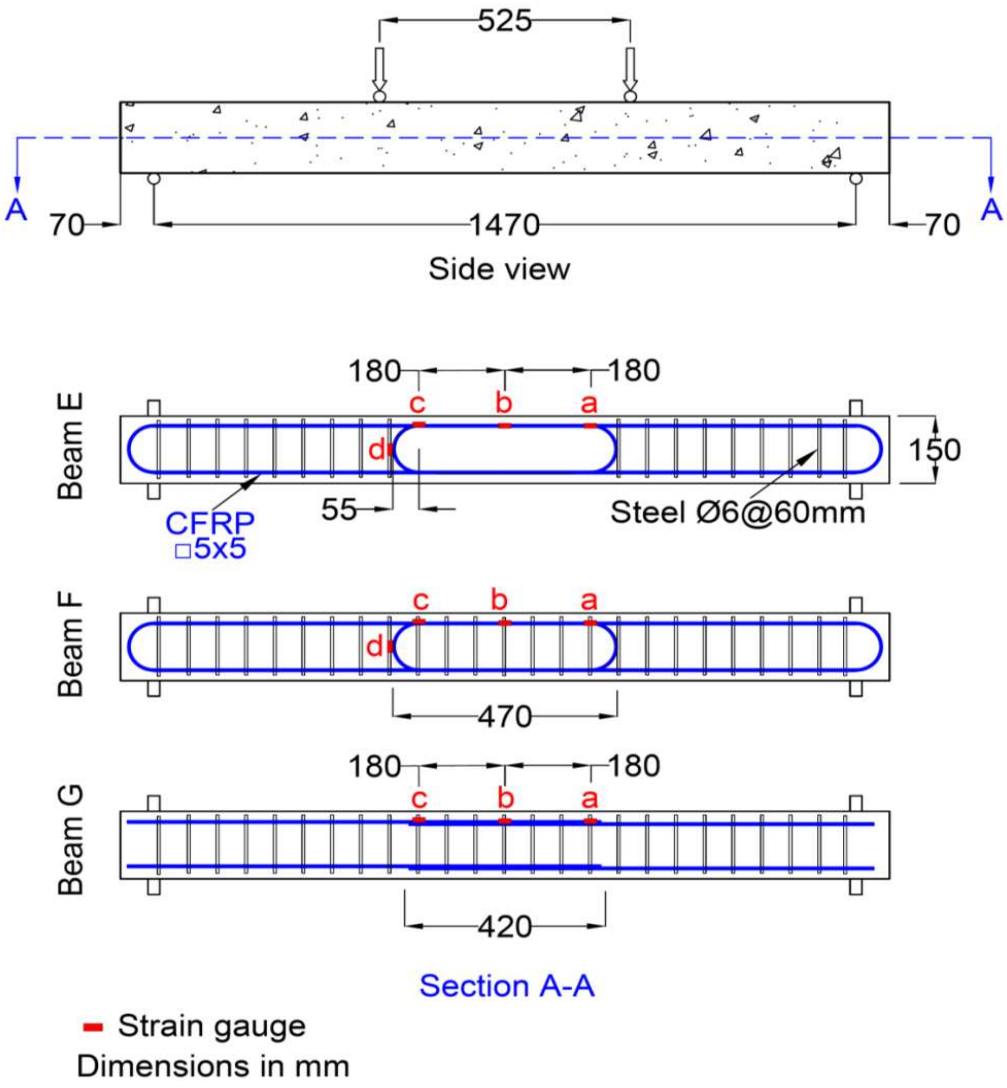

Figure 4.12 Location of strain gauges on CFRP reinforcement.

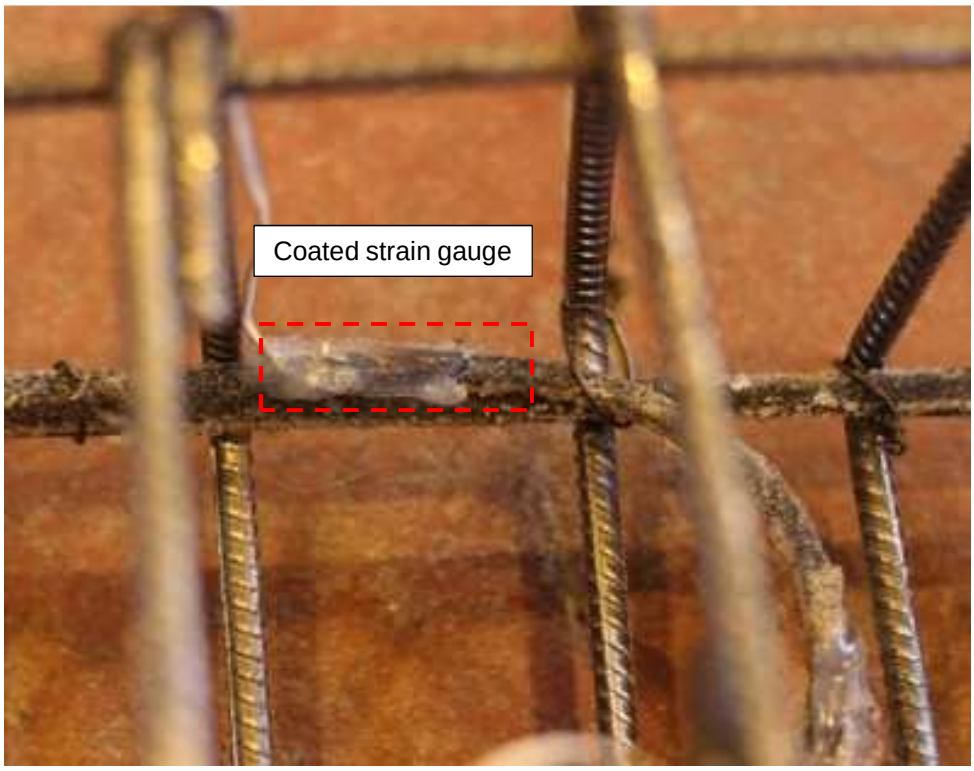

Figure 4.13 Strain gauge installed on CFRP loop and covered with coating material.

4.5.3 Steel Reinforcement

Steel reinforcement bars (with the properties given in section 4.4.3) were used as the upper reinforcement and shaped as stirrups (Figures 4.14-4.15) in accordance with the design dimensions shown in Figures 4.1-4.2. Afterwards, the hybrid (CFRP and steel) reinforcement cages were assembled. Concrete spacers were attached to the cages to give the required concrete cover.

Figure 4.14 Ribbed 6-mm steel rebar used as upper and shear reinforcement.

Figure 4.15 Steel stirrups used as shear reinforcement for beam specimens.

4.5.4 Formwork for Beam Specimens

The beam specimens were cast in plywood formwork made of 18-mm plywood sheets. The formwork was braced across the width to increase the stiffness of specimen and help tidying the thermocouples cables (Figure 4.16).

Figure 4.16 Reinforcement cages placed in plywood formwork ready for concrete casting.

4.5.5 Concrete Cast

Ready-mix concrete was cast in two layers inside the formwork and a mechanical vibrator was used to consolidate each layer of concrete. Once casting work was complete and while still placed in the formwork, the specimens were covered with polyethylene sheets and left for 48 hours for ambient curing.

4.5.6 Specimens Curing

After initial curing for 48 hours, the formworks were stripped and beams were moved to a conditioning room where specimens were kept for three months at a relative humidity maintained at about 47%. The curing conditions were intended to reduce the moisture content of specimens to alleviate the risk of concrete spalling when heated.

4.6 Instrumentations

As the beam specimens were to be tested in four-point bending, suitable instruments were needed to apply load and to measure the corresponding deflection of the specimens. Load was applied by means of a hydraulic actuator. Linear potentiometers and digital image correlation were used to record the beam specimens' corresponding deflection.

4.6.1 Linear Potentiometer

Linear potentiometer (LP) displacement transducers were used to monitor the mid-span deflection of the tested specimens (Figure 4.17). The displacement transducers had a stroke of 100 mm, run with 10V excitation voltage, and provided an accuracy up to 0.01 mm.

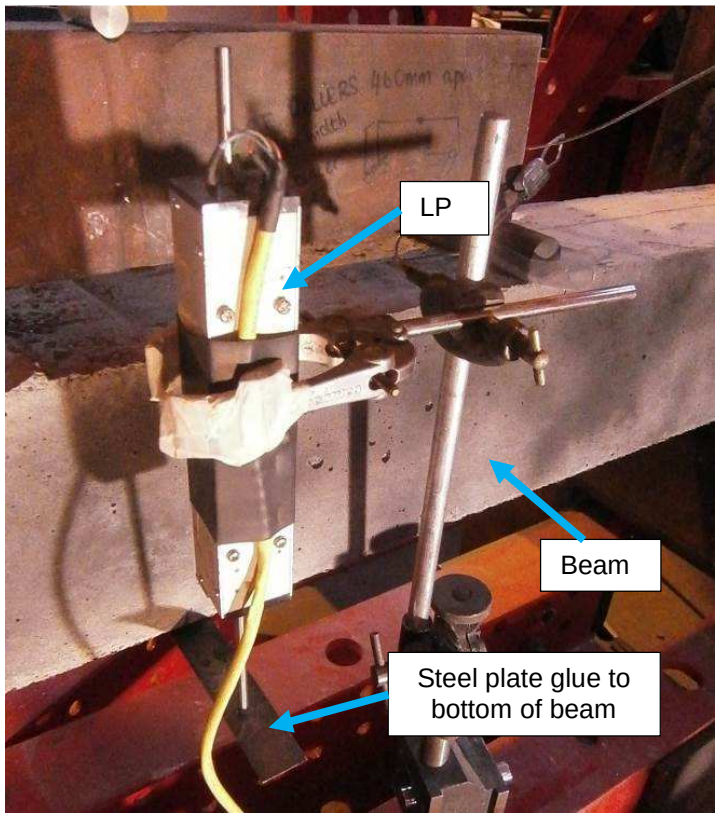

Figure 4.17 Linear Potentiometer displacement transducers to measure the deflection at the mid-span of beam.

4.6.2 Strain gauges

Foil strain gauges (TML FLA-5-11) with a gauge length of 5 mm were used to monitor the strain of the CFRP reinforcement within the loop overlap and the bar splice length in ambient temperature tests of phase II specimens. Four strain gauges were installed on CFRP loops and three on spliced straight bars at locations shown in Figure 4.12. The strain gauges are intended to provide information about the strain in the reinforcement which could be linked with the bond stress distribution for the CFRP loops and CFRP bars.

4.6.3 Canon DSLR Cameras

To conduct digital image correlation (DIC) analysis for central beams deflection, two Canon DSLR cameras were used. The beam specimens were initially painted with a high-contrast pattern (black with white speckles), then a Canon EOS 700D and a Canon 5D Mark II, whose high resolution was 18 MP and 21.2 MP respectively, were

placed on either side of the tested specimens and adjusted to capture images at a rate of 0.2 Hz (Figure 4.18).

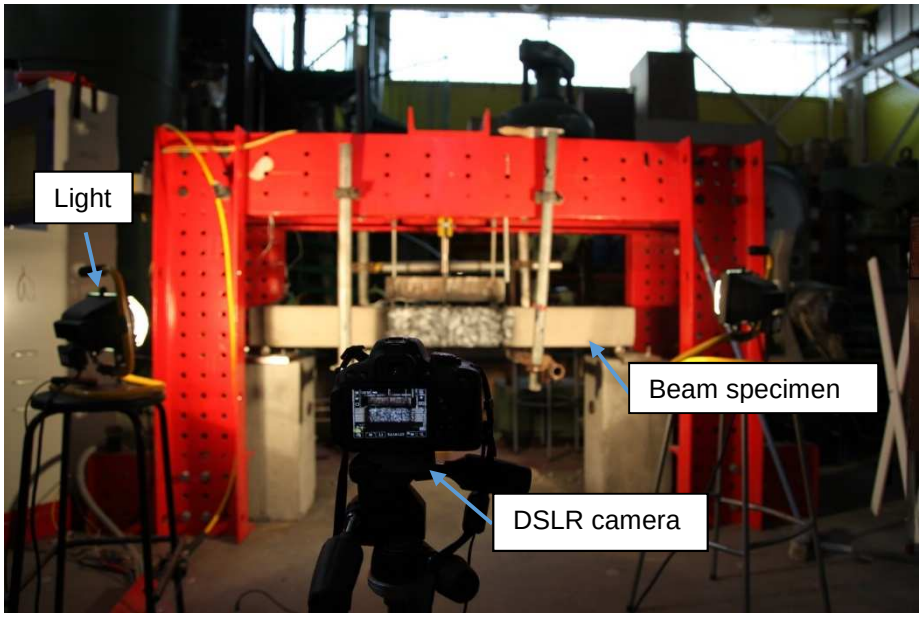

Figure 4.18 DSLR camera used to capture sequence of images of beam under testing for DIC analysis.

4.6.4 Instron 8800 Actuator

A 250-kN general purpose servo-hydraulic actuator with 250-mm stroke was used to apply load on the beam specimens during the ambient tests. The actuator is computer controlled, which allows precise control of the load value and loading rate, or displacement and displacement rate. The applied loading was transferred to the tested beam through a steel spreader beam (Figures 4.19-4.20).

4.7 Experimental Arrangements and Procedures

The beam specimens were tested in a four-point bending configuration at ambient temperature. The beam specimens were placed in the testing frame on roller supports and the load was transferred from actuator to the tested beam through a spreader beam placed on the top (Figure 4.19-4.20). High resolution cameras were placed at either side of the tested beam to capture images of specimens under testing at rate of 0.2 Hz for deflection measurement using DIC technique (Figure 4.18). Load and deflection

data were timely synchronised with DIC photos. The deflection of beams was also monitored through a linear potentiometer (LP) which was positioned on steel plate glued to the bottom of beam at the mid-span (see section 4.6.1). Using the hydraulic actuator (Instron 8800) in displacement control, load was applied at a displacement rate of 2 mm/min until failure occurred. The load-deflection response (from the actuator and the LP) of the tested beams was recorded by a data acquisition system at a rate of 10 Hz.

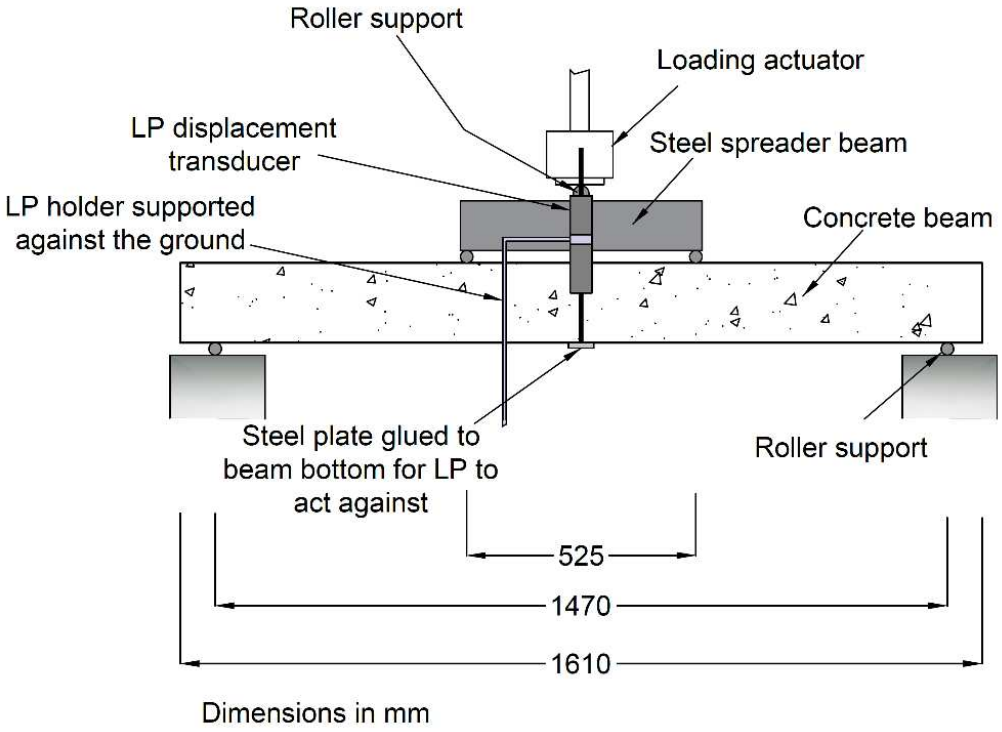

Figure 4.19 Schematic of four-point bending test at ambient temperature.

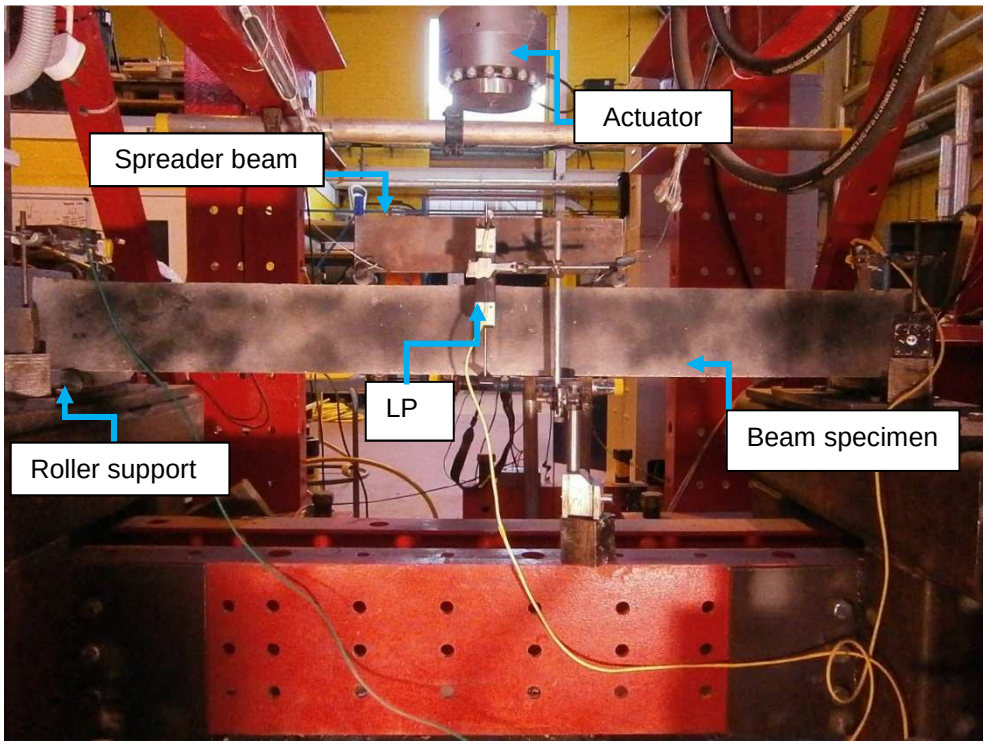

Figure 4.20 Test arrangement of four-point bending test at ambient.

4.8 Results

Load deflection Response:

The Figures 4.21 and 4.22 shows the load deflection response of beam specimens of phase I and II with different reinforcement arrangements tested in four-point bending configuration at ambient temperature. For specimen D2 there was a data logging error, and consequently only the failure load was captured. The deflection data used in Figures 4.21 and 4.22 were extracted from the LP readings. Comparisons of load-deflection response using the deflection data from LP and DIC of selected specimens are shown in Figures 4.23-4.24, which shows that both methods produce very similar results.

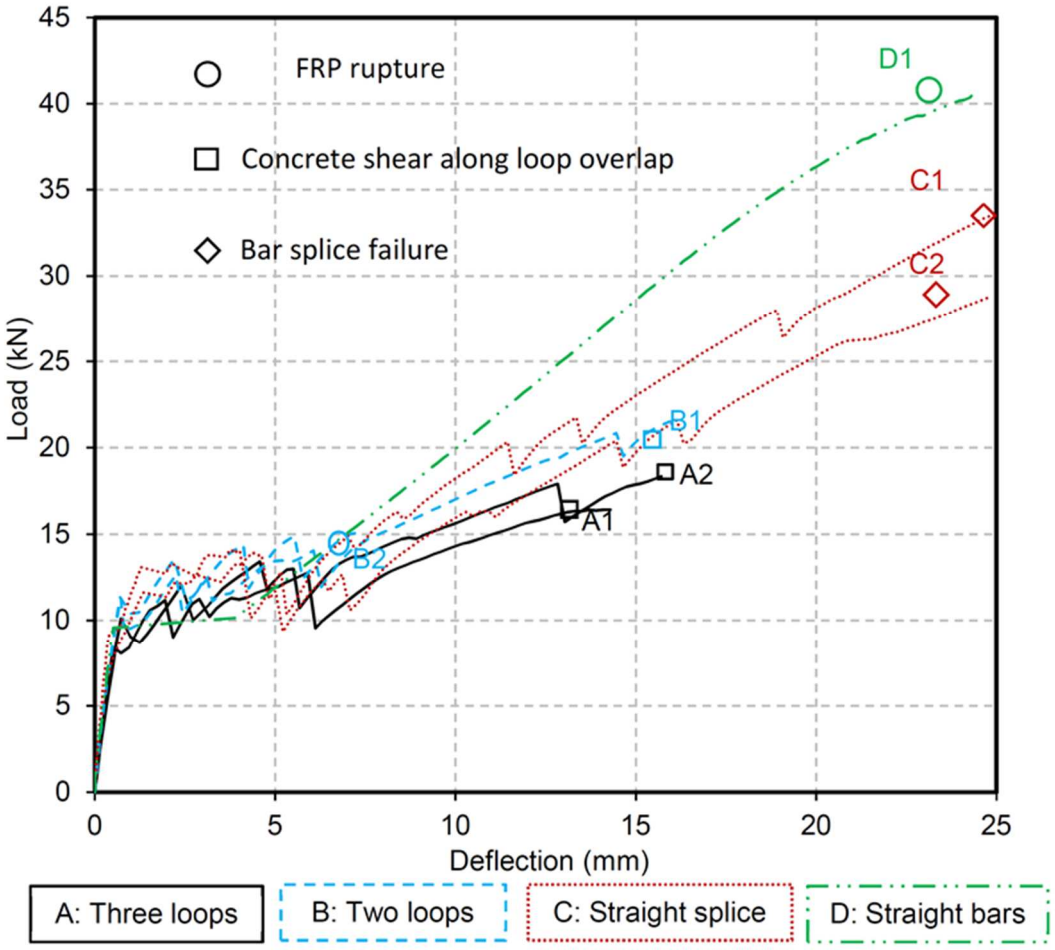

Figure 4.21 Load-deflection response of phase I beam specimens at ambient temperature.

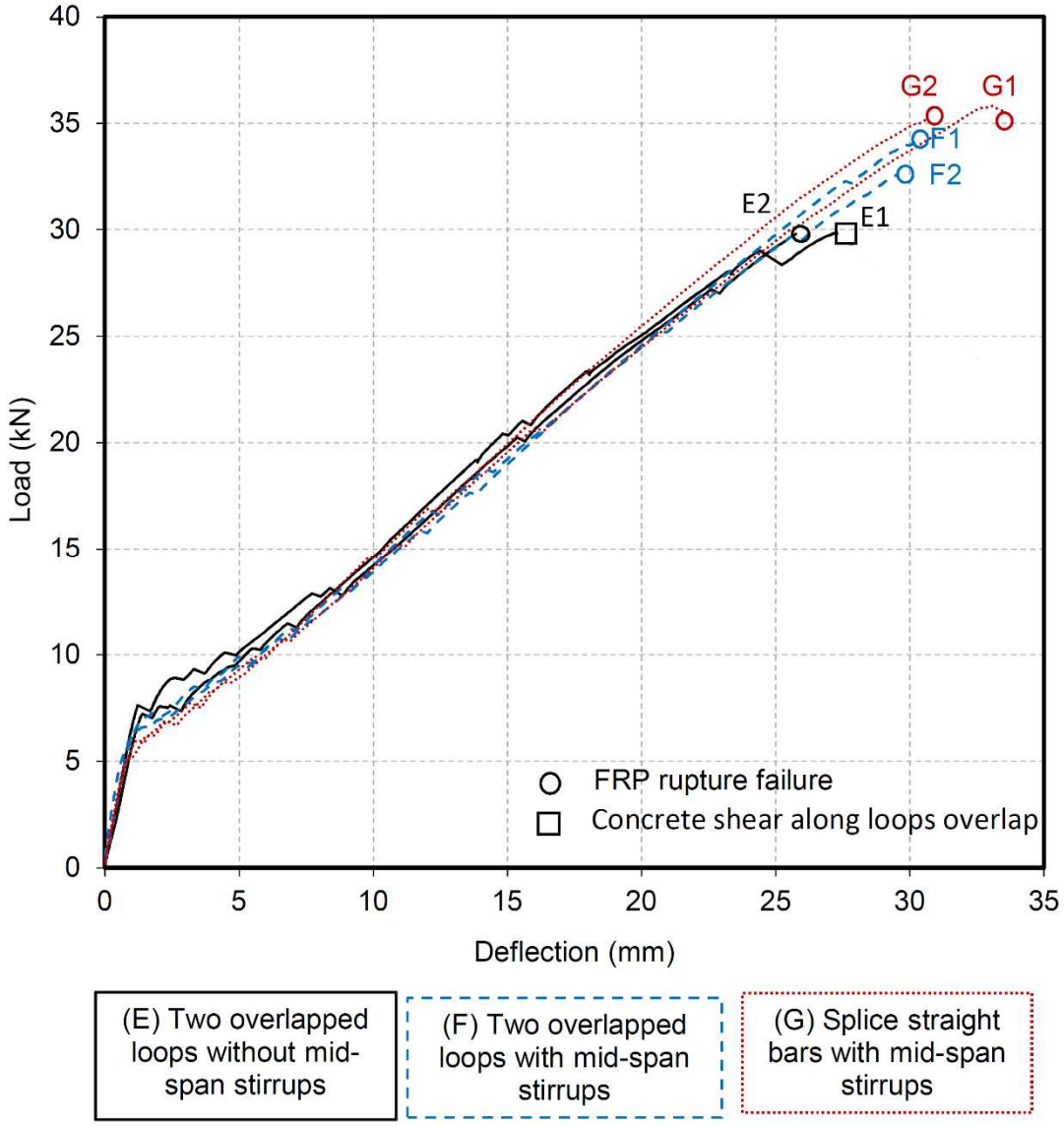

Figure 4.22 Load-deflection response of phase II beam specimen at ambient tests.

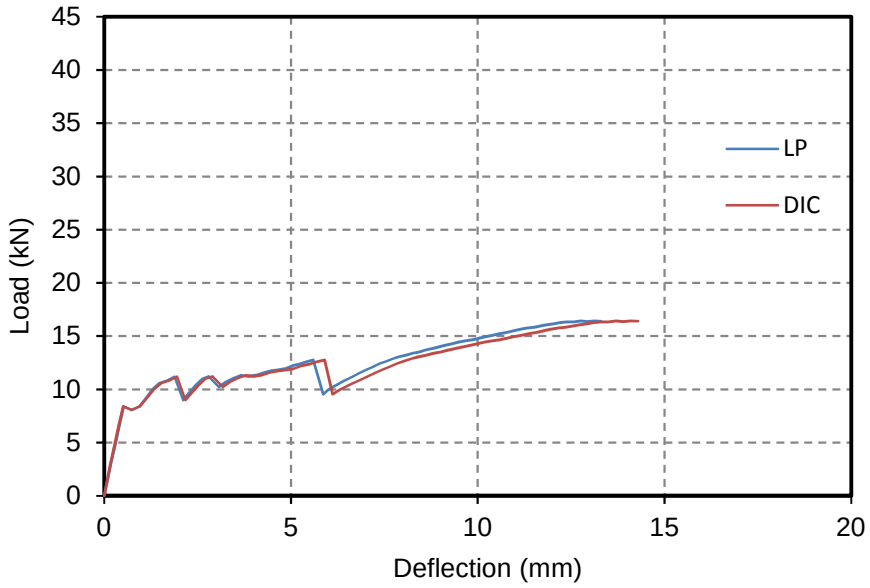

Figure 4.23 Comparison of load-deflection response of beam specimen A1 using deflection data from LP and DIC.

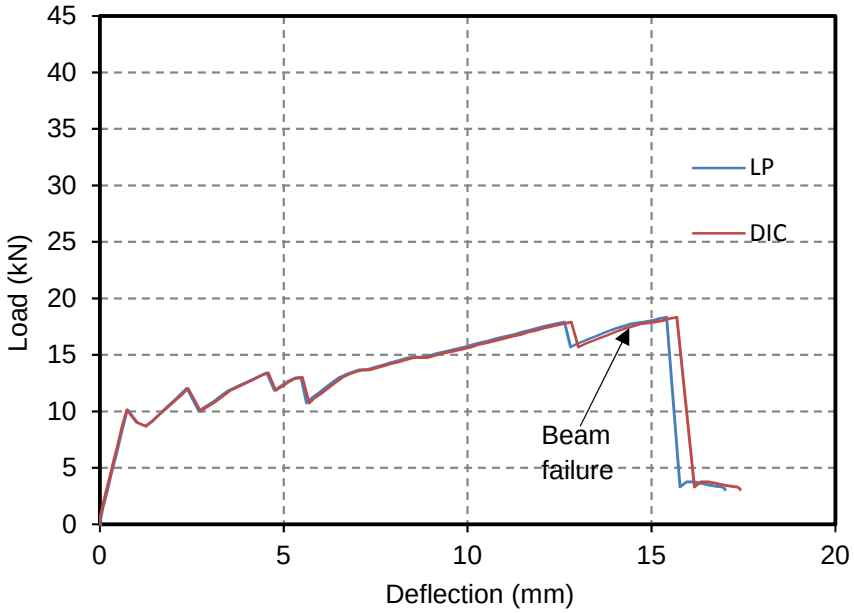

Figure 4.24 Comparison of load-deflection response of beam specimen A2 using deflection data from LP and DIC.

Specimens Failure loads and mechanisms

Table 4.6 lists the failure loads and mechanisms of beam specimens of phases I and II. Three types of failure mechanisms occurred. In beams with overlapping CFRP loops (A and B), except B2, a premature failure occurred as concrete shear along the overlap length. Figures 4.25 to 4.27 shows this type of failure. Beam specimens with spliced straight bars (type C) also failed prematurely in splice due to concrete splitting along the splice length as can been seen in Figure 4.28. Specimens with continuous straight bars developed the highest failure load and failure occurred as FRP rupture (complete cut of FRP reinforcement at failure location) as it can be seen in Figure 4.29. The areas where failure occurred in relation to reinforcement arrangements are shown in Figures 4.30-4.31.

For phase II specimens two types of failure mechanisms occurred. Only beam specimen (E1), reinforced with overlapped loops without mid span stirrups, failed due to concrete shear along overlap length (Figure 4.32). In all other beam specimens, failure occurred by FRP reinforcement rupture within the constant moment region outside the overlap or splice length. Figures 4.33 to 4.35 show this type of failure. The areas where failure occurred in relation to reinforcement arrangement are shown in Figure 4.36.

Table 4.7 Failure loads and mechanism of beam specimens at ambient temperature

Specimens	Age (Days)	Concrete cover for both bars (mm)[1]	Failure load (kN)	Failure mechanism
Phase I specimens				
A1 (Three loops)	259	25, 29	16.4	Shear in overlap
A2 (Three loops)	259	24, 25	18.3	Shear in overlap
B1 (Two loops)	272	17, 21	21.5	Shear in overlap
B2 (Two loops)	272	20, 20	15.1	FRP Rupture
C1 (Straight bars with splice)	273	24, 32	33.5	Splice failure
C2 (Straight bars with splice)	276	15, 18	28.8	Splice failure
D1 (Straight bars no splice)	269	21, 26	40.5	FRP rupture
D2 (Straight bars no splice)	271	28, 28	37.5	FRP rupture
Phase II specimens				
E1 (Two loops)	102	24	29.9	Shear in overlap
E2 (Two loops)	103	29	29.8	FRP rupture
F1 (Two loops)	104	29	34.1	FRP rupture
F2 (Two loops)	103	32	32.6	FRP rupture
G1 (Straight bars with splice)	104	31,28	35.8	FRP rupture
G2 (Straight bars with splice)	105	30	35.2	FRP rupture

[1]concrete cover measured at failure location. Concrete cover averaged at both bars when cover difference is 2 mm or less.

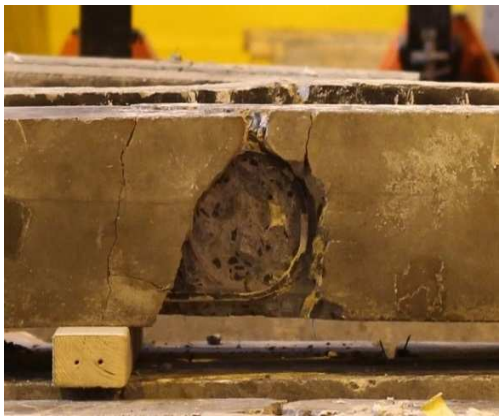

Figure 4.25 Bottom view of overlap failure of Specimen A1 (Three loops).

Figure 4.26 Bottom view of overlap failure of Specimen B1 (Two loops).

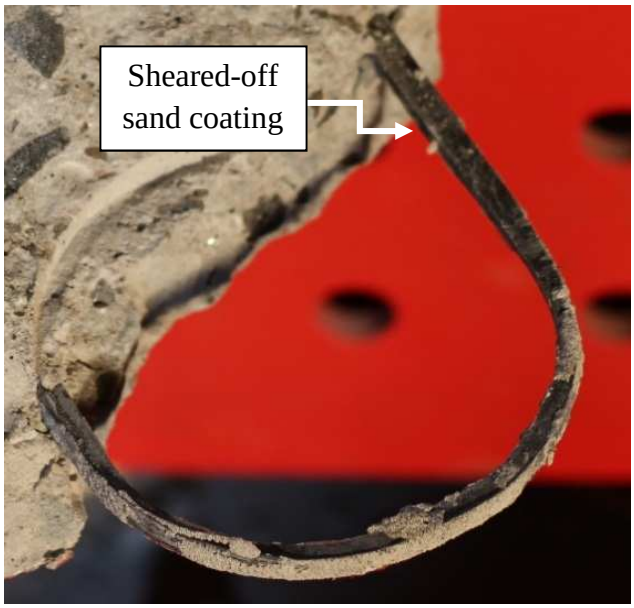

Figure 4.27 Shearing off of CFRP loop sand coating.

Figure 4.28 Concrete splitting along straight bars splice (bottom view of specimen C2).

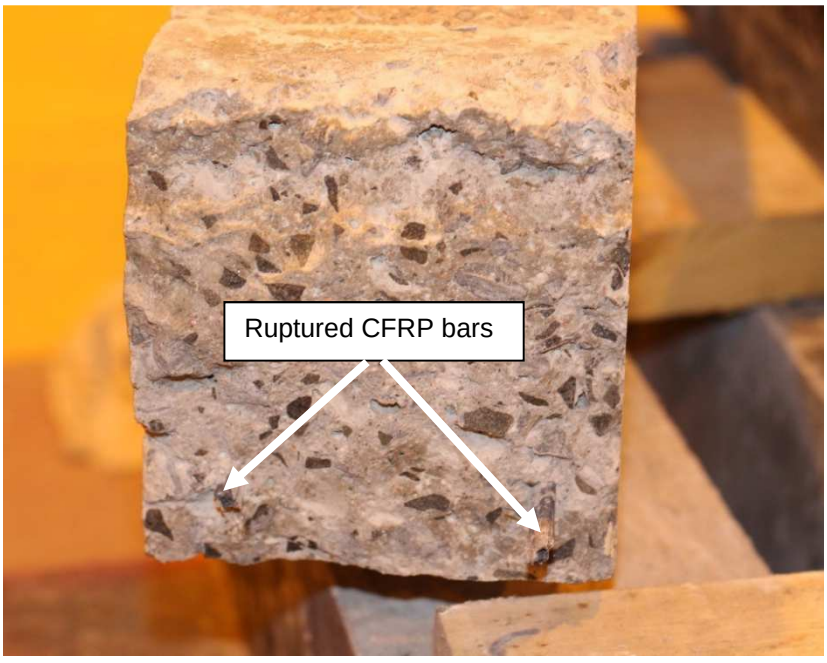

Figure 4.29 FRP reinforcement rupture in beam with continuous reinforcement (D2).

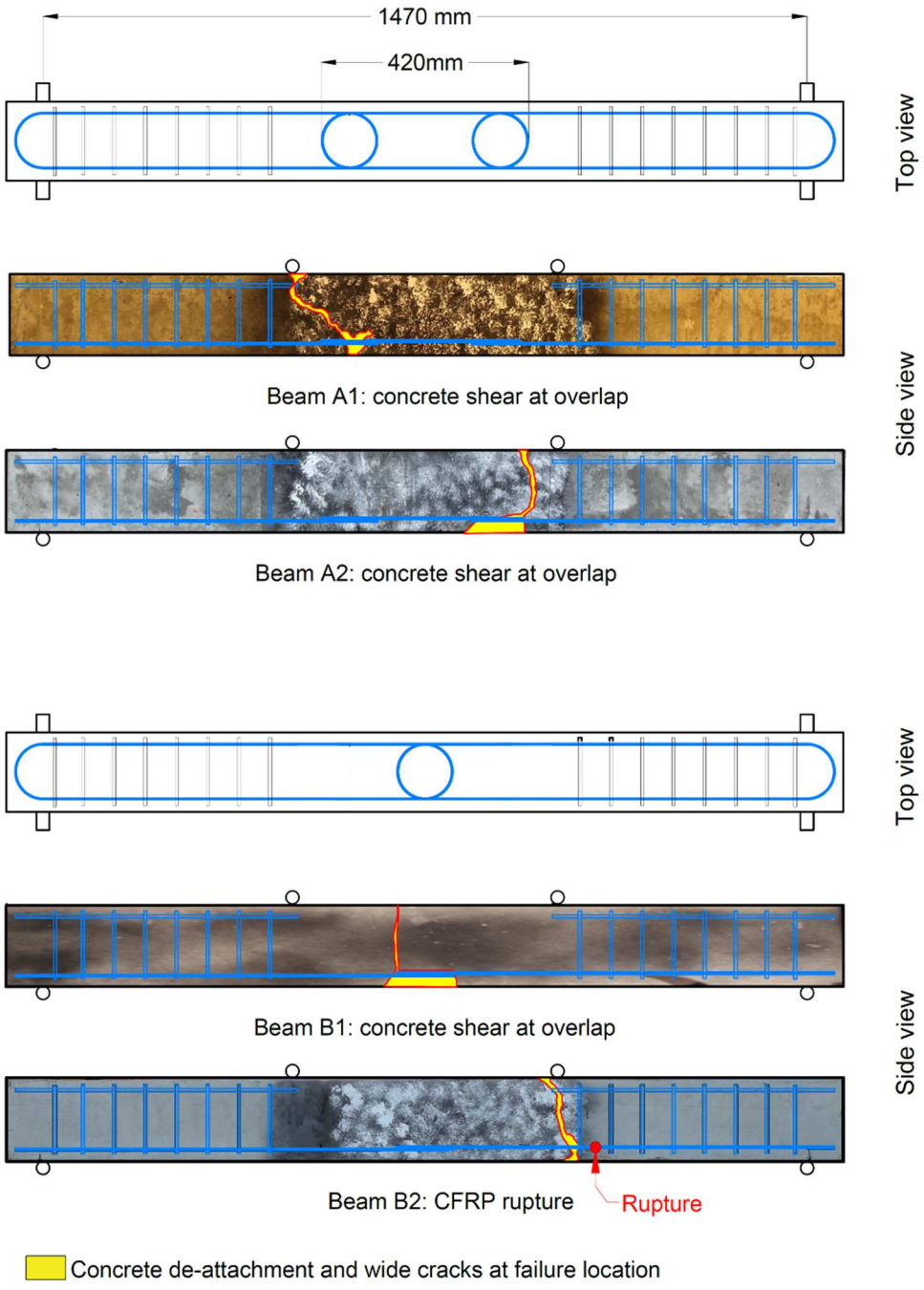

Figure 4.30 Failure zone and mechanism for beam specimens with CFRP loops at ambient temperature.

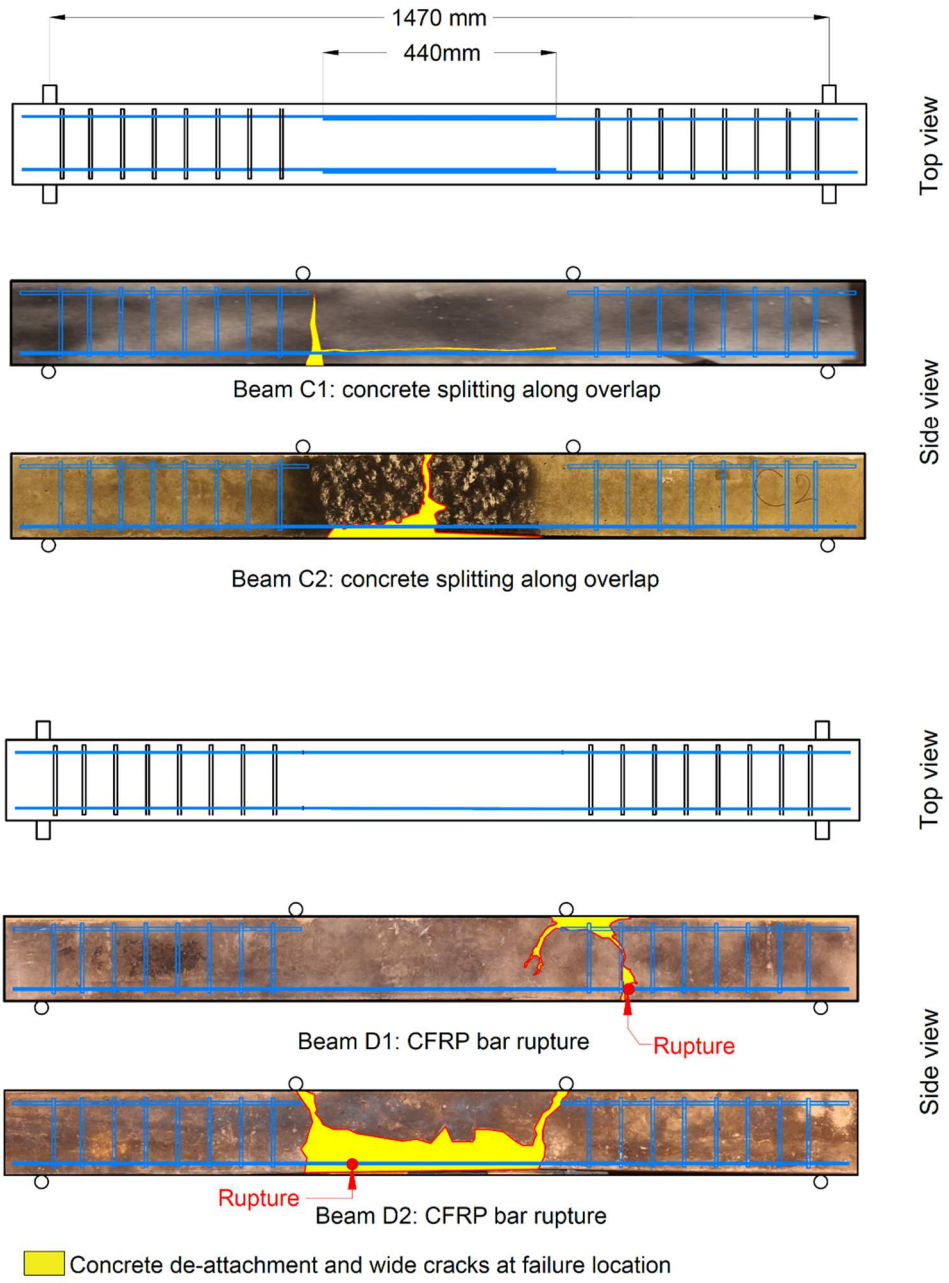

Figure 4.31 Failure zones and mechanisms for beam specimens with splice and continuous CFRP bars at ambient temperature.

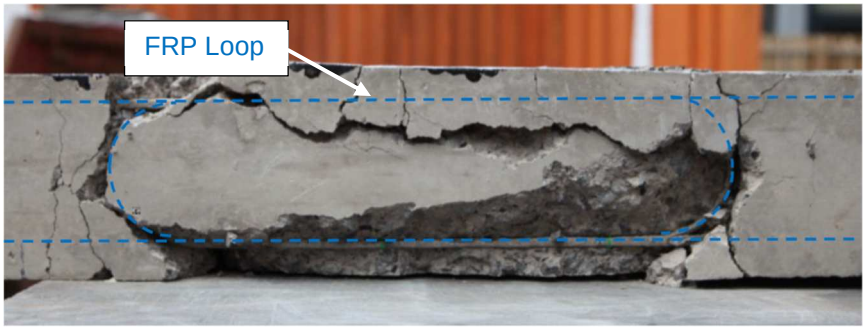

Figure 4.32 Concrete shear along loops overlap failure of specimen E1 (bottom view).

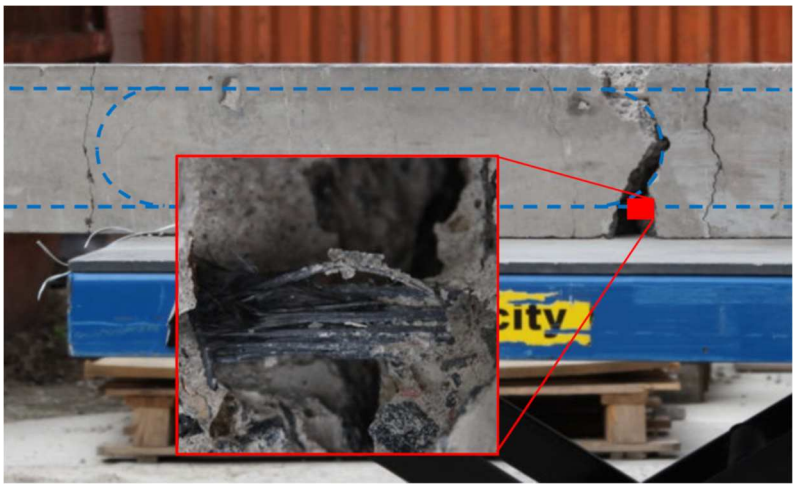

Figure 4.33 Rupture of CFRP loop within constant moment region and out of overlap length (bottom view of specimen E2).

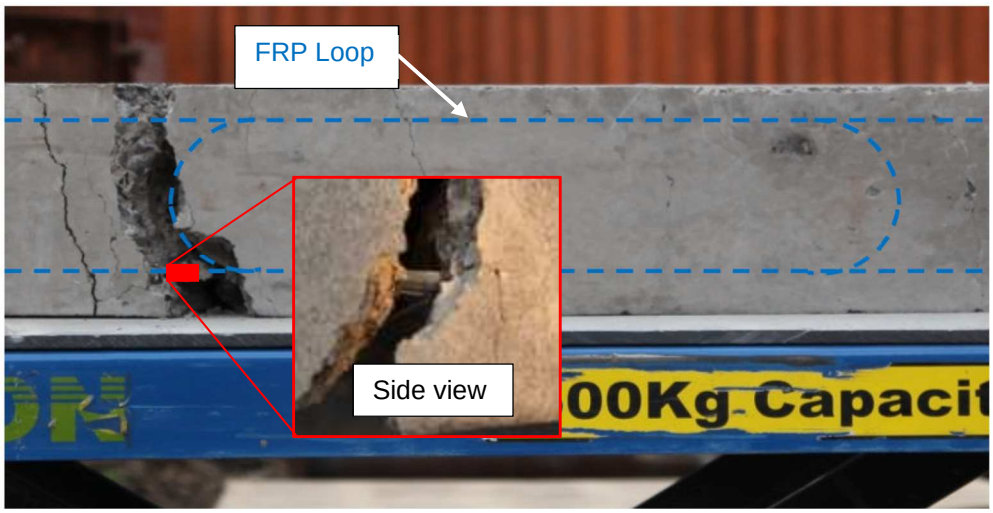

Figure 4.34 Rupture of CFRP loop within constant moment region and out of overlap length (bottom view of specimen F2).

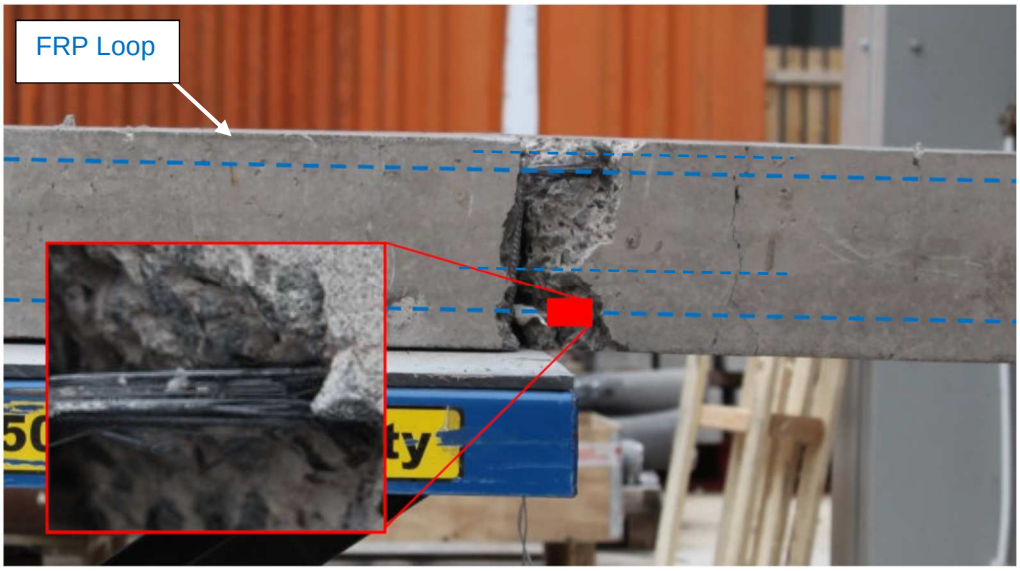

Figure 4.35 Rupture of CFRP bar within constant moment region out of overlap length (bottom view of specimen F2)

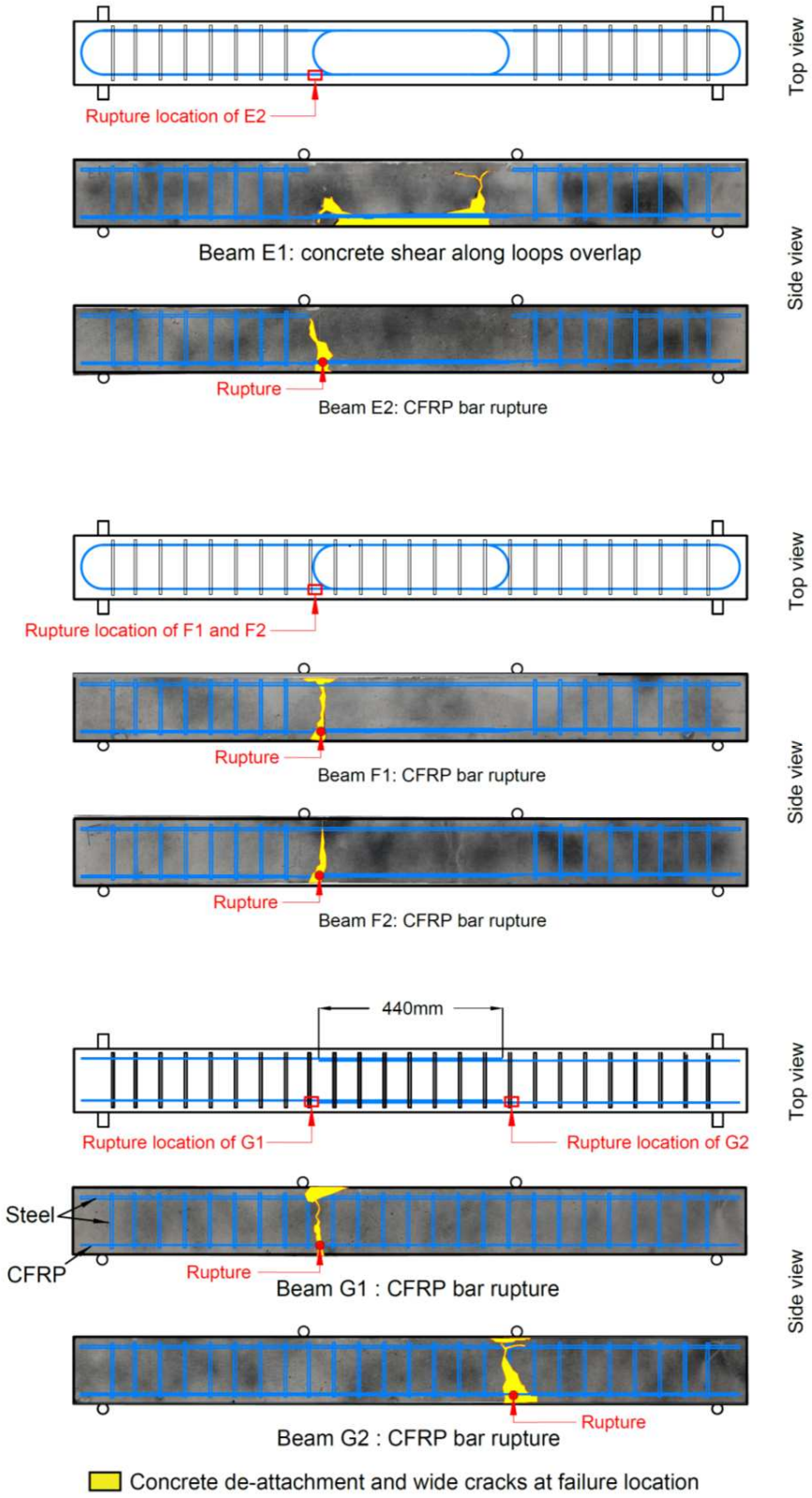

Figure 4.36 Failure zone and mechanism for beam specimens at ambient temperature.

Load- reinforcement strain response

Figure 4.37 below shows the change in CFRP reinforcement strain with applied load within the overlap and splice length for phase II specimens. Readings of strain gauges indicate a non-uniform distribution of forces along loops overlap and bars splice with strain values reduce toward the end of loops overlap and bars splice. This reflects the typical non-linear behaviour of bond forces.

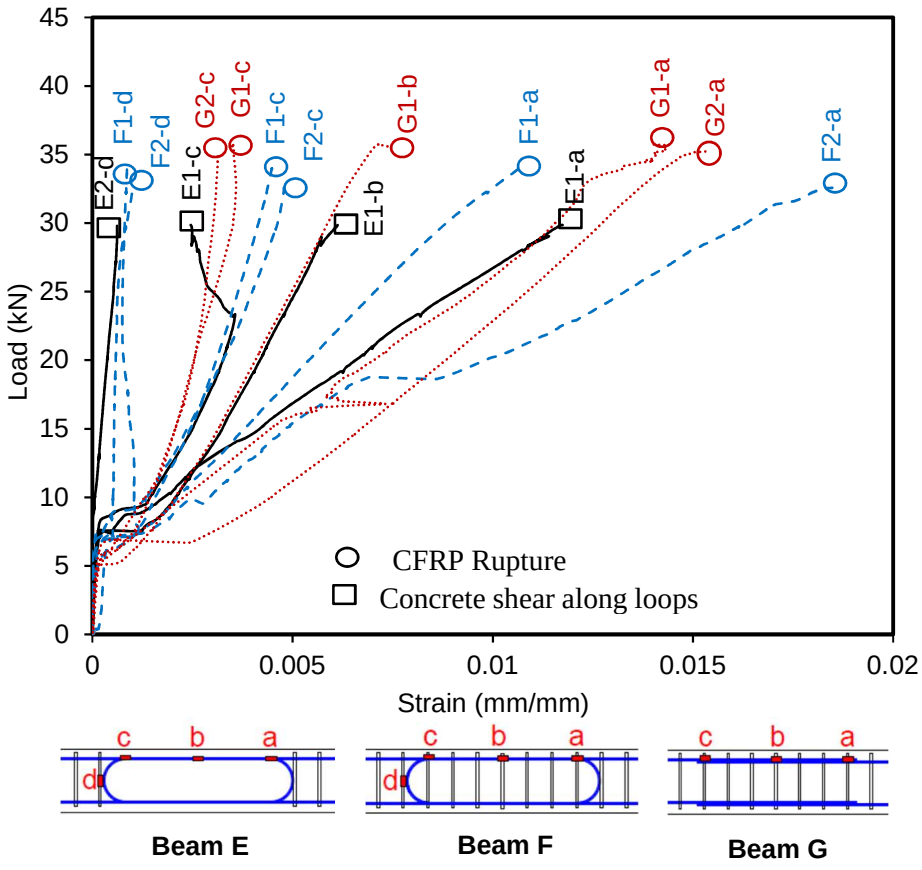

Figure 4.37 Load versus reinforcement strain responses of phase II specimens (some data is not included due to strain gauges failure).

Crack patterns:

Figures 4.38-4.41 below show the crack patterns in the beam specimens with different reinforcement arrangements. Images were taken between 0 to 5 seconds prior to failure.

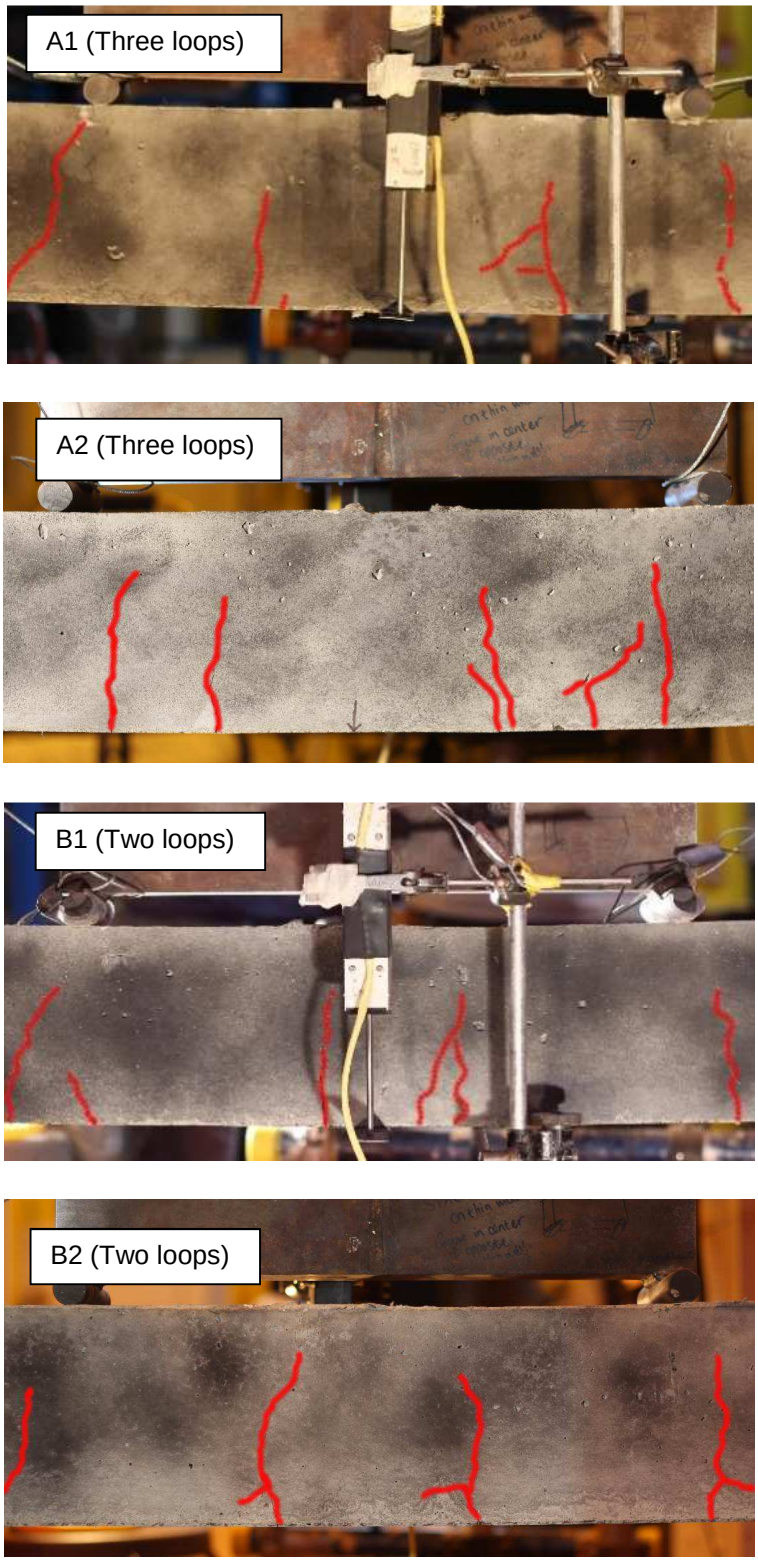

Figure 4.38 Crack patterns of beam specimens with CFRP loops prior to failure at ambient temperature (Phase I).

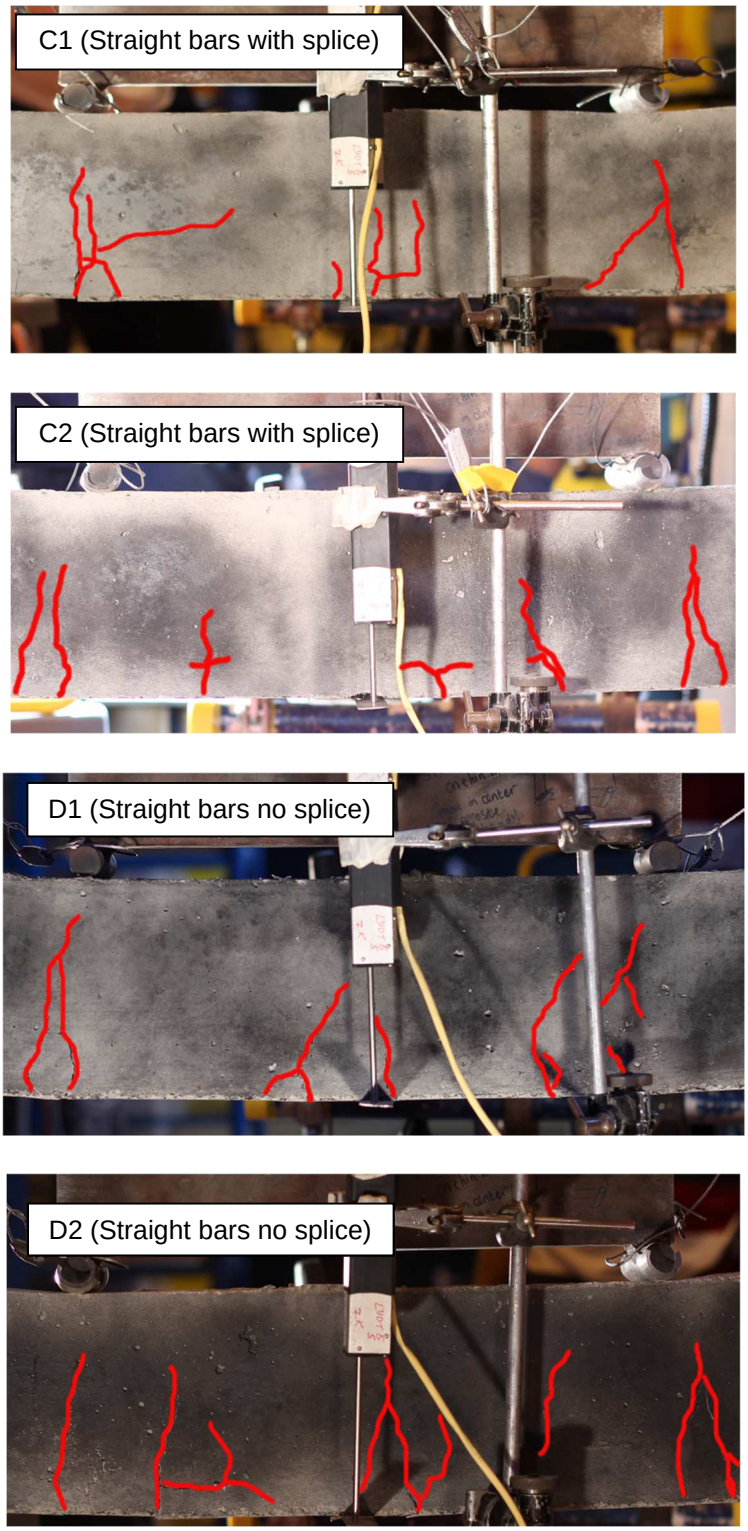

Figure 4.39 Crack patterns of beam specimens with CFRP straight bars prior to failure at ambient temperature (Phase I).

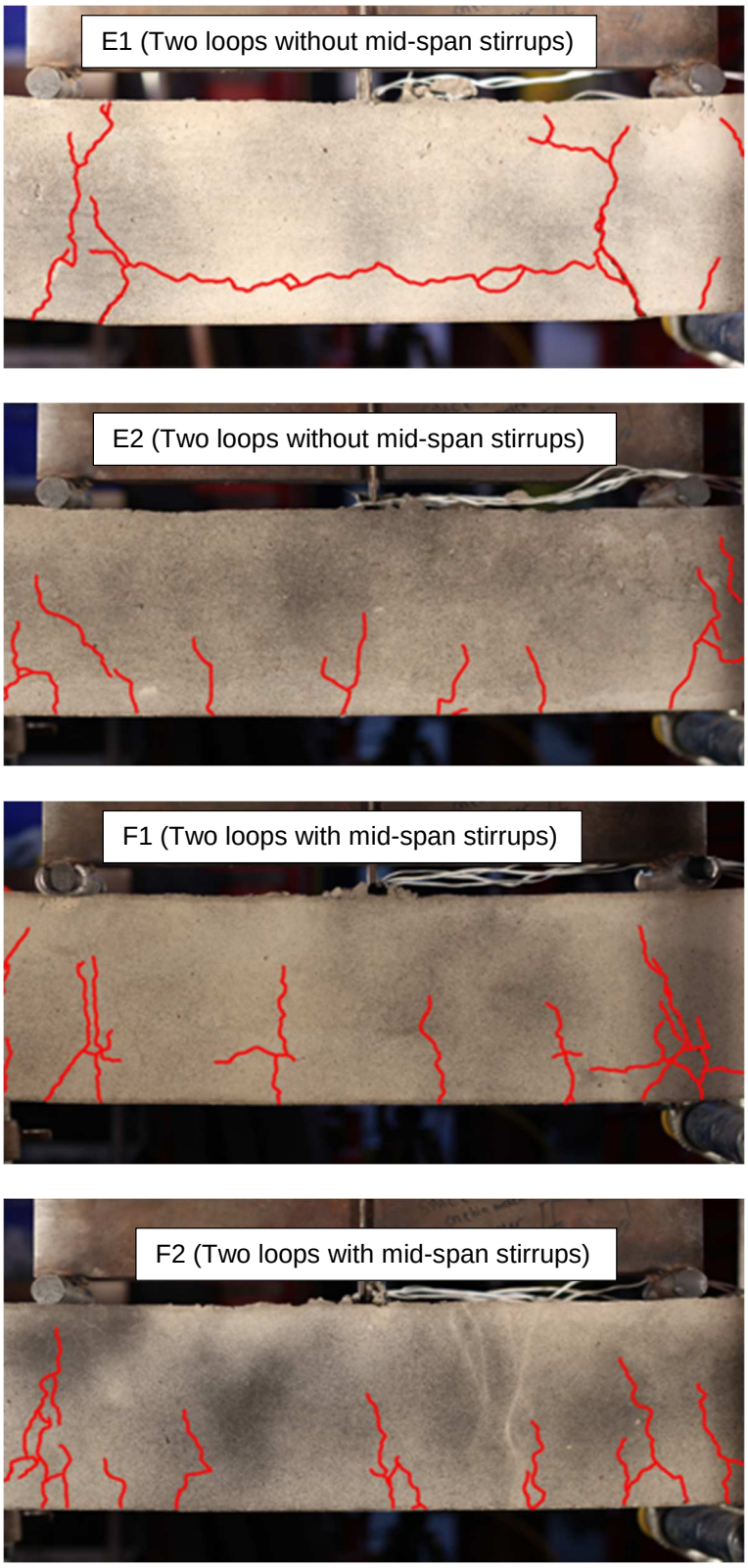

Figure 4.40 Crack patterns of beam specimens with CFRP loops prior to failure at ambient temperature (Phase II).

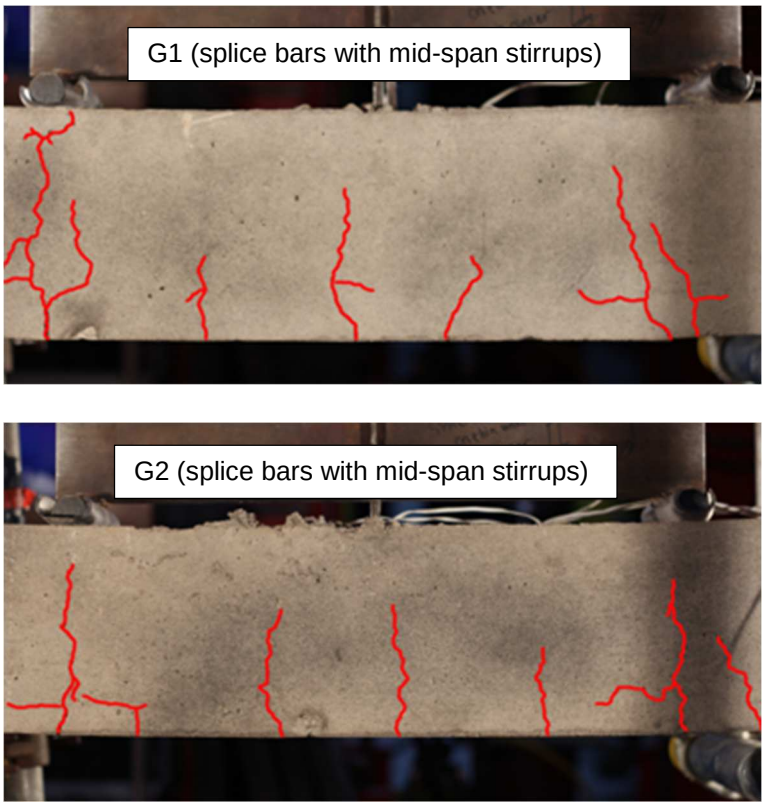

Figure 4.41 Crack patterns of beam specimens with CFRP spliced bars prior to failure at ambient temperature (Phase II)

4.9 Discussion of Ambient Temperature Tests Results

4.9.1 Load-deflection response

All of the beam specimens within each test phase exhibited similar values of stiffness prior to section cracking, irrespective of the type of reinforcement (see Figure 4.21 and Figure 4.22 for phase I and phase II specimens, respectively). This indicates that the geometry of reinforcement has no significant effect on the initial element response. This agrees with Carvelli (2013) findings when compared the initial response of slabs reinforced with straight and hooked reinforcement.

A comparison between the load-deflection response of one specimen of each type of phase I and II is shown in Figure 4.42 (load-deflection responses of all specimens are shown in Figures 4.21 and 4.22). It can be seen that the initial stiffness of beam specimens in phase I is about 19.5 kN/mm, while for phase II specimens it is about 7.4

kN/mm. The difference of initial stiffness between specimens of the two phases can be attributed to the differences in concrete cover (Table 4.7) and to the fact that the concrete compressive strength of phase II specimens (23.7 MPa) is almost half of phase I (42.4 MPa). The difference of concrete strength between the two phases as mentioned previously was not intentional, but it occurred due to a delivery of under-strength ready mix concrete.

The theoretical calculations of cracking load based on the ACI (2015) and ISIS (2007) equations of phase I and II beam specimens are 9.5 and 7.2 kN, respectively (see Appendix C.6 and Appendix D.2). These values are reasonably close to the cracking loads observed from the experimental data shown in Figure 4.42.

The post-cracking response showed a reduced stiffness for all specimens. Beam specimens from phase I (A, B, C, and D) had a different stiffness after cracking, which indicates a different level of bond quality and/or interaction mechanisms between the reinforcement and concrete. Post-cracking stiffness varied from ≈ 1.9 kN/mm for D1 specimen (continuous straight bars) to ≈ 0.8 kN/mm for A1 specimen (short overlapped loops). The beam specimens with the shortest overlapped length of 100 mm (beams with overlapped loops A and B) developed the lowest post-cracking stiffness and failure load. Beam specimens with spliced straight bars had a longer development length and achieved higher stiffness. Beam specimens with continuous straight bars (D) developed the highest stiffness and strength. Unlike the other specimens, beam specimens of type D had continuous reinforcement anchored outside the constant moment region and within a region confined with transverse reinforcement, which improved the bond between the reinforcement and concrete.

The post-cracking response of the phase II specimens (E, F, and G) showed that the stiffness of all beams was approximately the same (≈1 kN/mm), unlike in the case of phase I specimens (Figure 4.42). This indicates that the different reinforcement arrangements (overlapped loops and spliced bars) have similar interaction with concrete. This was confirmed by the strain data of reinforcement, as discussed in the following section 4.9.2.

The ISIS design guidelines (2007) specify permissible deflection of structural elements reinforced with FRP in a range of $l_n/180$ to $l_n/480$, (where l_n is span length), which depends on structure type and whether there are non-structural elements that will be affected by the corresponding deflection. In all specimens except B2, failure only occurred when these limits were exceeded.

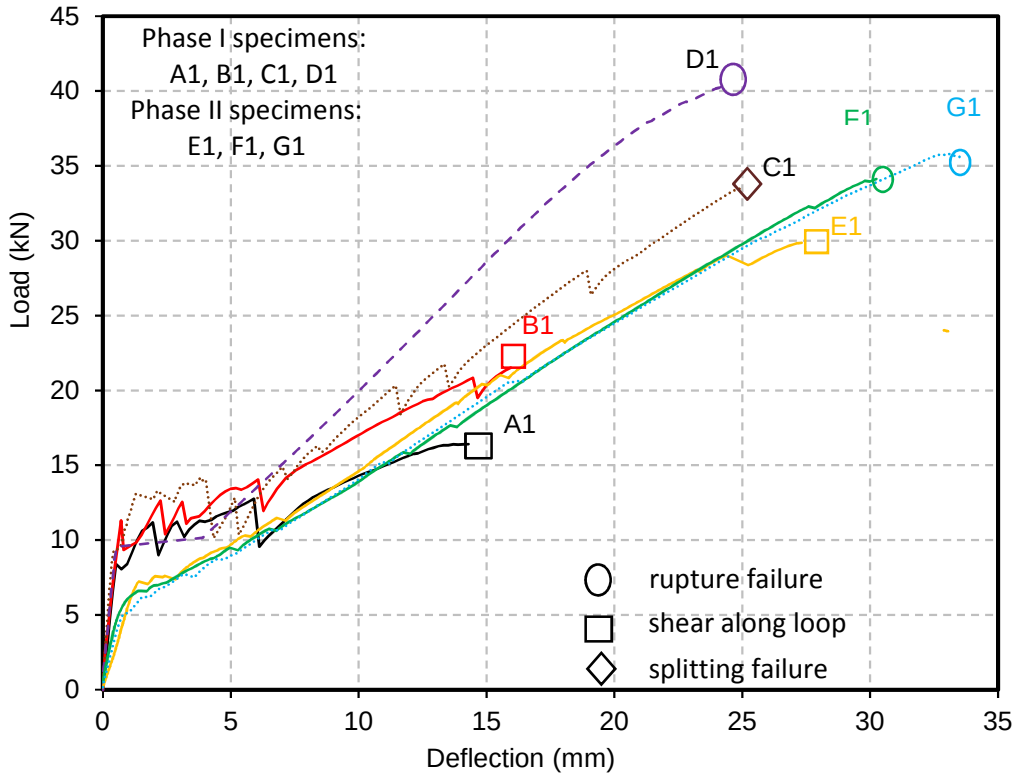

Figure 4.42 Load deflection response of one specimen of each type of phase I and phase II beam specimens. A: Three loops (short overlap), B: Two loops (short overlap), C: Straight splice, D: Continuous straight bars, E: Two loops (long overlap), F: Two loops (long overlap with mid-span stirrups), F: Splice bars with mid-span stirrups.

4.9.2 Reinforcement strain response

The strain data obtained along the loop overlap and bar splice lengths in the phase II specimens (Figure 4.37) showed that the different reinforcement arrangements (specimens E, F and G) developed similar strain distributions and magnitudes. Very low strain values were detected at the midpoint of the curved part of loops, indicating that the curved part was not significantly engaged (low forces were transformed to it).

This also indicates that the overlapped loop and splice bars had a similar bond interaction with concrete. This explains the observation made above (section 4.9.1), that specimens with loops and straight bars reinforcement exhibited very similar stiffness. The strain data showed that the strain value was higher at the overlap and splice start and reduced toward the end. Non-linear behaviour is associated with bond stress distribution of FRP, as documented in the literature (Baena et al., 2009; Nigro et al., 2011a). The maximum value of strain recorded for the specimens that failed by reinforcement rupture ranged between 1 and 1.8 % (Figure 4.37), which is lower than the rupture strain of the carbon fibre tow 2 % provided by the manufacturer (Table 3.1). However, rupture occurred out of the overlap / splice length, where no strain gauges were present, where the reinforcement ratio reduced, and the strain is expected to be higher as is discussed in the following section 4.9.3.

4.9.3 Failure loads and mechanisms

The brittleness of FRP reinforcement was evident in the failure behaviour of the beam specimens. In all of the beam specimens, failure was brittle and accompanied by a total loss of member load bearing capacity.

There was a great difference in failure values and mechanisms amongst the phase I tests (Figure 4.21 and Table 4.7). The beam specimens with continuous bars (type D) attained the highest failure load among specimens of phase I (Figure 4.21). The CFRP reinforcement developed its full strength and failed by rupture. This indicated that sufficient load transfer occurred between reinforcement and concrete. Beams with continuous bars had the advantages of an anchor length of 543 mm beyond constant bending moment region and also anchored within zones confined by steel shear stirrups. Wider cracks and higher deflection occurred in beams with straight bars prior to failure, in comparison with other specimens of phase I.

Beam specimens with spliced straight bars (type C) developed a lower failure load than beams with continuous bars. Failure occurred as concrete splitting along the splice length. Such a failure is reported in the literature (Harajli and Abouniaj, 2010; McIntyre et al., 2015) and is caused by the radial pressure at the reinforcement

interface overcoming the confinement pressure from the surrounding concrete (GangaRao et al., 2007; Quayyum, 2010; Aly et al., 2006). There were no clear indications of the splitting (apart from a few short cracks that appeared along the CFRP reinforcement level) prior to failure (Figure 4.39). Post-failure examination of specimens showed a detachment of a large area of concrete along the splice length (Figure 4.28). The occurrence of bond failure although the provided splice length (440 mm) exceeds the requirements (205 mm) by design guideline ISIS (2007), indicates that design equation might not be conservative for beams with similar size and concrete cover (see Appendix C.8).

Bond failure due to this concrete splitting was avoided in the phase II specimens by providing transverse reinforcement to increase confinement along bar splice as in case of beams type G. The steel stirrups provided extra confinement, which improved the bond strength and distribution along bar (Harajli and Abouniaj, 2010; Aly et al., 2006).

Specimens reinforced with short overlapped loops (type A and B), developed the lowest failure loads, because failure occurred prematurely due to concrete shear along loops overlap (Figures 4.25 and 4.26). The exception was specimen B2 that failed by reinforcement rupture, which was considered to be a premature failure because it happened at a load level significantly less than the load caused reinforcement rupture of specimens with continuous straight bars (D1 and D2). The rupture failure of the B2 specimen could be caused by a manufacturing defect or the bar being damaged during the specimen preparation process.

A visual inspection of failed specimens with short overlapped loops type A and B (except B2) showed a complete concrete detachment over the overlap length (Figures 4.25 and 4.26). No signs of fibre rupture were observed in any of the failed specimens. Signs of sand-coating shearing off at CFRP loop surface were observed (Figure 4.27), which is a common feature in FRP bond failure (Al-Zahrani et al., 1999; Baena et al., 2009; Harajli and Abouniaj, 2010).

The concrete shear along the loop overlaps that occurred in beam types A and B is attributed to the fact that the CFRP loops can generate a shear force in the

reinforcement direction that exceeds the shear resistance of concrete within an overlap zone by many folds, as shown in Appendix E.

In phase II beam specimens with CFRP loops (E and F) had longer overlap lengths than in phase I (A and B). In addition, transverse reinforcement was provided along the loop overlap length in beam type F. All phase II beam specimens (types E, F and G) failed in tension due to CFRP rupture, except for specimen E1. Beam specimens E1 and E2 have the same reinforcement arrangement and failure load; however, specimen E1 failed due to concrete shear along the overlap length. This can be interpreted as the shear resistance of concrete within loops overlap is very close to shear force in reinforcement direction generated by CFRP at rupture, 66.10 kN (see Appendix E). However, the theoretical estimation of the shear resistance of plain concrete within the loops overlap zone according to ISIS (2007) was just 31.51kN. This indicates that the design equation is very conservative for the case of overlapped loop reinforcement. In beam type F the transverse reinforcement along loops overlap length (Figure 4.2) enhanced the shear resistance between the overlapping loops significantly and prevented concrete shear along the loop overlap from occurring.

Rupture failure of beam specimens of phase II always occurred within the constant moment region outside the overlap length (Figure 4.36 and Figure 4.43) as it is where the reinforcement ratio reduced.

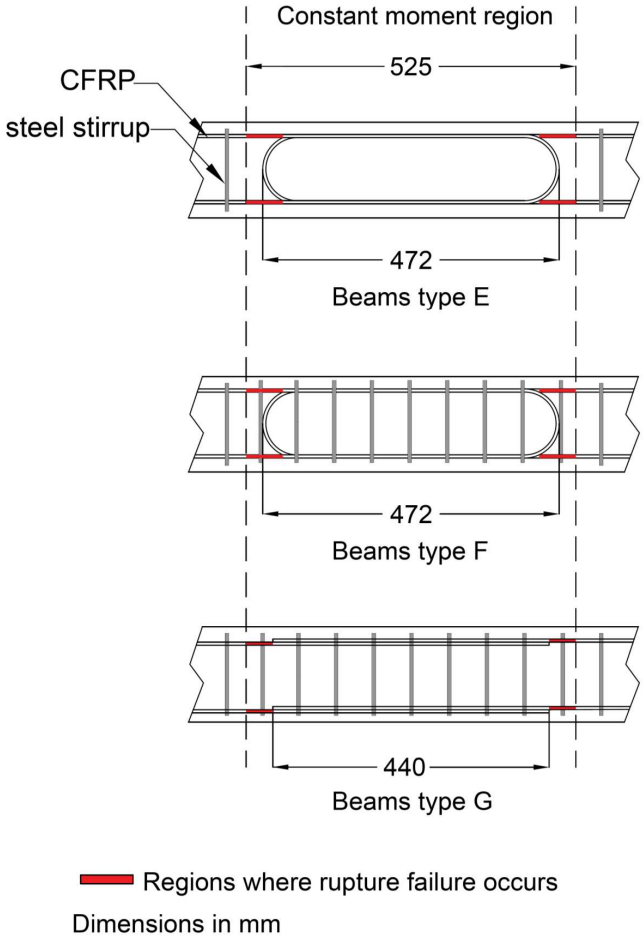

Figure 4.43 Regions out of single CFRP reinforcement within constant moment region where rupture failure occurred at ambient temperatures.

4.9.4 Cracks patterns

Flexural cracks appeared and propagated toward the compression zone as the load increased. Although failure occurred by concrete shear between the overlapping loops in beam types A and B, no horizontal cracks were observed at the reinforcement level prior to failure, which makes this failure very brittle (Figure 4.38). At failure a wide opening crack at mid-span propagated upwards causing beam separation into two parts (Figure 4.30). For beam specimens with spliced bars (type C) in addition to the flexural vertical cracks there were a few short horizontal cracks (Figure 4.39) which signalled the concrete splitting failure that occurred in this type of beam. Flexural cracks in specimens with continuous bars (type D) propagated further and were wider, because a higher load was attained (Figure 4.39).

A horizontal crack along the constant moment region at the reinforcement level occurred in beam specimen E1 prior to failure (Figure 4.40). This crack is indicating the failure mode, which occurred as concrete shear along loops overlap. The rest of phase II specimens had uniformly spaced flexural cracks that increased in width and length as the load increased (Figure 4.40-4.41), and which was the desired mode of failure at ambient temperature.

4.10 Summary

A series of four-point bending tests were carried out to evaluate the performance of a new design of CFRP loops as tension reinforcement against straight CFRP bars. At ambient temperature and while beam specimens were designed to fail in flexural by rupture of FRP reinforcement, when loops overlapped over short length beam specimens experienced a premature failure due to concrete shear along overlap length. Beam specimens with spliced straight bars also failed prematurely due to concrete splitting. Both failure modes are an indication for the need for longer overlap/splice length or increasing level of confinement around the reinforcement in failure regions. Beam specimens with continuous CFRP loops achieved higher resistance than other specimens and failed by bar rupture.

A second test series investigated the use of longer overlap length and the use of stirrups to avoid the undesirable shear and splitting failures that had occurred during the first series of tests. Results showed that such design adjustments can prevent premature failure and led FRP reinforcement to develop full strength and fail by rupture.

Chapter 5 – Heated Four-Point Bending Test

5.1 Overview

The previous chapter presented the first series of tests, in which beam specimens reinforced with either CFRP loops or straight bars were tested in bending at ambient temperature. The results showed that if sufficient overlap length and/or transverse reinforcement were provided, premature failures can be avoided and comparable performance between specimens reinforced with FRP loops and straight bars can be achieved at ambient temperature and failure by bar rupture can be developed.

This chapter presents the heated beam tests, in which same types of concrete beam specimens test at ambient (chapter 4) were tested in four-point bending test under sustained monotonic and transient localised heating over the mid-span region. The methodology, test arrangements, and results are included within this chapter, in addition to the discussion.

5.2 Test Specimens and Nomenclature

The dimension of beam specimens and reinforcement properties are the same as in ambient tests (see section 4.2).

5.2.1 Failure Criteria

The same failure criteria of beam specimens in ambient tests were used (see section 4.2.1).

5.3 Experimental Programme

A total of fourteen beam specimens, two in each group, were included in testing programme, as shown completely in Table 5.1. In the heated tests, all specimens were loaded under displacement control up to the sustained load value. After this, a localised heating was applied using the gas radiant panels over central region which was 550 mm and 970 mm long for beams of phase I and II respectively. A longer overlap length for loop reinforcement was used in phase II specimens therefore the heated region was extended.

Table 5.1 Beam specimens annotations and descriptions

Beam Type	Reinforcement	Heated Test (sustained load)
Phase I		
A	Spliced CFRP loops (two loops)	A3
		A4
B	Spliced CFRP loops (three loops)	B3
		B4
C	Spliced straight CFRP bars	C3
		C4
D	Continuous straight CFRP bars	D3
		D4
Phase II		
E	Spliced CFRP loops	E3
		E4
F	Spliced CFRP loops with mid span stirrups	F3
		F4
G	Spliced straight CFRP bars	G3
		G4
Total Number of specimens		14

5.4 Mechanical Properties of the Constituent Materials

5.4.1 CFRP Reinforcement

The CFRP reinforcement used had the same composition and manufacturing process as the CFRP reinforcement used in ambient specimens (see section 4.4.1).

5.4.2 Concrete

Beam specimens used for heated tests were cast using same concrete patch used for ambient tests which is reported in section 4.4.2.

5.4.3 Steel Reinforcement

The steel reinforcement used as compression steel and for the stirrups had the same properties as the steel reinforcement used in ambient test (see section 4.4.3).

5.5 Beam Specimens Preparation

5.5.1 Manufacturing of CFRP reinforcement

The CFRP reinforcement was manufactured in same process used for ambient specimens (see section 4.5.1).

5.5.2 Installing Thermocouples

Insulated type K thermocouples were used to monitor the temperature of CFRP reinforcement and concrete during heated tests. Figures 5.1-5.2 shows the location of thermocouples in the specimens of phase I and II respectively. The thermocouples were tied to the CFRP reinforcement to measure the temperature at the bottom of the reinforcement (Figures 5.3 to 5.8). In addition, in beam specimens B3 arrays of thermocouples (thermocouple trees) distributed vertically 20 mm apart, were used to monitor the concrete temperature at different depths (Figure 5.8). Thermocouple trees were attached at the bottom to the formwork using strong gum and tied above beam level to keep it vertical during concrete cast. The first thermocouple at the bottom of tree was placed 2 mm from the bottom surface of concrete.

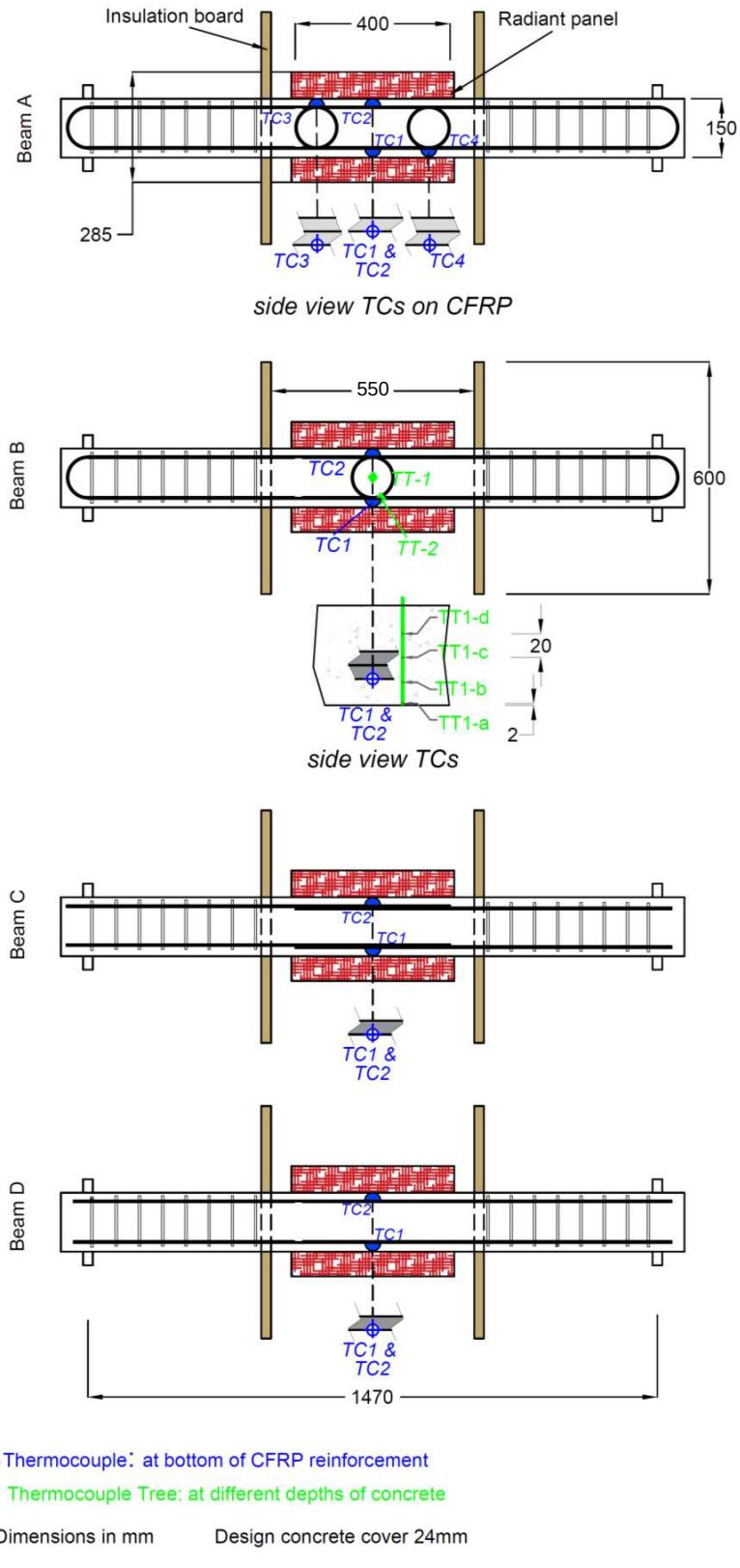

Figure 5.1 Location of thermocouples in beam specimens (Phase I).

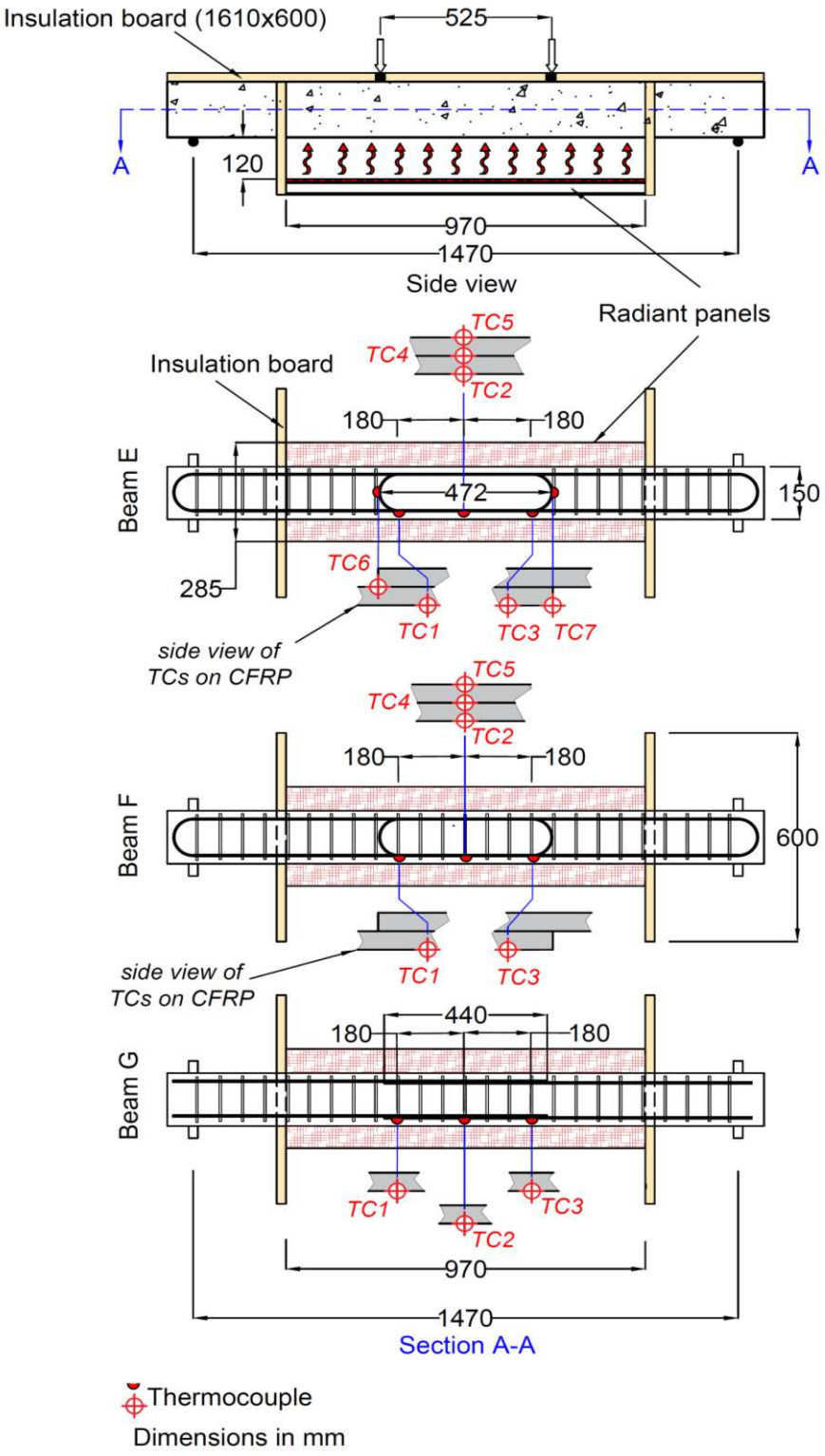

Figure 5.2 Location of thermocouple in beam specimens (Phase II).

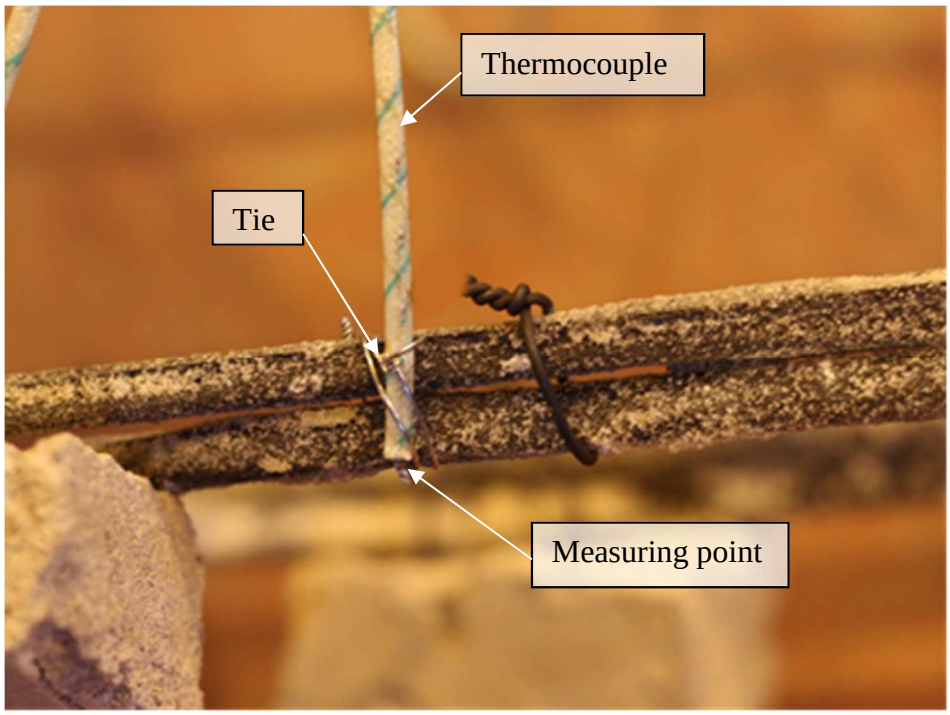

Figure 5.3 Tied thermocouple to measure temperature at the bottom of reinforcement.

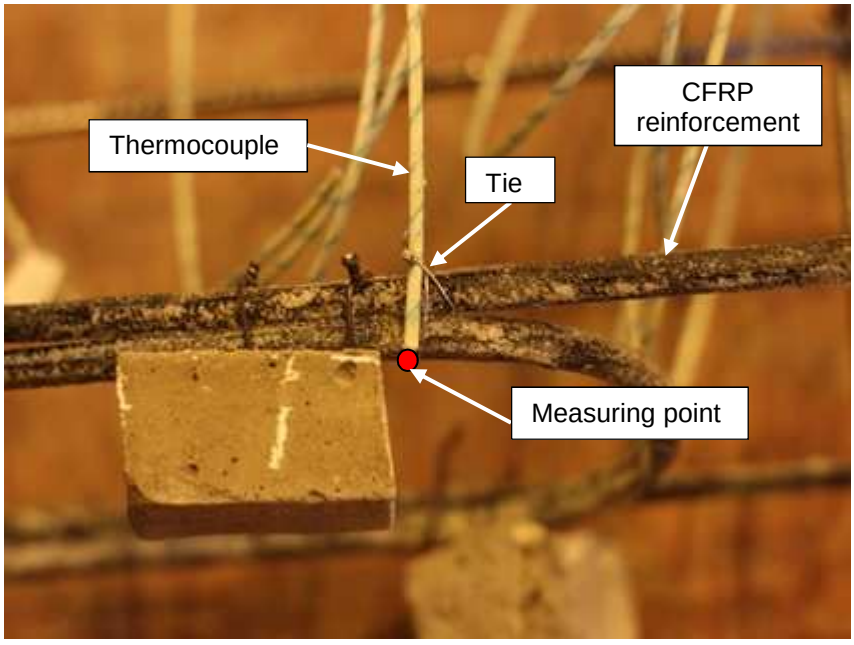

Figure 5.4 Tied thermocouple to measure temperature at the bottom of reinforcement (Specimen E3).

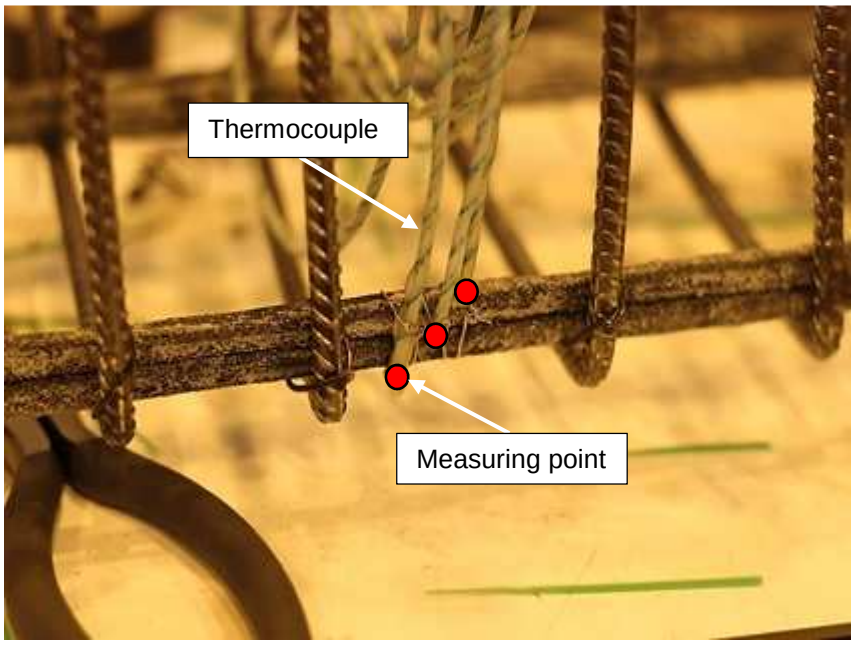

Figure 5.5 Three thermocouple tied at two overlapped loops to measure temperature at bottom, between, and above the loops (specimen F3).

Figure 5.6 Thermocouples fixed to CFRP reinforcement prior to concrete cast (Phase I).

Figure 5.7 Thermocouples fixed to CFRP reinforcement prior to concrete cast (Phase II specimens).

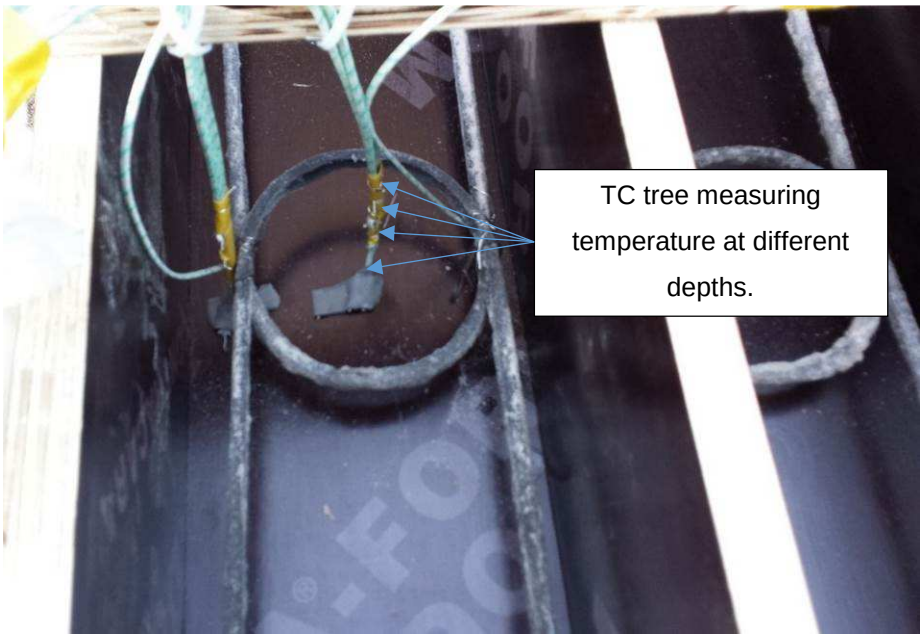

Figure 5.8 Thermocouple trees glued at the bottom to formwork while thermocouple array attached vertically to measure concrete temperature at different depths.

5.5.3 Formwork for the Beam Specimens

The beam specimens were cast in plywood formwork made of 18-mm plywood sheets. The formwork was braced across the width to increase the stiffness of specimen and help tidying the thermocouples cables (Figure 5.9).

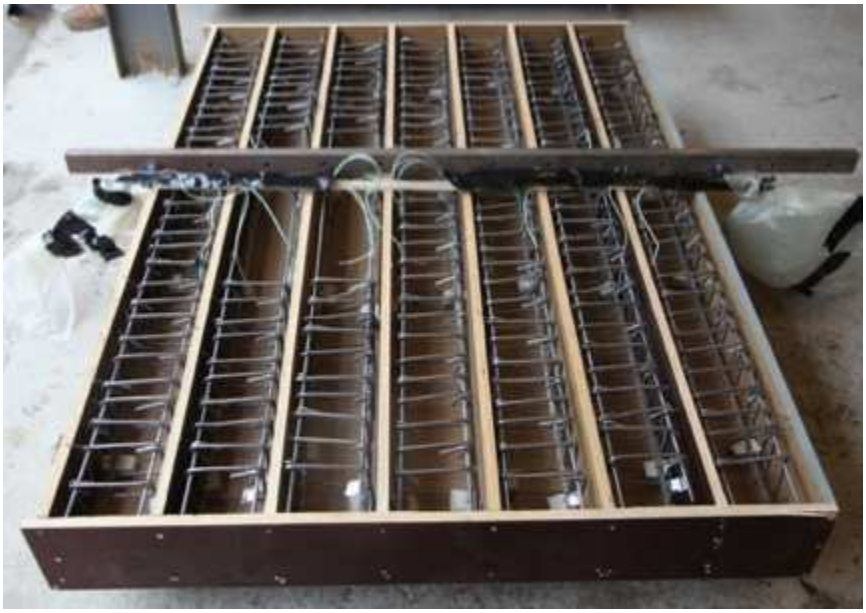

Figure 5.9 Reinforcement cages placed in plywood formwork ready for concrete casting.

5.5.4 Concrete Cast

The same procedure for casting the concrete for ambient test specimens was for the heated test specimens (see section 4.5.5).

5.5.5 Specimens Curing

Beam specimens of heated test were cured under the same conditions used for ambient test specimens (see section 4.5.6).

5.6 Instrumentations

The same instrumentation for applying the load and measuring the deflection that were used in ambient beam tests (see section 4.6) were used in beam heated tests. In addition, gas radiant panels and insulation boards were used which are described below.

5.6.1 Propane Gas Radiant Panel

Surface combustion radiant panels designed to provide a uniform heat were used to heat the central region of the tested beams. Each panel had a cross-sectional dimension of 440×285 mm and run on a mixture of air and propane gas (Figures 5.10-5.13).

5.6.2 Superwool Insulation Boards

Superwool board is a thermal insulation product which contains alkaline earth silicate (AES) wools held together by an organic binder. It can be used up to temperature of 1150 °C. Superwool insulation boards were used to confine heat generated by gas radiant panels to the central region of the beam (Figures 5.10-5.13). The boards were placed on either side of the radiant panel. The width of the board (600 mm) exceeded the width of the radiant panel (285 mm). The insulation boards were also placed on the top of the beams to protect the hydraulic loading jack from heat.

5.7 Heated Tests

5.7.1 Experimental Arrangements and Procedures

During the elevated temperature tests, the beam specimens were tested in a separate frame to avoid any effect of heat from the gas radiant panel on the actuator. The load was applied to a spreader beam by a 10-tonne hydraulic jack which was connected to another 25-tonne hydraulic jack placed under the actuator (Figures 5.10-5.14). The actuator pushed down the stroke of jack beneath it which in turn caused the stroke of jack placed on the tested specimen to extend and apply load. This testing system has been used in the Structures Laboratory of the University of Edinburgh. It has been calibrated to account for the difference between load applied on the 25-tonne hydraulic jack and load produced by the 10-tonne hydraulic jack on the tested specimens. The deflection of the beam specimens was monitored by means of two LPs placed at the top surface of the beam and DIC through two DSLR cameras covering both sides of the beams.

The beam specimens were initially loaded in displacement control at a rate of 1 to 2 mm/min (the variation was due to the use of the hydraulic jack for loading) up to the sustained load. For phase I specimens, the value of sustained load was chosen to be 35% of average ambient strength of control specimens (continuous straight bars Group D), 14 kN, (see Table 4.7). For phase II specimens (except E3) the sustained load was also chosen as 35% of average ambient strength of all phase II specimens (11.6 kN) as there was a small variation in ambient strength between specimens (Table 4.7). The sustained load value (35% of ambient capacity for control specimen type D of phase I and all phase II beams specimens) was chosen as it corresponds with beam deflection of ≈ 6.5 mm, (Figures 4.21-4.22), which falls at the serviceability limit of maximum allowable deflection based on beam span/240 (1470 mm/240 = 6.13 mm) as specified by ACI (2015).The sustained load for specimen E3 was 18.5 kN which corresponds with 55% of the ambient strength, is maximum allowable sustained stress level permitted by ACI (2015) for CFRP reinforcement. After the sustained load was reached, heat was applied using the gas radiant panels until failure occurred. The size of heated zone in phase I test was 550 mm (Figure 5.10). In phase II of the heated zone was increased to 970 mm by using an array of two gas radiant panels (Figure 5.12).

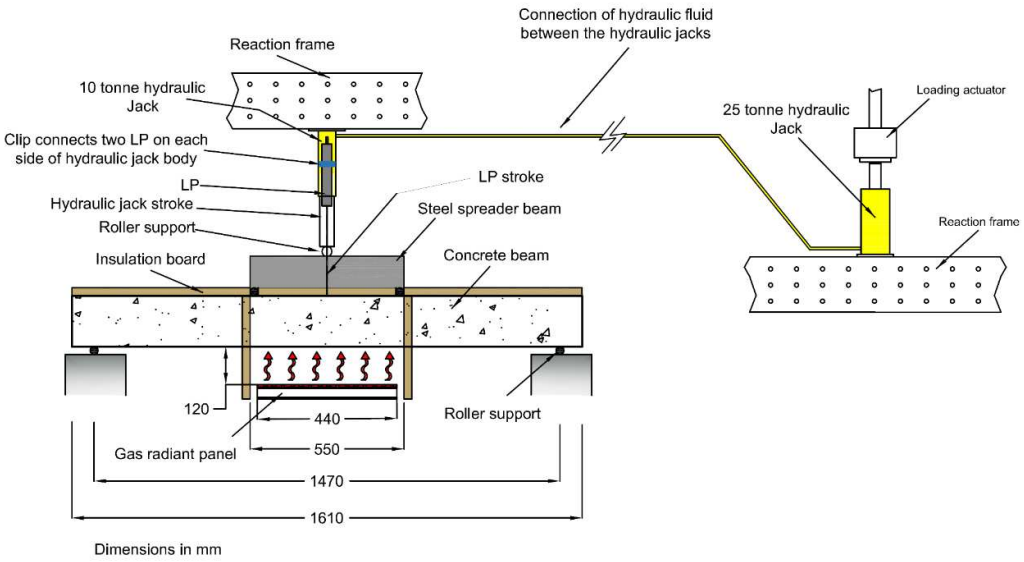

Figure 5.10 Schematic of four-point bending test with localised heating.

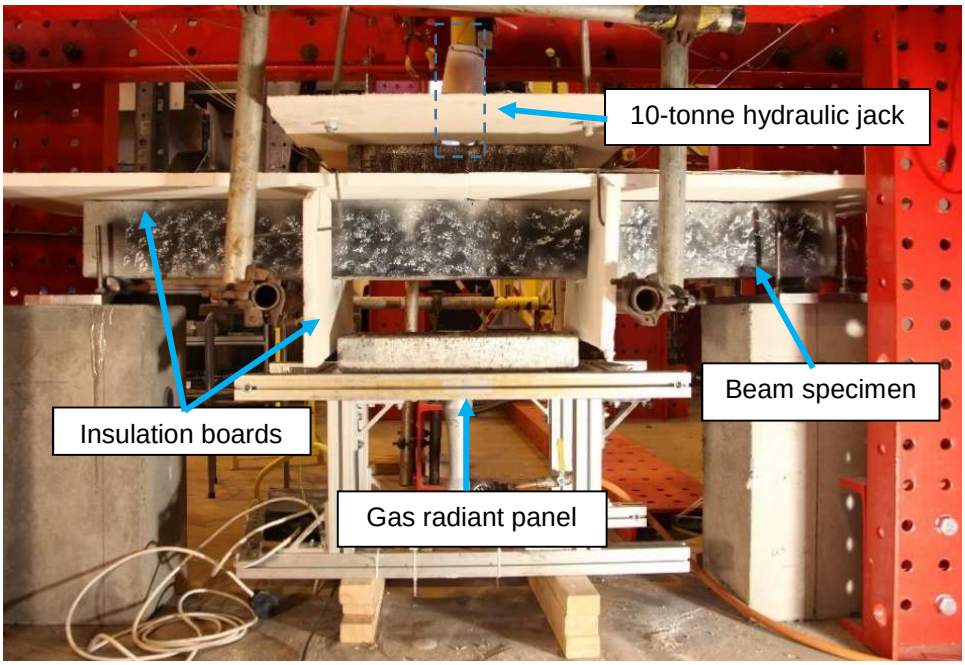

Figure 5.11 Testing arrangement of four-point bending test with localised heating.

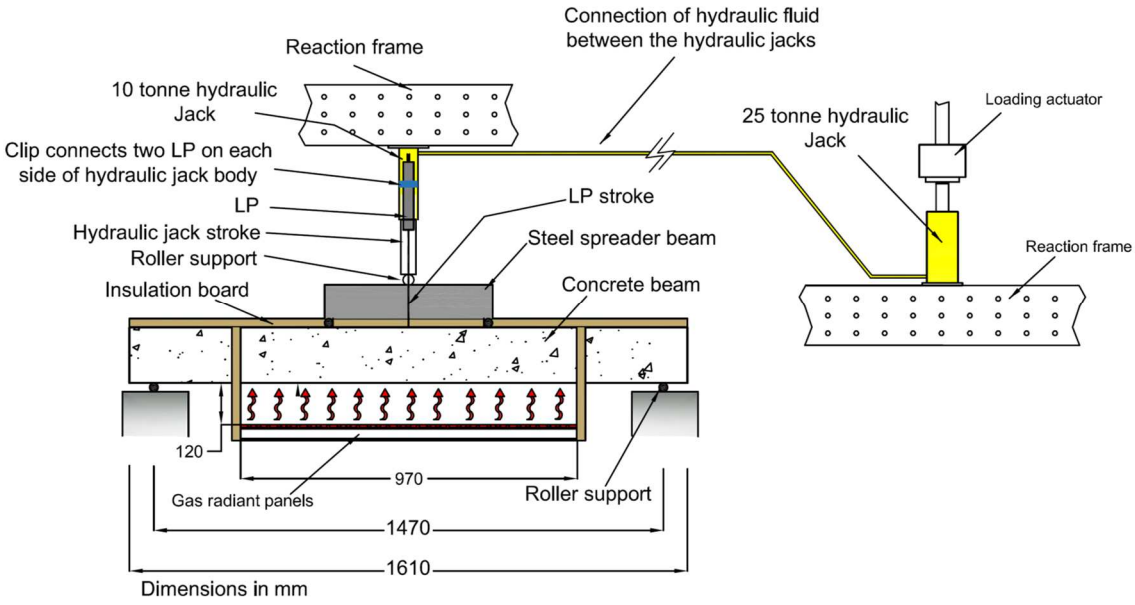

Figure 5.12 Schematic of four-point bending test with localised heating.

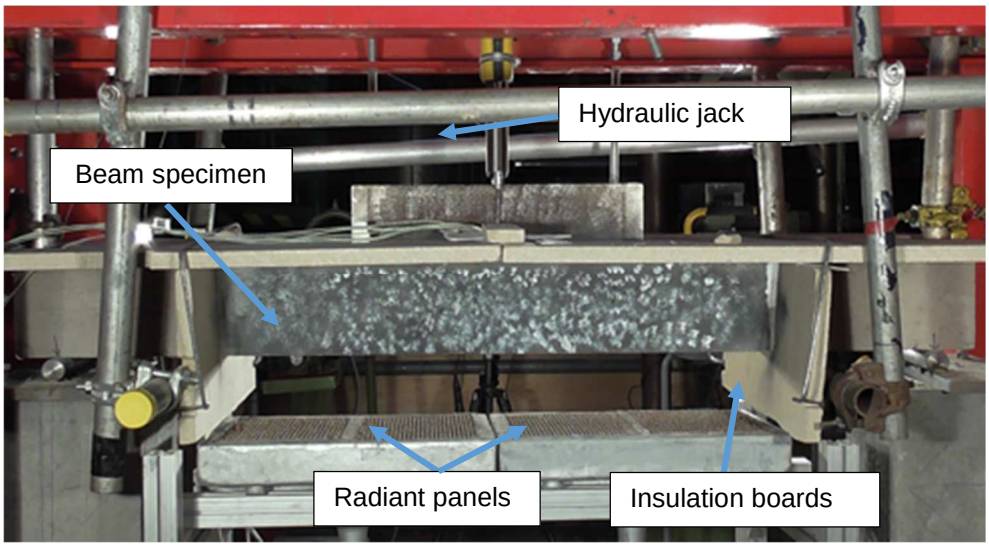

Figure 5.13 Testing arrangement of four-point bending test with localised heating.

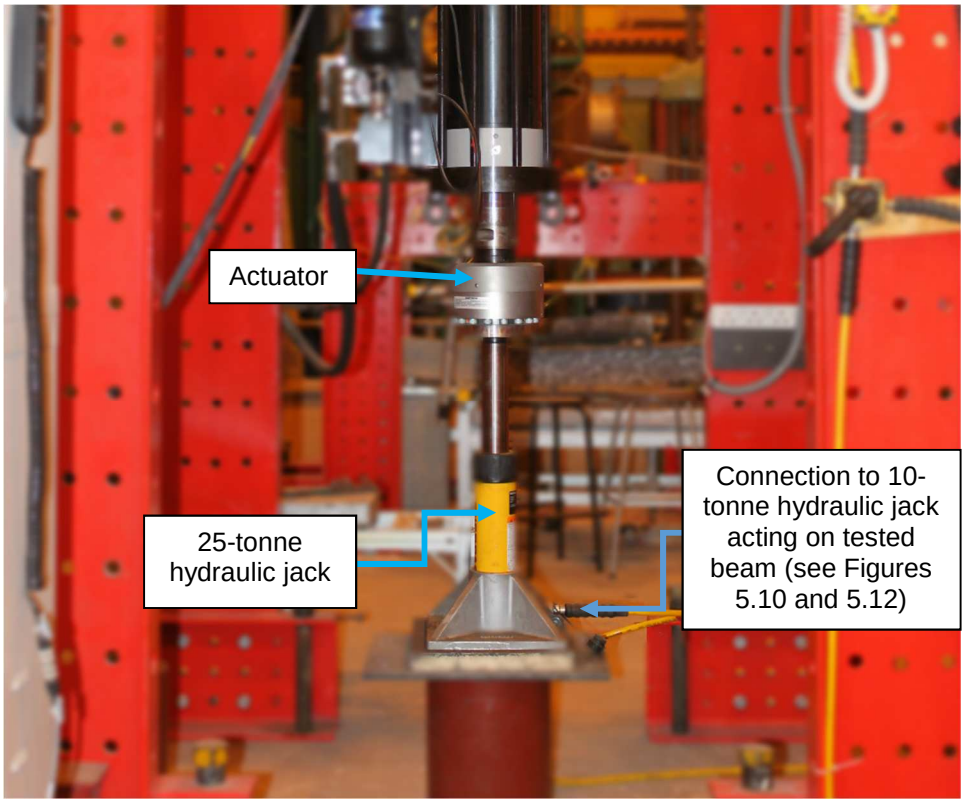

Figure 5.14 Instron actuator pressing 25-tonne hydraulic jack to transfer load to a parallel connected 10-tonne hydraulic jack acting on test beam

5.7.2 Results

Deflection-time response:

Figure 5.15 shows the deflection-time response and failure modes of phase I beam specimens with different reinforcement arrangements under the sustained load and heating. The initail stiffness of beams with different reinforcement arrangements was the same prior to cracking. Post to ignition, however, reinforcement types has a great influence on load-deflection response.

For phase II beam specimens and as observed in ambient tests, reinforcement type has no effect on the initial stiffness of beams (Figure 5.16). Under heating the load value was sustained, however, it can be noticed that beams deflection continued to increase which indicates a degredation of reinforcement bond strength.

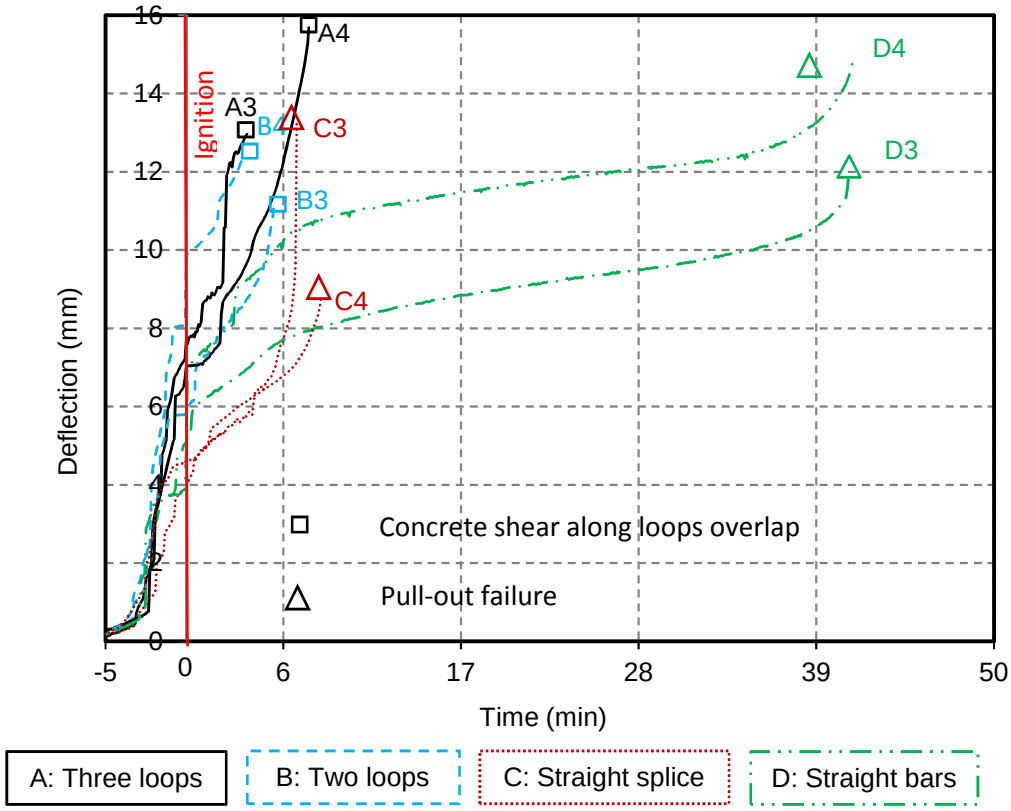

Figure 5.15 Deflection-time response of different beam specimens in heated test (Phase I).

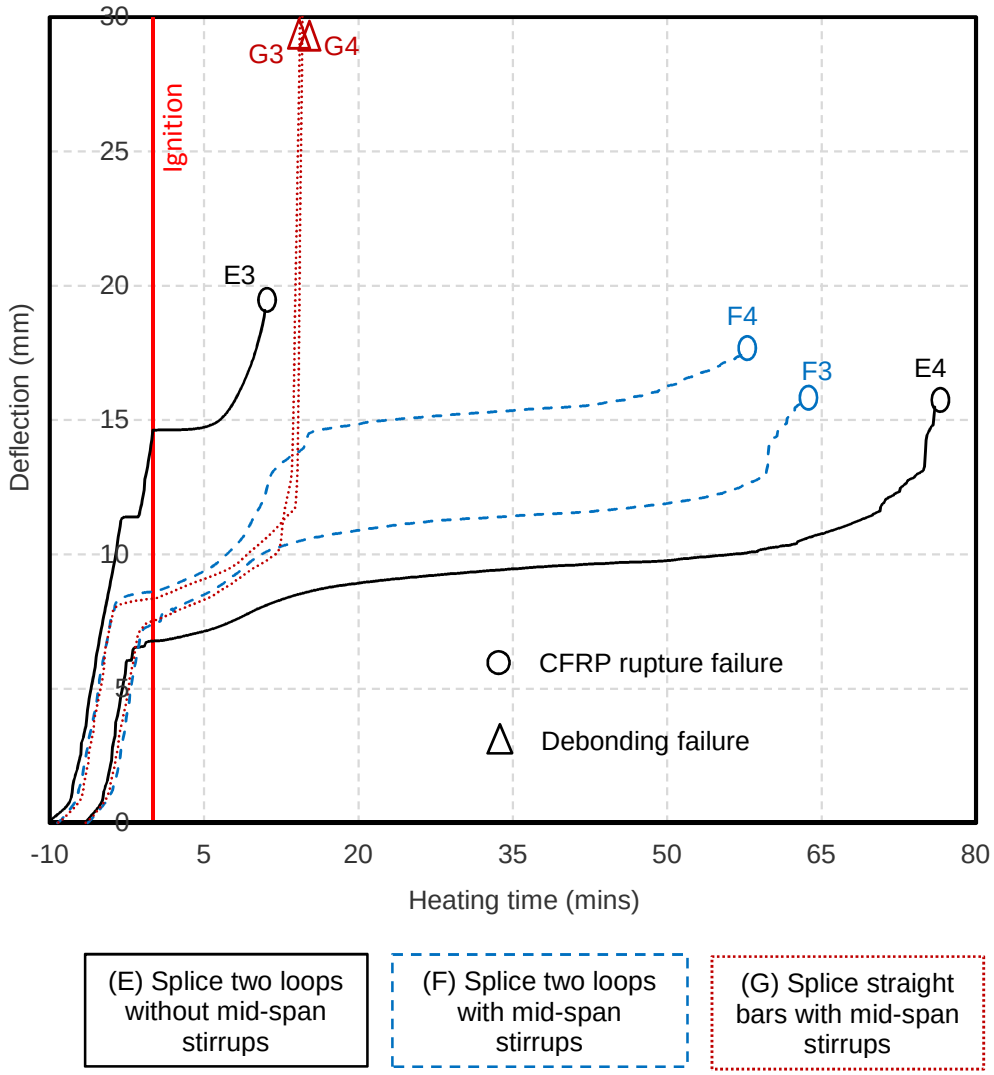

Figure 5.16 Displacement-time response of beam specimens under heating (Phase II).

Fire Resistance Time and Failure Mechanisms:

Table 5.2 below lists the fire resistance time and failure mechanisms of beam specimens with different reinforcement arrangements. Beam specimens with loops overlapped over a short length (type A and B) failed prematurely by concrete shear along loops overlap (Figure 5.17-5.18). Beam specimens with spliced bars (type C) achieved a short fire resistance as elevated temperatures caused reinforcement to pull-out (Figure 5.19). As in ambient temperature tests, beam specimens with

continuous bars (type D) achieved the highest resistance however failure mode changed to pull-out under heating (Figure 5.20).

Table 5.2 Fire resistance time and mechanism of beam specimens in heated test

Specimens	Age (Days)	Concrete cover for both bars (mm)[1]	Average concrete cover (mm)	Sustained load (kN)	Heating duration (min:sec)	Failure mechanism
Phase I						
A3 (Three loops)	342	22, 25	23.5	14.0	8:20	Shear in overlap
A4 (Three loops)	398	27, 32	29.5		7:35	Shear in overlap
B3 (Two loops)	354	23, 25	24		5:30	Shear in overlap
B4 (Two loops)	403	15, 24	19.5		3:35	Shear in overlap
C3 (bars with splice)	381	21, 26	23.5		7:59	Pull-out
C4 (bars with splice)	403	20, 30	25		8:19	Pull-out
D3 (bars no splice)	342	24, 32	28		45:35	Pull-out
D4 (bars no splice)	409	25, 27	26		41:10	Pull-out
Phase II						
E3 (Two loops)	175	27	27	18.5	9:20	FRP rupture
E4 (Two loops)	181	27	27	11.6	76:05	FRP rupture
F3 (Two loops)	187	27	27		62:55	FRP rupture
F4 (Two loops)	190	29	29		57:10	FRP rupture
G3 (bars with splice)	182	26	26		14:40	Pull-out
G4 (bars with splice)	189	31	31		15:00	Pull-out

[1]concrete cover measured at failure location. Concrete cover averaged at both bar when cover difference is 2 mm or less.

Table 5.2 also lists the fire resistance time and failure mechanisms of beam specimens of phase II specimens. Results show that while all beams with spliced bars failed due to debonding by pull-out, CFRP loops maintained interaction till failure occurred due to rupture. Load value appeared to be an important factor as beam with higher sustained load achieved a lower fire resistance time (Table 5.2). There is a trend observed in terms of rupture location, it always occurred just outside of overlap zone. For specimens E3 the test was restarted due to difficulties with propane gas flow. The specimen was loaded and heated for 8 minutes before load and heating

were removed and restarted. This procedure is expected to influence the achieved fire resistance.

Figures 5.17 to 5.23 are photographs show typical failure mechanisms encountered in each specimen type. Figures 5.24 and 5.27 show failure zone in all specimen in respect to reinforcement arrangements.

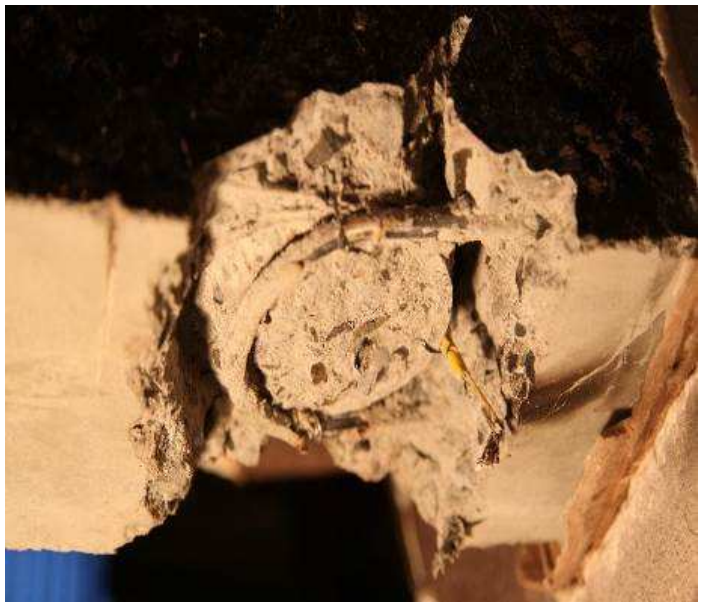

Figure 5.17 Concrete shear along CFRP loops overlap of specimen with three loop A4 (bottom view).

Figure 5.18 Concrete shear along CFRP loops overlap of specimen with two loop B3 (bottom view).

Figure 5.19 Wide crack caused by reinforcement pull-out of beam with spliced straight bars C4 (bottom view).

Figure 5.20 Failure at mid span caused by reinforcement pull-out of beam specimen with continuous reinforcement D3 (side view).

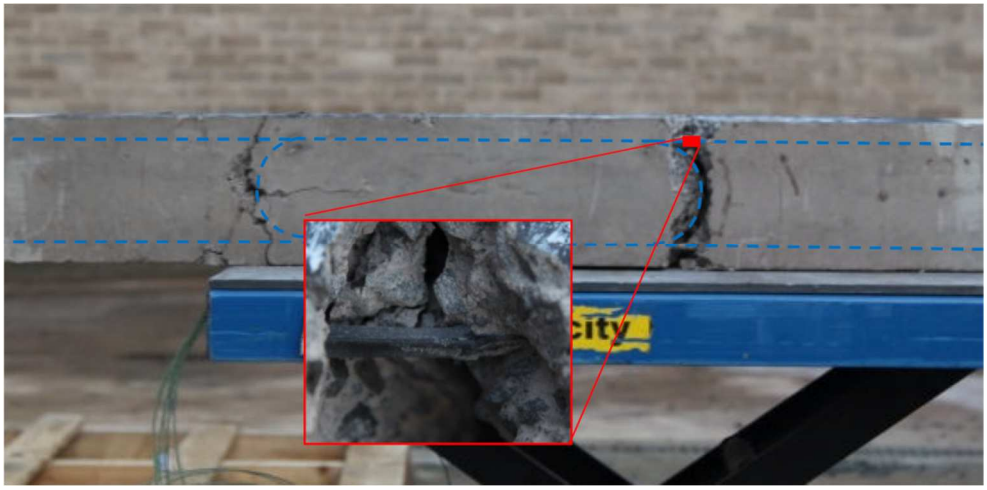

Figure 5.21 Rupture of CFRP loop within constant moment region and out of overlap length (bottom view of specimen E3).

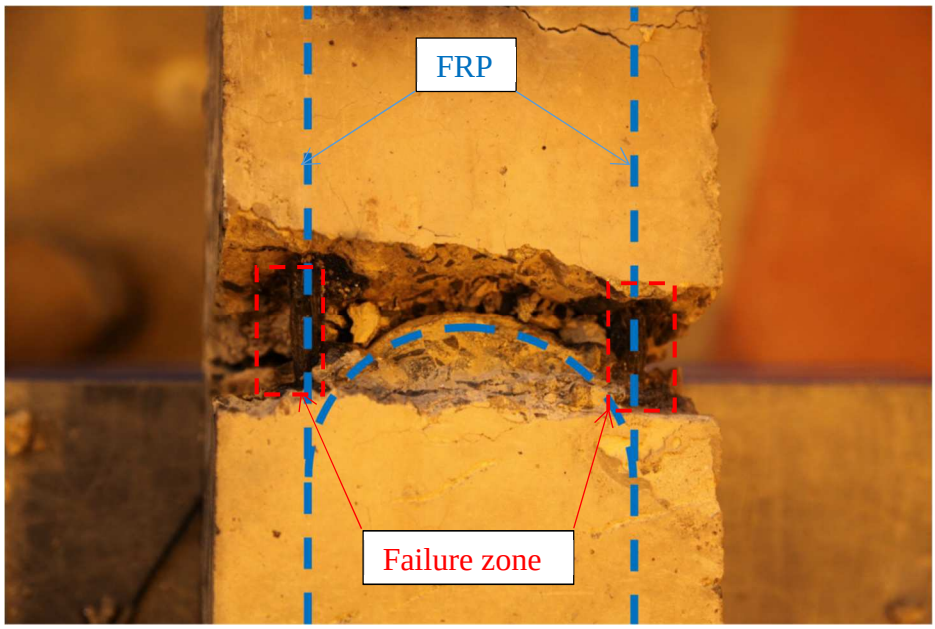

Figure 5.22 Rupture of CFRP loop within constant moment region and out of overlap length (bottom view of specimen F3).

Figure 5.23 Crack open as splice bar pull-out due to debonding at elevated temperature (side view of specimen G2).

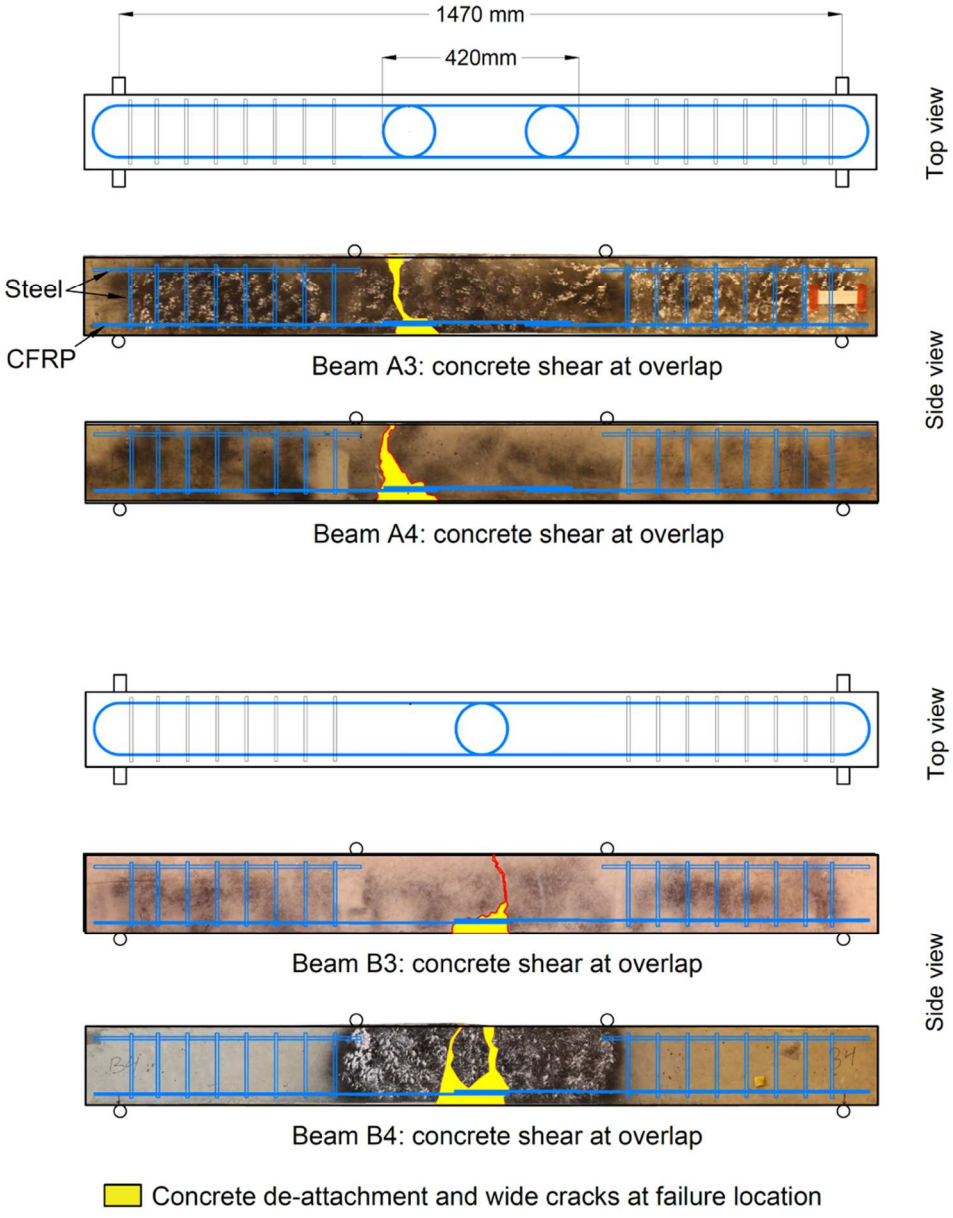

Figure 5.24 Failure zone and mechanism for beam specimens with CFRP loops at elevated temperatures.

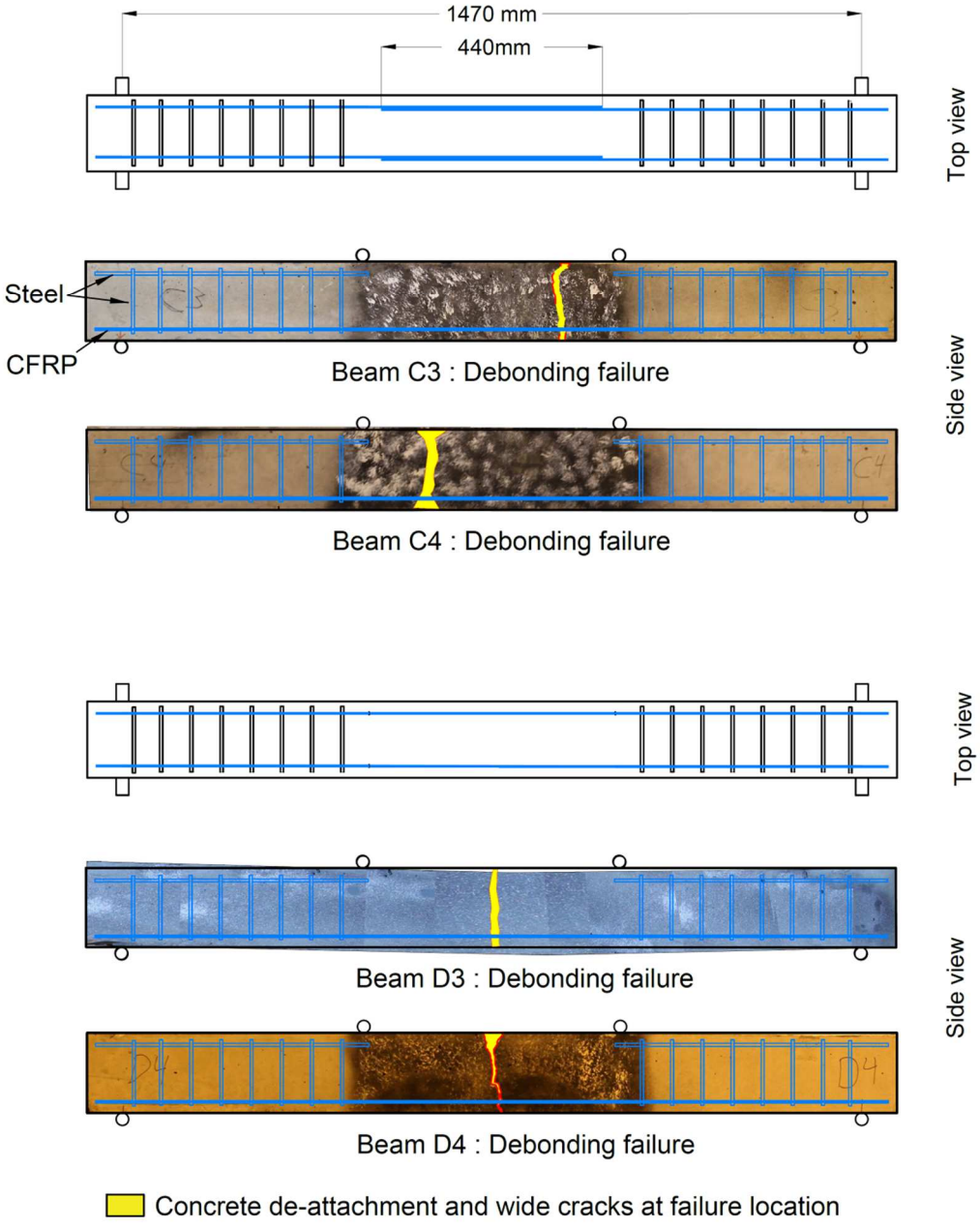

Figure 5.25 Failure zones and mechanisms for beam specimens with splice and continuous CFRP bars at elevated temperatures.

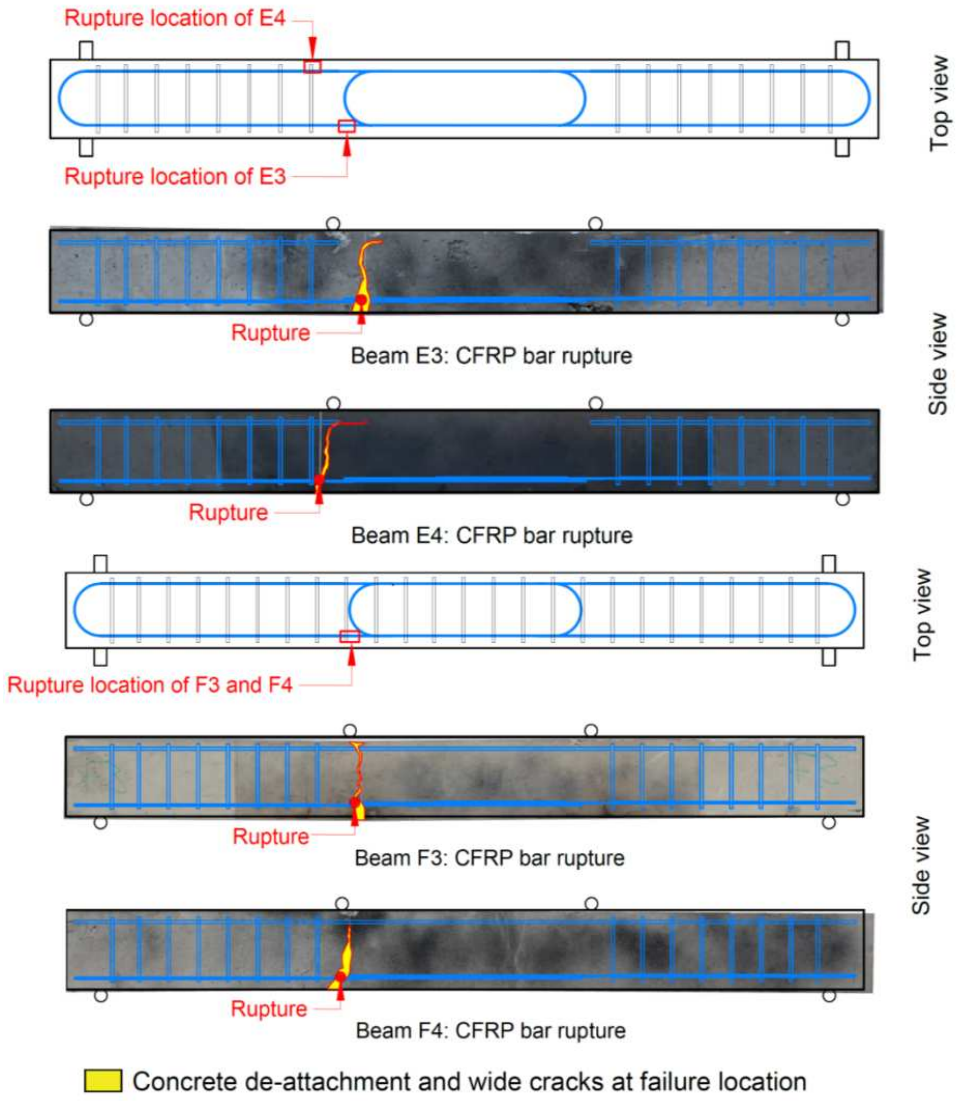

Figure 5.26 Failure zone and mechanism for beam specimens with CFRP loops at elevated temperatures.

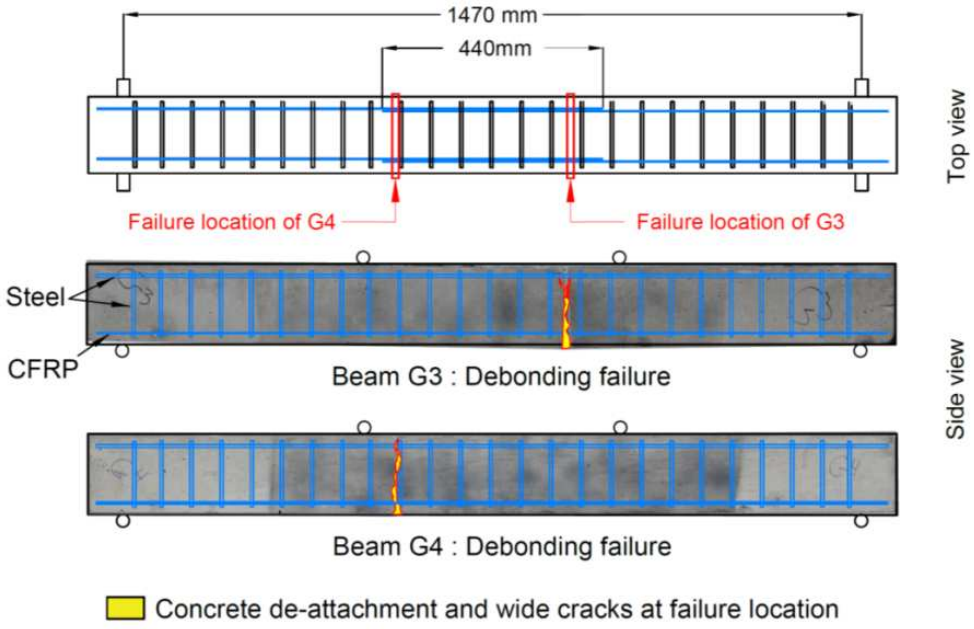

Figure 5.27 Failure zone and mechanism for beam specimens with CFRP spliced bars at elevated temperatures.

Crack patterns

Figures 5.28 and 5.31 below show the crack patterns in the beam specimens with different reinforcement arrangement in heated tests. The images were taken between 0 and 5 second prior to failure. The locations where cracks appeared or propagated during the heating phase are marked with yellow marks.

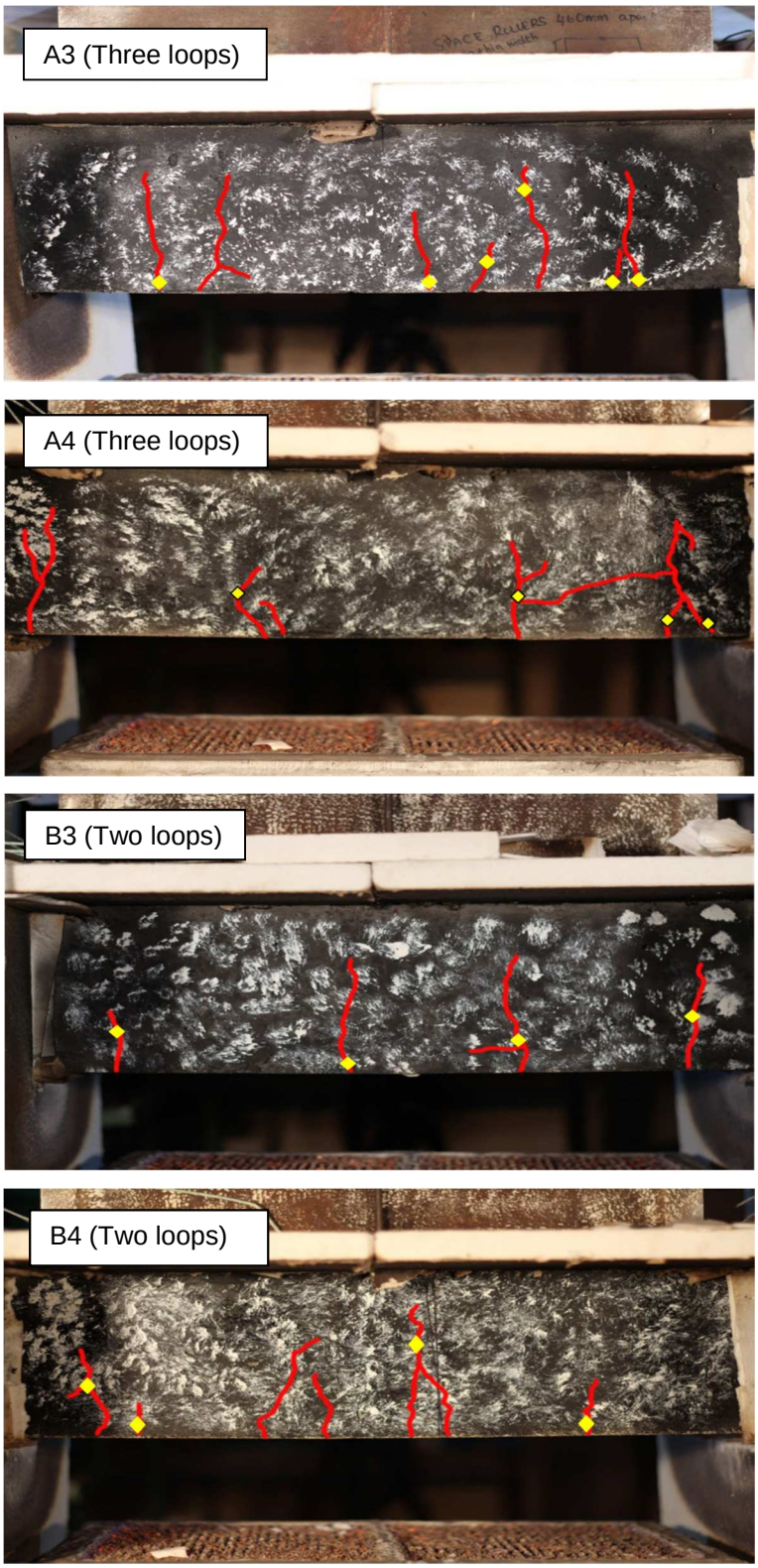

Figure 5.28 Crack patterns of beam specimens with CFRP loops prior to failure at elevated temperatures (the yellow marks indicate locations where cracks start or propagate under heating).

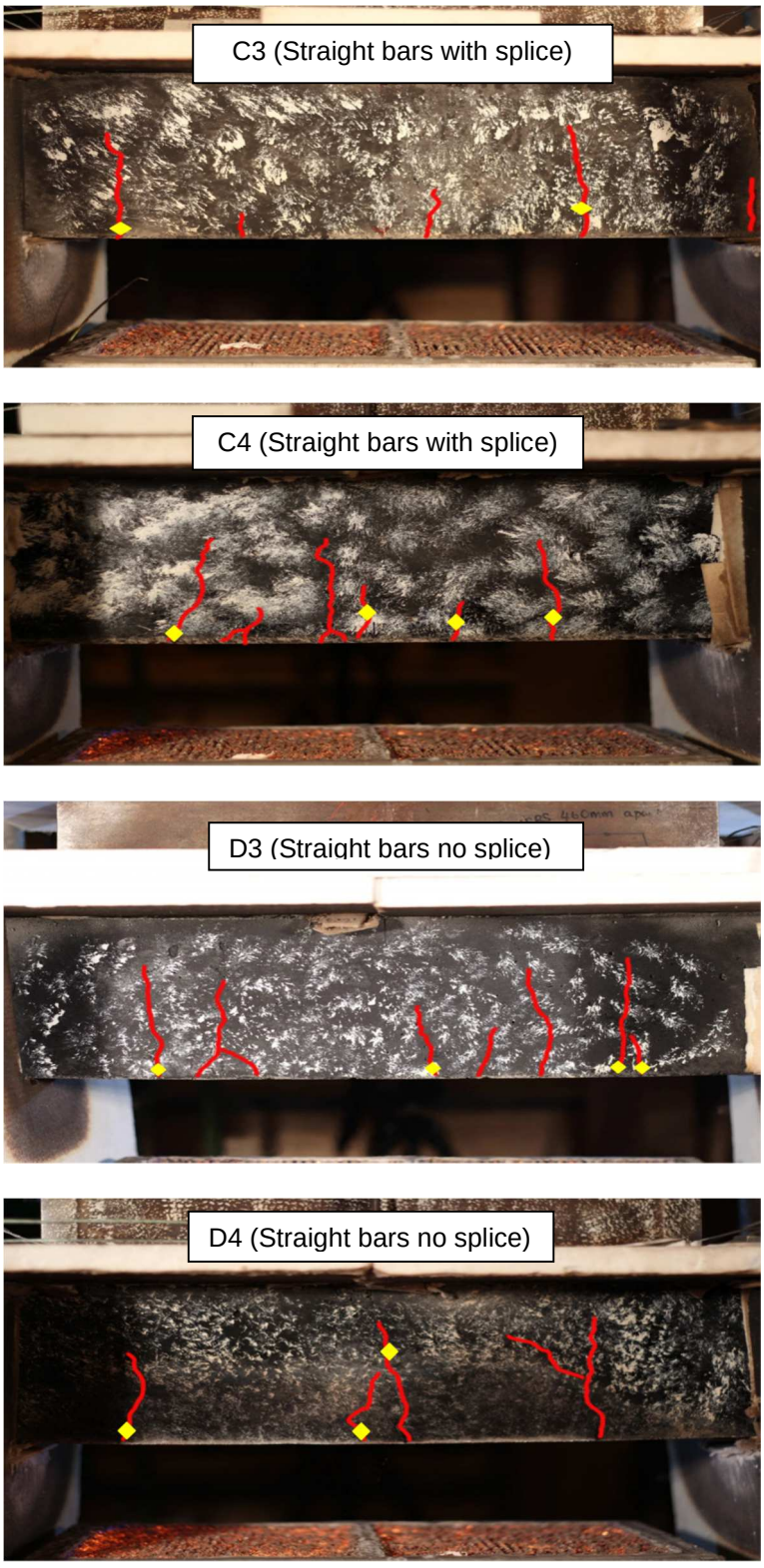

Figure 5.29 Crack patterns of beam specimens with CFRP straight bars prior to failure at elevated temperatures (the yellow marks indicate locations where cracks start or propagate under heating).

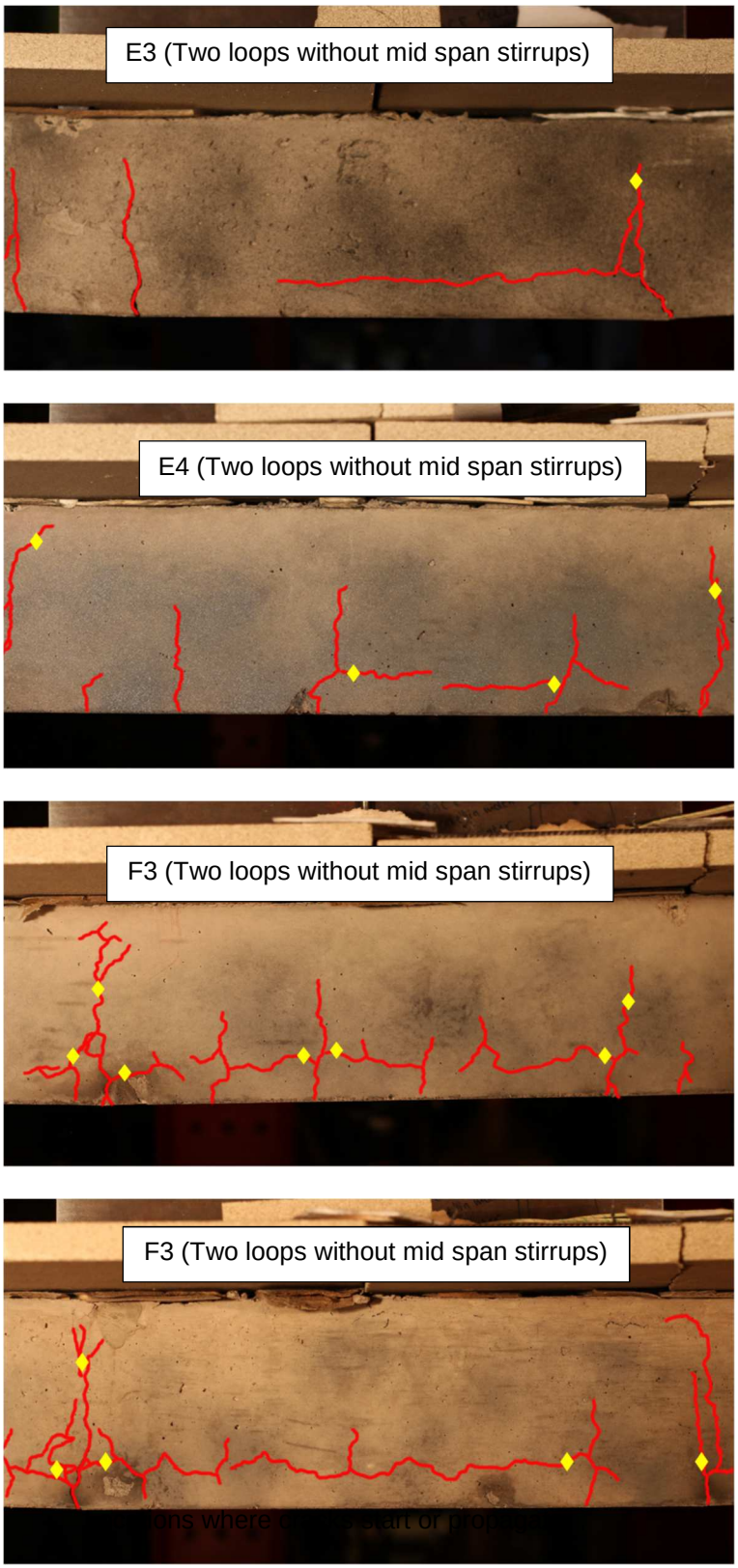

Figure 5.30 Crack patterns of beam specimens with CFRP loops prior to failure at elevated temperature.

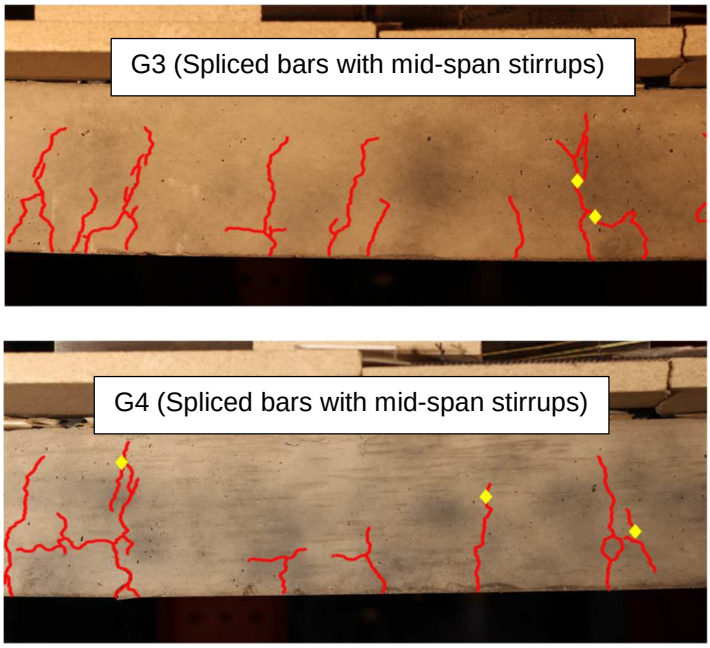

Figure 5.31 Crack patterns of beam specimens with splice CFRP bars at elevated temperatures.

CFRP Reinforcement and Concrete Temperature Propagation

The figures below show the temperatures recorded in the CFRP reinforcement for the beam specimens with different reinforcement arrangements.

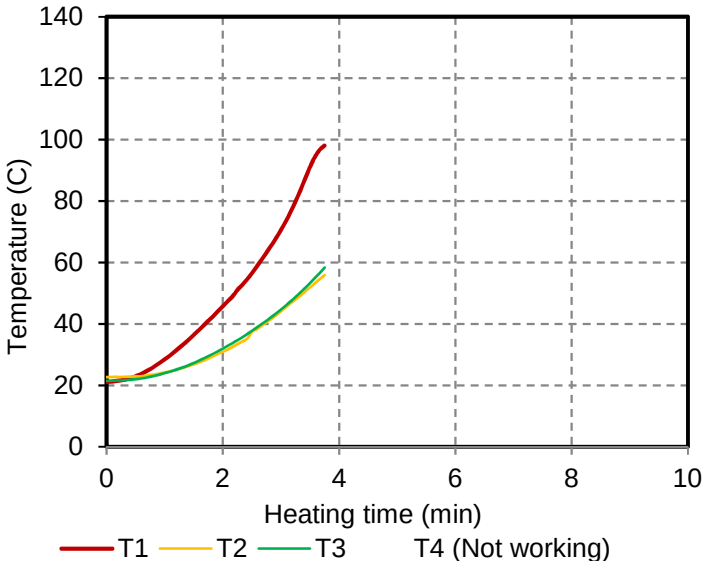

Figure 5.32 Temperature propagation at bottom of reinforcement after ignition (Specimen A3).

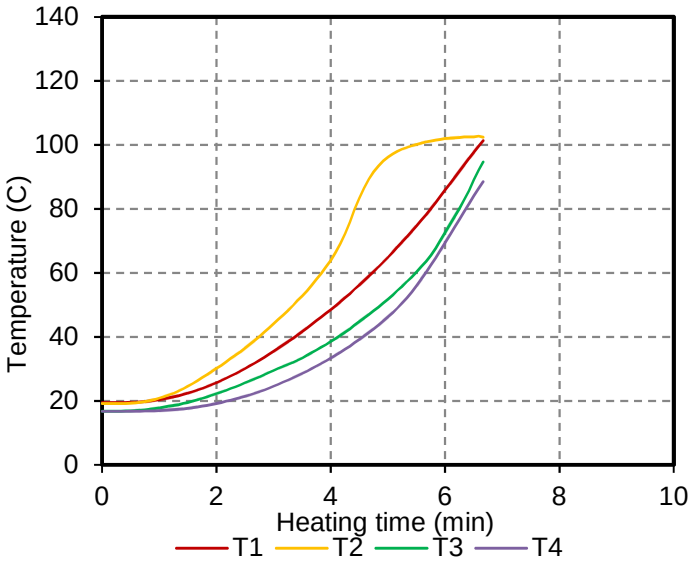

Figure 5.33 Temperature propagation at bottom of reinforcement after ignition (Specimen A4).

Figures 4.48-4.55 show the temperatures of the thermocouples installed on CFRP reinforcement and thermocouple trees (see section 5.5.2) measuring concrete temperature at different depth of beam specimen B3 (with three CFRP loops).

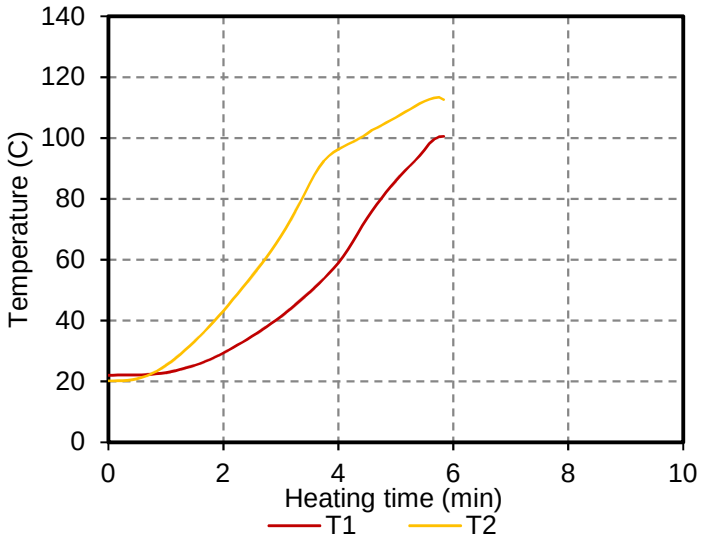

Figure 5.34 Temperature propagation at bottom of reinforcement after ignition (Specimen B3).

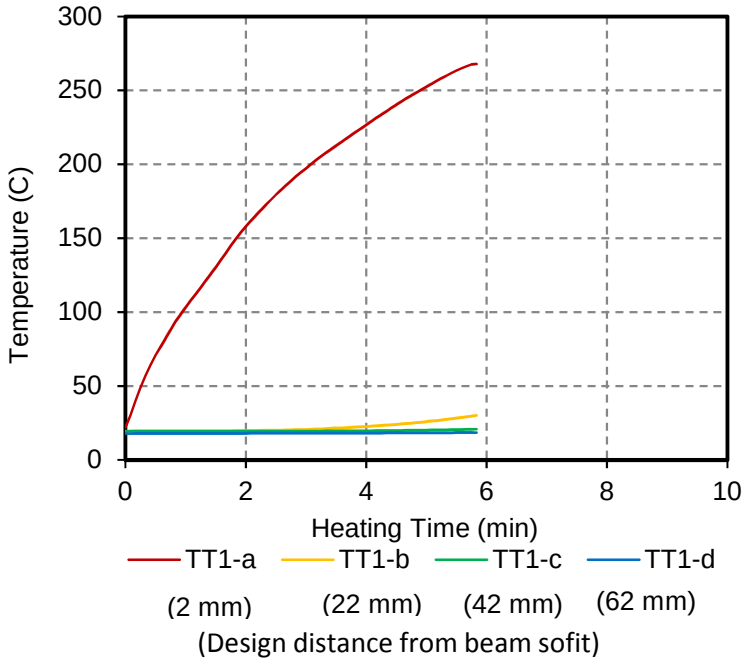

Figure 5.35 Temperature propagation of concrete at different heights from readings of thermocouple tree TT1 (Specimen B3).

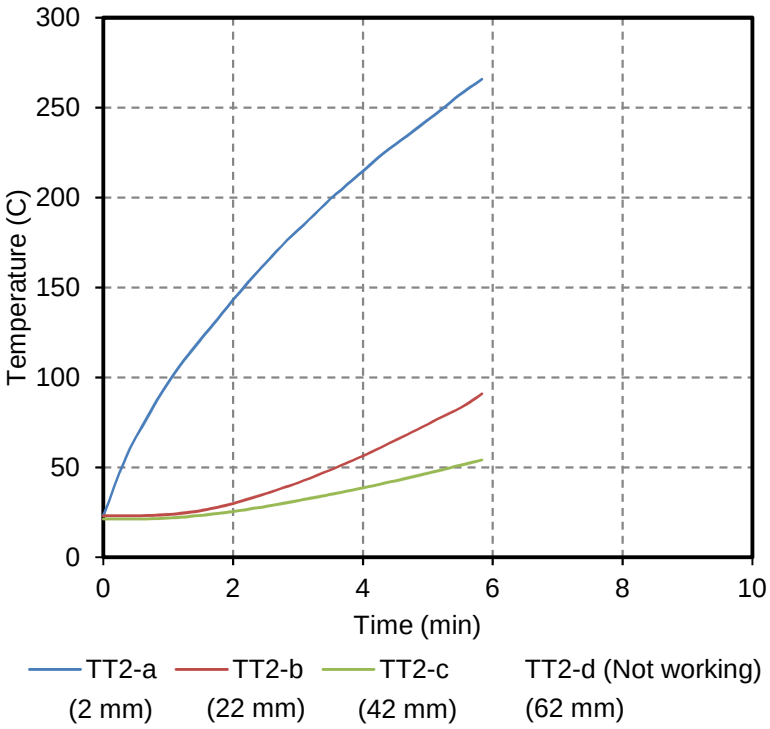

Figure 5.36 Temperature propagation of concrete at different heights from readings of thermocouple tree TT2 (Specimen B3).

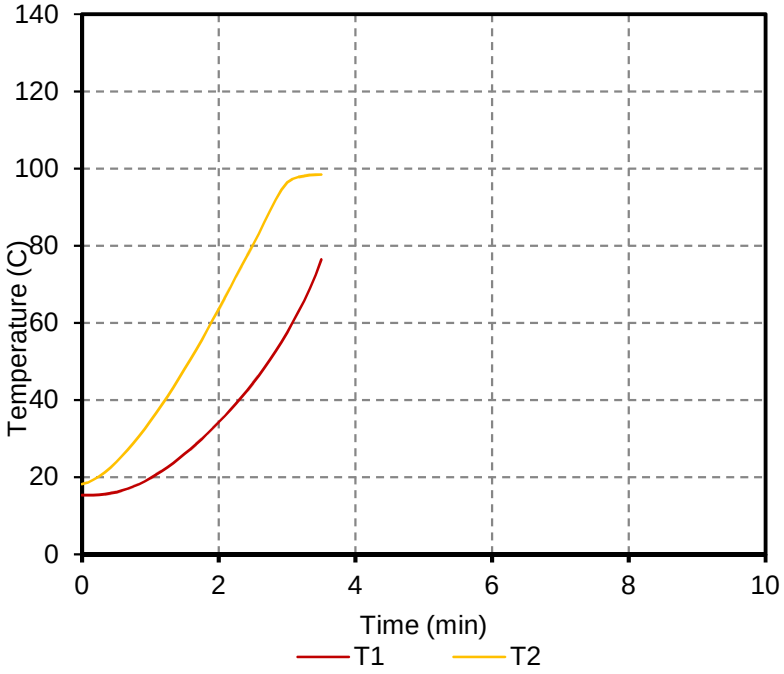

Figure 5.37 Temperature propagation at bottom of reinforcement after ignition (Specimen B4).

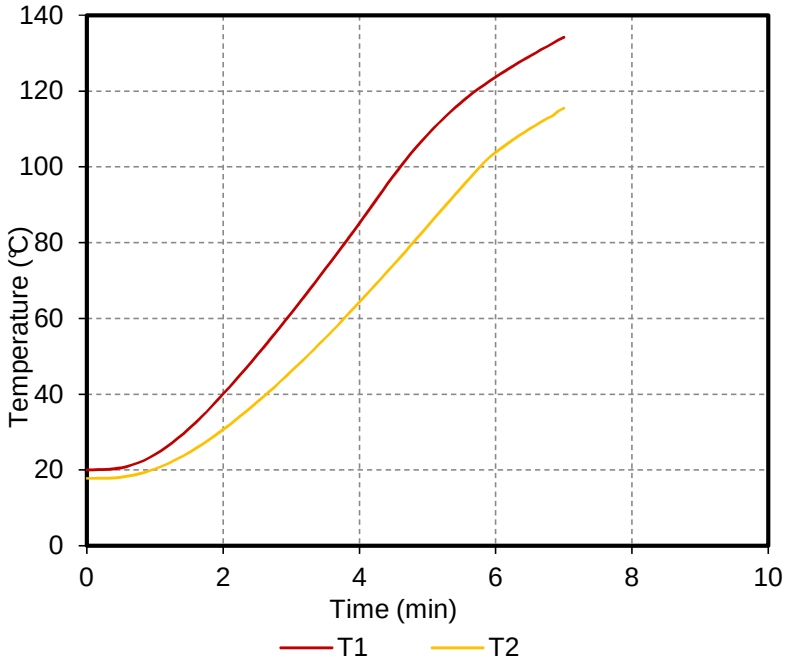

Figure 5.38 Temperature propagation at bottom of reinforcement after ignition (Specimen C3).

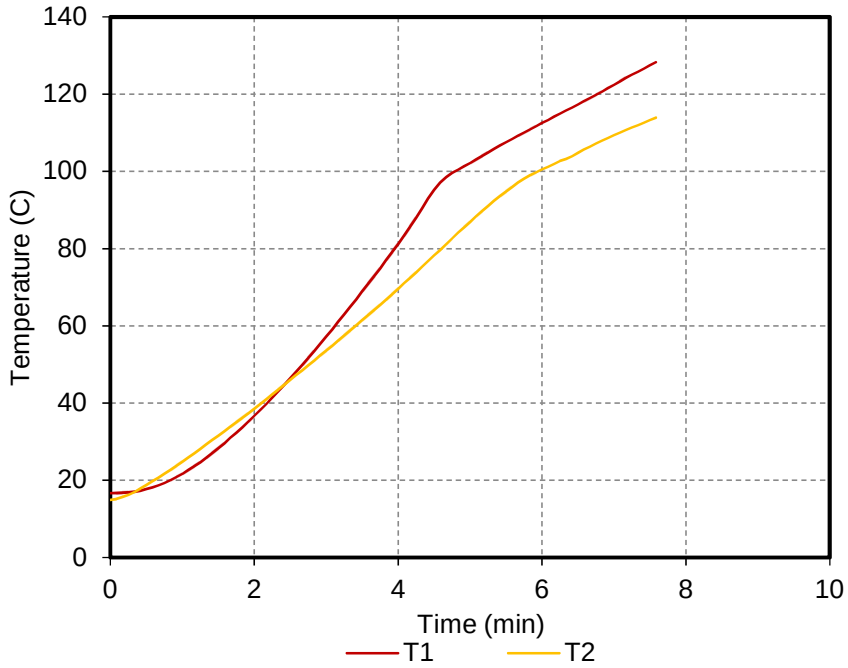

Figure 5.39 Temperature propagation at bottom of reinforcement after ignition (Specimen C4).

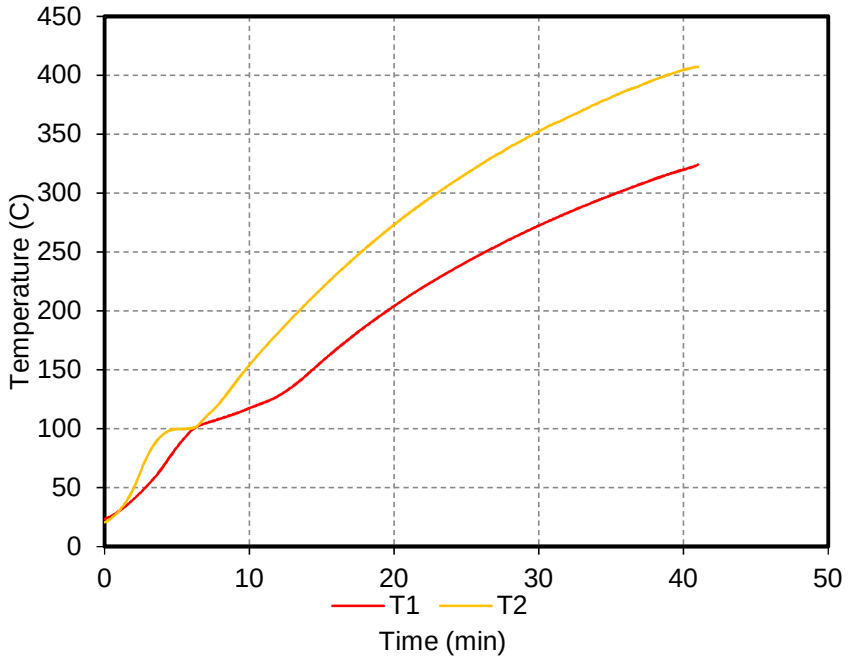

Figure 5.40 Temperature propagation at bottom of reinforcement after ignition (Specimen D3).

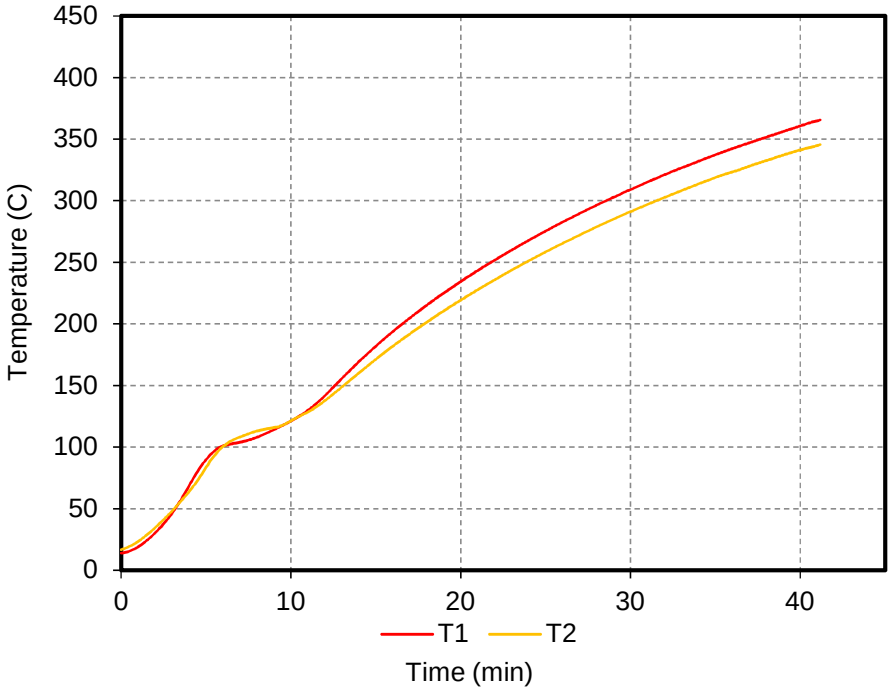

Figure 5.41 Temperature propagation at bottom of reinforcement after ignition (Specimen D4).

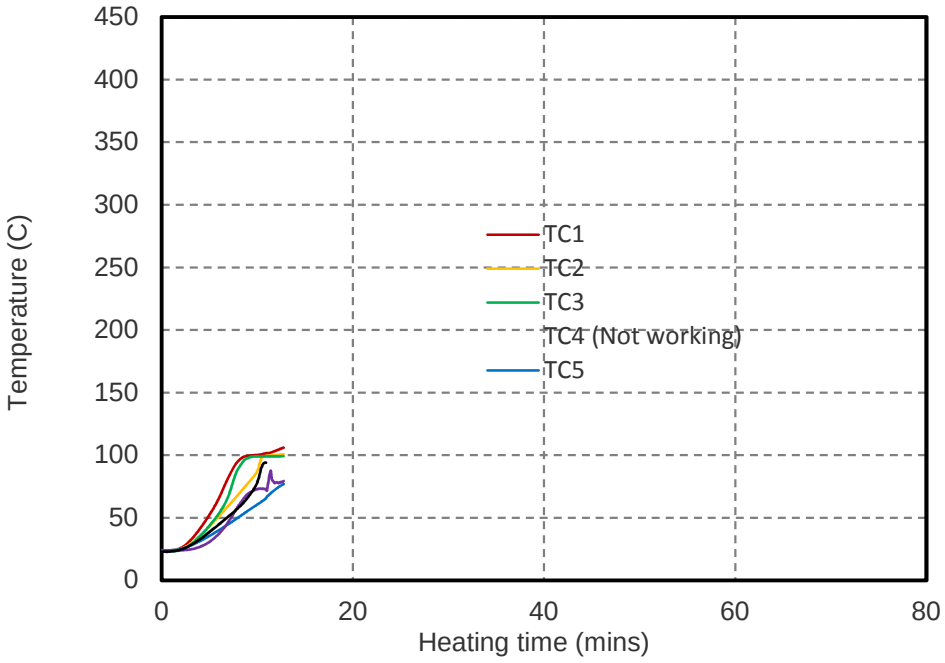

Figure 5.42 Temperature propagation at bottom of reinforcement after ignition (Specimen E3: Loops without mid-span stirrups).

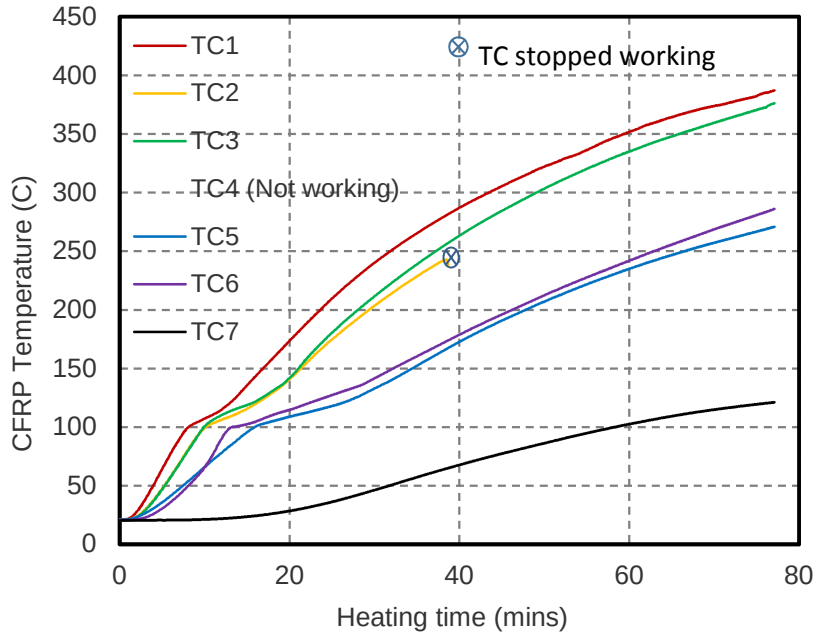

Figure 5.43 Temperature propagation at bottom of reinforcement after ignition (Specimen E4: Loops without mid-span stirrups).

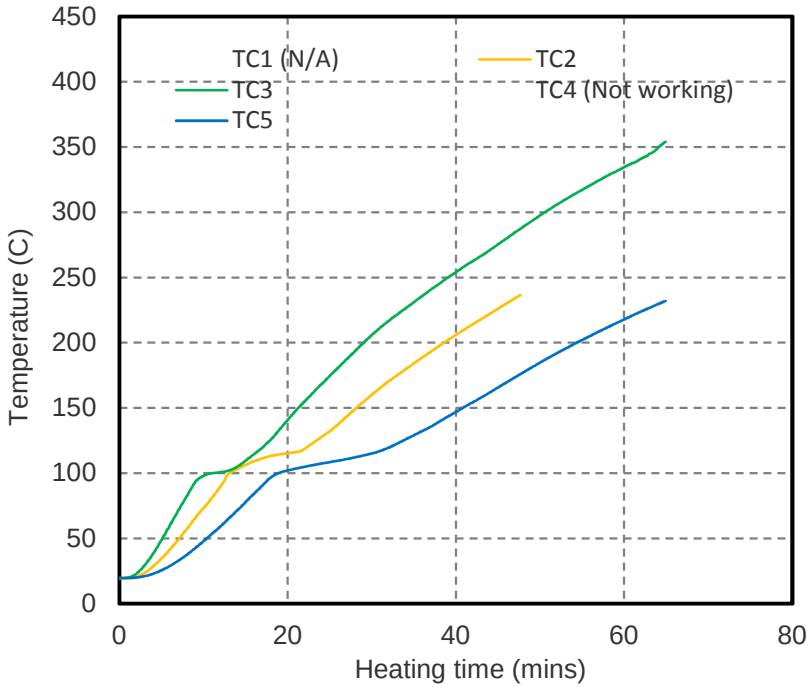

Figure 5.44 Temperature propagation at bottom of reinforcement after ignition (Specimen F3: Loops with mid-span stirrups).

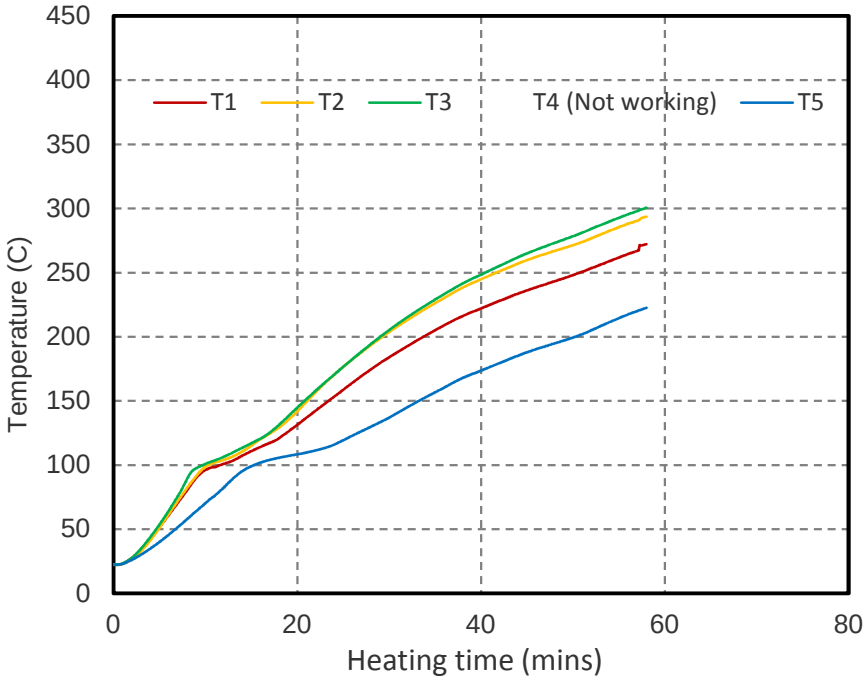

Figure 5.45 Temperature propagation at bottom of reinforcement after ignition (Specimen F4: Loops with mid-span stirrups).

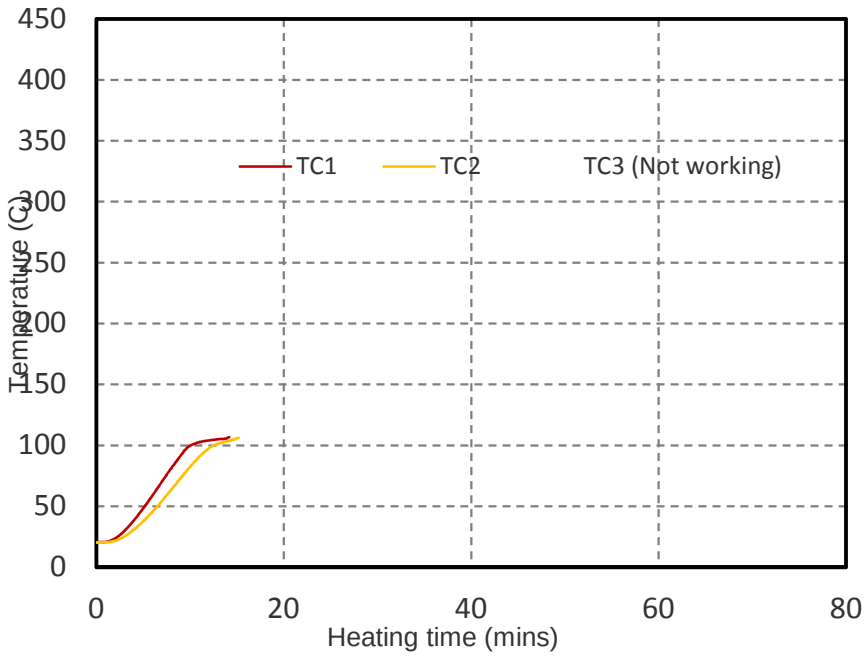

Figure 5.46 Temperature propagation at bottom of reinforcement after ignition (Specimen G3: spliced bars with mid-span stirrups).

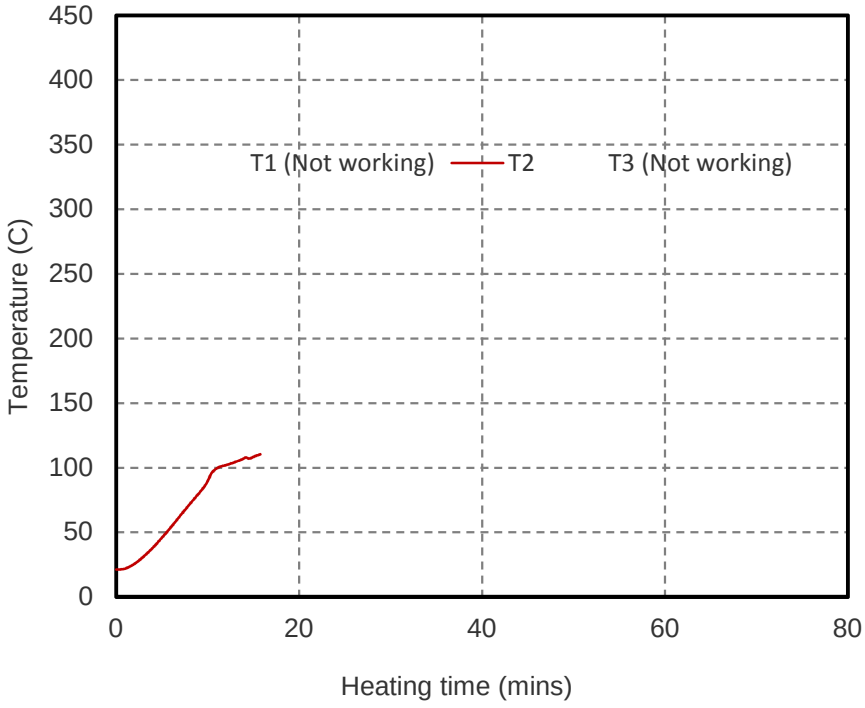

Figure 5.47 Temperature propagation at bottom of reinforcement after ignition (Specimen G4: spliced bars with mid-span stirrups).

5.8 Discussion of Heated Tests Results

Under heating and sustained load there were distinct differences in fire resistance times and failure modes between beam specimens with different reinforcement arrangements.

5.8.1 Deflection response under heating

As a general trend, all specimens exhibited increasing deflection after ignition and under sustained load. The deflection response of one specimen from each beam type is shown in Figure 5.48. Deflection response under heating and sustained load shows an increasing in beams deflection, which can be attributed to a combination of two factors:

1. The first factor is deflection induced by a thermal gradient across the section, which had the quickest effect on deflection. Results from the phase I beam specimens showed vast temperature variation of about 230 °C within 60 mm from the beam soffit (Figure 5.35).
2. The second factor is bond degradation between the CFRP reinforcement and concrete. The sensitivity of the FRP bond strength to elevated temperatures is reflected by the dynamic mechanical analysis results for the EL2 epoxy resin used in the reinforcement (Appendix A.2). The temperature of the CFRP reinforcement in the heated tests (Figures 5.32-5.47) easily exceeded the glass transition temperature of the matrix, T_g = 87.6 °C, (Appendix A.2). This severely reduced the bond stress between the reinforcement and concrete, and consequently increased the deflection of the beams.

For the beams with continuous straight bars in post-ignition (under the sustained load), three phases of deflection response can be recognised (Figure 5.15 and 5.48). In the first phase (over 7 minutes from ignition), the deflection of beam increases influenced by thermal gradient and CFRP bond degradation. However, unlike the beam specimens with spliced bars (type C and G), failure did not occur at the end of this phase, because anchorage was provided outside the heated zone. In the second phase, the deflection rate of the beam specimen decreased even though the reinforcement temperature continued to increase, because the reinforcement acted as a tie within the beam. This tie-action could occur due to the CFRP reinforcement being de-bonded from the concrete within the heated region, but the end anchorage of the bars was provided in areas not directly exposed to fire (Figure 5.49), and provides additional strength to beams to resist thermo-mechanical load (Rafi et al., 2007; Rafi and Nadjai, 2011; Carvelli et al., 2013). The deflection rate is reduced, but did not stop, because heat gradually propagated toward the regions not directly exposed to fire (cold regions) and caused bond degradation of the reinforcement portions that act as anchorage. After an extended period of fire exposure (40-45 minutes) and due to heat conducted from the heated zone, the anchorage could no longer sustain the transferred loads. In the third phase and in a similar manner to

spliced bars specimens, the deflection rate accelerated and was followed by failure due to bar pull-out.

The absence of reinforcement continuity significantly influenced the response of beam specimens with spliced straight bars (types C and G). These beams type exhibited an increasing deflection over a short time of heating before the deflection rate accelerated prior to pull-out failure. A similar trend of deflection response was observed in beam specimens with short overlapped loops (types A and B), however failure was more brittle.

Three phases of the load-deflection response can also be recognised in the beam specimens with long CFRP loops (E and F) after ignition (Figure 5.16). The initial phase (≈ 12 minutes after ignition), caused the beam deflection to increase, due to the thermal gradient across the beam section and reinforcement bond degradation. Failure did not occur at this stage as the CFRP loops had second load carrying mechanism, by direct bearing on the concrete (instead of bond). Despite the increasing temperature, in the second phase the deflection rate reduced, as the loop reinforcement was anchored to the concrete at the curved parts. In the third phase, the progressive rupture of fibres was evident as an increased deflection rate leading eventually to failure (Figure 5.16). As the matrix softened, it lost the ability to provide load sharing between the fibres, and this caused an unequal load distribution between individual fibres, resulting in fibre rupture.

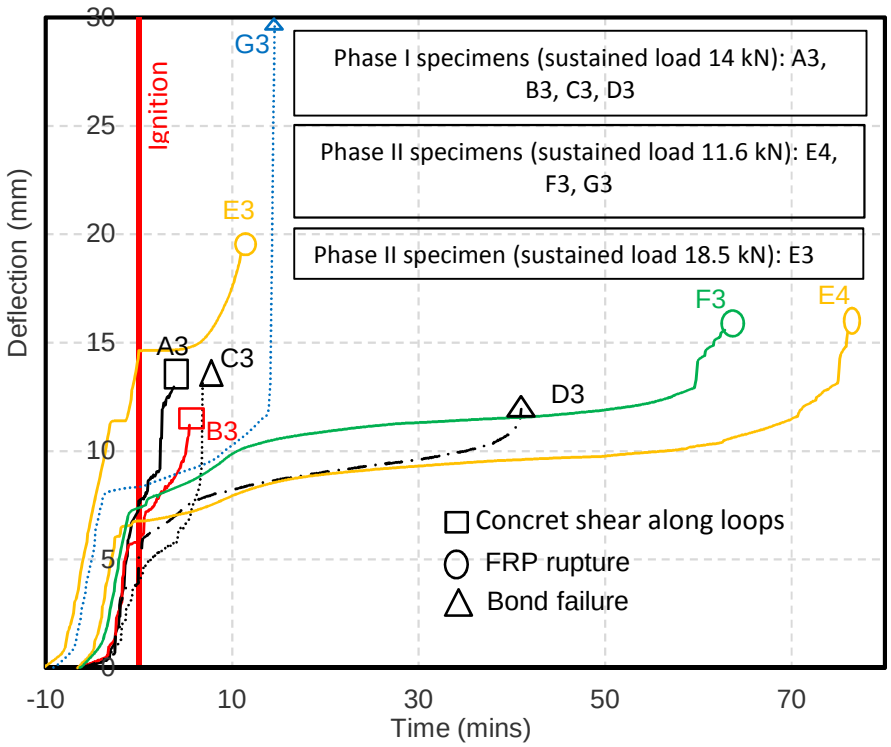

Figure 5.48 Load deflection response of one specimen of each type of phase I and phase II beam specimens under heating. A: Three loops (short overlap), B: Two loops (short overlap), C: Straight splice, D: Continuous straight bars, E: Two loops (long overlap), F: Two loops (long overlap with mid-span stirrups), F: Splice bars with mid-span stirrups.

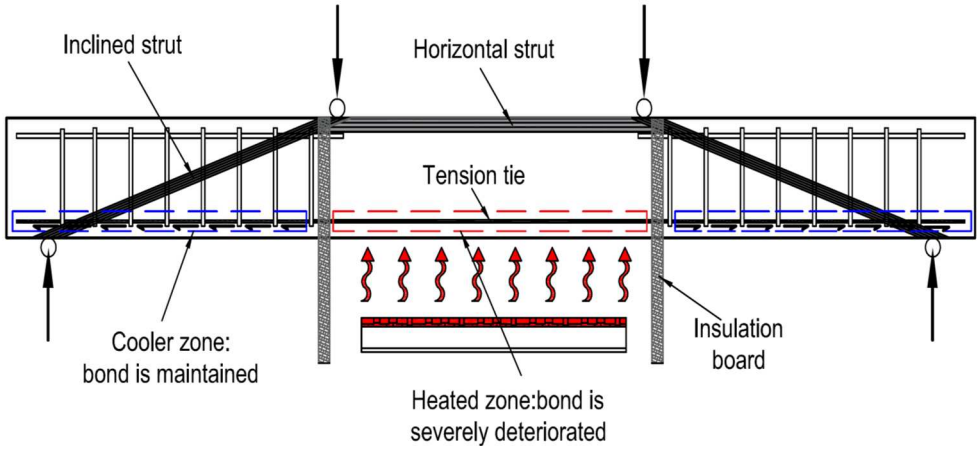

Figure 5.49 Beam with continuous CFRP bars transform to tie-arch action when de-bond occurs at heated region

5.8.2 Failure mechanisms

The heated tests upon specimens with CFRP loops (types A and B, short overlapped loops) had the same failure mode as during the ambient temperature tests. Failure occurred by concrete shear along the loop overlap after a short time of fire exposure (up to 6 minutes). The failure was sudden and accompanied by complete detachment of the concrete along the circular overlap zone (Figures 5.17 to 5.18). Even though the sustained load was lower than the ambient failure load, the thermal stresses generated from temperature gradients across the section are likely to have initiated failure. The shear strength of the concrete will also have been affected by the presence of pore water, especially as the thermocouples readings on the reinforcement prior to failure showed temperatures in the range of 100 – 115 °C. Visual inspection after failure showed no sign of rupture in the CFRP loop, which confirmed that failure was initiated solely due to concrete shear along splice. The reinforcement sand coating, however, was removed from some parts.

The failure mechanism of the beams with spliced straight bars (type C) changed from concrete splitting (as observed in ambient tests), to bond failure by bar pull-out. This failure was initiated after a short time of fire exposure. A similar trend has been reported by McIntyre et al. (2015). As the reinforcement temperatures increased, the bond strength along splice was reduced until the specimen reached a level where the reinforcement could no longer sustain the transferred load, and failure occurred at the cracks. Visual inspection after failure showed that some longitudinal cracks were formed along the bottom of the beam specimens as shown in Figure 5.19. The crack patterns are discussed in section 5.8.3.

Failure of the beams with continuous straight bars (type D) bridging the heated zone also changed from rupture during the ambient temperature tests to pull-out failure under heating and sustained load. During heating and prior to failure, a clear smell of burned polymer was detected and some traces of black also formed around the cracks within the heated region. These were signs of the CFRP polymer matrix being severely degraded. Thermocouple data show that during heating, the reinforcement

temperature at the mid-span reached temperatures in the range of 350 – 400 °C (Figures 5.40-5.41), much higher than the polymer glass transition temperature (T_g = 87.6 °C). However, cold anchorage of the bars in areas not directly exposed to fire enabled the beams to support loads and achieve fire resistance time exceeding 40 minutes, longer than any other specimens in phase I of beam tests.

The concept of providing an anchor for continuous reinforcement in areas not directly exposed to fire to enhance FRP reinforcement performance at elevated temperatures has been previously investigated by other researchers and the cases of both bond and flexural failures have been reported (see section 2.12). In the current research, although the provided anchorage length out of the heated region (≈530 mm) exceeded the required development length (l_d = 155 mm) by ISIS (2007) (Appendix C.7) and the anchorage lengths used in studies (Nigro et al., 2012; Nigro et al., 2011b; Rafi et al., 2007; McIntyre et al., 2015), failure still occurred due to bond loss. This indicates that the CFRP reinforcement failure mode under heating, whether pull-out or rupture, is not solely affected by the anchorage length. The size of the heated region, load value, and heat flux penetrating the beam section also appear to affect CFRP reinforcement failure mode. Pull-out and rupture failure intrigued due to degraded bond with concrete and reduced the tensile strength of rebar at higher temperatures. Therefore, depending on the amount of heat that has been conducted to cooler regions and bar critical rupture temperatures under specific load, failure mode is determined.

Post failure examination of type D beam specimens showed that the polymer matrix of CFRP bars was burned out and the reinforcement turned into a bundle of fibres, confirming that the reinforcement within the heated region behaves as a tie, resulting in tie-arch action in the beam (Figure 5.49). The CFRP reinforcement in the cold anchorage areas was heated by conduction through the concrete in the absence of oxygen (or with limited oxygen supplied through the cracks). Once the bar pulled out, the exposed area of CFRP bars ignited, as shown in Figure 4.20.

During the elevated temperatures tests of phase II specimens, the benefit of the CFRP loops became clear. The beams with straight bars (type G) failed due to

reinforcement pull out after a short time (≈ 15 minutes) of fire exposure. Conversely, under the same sustained load, the specimens with CFRP loop reinforcements retained sufficient strength to carry the sustained applied load for a period up to five times longer than the spliced straight bars, and failed by CFRP rupture.

The failure mode of beams with splice straight bars (type G) changed from reinforcement rupture at ambient temperature to pull-out of the reinforcement. Pull-out failure occurred because the CFRP bars could no longer transfer force to concrete through bar surface due to the softening of matrix resin. Pull-out failure is associated with rapidly increased deflection and widening of flexural cracks at splice end (Figures 5.23 and 5.27). A similar trend was also observed by other researchers (Harajli and Abouniaj, 2010; Weber, 2008; McIntyre et al., 2015).

Specimens with CFRP loops and long overlap lengths (types E and F) failed by CFRP rupture, rather than by bond failure, at longer durations of heating (57-76 minutes) more than any other specimen type, including the straight continuous bars which relied upon cold anchorage. Rupture of the reinforcement indicated that the reinforcement was sufficiently anchored in the concrete for the FRP to reach its ultimate tensile capacity at elevated temperatures. When the interlock and friction mechanisms of bond force transfer were lost due to softening of the matrix, tensile forces could still be resisted through the carbon fibres in the loops. Although the weaker section of the CFRP loops was the curved part (as demonstrated through tension and push-off tests in Chapter 3) rupture failure did not occur there due to the additional available strength at the loops overlap (the reinforcement area is doubled). The CFRP rupture location during heating was the same as the rupture location at ambient tests, i.e. just outside the overlap zone where the reinforcement ratio was reduced (Figures 5.26 and 4.43). The occurrence of rupture failure within the straight portion of the loop revealed that failure at the curved part of loop can be avoided (and consequently the strength increased) through overlapping, as additional strength will be available for the curved part. The rupture load during heating was lower than at ambient temperatures because the matrix softened, as discussed above. The progressive rupture of fibres was indicated by an increase in the deflection rate

leading to eventual failure (Figure 5.16). To investigate the influence of load value, beam specimen E3 was put under higher value of load, and much shorter fire resistance was observed. However, for this particular specimens there were difficulties with propane flow therefore after initial loading and heating for 8 minutes the test was stopped and load was removed. When the test was restarted failure occurred after 9 minutes of heating. This process is expected to affect the bond status between FRP and concrete and increase beam cracks propagation which influence the achieved fire resistance. Therefore, the load effect can not be concluded based on the results from specimen E3 due to the undefined error.

Figure 5.50 compares the fire resistance time and failure mode of specimens with different reinforcement arrangements.

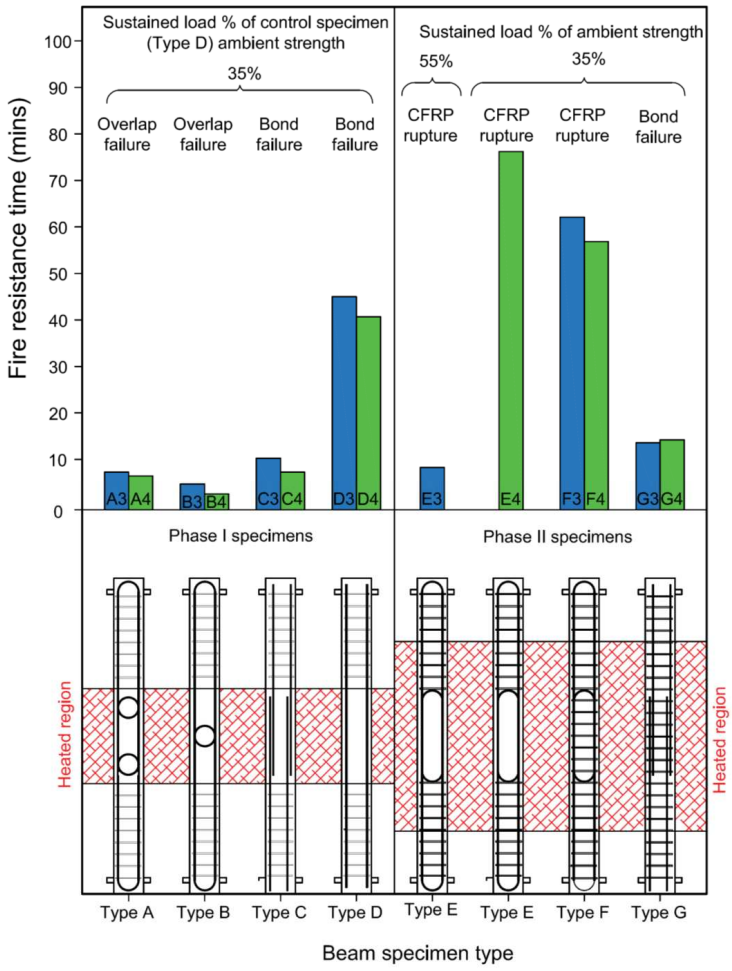

Figure 5.50 Comparison of fire resistance time and failure mode of beam specimens with different reinforcement arrangements.

Comparing the fire performance of different specimens shows that the CFRP loops (as in beams E and F) increased the fire resistance time by 380-500% (Figure 5.50) compared to the straight spliced specimens under same sustained load. The fire resistance time for the CFRP loops was also up to 70% higher than that for the specimens reinforced with continuous bars (type D) that relied upon cold anchorage outside the heated region. Furthermore, in the case of the CFRP loop specimens (E and F), the failure mechanism was maintained as rupture under heating (whereas the straight bars eventually failed due to bond), which implies that enhancing the reinforcement tensile strength could potentially improve the fire resistance time.

5.8.3 Crack patterns

Although the load was constant during heating, the crack openings increased, and in a few cases new cracks appeared. This was due to bond degradation and thermal stresses. In all of the beam specimens, failure occurred at crack locations. The reinforcement would have been hotter at the crack locations due to local heat penetration. This results in lower tensile and bond strength and therefore triggered failure at cracks.

Post-failure inspection of the beam specimens with the spliced bars (types C and G) showed longitudinal cracks appeared along the reinforcement at the bottom of beams within the heated region (Figures 5.19). The longitudinal cracks along the reinforcement could have been caused by transverse thermal expansion of the CFRP reinforcement. Elevated temperatures cause transverse expansion of CFRP, which generates tensile stresses at the contact surface with concrete, which can result in splitting cracks in the concrete. For FRP reinforcement the coefficient of thermal expansion (CTE) in the longitudinal direction is low and controlled by fibres, but that in the transverse direction is controlled by the matrix and is 3 to 8 times higher than concrete (Gentry and Husain, 1999; Aiello et al., 1999). The mismatch in transverse thermal expansion between the FRP and the concrete induces radial pressures upon

the concrete cover when the temperature increases (Rafi et al., 2007; Aiello et al., 2001; Galati et al., 2006).

No signs of longitudinal cracks were observed in the beam specimens with continuous straight bars (type D), although they were heated for longer periods. The reason for this could be that the beams with spliced bars (types C and G) had double reinforcement areas (higher transverse expansion) within the heated region. In addition, the beams with continuous bars anchorage were anchored outside the heated region, therefore tension in the reinforcement could reduce the radial pressure due to Poisson's deformation (Aiello et al., 2001). In terms of the failure location, failure occurred at the cracks within the splice length for beam specimens (types C and G), but at a crack located right at the mid-span for specimens with continuous bars (type D) (Figures 5.20 and 5.25).

The beams with short overlapped loops (A and B) did not exhibit any horizontal cracks along the overlap length prior to failure along the overlap length (as for the ambient temperature tests). This made failure very brittle, without any visible warning. For the phase II beam specimens with overlapped loops (E and F) no new flexural cracks appeared during heating, but new horizontal cracks formed at the reinforcement level within the heated region (Figure 5.31). Similar cracks have been observed by other researchers (Abbasi and Hogg, 2006). No horizontal cracks appeared during the ambient tests with one exception of specimen E1, which failed due to concrete shear along the loops splice. These horizontal cracks probably did not result from pore pressure generated from moisture conversion into steam, because they formed gradually and propagated slowly even beyond 115 °C. As in the case of spliced bar, the transverse thermal expansion of polymeric matrix is the probable cause.

Physical measurement of the crack openings during the heated tests was not feasible due to the elevated temperature of the radiant panels. However, CFRP loop reinforcement is expected to a certain degree to restrain crack formation and widening due to two qualities. First, mechanical interlock with the concrete through the curved parts of the loops at both ends, which provide an alternative interaction

mechanism with the concrete. Second, the coefficient of thermal expansion in the longitudinal direction of the CFRP reinforcement is significantly lower than concrete.

5.9 Summary

- At ambient temperature loop reinforcement can be designed to have a similar performance to straight reinforcement.
- Short fire resistance achieved with beam specimens reinforced with spliced bar confirms the sensitivity of FRP reinforcement bond strength to elevated temperatures.
- Providing beams with continuous reinforcement anchored in areas not directly exposed to fire can enhance fire resistance for localised heating. However, bond failure can still occur when heat propagate toward anchorages.
- Significant improvement in fire resistance time was achieved with CFRP loop reinforcement.
- Mechanical interlock between the loops and concrete can sustain load when the bond has degraded.
- Shear in the concrete along loop reinforcement within the overlap region is critical. Therefore, it is important to provide sufficient overlap length or use transverse reinforcement to enhance shear resistance of overlap zone.
- Cracks opening over the unbonded length is a concern as loops rupture failure consistency occurs at there.

Chapter 6 – Analysis of the Bond-Slip Response

6.1 Overview

The previous chapters have presented and discussed experimental work, in which the performance of CFRP loop reinforcement was evaluated at ambient and elevated temperatures. It was demonstrated that the CFRP loops provided a significant enhancement in fire resistance. To facilitate the design and assessment of the bond performance of CFRP loop reinforcement, an analysis tool for the bond stress-slip behaviour is needed. In this chapter, a Matlab programme is developed to calculate the response of the embedded length of FRP reinforcement at ambient and elevated temperatures. The programme is based on 1D finite element model and it was also used to predict the performance of the beam specimens tested during phase I and II of the experimental programme at ambient and elevated temperatures.

6.2 Analytical Model for Bond-Slip Response

The bond stress distribution is important as it describes the interaction between the reinforcement and concrete. Typically, the bond behaviour between bar and concrete is described by a relation between the local bond stress and relative slip (see section 2.9 for more details). Although many analytical solutions have been developed to calculate bond stress distribution for steel reinforcement, far less work are available for FRP bar reinforcement. Nigro et al. (2012) developed an iterative finite difference procedure to calculate development length and bond stress distribution for FRP bars. Nigro et al. (2012) also compared the analytical predictions with experimental results

and a good correlation was reported. The solution is based on boundary conditions of slip, bond stress, and axial stress equal to zero at bar unloaded end. While these conditions are valid for calculation of bond stress distribution along bars development length, they are not adequate for the case of loop reinforcement. At asymmetry points of loop reinforcement slip and bond stress are zero but axial stress may not be zero.

Idealising bond stress-slip response as one dimensional finite element problem is an approach that was used by Yankelevsky (1985) for steel reinforcement. The solution is based on using differential equations to describe the local equilibrium state of a short length of a reinforcing bars, and solving these to determine the variation along the reinforcement. This approach was adopted in the current work because the boundary conditions can be adjusted to simulate the case of FRP loop reinforcement. The local bond constitutive law used by Yankelevsky (1985) is for steel and it consists of four zones as shown in Figure 6.1. As discussed in section 2.9 such model is not suitable for FRP reinforcement due to the differences in materials properties. An alternative local bond constitutive law for FRP reinforcement was used and it is discussed in the following section 6.2.1. Details of Yankelevsky (1984) solution procedure is described in more details in section 6.2.2.

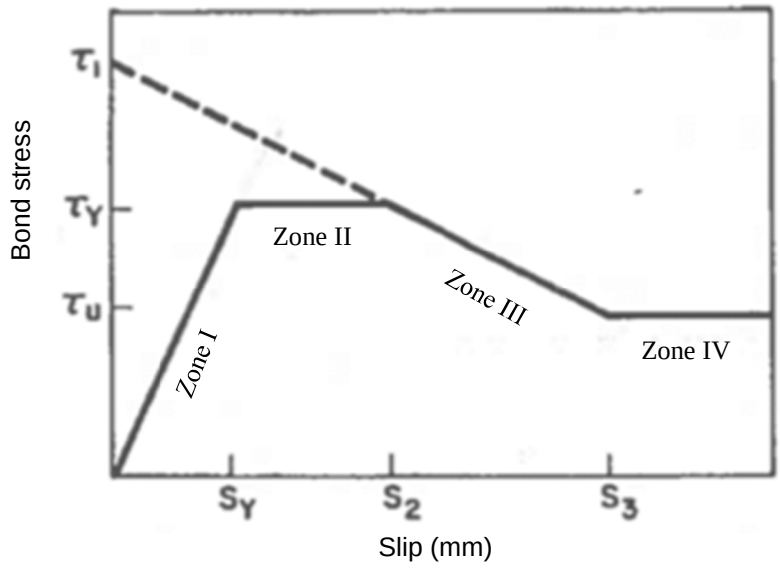

Figure 6.1 Bond law used in Yankelevsky (1985).

6.2.1 The Local Bond Stress – Slip Constitutive Response

As discussed in section 2.9 there are many bond stress-slip law developed for FRP reinforcement. Cosenza et al. (2002), for example, proposed a double branch bond stress-slip law (Figure 6.2). The ascending and softening branches are identified by the maximum shear stress τ_m and a corresponding slip s_m, in addition to curve fittings parameters α and p, which describe the shape of the non-linear ascending branch and the slope of the descending branch. Equations 6.1 and 6.2 describe each branch of the bond law. Cosenza et al. (2002) bond stress-slip law was favoured in the current study to be used within the analytical solution because the availability of bond test data for sand coated CFRP bars which can be used to define the bond law parameters.

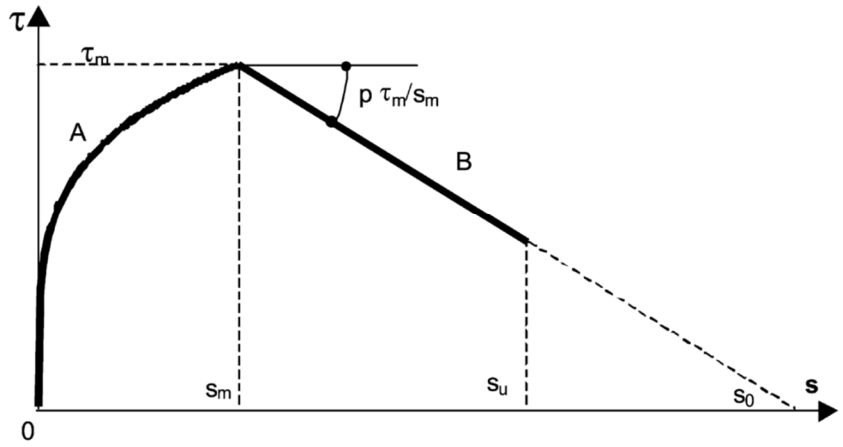

Figure 6.2 Modified bond-slip law (Cosenza et al., 2002).

$$\tau(s) = \tau_m \left(\frac{s}{s_m}\right)^{\alpha} \qquad \text{for } s < s_m \tag{6.1}$$

$$\tau(s) = \tau_m \left(1 + p - p\frac{s}{s_m}\right) \qquad \text{for } s_m < s < s_u \tag{6.2}$$

No pull-out or notched beam bond tests have been conducted as a part of the current research. Also the lateral (out of plane) movement occurred in push-off specimens (see section 3.5.8) induced error in the deformation measured with DIC and therefore parameter of bond stress-slip response could not be generated. Consequently some assumptions and simplifications have been made to identify the bond law parameters required for the model of Cosenza et al. (2002).

- The value for α was assumed to be 1, which gives a linear ascending branch (Figure 6.3). Linear and low order ascending branches were reported in various pull-out test results in the literature (Baena et al., 2009).

- The reinforcement used in the current study is sand-coated CFRP, and consequently bond law parameters obtained from pull-out tests on carbon fibre sand-coated bars was gathered from the literature, giving the maximum bond stress and corresponding slips shown in Table 6.1. The data used is for bars with circular cross-sections and for sizes different from that used in the current research, due to the scarcity of data.

- The value of p describes the softening branch. In Cosenza et al. (2002) the residual bond strength is neglected and the bond strength is assumed to diminish to zero (Figure 6.2). Therefore, the value of p was calculated based on the initial slope of the softening branch of the bond law of the data gathered from the literature as shown in Figures 6.4 and 6.5. The calculated p parameters are listed in Table 6.1.

Based on all of the above, the averaged bond model parameters are (Table 6.1):

τ_m = 14.55 MPa, s_m = 0.28 mm, α = 1, p = 21.71, s_0 = 4.26 mm (calculated from equation 7.2)

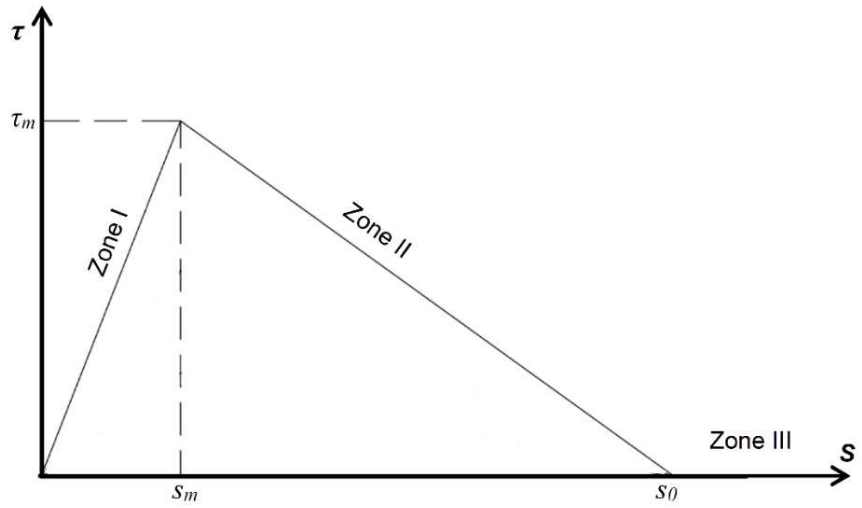

Figure 6.3 Linear double branched bond law used in the current study.

Table 6.1 Bond model parameters from literature

Source	Size	τ_m (MPa)	s_m (mm)	p
(Baena et al., 2009)	#3	16.44	0.38	21.24
(Baena et al., 2009)	#4	13.50	0.15	29.27
(Achillides et al., 2004)	10 mm	13.70	0.30	14.63
Average value		14.55	0.28	21.71

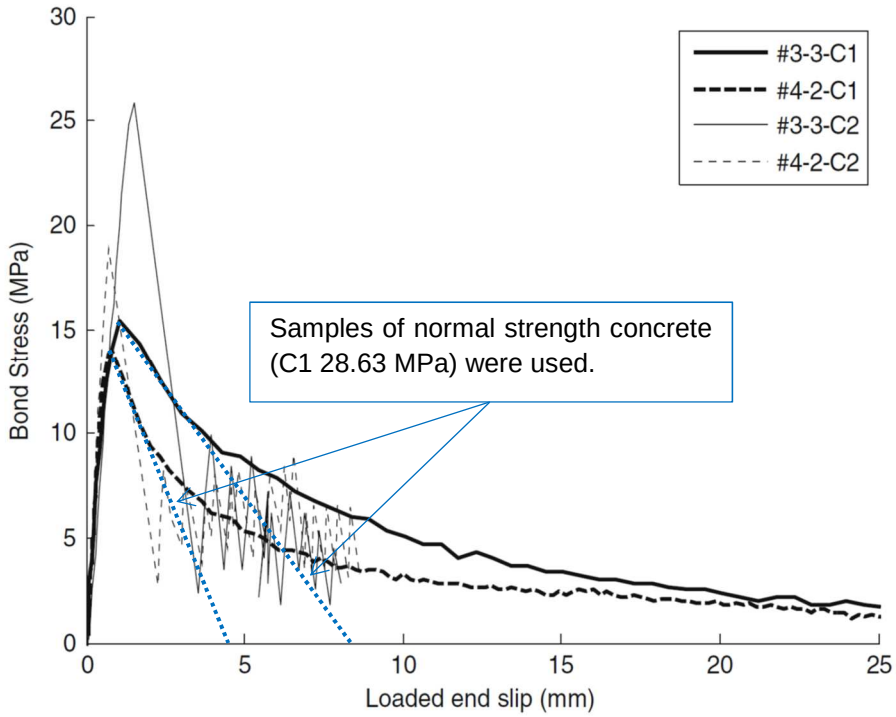

Figure 6.4 Bond stress-slip response of CFRP bars using pull-out test (Baena et al., 2009).

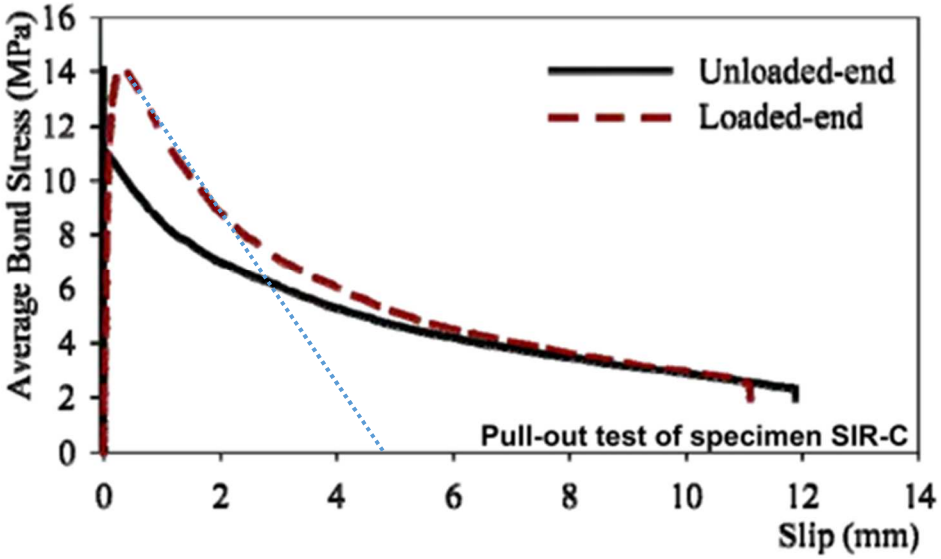

Figure 6.5 Bond slip response of sand-coated CFRP bar (Achillides et al., 2004).

6.2.2 Mathematical Formulation of Bond Stress-Slip Response

Yankelevsky (1985)'s finite element solution method was used to determine the bond stress-response response of the FRP reinforcement used in this study. Yankelevsky subdivided the reinforcing into short elements. A global stiffness matrix was built and used to calculate slip at each node under the effect of the applied external axial forces. For steel reinforced concrete, Yankelevsky validated his model against experimental data and a good agreement was found.

For each of the zones in the bond law, Yankelevsky (1985) derived the local relationship between nodal force and slip in terms of stiffness coefficients, *k*. The bond-slip analysis is then solved as a 1D finite element problem. The deformation in concrete was not considered by Yankelevsky (1985). Pecce et al. (2001) based on pull-out tests results of FRP bars found that for a reasonable variation of concrete strength (39 to 52 MPa) no significant affect on bond response was observed. In addition, Nigro et al. (2012) did not include the concrete deformation in their finite difference solution for FRP bond analysis and a good agrement with experimental data was reported. Thereforfe in the current study the concrete deformation was also ignored for simplification. Moreover, as linear double-branched bond law (Figure 6.3) is used in

this study to model the FRP reinforcement, only the equations for the ascending and descending branches of bond law in Yankelevsky (1985) are needed.

Considering a finite bar segment (Figure 6.6) with *D* diameter, with axial force *P(x)* and circumferential shear stress, *τ(x)*, acting at distance, *x*, the equilibrium requirement as formed by Yankelevsky (1985) are shown in Equations 6.3-6.12:

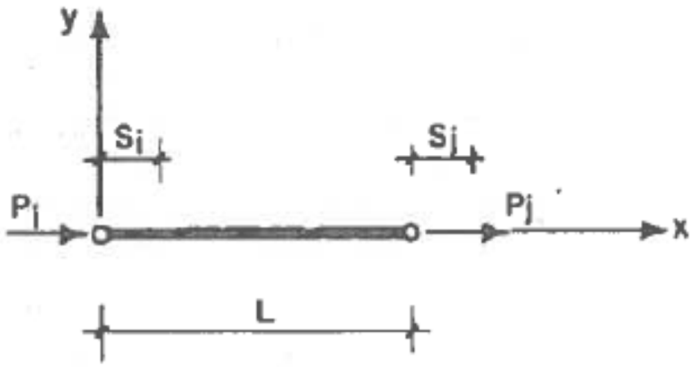

Figure 6.6 Nodal axial forces and slip of a finite element (Yankelevsky, 1985).

For the ascending branch (zone I in Figure 7.1):

$$\begin{Bmatrix} P_i \\ P_j \end{Bmatrix} = \begin{pmatrix} k_{11}^1 & k_{12}^1 \\ k_{21}^1 & k_{22}^1 \end{pmatrix} \cdot \begin{Bmatrix} S_i \\ S_j \end{Bmatrix} \tag{6.3}$$

$$k_{11}^1 = k_{22}^1 = \frac{\alpha_1 EA}{\tanh\ (\alpha_1 L)} \tag{6.4}$$

$$k_{12}^1 = k_{21}^1 = \frac{-\alpha_1 EA}{\sinh\ (\alpha_1 L)} \tag{6.5}$$

$$\alpha_1 = \sqrt{\frac{4\tau_y}{s_y ED}} \tag{6.6}$$

For the descending branch (zone III in Figure 7.1):

$$\begin{Bmatrix} P_i \\ P_j \end{Bmatrix} = \begin{Bmatrix} P_i^3 \\ P_j^3{}_j \end{Bmatrix} + \begin{pmatrix} k_{11}^3 & k_{12}^3 \\ k_{21}^3 & k_{22}^3 \end{pmatrix} . \begin{Bmatrix} S_i \\ S_j \end{Bmatrix} \quad (6.7)$$

$$k_{11}^3 = k_{22}^3 = \frac{\alpha_2 EA}{\tanh\ (\alpha_2 L)} \quad (6.8)$$

$$k_{12}^3 = k_{21}^3 = \frac{-\alpha_2 EA}{\sinh\ (\alpha_2 L)} \quad (6.9)$$

$$P_i^3 = -P_i^3 = \frac{-\alpha_2 \tau_1 EA}{K_2}\ t_g(\frac{\alpha_2 L}{2}) \quad (6.10)$$

$$K_2 = \frac{\tau_y - \tau_u}{S_3 - S_2} \quad (6.11)$$

$$\alpha_2 = \sqrt{\frac{4K_2}{ED}} \quad (7.12)$$

Where P_i is the nodal axial force, L is the bar segement length, E is the reinforcement Young's modulus, D is the bar diameter, s is the nodal slip, and τ is the local bond stress (Figure 6.1).

6.3 Programme For Bond Stress-Slip Analysis

6.3.1 Programme Description

A script was written using Matlab 2012b to conduct the 1D finite element analysis of the reinforcing bar using the mathematical equations derived by Yankelevsky (1985) (see equations 6.3 -6.12). The programme calculates the nodal displacement under the

applied force, which is then used to calculate the strain in the elements, and the axial stress. Nodal displacement is also used to calculate the corresponding bond stress at each node from the bond constitutive law (Figure 6.3). The input data required are the bond law parameters, the applied axial force, bar size, bar length, bar longitudinal Young's modulus, element size, load steps, and maximum number of iterations. The Matlab script is provided in Appendix F.

6.3.2 Solution Procedure

The solution procedure described in Yankelevsky (1985) was used in designing the Matlab programme. At the beginning of the ascending branch (Zone I in Figure 6.3) stiffness coefficients properties are assigned to all bar elements, then the global stiffness and force matrices are formed. The corresponding nodal displacements are calculated for the first load increment. Before the second load increment is applied, the values of nodal displacement are checked. If both nodes of an element exceeded the zone slip limit (s_m *or* s_n), the properties of that zone are assigned to the element and another iteration is made. Iterations within the load increment are continued until convergence is achieved, or the maximum number of iterations defined by the user is reached, which trigger a notifying message for the user. The same procedure is then repeated for the rest of load steps. Depending on the cumulative slip at each node from previous load steps stiffness coefficients properties are assigned to elements in the new load step. Strain in the elements is calculated from nodal displacements and used to calculate the axial stress. The bond stress at the nodes is calculated from nodal displacement using the bond constitutive law.

6.4 Assessment of Bond Performance at Ambient Temperatures

The bond between reinforcement and concrete is a vital aspect in the designing of concrete elements reinforced with FRP reinforcement. Although some work has been done to develop bond laws for FRP reinforcement, there is a lack of simplified tools

to investigate bond performance of internal FRP reinforcement in concrete especially at elevated temperatures.

The bond performance of FRP reinforcement can be assessed through calculating slip, axial stress, and bond stress distribution along reinforcement, which can be achieved using the simplified 1D finite element problem discussed above.

6.4.1 The Case of a Straight Reinforcing Bar

The programme can be used to predict bond stress and slip distribution along a straight bar embedded in concrete when the mechanical properties of an FRP bar are known, in addition to bond law parameters. Therefore, the programme can be used to check if the provided embedded length is sufficient to resist the applied forces. If slip along reinforcement was found to diminish at the end of reinforcement, this indicates the embedded length is either equal or more than the development length of bar.

Finding the development length (shortest embedded length required for bar to develop its full tensile capacity) in the current version of the programme has to be done by trying different embedded lengths until the conditions of development length are met.

The Matlab programme was used to assess if the embedded length of splice straight bars used in beam specimen type G is sufficient for reinforcement to develop it ultimate tensile strength. Bond law parameters from the literature for carbon fibre sand-coated bars were used (Table 6.1). The theoretical ultimate tensile stress, 1322 MPa (Appendix D), of CFRP reinforcement was considered as applied axial stress.

The value of development length for CFRP bar to develop its full strength was found to be 405 mm. Bar length was calculated to nearest 1 mm and slip value to nearest 0.0001 mm . Figures 6.7 and 6.9 show slip, axial stress, and bond stress distribution along the bar. Because the provided embedded length in beam specimens type G (440 mm) exceeds the calculated development length (405 mm) rupture failure is expected. This was confirmed by experimental results (Table 4.7) of beam specimens. Splice length is typically recommended by design guidelines to be more than the development length (see section 2.5.2).

The value of development (405 mm) is based on element size of 1 mm and 10 load equal steps. Convergence analysis was done to investigate the influence of element size and load step size on obtained results. Different element sizes, 0.5, 1, 2, and 3 mm, were used in the calculation of development length and variation of up to 3.5% was observed. Different equal load steps, 10, 20, and 30, were also used which caused variation in results up to 1.5%. The slip, axial force, and bond stress distribution along the development length using different element and load steps sizes are provided within Appendix G. For the purpose of the current work the variation in results is considered not to be significant and element size of 1 mm and 10 equal load steps were decided to be used for the rest of analysis within this chapter.

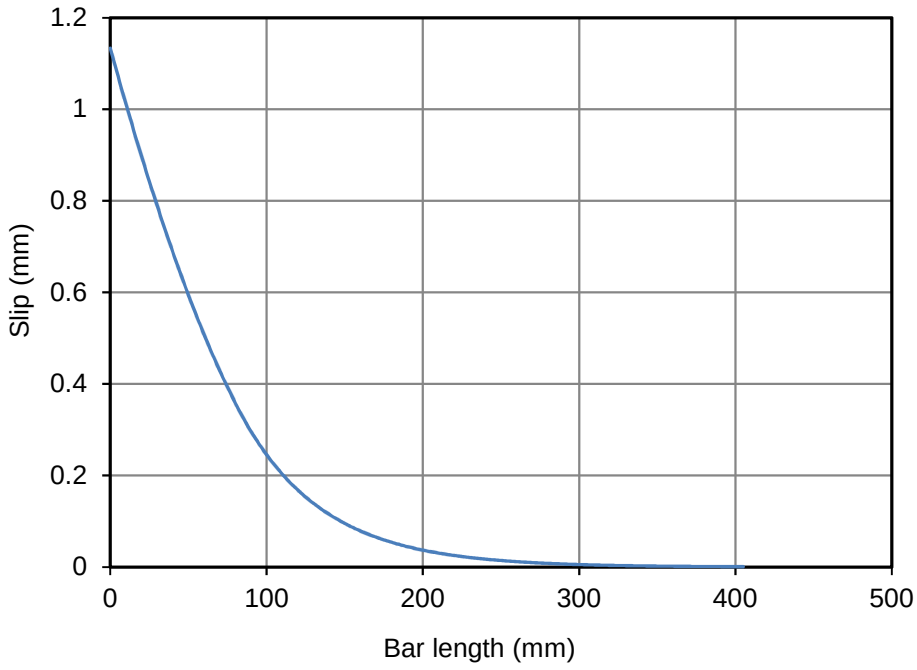

Figure 6.7 Slip response of CFRP reinforcement at ultimate tensile stress.

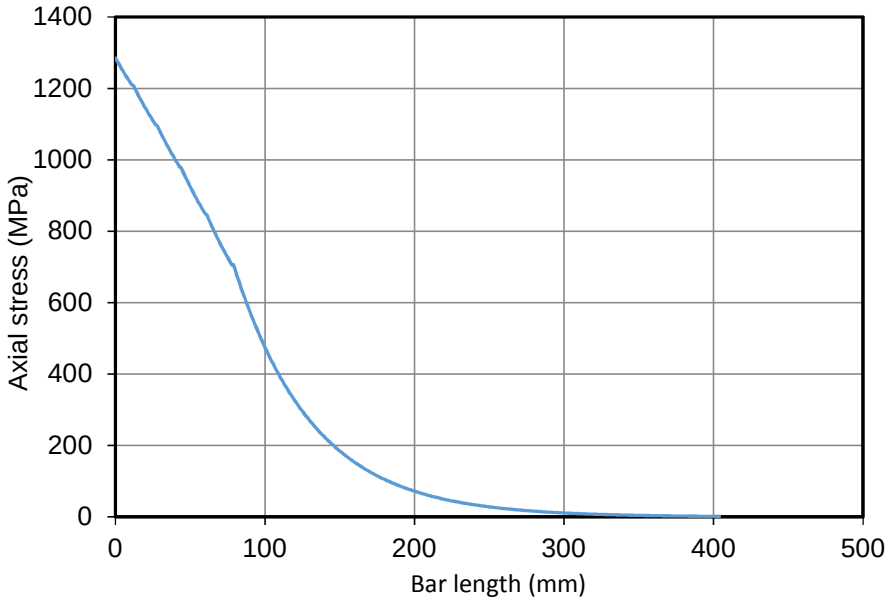

Figure 6.8 Axial stress response of CFRP reinforcement at ultimate tensile stress.

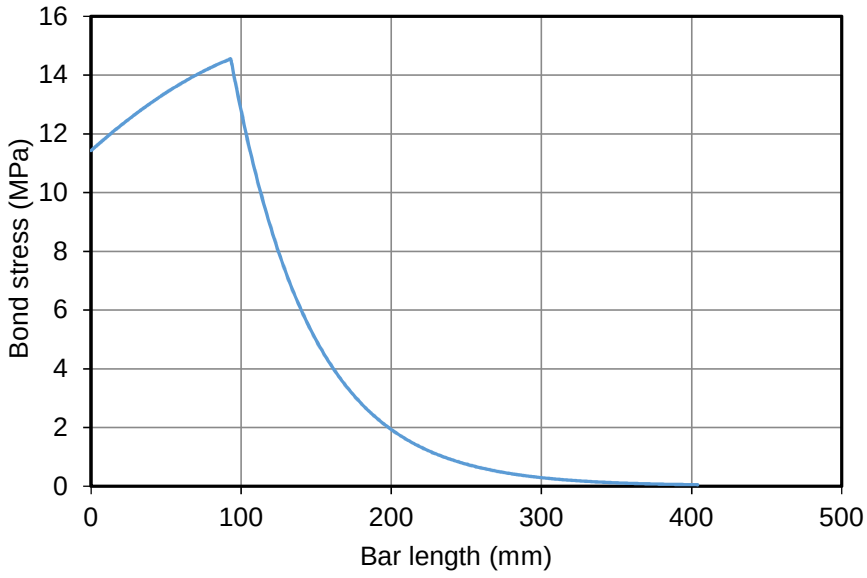

Figure 6.9 Bond stress response of CFRP reinforcement at ultimate tensile stress.

6.4.2 The Case of FRP Loop

The geometry of the FRP loops provides them with an extra load-carrying mechanism due to the continuity of the loop, as opposed to the free end of a straight bar. The FRP loops are symmetrical along the axial axis, so a fixed boundary condition was introduced at the midpoint of the curved part (Figure 6.10).

To simplify modelling, the curved part was replaced with a straight portion of the same length, terminated with the fixed end shown in Figure 6.10. This simplification is conservative, because curved reinforcement provides better bond with the concrete compared to straight reinforcement (Ehsani et al., 1995; Ehsani et al., 1996; Imjai et al., 2007a; Imjai et al., 2009). A more accurate representation of the curved part could be simulated by calibrating the stiffness coefficients for the finite elements within the curved part; however, this was not considered in the current study.

The fixed end boundary condition was incorporated in the Matlab script by deleting the column and row in matrices of slip, stiffness, and force that correspond with the fixed end node. In Matlab script when the value of input parameters *fbc* (fixed boundary condition) is set to 1, the Matlab script will consider the bar to have a fixed end, while when set to zero the bar end is considered not fixed (straight bar).

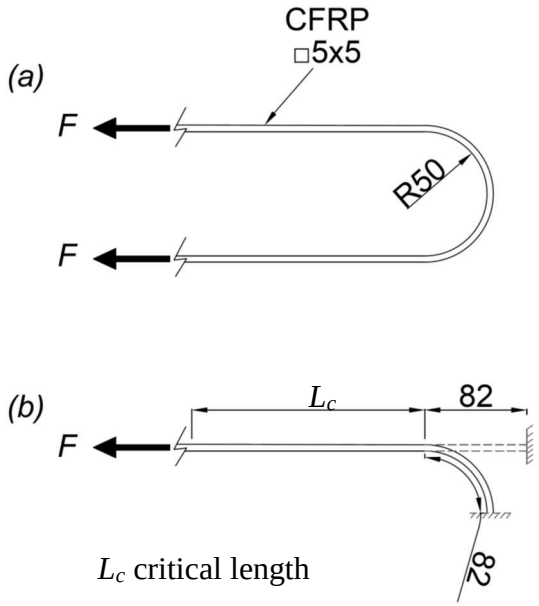

Figure 6.10 Simplification of CFRP loop into 1D problem.

The curved FRP reinforcement has less tensile capacity than the straight portion due to the multi-axial loading status and lower strength of the FRP reinforcement in the transverse direction (Guadagnini et al., 2006; Imjai et al., 2009; Imjai et al., 2007b; Imjai et al., 2007a), see section 2.6, and also as observed during the loop tension and push-off tests (Chapter 3) in which rupture failure occurred at the start of the curved part. Therefore, in the current study a *critical length* , (L_c in Figure 6.10), of FRP loop was defined as the length of the straight portion of reinforcement between the loaded end and the start of curved part that allows the ultimate tensile stress to be developed at the loaded end, with the stress at the curved part equal to the tensile capacity of the bend.

The strength of the curved FRP bar can be estimated using equation 6.13 from the Japanese design guidelines (JSCE, 1997), and since adopted by other design guidelines ACI (2015) and ISIS (2007).

$$f_{fb} = \left(0.05\frac{r_b}{d_b} + 0.3\right) f_{fu} \leq f_{fu} \qquad (6.13)$$

Where f_{fb} is the design tensile strength of the bend of the FRP bar, (MPa); r_b is the radius of the bend, (mm); d_b is the diameter of reinforcing bar, (mm); and f_{fu} is the design tensile strength of FRP, considering reductions for service environment, (MPa).

The Matlab programme was used to calculate the critical length (L_c) by changing the value of the embedded length until the conditions for critical length were met. The programme was used to assess the slip, axial stress, and bond stress responses for this embedded length.

As a practical example, the programme was used to assess the bond response of a CFRP loop used in beam specimens of phase II. During the tension tests on loops described in Chapter 3, the average tensile capacity of the bend was found to be 852 MPa based on tensile test 42.6 kN (Table 3.7). This corresponds to a 36% strength reduction compared to the estimated ultimate strength of the straight reinforcement

1322 MPa (Appendix D). The empirical equation 6.13, however, predicts the tensile strength of the curved part to be 1058 MPa, (d_b = 5 mm; r_b = 50mm), equation 6.14, which is 24% more than observed experimentally. However, the tensile test was conducted upon bare loops (not embedded in concrete), and therefore it is expected to underestimate the bend capacity to some extent. The bend tensile capacity based on both the JSCE (2007) equation and tensile capacity were considered below for comparison.

The critical length was found to be 123 mm (using the experimentally obtained bend strength) or 143 mm (from equation 6.13). Figures 6.11 to 6.13 show the slip, axial stress, and bond stress distributions along the loop development length. Specimens of type E and F had greater embedded lengths than either 123 mm or 143 mm, and consequently the reinforcement was expected to develop its full strength and rupture occurred within the straight portion of loop, which is in agreement with experimental results (Table 4.7).

$$f_{fb} = \left(0.05\frac{50}{5} + 0.3\right)1322 \approx 1058 \text{ MPa} \tag{6.14}$$

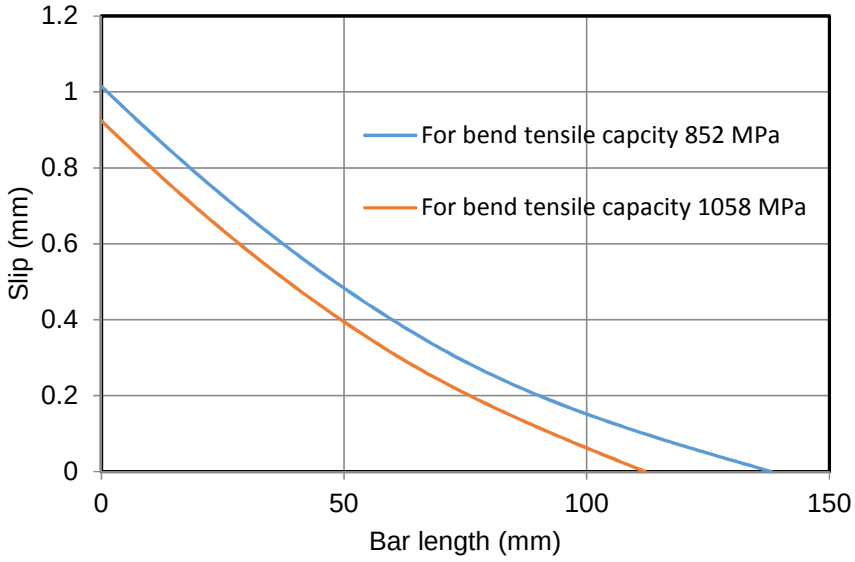

Figure 6.11 Slip response along CFRP loop development length.

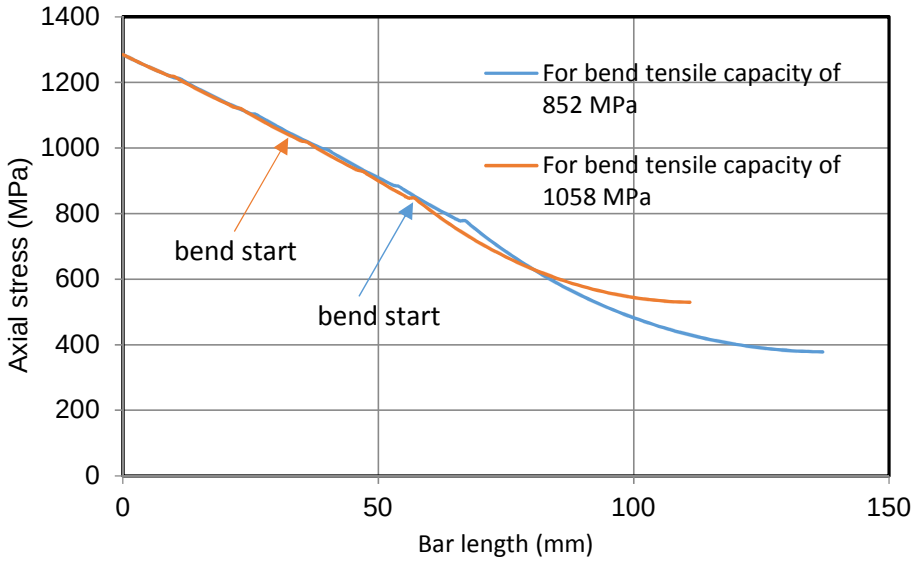

Figure 6.12 Axial stress response along CFRP loop development length**.**

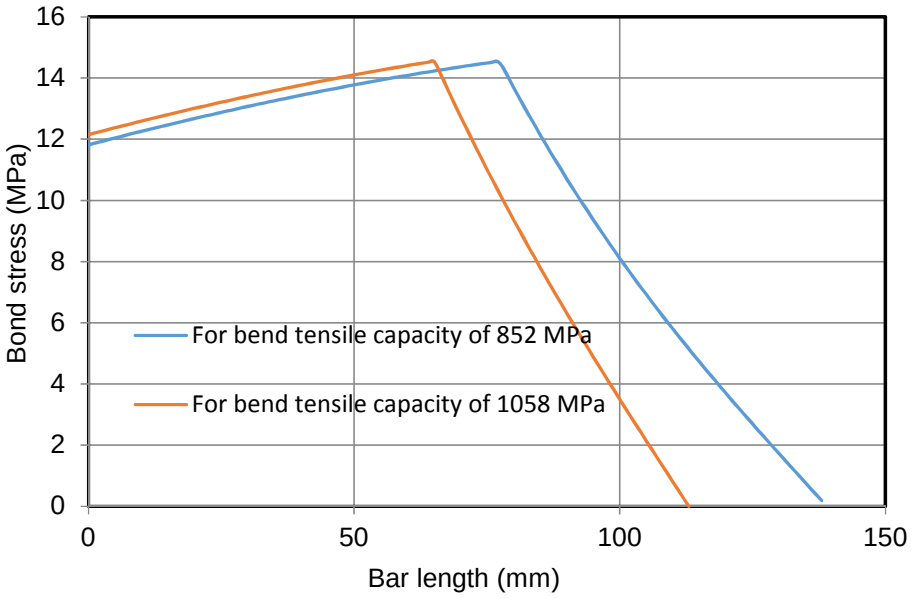

Figure 6.13 Bond stress response along CFRP loop development length.

6.5 Assessment of Bond Performance at Elevated Temperatures

The bond of FRP reinforcement degrades at elevated temperatures due to softening of the polymer matrix (see section 2.10). If the reduction of the bond strength and reinforcement mechanical properties with respect to temperature are known, the same analysis steps that were used at ambient temperature conditions (section 6.4) can be used for elevated temperatures to assess bond stress-slip response.

The deterioration in the FRP tensile strength and Young's modulus with temperature is shown in Figure 2.16 which is based on experimental data from literature. Same data was used by Nigro et al. (2008) to obtain equations describing tensile strength and Young's modulus deterioration with temperature for different types of FRP (carbon, glass, and aramid), equations 7.15 and 7.16.

$$\rho_f(T) = \frac{f_{fu}(T)}{f_{fu}} = \frac{0.05}{0.05 + 8.0\times10^{-11}\times T^{3.55}} \tag{6.15}$$

$$\rho_E(T) = \frac{E_f(T)}{E_f} = \frac{0.28}{0.28 + 6.0\times10^{-12}\times T^{4.3}} \tag{6.16}$$

Where $\rho_f\ (T)$ and $\rho_E(T)$ are reduction factors for tensile strength and the Young modulus of the bars, respectively, based on the temperature, T, in the bar.

To account for the effect of temperature on bond strength a semi-empirical model developed by Katz and Berman (2000) was utilised, equation 6.17. The model uses three parameters: glass transition temperature and degree of crosslinking of polymer at the reinforcement surface, in addition to residual bond stress. Refer to section 2.11.2 for more details. The glass transition temperature used in the model was measured using a differential scanning calorimeter (DSC). In this research, glass transition temperature was determined based on tan δ using DMA test (refer to section 3.2.2 and Appendix A). Any difference that could result from measuring T_g with the two different test methods was not considered as a part of the current study. The residual

bond strength in this model is defined as the residual bond strength at a high temperature (<350 °C) where no further reduction occurs (Katz and Berman, 2000).

$$\tau^* = 0.5(1-\tau_r^*)tanh\left\{-\frac{0.02}{C_r}\left[T-k_1\left(T_g+\frac{k_1}{0.02}C_r\right)\right]\right\}+0.5(1+\tau_r^*) \quad (6.17)$$

$$k_1 = \begin{cases} 1, & T_g \le 80, \\ 1-0.025(T_g-80), & 80 < T_g < 120, \\ 0, & T_g \ge 120 \end{cases}$$

Where τ^* normalized residual bond strength, C_r degree of cross linking for polymeric matrix, T_g is the glass transition temperature in °C.

In the current study under the effect of temperature due to data scarcity and as a simplification, only the peak bond strength τ_m was amended in the bond law according to equation 6.17. The values of s_m and s_n were kept unchanged as at ambient temperature (Figure 7.14). Such a simplification appears not to influence the accuracy of the produced bond stress-slip response in any significant way, as when was used by Nigro et al. (2012) and good agreement with experimental tests was reported. When bond law is updated for specific temperature, the Matlab programme can then be used in same manner described previously for ambient temperature to calculate development or critical length of CFRP straight bars and loop reinforcement. It can also be used for design or assessment for specific fire ratings, provided that temperature-time data is available (e.g. Standard temperature-time curve ISO 834).

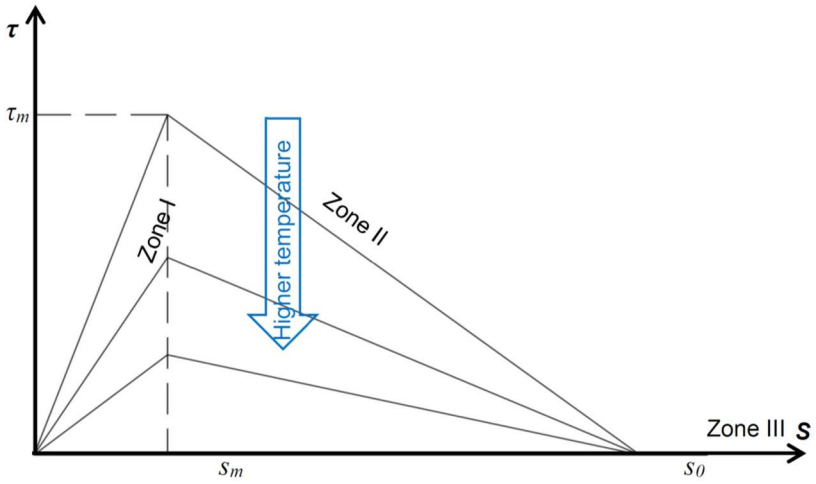

Figure 6.14 Linear double branched bond law used in the current study.

6.5.1 Development Length of Straight Bars at Elevated Temperatures

As bond strength reduces with temperature, a longer embedded length will be needed to resist the applied forces than at ambient temperature. To calculate the development length for a straight bar or to evaluate the response of an embedded length at a specific temperature, the bond strength and mechanical properties have first to be calculated using equations 6.15 and 6.16. These data are then used as inputs to the Matlab programme and the same procedure that was discussed for the ambient temperature case (section 6.4.1) was followed, as demonstrated by the example below.

In the heated tests of beam specimens with spliced bars (group C and G), failure occurred by pull-out when the reinforcement temperature was in the range of 115-135 °C (Figures 4.38, 4.39, 5.46, and 5.47). The axial stress in the reinforcement under the sustained load was theoretically calculated using a triangular stress block (Appendix H). Considering the actual concrete cover, the highest value of axial stress in beam specimens with a splice bar was calculated to be 521 MPa for beam specimen C4. The reduction of bond strength, tensile strength, and Young's modulus were calculated using equations 6.15 and 6.16 for a temperature of 135 °C for use in the analysis. Calculations were also conducted for ambient temperature (20 °C), T_g (87.6 °C) and 200 °C to demonstrate the effect of temperature on slip and bond stress (Table 6.2). The value for polymer cross linking, C_r, is determined experimentally which was not done as a part of the current study. However, a value of C_r = 0.9 reported by (Katz and Berman, 2000) for GFRP bar with helical-wrap and sand coating at surface was used due to limited data in the literature.

Table 6.2 Theoretical reduction in CFRP bond strength and mechanical properties with temperature.

Temperature °C	$\rho_f(T)$	$\rho_E(T)$	τ^*	f_{fu} (MPa)	E_f (MPa)	τ_m (MPa)
Ambient	1	1	1	1322	103210	14.55
T_g 87.6	0.99	1	0.84	1309	103210	12.22
135	0.94	0.97	0.44	1242	100114	6.40
200	0.81	0.86	0.13	1071	88761	1.89
387	0.29	0.26	0	383	26834	0

where: ρ_f and ρ_f are tensile strength and Young's modulus reduction factors, τ^* normalized residual bond strength, f_{fu} ultimate tensile strength, E_f Young's modulus for FRP, τ_m is maximum bond strength.

Using the Matlab programme it was found that the development length for axial stress of 521 MPa at a temperature of 135 °C is 500 mm (Figures 6.15-6.17). The embedded length provided in the beam specimens with splice bars (types C and G) was only 440 mm, and consequently debonding (pull-out) failure was expected, which is in agreement with the experimental results. The effect of temperature on the development length, axial stress and bond stress distribution are shown in Figures 6.15 to 6.17. The values of development length at each temperature are listed in Table 6.3. The degradation of bond strength with temperature was highly non-linear as it can be noticed in Table 6.2 and Figures 6.15-6.17. At temperatures 135 and 200°C the bond stress over some part of embedded length underwent softening (Figure 6.17) because the maximum bond stress is reduced.

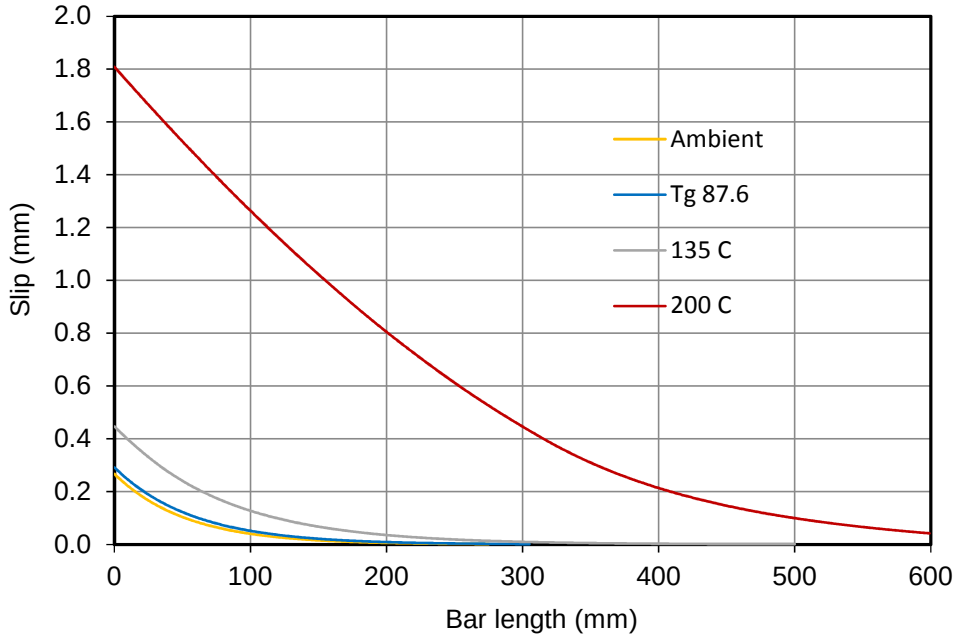

Figure 6.15 Analytical slip response with temperature of CFRP bar.

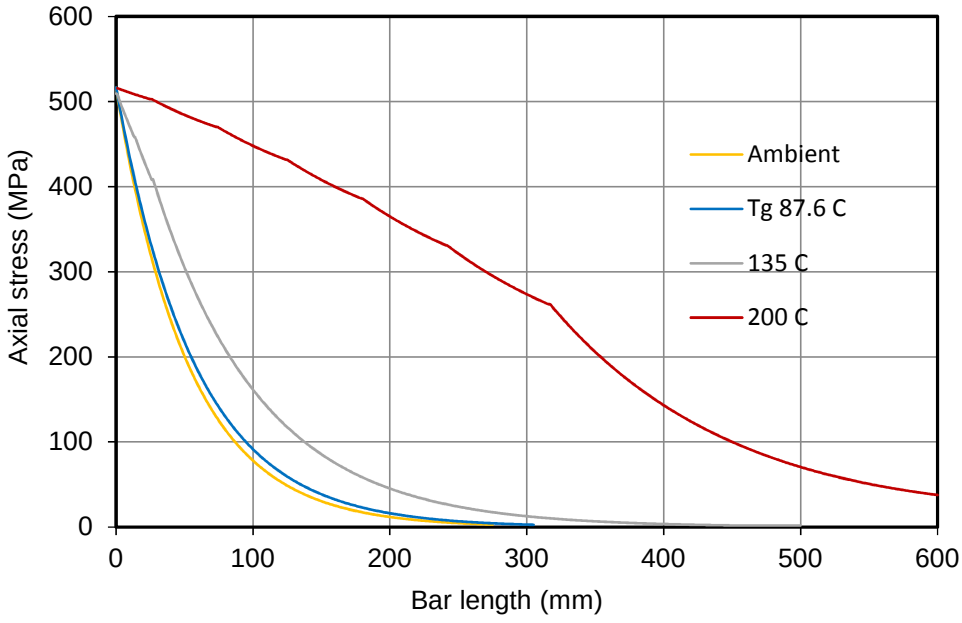

Figure 6.16 Analytical axial stress distribution along bar under different temperatures.

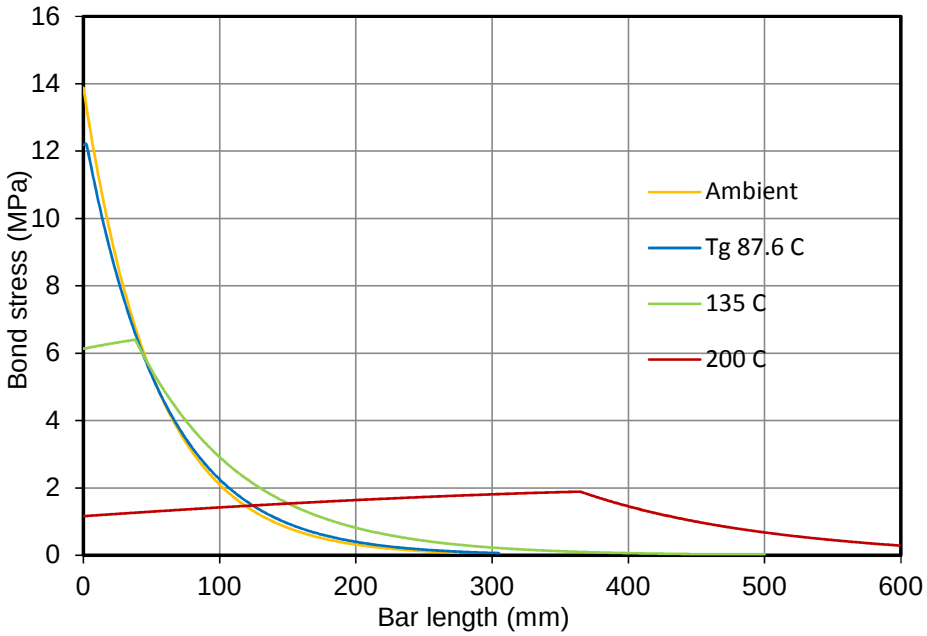

Figure 6.17 Analytical bond strength distribution along CFRP bar at different temperatures.

Table 6.3 Analytical development length for straight bars at different temperature.

Temperature °C	Axial stress (MPa) [1]	τ_m (MPa)	Development length (mm)
Ambient	521	14.55	275
T_g 87.6		12.22	305
135		6.40	500
200		1.89	>600

[1]caused by the applied sustained load during the heated test

6.5.2 Development Length of CFRP Loop at Elevated Temperatures

For a straight bar, failure occurs once the surface bond cannot maintain the applied forces. A CFRP loop, however, can sustain a higher load as it has an additional interaction mechanism with concrete. For CFRP loops to sustain load at a specific temperature, the applied forces must be less than the tensile stress of the straight portion of CFRP loop and the amount of force transferred to the curved part should be less than the tensile strength of the curved part at that temperature, too.

Beams reinforced with CFRP loops can be designed to perform at elevated temperatures by providing sufficient *critical length* for the required level of load. The

Matlab programme can be used to determine the *critical length* of a CFRP loop at elevated temperatures in the same manner used under ambient conditions (section 6.4.2), but with reducing the bond strength and mechanical properties of the CFRP reinforcement.

As a demonstration of utilising the Matlab programme to evaluate the bond performance of CFRP loops at elevated temperatures, a beam specimen from phase II was analysed. In the heated test of phase II, the highest value of axial stress and temperature during heated tests of beam specimens with overlapped CFRP loops types E and F were 387 °C (Figure 5.29) and 457 MPa (Appendix H). The reduction in bond strength, CFRP tensile strength, and Young's modulus was calculated using equations 6.15 and 6.16. The calculated values are listed in Table 6.2. The tensile strength of the curved part of the loop based on CFRP reduced tensile strength at a temperature of 387 °C was calculated using Equation 6.14 and was found to be 306 MPa. The analysis was also done at ambient temperature, T_g (87.6), 135 and 200 °C for comparison.

At ambient temperature, T_g (87.6), 135, and 200 °C the tensile strength of curved part of loop exceeds the level of the applied stress (457 MPa) therefore no additional embedded length is needed (Table 6.4). The slip, axial stress, and bond stress distribution along curved part of loop is shown in Figures 7.18-7.20. The figures show an expected pattern, as temperature increases bond strength reduces, higher stresses are transferred to the fixed end, and higher values of slip occur.

At temperature of 387 °C the bond strength is effectively zero as suggested by Katz and Berman (2000) model based on pull-out test at elevated temperatures concluded that force transfer between FRP bars and concrete beyond 250 °C is negligible. Therefore, the tensile capacity of the curved part will control the failure load, as it is the weakest part of the CFRP loop reinforcement, and all axial stress in reinforcement will be transformed to it completely. For the case of beam specimens with CFRP loop reinforcement, failure is expected to occur at a temperature of 387 °C, because the axial stress level in reinforcement is 457 MPa, which exceeds the estimated capacity of the curved part of loop 306 MPa. However, for the case of beam specimens type E and F, failure did not occur at the bend because additional strength was provided by

the overlap (doubled reinforcement area). Failure instead occurred within the straight portion of reinforcement, which has a reduced estimated tensile capacity of 383 MPa (Table 6.4) and it is less than the axial stress of 457 MPa generated by the sustained load.

When comparing the bond-slip response of the two types of reinforcement, it is noticed that for bar reinforcement the calculated development length increased significantly as the temperature increased from ambient to T_g, 135, and 200 °C (Table 6.3). Loop reinforcement, on the other hand, was less sensitive to increase in temperature (Table 6.4) due to the additional interaction mechanism with concrete which is idealised as a fixed end in the finite element model (Figure 6.10). In all the analysis that was performed the numerical solution was found to converge easily and no more than 10 iterations were needed within load steps.

Table 6.4 Analytically critical length of CFRP loop under the sustained load at different temperatures.

Temperature °C	Axial stress (MPa)	Tensile strength (MPa)	Bend tensile strength (MPa)[1]	Loop critical length (mm)
Ambient	457	1322	1058	0
T_g 87.6		1309	1047	0
135		1243	994	0
200		1071	857	0
387		383	306	-

[1]Based on reduced tensile strength due to temperature using Equation 7.15, and bend strength using Equation 7.13.

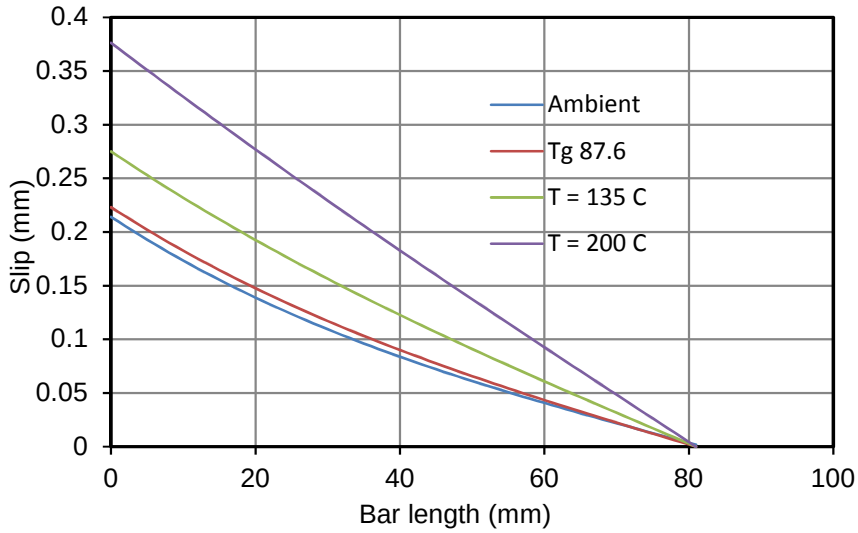

Figure 6.18 Analytical slip response with temperature of CFRP loop.

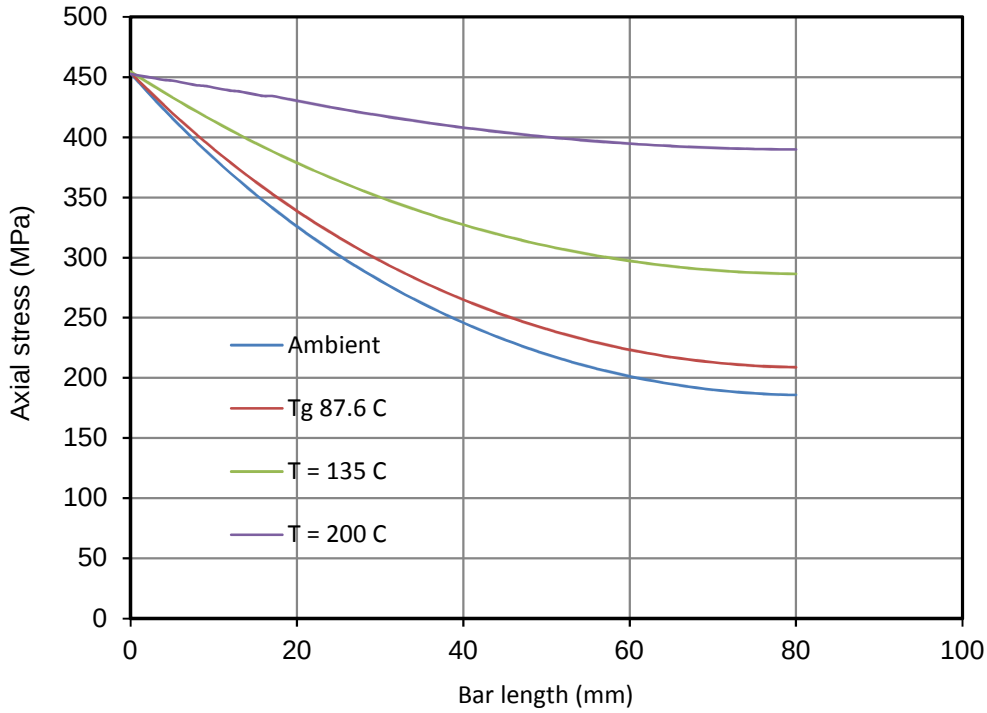

Figure 6.19 Analytical axial stress distribution along CFRP loop under different temperatures.

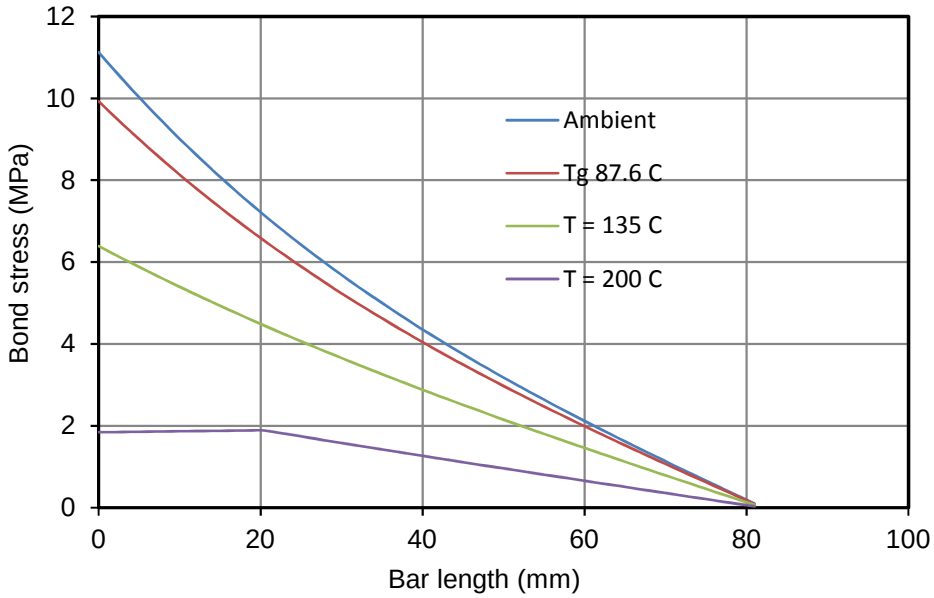

Figure 6.20 Analytical bond strength distribution along CFRP bar at different temperatures.

6.6 Limitation of the Matlab Programme for Bond Analysis and Suggested Improvements

The Matlab programme is a useful tool for bond analysis of FRP reinforcement; however, it has some limitations and some aspects to be improved.

The stiffness parameters are assigned to elements based upon the zone of the bond law (Figure 6.3) that the element is considered to be in. The stiffness coefficients of the element are only updated when the slip at both nodes of elements exceeds the zone limit (s_m or s_n). This procedure increases the dependent of the results on element size. A small element size would be recommended to limit this effect. As a further development, the element subdividing technique used by Yankelevsky (1985) can be added to the programme to evade the influence of element nodes falling within different zones of bond law. In this technique elements in transition between two zones are subdivided into two elements with lengths relative to slip value at the nodes. This can reduce the number of iterations and enhance the accuracy of the programme, especially when a bigger size element is used.

While the Matlab programme can produce bond-slip response of a specific length, it does not automatically calculate the development length and *critical length* of the CFRP loop based on entered data, but the user has to try different lengths until the desired conditions are met. A development in form of an automated calculation of development length for straight bars and critical length for loops is suggested.

In elevated temperatures analysis, the temperature was assumed to be constant along the reinforcement. While this can be considered as a reasonable simplification for short lengths, when the analysis is intended for long spans, providing the ability to enter the temperature profile along the reinforcement can be valuable.

6.7 Summary

- One dimensional finite element model from the literature for bond-slip of stress of steel reinforcement was modified to suit FRP reinforcement.

- A Matlab programme was developed based on the analytical model to calculate slip and bond stress distribution along a given length of reinforcement. The Matlab programme can be used to determine the development length for straight bars and critical length of loop reinforcement.
- When combined with an empirical model to calculate bond strength reduction with temperature, the Matlab programme can be used to assess the bond performance of FRP reinforcement at elevated temperatures and can also be used to calculate the required embedded length to perform at specific temperatures.
- The slip, axial stress, and bond stress distribution along reinforcement shows as temperature increases bond strength reduces, higher stresses are transferred to toward the unloaded end, and higher values of slip occur.
- Bond-slip response at elevated temperatures illustrated that loop reinforcement is less sensitive to increase in temperature due to the additional interaction mechanism with concrete which is idealised as a fixed end in the finite element model.
- The numerical analysis was used to predict bond performance of straight bars and loop reinforcement within concrete beam at ambient and elevated temperature, and the obtained results correlate with the experimental observations.

Chapter 7 – Conclusions and Recommendations

7.1 Summary

The experimental and numerical studies presented in this thesis sought to examine the performance of a novel design of FRP loop as internal reinforcement for concrete beams to enhance their performance in fire. To achieve this objective, a literature review was conducted; proof of concept assessment in form of tension and push-off tests were performed, beam bending tests upon beams reinforced with loop reinforcement and other with straight bars were conducted at ambient and elevated temperatures, and finally a numerical analysis tool for bond stress-slip analysis was developed.

A procedure in which closed FRP loops reinforcement can be produced was suggested within the current work. Sufficient experimental data were obtained from the conducted tests to evaluate the flexural strength, deflection, failure modes, and fire resistance time of beams reinforced with CFRP loop. The developed numerical analysis tool was found to be capable of producing bond stress-slip response for FRP loop and straight reinforcement at ambient and elevated temperatures. Thus, the objectives of this thesis, as outlined in section 1.3, have been achieved.

7.2 Conclusions

The primary conclusions that can be drawn from the experimental and numerical work presented within current this thesis are:

- Loop reinforcement can be designed to have a similar performance to straight reinforcement at ambient temperature. This has been shown through the results of push-off tests, beam tests, and the numerical analysis.

- Experimental tests at elevated temperatures showed a significant improvement in fire resistance (up to ≈ 5 times) can be achieved with loop reinforcement over straight bars due to the additional interaction mechanism with concrete through bearing at the loop ends.

- Force transfer between FRP straight bars and concrete rely on surface bond therefore the structural stability significantly deteriorates at elevated temperatures due to polymeric matrix softening. This was observed in the reduced load bearing capacity and increased slippage of reinforcement.

- The surface bond of loop reinforcement is also damaged by elevated temperatures, however, the reinforcement continuity (closed loop) enables forces transfer to be maintained with concrete.

- The numerical analysis provided an insight to the differences in bond stress-slip responses between loop and straight bars reinforcement. In case of straight bar, increase in temperature leads to a reduction of bond stress and therefore longer embedded length is required to maintain the applied forces. On the other hand, loop reinforcement is less sensitive to increase in temperature because when surface bond degrades higher axial stresses are transferred toward loop end at which slip diminishes due to symmetry.

- Under heating the dominant failure mode for specimens with straight bars was debonding in form of reinforcement pull-out. On the other hand, reinforcement rupture governs the failure in case of loop reinforcement. Therefore, enhancing reinforcement tensile strength can increase the fire resistance time of CFRP loops, while this is not effective for straight bars as failure occurred due to debonding.

- Force transfer can be done between loops through overlapping. However, it is important to provide sufficient overlap length or use transverse reinforcement to avoid shear along reinforcement of the concrete within the overlap region.

A series of more specific conclusions can be drawn from the individual chapters of this thesis.

The following conclusions were drawn on the basis of the literature review presented in Chapter 2:

- The sensitivity of FRP bond strength to temperature is reported by many studies and recognised in design guidelines, therefore some advice against utilising of FRP as an internal reinforcement for concrete where fire performance is critical.
- FRP and its sub components are produced with a variety of properties which makes it difficult to make a generalisation about FRP characteristics.
- The proposed measures to enhance the performance of FRP reinforcement in fire concentrate on providing thermal insulations to structural elements incorporating FRP or providing anchorage to reinforcement in areas not exposed to fire.

The following conclusions were drawn on based of the experimental program of tension and push-off test presented in Chapter 3:

- Closed FRP loop reinforcement can be produced in a simple procedure of winding up epoxy-saturated fibre around a mould.
- The continuity of loop reinforcement enables reinforcement to sustain tension forces even in the absence of surface bond with concrete.
- The curved part of loop is weakest because of the multiaxial stress state that occurs there due to axial force in reinforcement and transverse forces caused by bearing against concrete. The effect is exaggerated by the fact that FRP is weaker in a transverse direction.
- Push-off tests can provide a quick and useful assessment to bond performance of FRP reinforcement at ambient and elevated temperatures.

- At ambient temperature there was no clear distinction in performance between different reinforcement types. The dominant failure mode occurred between different reinforcement arrangements was bar rupture within the free length of the reinforcement. This indicates that the reinforcement was sufficiently bonded to the concrete for it to reach its ultimate capacity.
- At elevated temperatures (T_g 84.7 °C and 130 °C), the benefit of CFRP loop became evident. Both specimens with straight and hooked reinforcement experienced a severe reduction in bond strength and failed due to debonding by pull-out. Specimens with the CFRP loop achieved failure load three times higher than other samples, because when the interlock and friction mechanisms of bond force transfer were lost due to softening of the resin, tensile forces in the reinforcement (FRP fibres) could still be resisted through bearing at loop ends. The rupture failure location changed from free length as in ambient temperature to the curved part of loop. This is because when surface bond degrades under elevated temperatures, more force is transferred to the critical section of the loop, which is the curved part.

The following conclusions were drawn on based of the experimental program of beam tests presented in Chapters 4 and 5:

- The push-off test provided a quick assessment of CFRP loops against straight and hooked bars; however, the test does not closely represent the case of reinforcement in beams. That is because the configuration of push-out test induced confinement on reinforcement, lacked local bar buckling, and the thick concrete cover also minimises the chance of concrete splitting. Therefore, further testing of four-point bending tests upon beams reinforced with loops was needed.
- Based on load-deflection response, ultimate strength, and failure mode it was found that beam with FRP loop reinforcement can be designed to have a similar performance of beams with straight bars.
- When loops are overlapped, sufficient overlap length is needed to avoid a premature shear failure of concrete within the overlap zone. Providing

transverse reinforcement was found to effectively enhance the shear capacity of concrete within the overlap zone. Transverse reinforcement also enhanced the confinement level and can prevent splitting failure from occurring along bars splice length.

- Under heating and sustained load, beam specimens exhibited increased deflection over time, which is attributed to thermal gradient across the section and degrading of CFRP reinforcement bond.
- The sensitivity of FRP bond reinforcement reported in the literature was confirmed with short fire resistance time achieved by beams with spliced bars. Failure due to reinforcement pull-out occurred after 10-15 minutes of heating. Confinement levels added by transverse reinforcement was found not to be sufficient to deter debonding failure at elevated temperatures.
- Providing anchorage to bars in areas not directly exposed to fire was found to considerably increase fire resistance time (≈ 45 minutes). However, failure can still occur due to debonding, as heat propagates toward the anchorages.
- Loop reinforcement was found to provide a significant improvement in the fire resistance time. Loops reinforcement successfully maintained interaction with concrete at elevated temperatures (up to 390 °C) well above glass transition temperature of polymeric matrix (87.6 °C). Fire endurance increased between 4 to 5 times in comparison with spliced bars. The utilising of CFRP loops also influenced the load-deflection response. The rate of deflection is reduced when the curved part of the loop is engaged and restricted the reinforcement slip.
- A clear distinction in failure modes was observed in beams heated test. While the dominant failure mode for straight bars was pull-out, in the case of CFRP loop specimens (with sufficient overlap length) the failure mechanism was maintained as rupture under heating, which entails that enhancing the reinforcement tensile strength can improve fire resistance time.
- The occurrence of rupture failure within the straight portion of the loop revealed that failure at the curved part of loop can be avoided (and

consequently the strength increased) through overlapping, as additional strength will be available for the curved part.

The following conclusions were drawn on based of numerical analysis presented in Chapter 6:

- The reforming of bond numerical solution for steel from the literature to be applicable to FRP straight and loop reinforcement was successful and can be used to determine bond-stress slip response of loop and straight bar reinforcement. A Matlab script was developed to perform the numerical analysis.
- The reformed numerical model was also able to calculate bond stress-slip responses at elevated temperatures when conjoined with a semi-empirical model from the literature to estimate the reduction in bond strength and other mechanical properties under to heating.
- The model was found to be a useful tool to aid the design of loop and bar reinforcement for elevated temperatures. The outcome predictions were comparable to the experimental results in terms of failure mode and critical temperature. More refined data for bond law parameters are expected to enhance the results accuracy.

7.3 Limitations of the Current Work

Although the work has met its aims and objectives there were some limitations which listed below:

- The size dependency of beam specimens was not examined within the current work. The experimental program was conducted upon concrete beams with a relatively shallow depth. This might have an effect on crack formation which may influence fire resistance as discussed within the thesis.
- The reinforcement used within this study has a square cross section which develops higher bond strength than more common round shape (CEB-FIP,

2000). However, the parameters for bond-slip response used in the numerical analysis was for round bars and that because of data scarcity.

- Some fluctuating in tension capacity of reinforcement was observed in early stage testing (tension and push-off tests) which can be attributed to variation in the composite occurred during the manual manufacturing process and/or to uncertainties caused by tests configurations.
- In the numerical analysis the temperature was assumed to be constant along the reinforcement. While this can be considered as a reasonable simplification for short lengths, it could reduce the accuracy of results when the analysis is made for long spans.

7.4 Future Work

Although a number of significant conclusions have been drawn regarding the performance of FRP loop reinforcement, further research is required to investigate some aspects of ambient and fire behaviour in more details. Also to explore further developments and applications. Some of the most important recommendations for further research are listed below:

7.4.1 CFRP Loops Design

1. The hand winding process of CFRP loops yielded reinforcement with low fibre fraction volume. Higher fibre fraction could be improved through mechanical winding under higher tension, or the use of vacuum bagging.
2. The square cross-section used is less common than circular. The cross-section shape could have influence on the tensile capacity of the curved portion of loop, however this was not discussed with this study.
3. The capacity of CFRP loops is controlled by the curved portions. Therefore, developing techniques to enhance bend capacity will result in improved performance at elevated temperatures. However, the impact of any added complexity should be assessed on the manufacturing process and cost.

7.4.2 Experimental Work

4. Bond law parameters that were used in the bond model were averaged values from the literature of reinforcement with the same fibre type and similar surface configurations. However, there are differences in terms of bar cross-section shape and size. Conducting pull-out tests on reinforcement bars to obtain bond law parameters are expected to improve the accuracy of the numerical analysis results.
5. The tensile capacity of CFRP reinforcement was theoretically estimated based on reinforcement rupture failure load of beam specimens. Performing tensile tests is a more accurate measure of reinforcement mechanical properties.
6. The size effect has not been investigated within the current work. Useful information about size dependency can be gained through beam tests with different aspect ratios.
7. Loops overlap length was found to be crucial as insufficient length can cause a premature failure. Further experimental and analytical work is needed for better understanding of stresses generated in overlap zone.
8. Cracking opening along the unbonded length under heating requires more investigations as it is expected to influence the fire resistance of reinforcement.

7.4.3 Numerical Analysis

9. The numerical analysis produces a bond-stress response for a specified length, but it does not automatically determine development or critical length. The user has to attempt different lengths until the desired conditions are met (zero slip at end for straight bars and axial stress at bend less than bend capacity for CFRP loop reinforcement case). A development in form of an automated calculation of development length for straight bars and critical length for loops is suggested.

7.4.4 Further Applications

10. FRP reinforcement is used for strengthening applications where FRP strips or sheets are adhered to structural elements by polymeric matrix. These systems

are very vulnerable in case of fire. FRP loop technique may be exploited for strengthening applications. The additional interaction mechanism through bearing at loop ends, which was demonstrated within the current work to be effective, is expected to enhance fire endurance of strengthening systems as well. Mechanical anchor then has to be provided at loops ends, a conceptual design is shown in Figure 8.1. Near surface mounted (NFM) technique may also provide the mechanical anchoring needed for loop to perform in fire. Additional bond to the strengthened element by polymeric matrix can be added. Experimental study has to be done to confirm the feasibility of such technique.

Figure 7.1 A Conceptual design of CFRP loop as a flexural strengthening technique.

References

ABBASI, A. & HOGG, P. J. 2006. Fire testing of concrete beams with fibre reinforced plastic rebar. *Composites Part A: Applied Science and Manufacturing,* 37**,** 1142-1150.

ACHILLIDES, Z. & PILAKOUTAS, K. 2004. Bond Behavior of Fiber Reinforced Polymer Bars under Direct Pullout Conditions. *Journal of Composites for Construction,* 8**,** 173-181.

ACI 2012. Guide Test Methods for Fiber-Reinforced Polymers (FRPs) for Reinforcing or Strengthening Concrete and Masonry Structures ACI 440.3R-12. American Concrete Institute, Farmington Hills, MI, USA.

ACI 2006. Guide for the Design and Construction of Structural Concrete Reinforced with FRP Bars *ACI 440.1R-06.* American Concrete Institute, Farmington Hills, MI.

ACI 2015. Guide for the Design and Construction of Structural Concrete Reinforced with Fiber Reinforced Polymer (FRP) Bars *ACI 440.1R-06.* American Concrete Institute, Farmington Hills, MI

AHMED, E. A., EL-SAYED, A. K., EL-SALAKAWY, E. & BENMOKRANE, B. 2010. Bend Strength of FRP Stirrups: Comparison and Evaluation of Testing Methods. *Journal of Composites for Construction,* 14**,** 3-10.

AIELLO, M. A., FOCACCI, F., HUANG, P. C. & NANNI, A. 1999. Cracking of Concrete Cover in FRP Reinforced Concrete Elements under Thermal Loads. *4th International Symposium on FRP for Reinforcement of Concrete Structures (FRPRCS4).* Baltimore.

AL-ZAHRANI, M. M. 1995. *Bond Behaviour of Fibre Reinforced Plastic (FRP) Reinforcement with Concrete.* PhD, The Pennsylvania State University.

ALY, R., BENMOKRANE, B. & EBEAD, U. 2006. Tensile Lap Splicing of FRP Reinforcing Bars in Concrete. *ACI Structural Journal,* 103**,** 226-234.

AMETRANO, D. 2011. *Bond characteristics of glass fibre reinforced polymer bars embedded in high performance and ultra-high performance concrete.* Master of Applied Science, Ryerson University.

BAENA, M., TORRES, L., TURON, A. & BARRIS, C. 2009. Experimental study of bond behaviour between concrete and FRP bars using a pull-out test. *Composites Part B: Engineering,* 40**,** 784-797.

BAKIS, C. E., UPPULURI, V. S., NANNI, A. & BOOTHBY, T. E. 1998. Analysis of bonding mechanisms of smooth and lugged FRP rods embedded in concrete. *Composites Science and Technology,* 58**,** 1307-1319.

BISBY, L. A., GREEN, M. F. & KODUR, V. K. R. 2005. Response to fire of concrete structures that incorporate FRP. *Progress in structural engineering and materials,* 7**,** 136-149.

BISBY, L. A., GREEN, M. F. & KODUR, V. R. 2002. Studies on the fire behaviour of FRP reinforced and/or strengthened concrete members. *Second International Conference on the Durability of Composites for Construction.* Montréal, Québec.

BLONTROCK, H., TAERWE, L. & MATTHYS, S. Year. Properties of fiber reinforced plastics at elevated temperatures with regard to fire resistance of reinforced concrete members. *In:* C. W. DOLAN, S. H. R., A. NANNI, , ed. The 4th International Symposium on Fiber Reinforced Polymer Reinforcement for Reinforced Concrete Structures (FRPRCS-4), 1999 Baltimore, USA. 43-54.

BLONTROCK, H., TAERWE, L. & MATTHYS, S. Year. Properties of Fiber Reinforced Plastics at Elevated Temperatures with Regard to Fire Resistance of Reinforced Concrete Members. *In:* FARMINGTON HILLS, M. A. C. I., ed. 10th international symposium on fibre-reinforced polymer reinforcement, 2011 Tampa, Florida, USA. 43-54.

BRITISH STANDARD INSTITUTION 1987. Fire Tests on Building Materials and Structures. Part 20 Method of Determination of Fire Resistance of Elements of Constructions. *BS 476.*

CAO, S., WU, Z. & WANG, X. 2009. Tensile Properties of CFRP and Hybrid FRP Composites at Elevated Temperatures. *COMPOSITE MATERIALS,* 43**,** 315-330.

CARVELLI, V., PISANI, M. A. & POGGI, C. 2013. High temperature effects on concrete members reinforced with GFRP rebars. *Composites Part B: Engineering,* 54**,** 125-132.

COSENZA, E., MANFREDI, G. & REALFONZO, R. 1997. Behavior and Modeling of Bond of FRP Rebars to Concrete. *Journal of Composites for Construction,* 1**,** 40-51.

COSENZA, E., MANFREDI, G. & REALFONZO, R. 2002. *Development length of FRP straight rebars* [Online]. [Accessed 7 33].

CSA 2012. Design and Construction of Building Components with Fibre-Reinforced Polymers. *CAN/CSA-S806-12.* Canadian Standards Association, Ottawa, Ontario.

EHSANI, M. R., SAADATMANESH, H. & TAO, S. 1995. Bond of Hooked Glass Fiber Reinforced Plastic (GFRP) Reinforcing Bars to Concrete. *ACI Materials Journal,* 92**,** 391-400.

EHSANI, M. R., SAADATMANESH, H. & TAO, S. 1996. Design Recommendations for Bond of GFRP Rebars to Concrete. *Journal of Structural Engineering,* 122**,** 247-254.

ELIGEHAUSEN, R., POPOV, E. P. & BERTERO, V. V. 1983. Local Bond Stress-Slip Relationships of Deformed Bars Under Generalized Excitations. Berkeley: University of California.

FIP 2000. Bond of reinforcement in concrete. *fib Bulletin No. 10.* Stuttgart: International Federation for Structural Concrete (fib).

FIP 2001. Externally bonded FRP reinforcement for RC structures. Stuttgart.

FIP 2007a. FRP reinforcement in RC structures. Lausanne, Switzerland: International Federation for Structural Concrete.

FIP 2007b. FRP reinforcement in RC structures. *fib Bulletin No. 40.* Stuttgart: International Federation for Structural Concrete (fib).

FIRMO, J. P. L. D. C. 2015. *Fire behaviour of reinforced concrete structures strengthened with CFRP strips.* PhD Degree in Civil Engineering, University of Lispon.

GANGARAO, H. V. S., TALY, N. & VIJAY, P. V. 2007. *Rgeeinforced Concrete Design With FRP Composites,* CRC Press.

GENTRY, T. & HUSAIN, M. 1999. Thermal Compatibility of Concrete and Composite Reinforcements. *Journal of Composites for Construction,* 3**,** 82-86.

GOMES, M. M., CORREIA, J. R., BRANCO, F. A., SOUSA, J. M. P. A. J., LEMOS, F. & DIOGO, A. C. Year. Tensile and shear behaviour of GFRP pultruded laminates at elevated temperaute. *In:* 6th International Conference on Fiber Reinforced Polymer (FRP) Composites in Civil Engineering, 13–15 June 2012 Rome, Italy.

GREEN, M. F., BENICHOU, N., KODUR, V. & BISBY, L. A. 2007. Design guidelines for fire resistance of FRP-Strengthened concrete structures. *The 8th International Symposium on Fiber Reinforced Polymer Reinforcement for Concrete Structures, FRPRCS-8.* Patras, Greece.

GUADAGNINI, A., IMJAI, T. & PILAKOUTAS, K. 2006. Curved non ferrous reinforcement for concrete structures. *Measuring, Monitoring and Modeling Concrete Properties***,** 719-728.

HARAJLI, M. & ABOUNIAJ, M. 2010. Bond Performance of GFRP Bars in Tension: Experimental Evaluation and Assessment of ACI 440 Guidelines. *Journal of Composites for Construction,* 14**,** 659-668.

IMJAI, T., GUADAGNINI, M. & PILAKOUTAS, K. 2007a. Mechanical Performance of Curved FRP Rebars - Part I: Experimental Study. *In:* SMITH, S. T. (ed.) *Asia-Pacific Conference on FRP in Structures (APFIS 2007).* Hong Kong, China.

IMJAI, T., GUADAGNINI, M. & PILAKOUTAS, K. 2007b. Mechanical Performance of Curved FRP Rebars - Part II: PERFORMANCE OF CURVED FRP REBARS - PART II: Analytical Study. *In:* SMITH, S. T. (ed.) *Asia-Pacific Conference on FRP in Structures (APFIS 2007).* Hong Kong, China.

IMJAI, T., GUADAGNINI, M. & PILAKOUTAS, K. 2009. Curved FRP as concrete reinforcement. *Engineering and Computational Mechanics,* 162**,** 171 –178.

ISIS 2003. An Introduction to FRP Composites For Construction. Manitoba, Canada: Intelligent Sensing for Innovative Structures.

ISIS 2007. Reinforcing Concrete Structures with Fibre Reinforced Polymers. *Design Manual No.3, Version 2.* Manitoba, Canada: Intelligent Sensing for Innovative Structures.

JSCE 1997. Recommendation for Design and Construction of Concrete Structures Using Continuous Fibre Reinforcing Materials. *Researc Committee on Continuous Fiber Reinforcing Materials.* Tokyo.

KATZ, A. 1999. Bond mechanism of FRP rebars to concrete. *Materials and Structures* 32**,** 761-768

KATZ, A. & BERMAN, N. 2000. Modeling the effect of high temperature on the bond of FRP reinforcing bars to concrete. *Cement and Concrete Composites,* 22**,** 433-443.

KATZ, A., BERMAN, N. & BANK, L. C. 1999. Effect of High Temperature on Bond Strength of Rebars. *Journal of Composites for Construction,* 3.

KODUR, E. K. R., BISBY, L. A. & FOO, S. H.-C. 2005. Thermal Behavior of Fire-Exposed Concrete Slabs Reinforced with Fiber-Reinforced Polymer Bars. *ACI Structural Journal,* 102**,** 799-807.

LEES, J. M. & WINISTÖRFER, A. U. 2011. Non-laminated FRP Strap Elements for Reinforced Concrete, Timber and Masonry Applications. *Journal of Composites for Construction,* 15**,** 146-155.

MALVAR, L. J. 1994. Bond stress-slip characteristics of FRP rebars. *Report TR-2013-SHR.* Port Hueneme, California: Naval facilities Engineering Service Center.

MASMOUDI, R., MASMOUDI, A., BEN OUEZDOU, M. & DAOUD, A. 2011. Long-term bond performance of GFRP bars in concrete under temperature ranging from 20 degrees C to 80 degrees C. *Construction and Building Materials,* 25**,** 486-493.

MCINTYRE, E., BILOTTA, A., BISBY, L. & NIGRO, E. 2014. Mechanical Properties of Fibre Reinforced Polymer Reinfrocement for Concrete at Hight Temperature. *8th International Conference on Structures in Fire.* Shanghai, China.

MCINTYRE, E. R. E., BISBY, L. A. & STRATFORD, T. J. 2015. Title: Elevated Temperature Performance of Concrete Beams Reinforced with FRP Bars. *In:* KODUR, V. K. R. & BANTHIA, N. (eds.) *Fifth International Workshop on Performance, Protection & Strengthening of Structures under Extreme Loading.* East Lansing, MI, USA.

MEIER, U. & WINSTÖRFER, A. 2007. Advanced Thermoplastic CFRP Tendons. *International Workshop on Thermoplastic Matrix Composites.* Ostuni (BR), ITALY

MENARD, K. P. 2008. *Dynamic Mechanical Analysis: A Practical Introduction*, CRC Press

MOSLEY, W. H., HULSE, R. & BUNGEY, J. H. 2007. *Reinforced Concrete Design: to Eurocode 2,* New York, Palgrave Macmillan; edition.

MUNOZ, M. B. 2010. *Study of Bond Behaviour Between FRP Reinforcement and Concrete.* PhD, Universitat of Girona.

NADJAI, A., TALAMONA, D. & ALI, F. Year. Fire performance of concrete beams reinforced with FRP bars. *In:* CHEN, J. F. & TENG, J. G., eds. International Symposium on Bond Behaviour of FRP in Structures 2005. International Institute for FRP in Construction.

NIGRO, E., CEFARELLI, G., BILOTTA, A., MANFREDI, G. & COSENZA, E. 2011a. Fire resistance of concrete slabs reinforced with FRP bars. Part I: Experimental investigations on the mechanical behavior. *Composites Part B: Engineering,* 42**,** 1739-1750.

NIGRO, E., CEFARELLI, G., BILOTTA, A., MANFREDI, G. & COSENZA, E. 2011b. Fire resistance of concrete slabs reinforced with FRP bars. Part II: Experimental results and numerical simulations on the thermal field. *Composites Part B: Engineering,* 42**,** 1751-1763.

NIGRO, E., CEFARELLI, G., BILOTTA, A., MANFREDI, G. & COSENZA, E. 2012. Behavior of FRP Reinforced Concrete Slabs in Case of Fire: Theoretical Models and Experimental Tests. *Advances in Structural Engineering,* 15**,** 637-652.

NIGRO, E., CEFARELLI, G., BILOTTA, A., MANFREDI, G. & COSENZA, E. 2013. Adhesion at High Temperature of FRP Bars Straight or Bent at the end of Concrete Slabs. *Journal of Structural Fire Engineering,* 4**,** 71-85.

NIGRO, E., CEFARELLI, G., MANFREDI, G. & COSENZA, E. Year. Valutazione della resistenza in caso di incendio di solette di calcestruzzo armate con barre di FRP: metodo generale e metodi semplificati. *In:* XVII Congresso C.T.E., 2008 Milan, Italy. C.T.E.

OKELO, R. & YUAN, R. 2005. Bond Strength of Fiber Reinforced Polymer Rebars in Normal Strength Concrete. *Journal of Composites for Construction,* 9**,** 203-213.

ORANGUN, C. O., JIRSA, J. O. & BREEN, J. E. 1977. A Reevaluation of Test Data on Development Length and Splices. *ACI JOURNAL,* 74**,** 114-122.

PECCE, M., MANFREDI, G., REALFONZO, R. & COSENZA, E. 2001. Experimental and Analytical Evaluation of Bond Properties of GFRP Bars. *Journal of Materials in Civil Engineering,* 13**,** 282-290.

QUAYYUM, S. 2010. *Bond behaviour of fibre reinforced polymer (FRP) rebars in concrete.* Master of Applied Science, University of British Columbuia.

RAFI, M. M. & NADJAI, A. 2011. Fire Tests of Hybrid and Carbon Fiber-Reinforced Polymer Bar Reinforced Concrete Beams. *ACI Materials Journal,* 108**,** 252-260.

RAFI, M. M., NADJAI, A. & ALI, F. 2007. Fire resistance of carbon FRP reinforced-concrete beams. *Magazine of Concrete Research.* Institution of Civil Engineers.

SAAFI, M. 2002. Effect of fire on FRP reinforced concrete members. *Composite Structures,* 58**,** 11-20.

SAUDER, C., LAMON, J. & PAILLER, R. 2004. The tensile behavior of carbon fibers at high temperatures up to 2400 °C. *Carbon,* 42**,** 715-725.

SHEHATA, E., MORPHY, R. & RIZKALLA, S. 2000. Fibre reinforced polymer shear reinforcement for concrete members: behaviour and design guidelines. *Canadian Journal of Civil Engineering,* 27**,** 859-872.

THAMRIN, R. & KAKU, T. Year. DEVELOPMENT LENGTH EVALUATION OF REINFORCED CONCRETE BEAM WITH CFRP BARS. *In:* CHEN, J. F. & TENG, J. G., eds. The International Symposium on Bond Behaviour of FRP in Structures, 2005. International Institute for FRP in Construction, 385-392

TIGHIOUART, B., BENMOKRANE, B. & MUKHOPADHYAYA, P. 1999. Bond strength of glass FRP rebar splices in beams under static loading. *Construction and Building Materials,* 13**,** 383-392.

WALSH, P. J. & CORPORATION, Z. 2001. *ASM Handbook,* Material Park, Ohio, ASM International.

WEBER, A. 2008. Fire-resistance tests on composite rebars. *Fourth International Conference on FRP Composites in Civil Engineering.* Zurich, Switzerland.

WHITE, D. J., TAKE, W. A. & BOLTON, M. D. 2003. Soil deformation measurement using particle image velocimetry (PIV) and photogrammetry. *Geotechnique* 53**,** 619–631.

WINISTORFER, A. & MOTTRAM, J. T. 2001. Finite Element Analysis of Non-Laminated Composite Pin-Loaded Straps for Civil Engineering. *Journal of COMPOSITE MATERIALS,* 35**,** 577-602.

YANKELEVSKY, D. Z. 1985. New Finite Element For Bond-Slip Analysis. *Journal of Structural Engineering,* 111

Appendix A – Dynamic Mechanical Analysis Results

This appendix includes the results of dynamic mechanical analysis (DMA) tests that were conducted to determine the glass transition temperature (T_g) of CFRP reinforcement produced for beam tests. The test results illustrate the changes in storage modulus with temperature. T_g was determined on the basis of highest tan δ.

A.1 DMA Results of CFRP Reinforcement Used in Beam tests

The figures below illustrate the changes in storage modulus with temperature and corresponding tan δ which was used to determine T_g for the CFRP reinforcement patch used in phase I of beam test. (refer to section 4.5.1). From Figures A.5 and A.6 The average value of T_g is 87.6 °C.

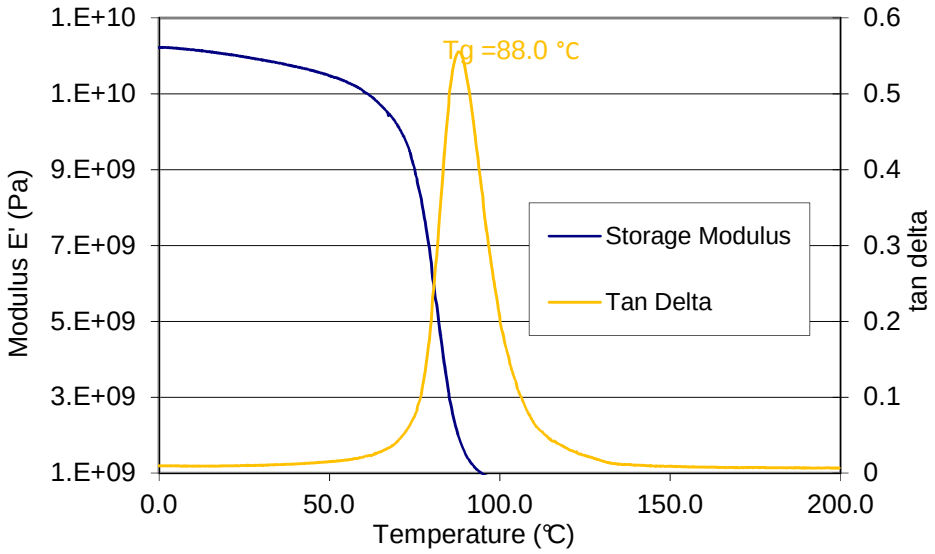

Figure A.1 DMA results for sample S5 with EL2 resin.

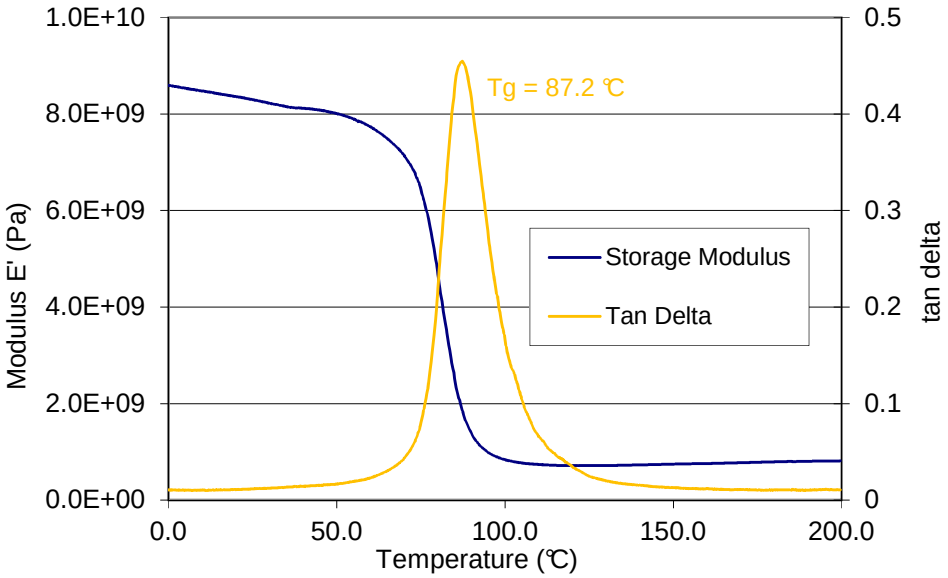

Figure A.2 DMA results for sample S6 with EL2 resin.

Appendix B – CFRP and Gas Temperature Progression in Tension Tests

This appendix includes data describes CFRP loop reinforcement and gas temperatures during the heated tension tests, refer to section 3.3.2 for more details.

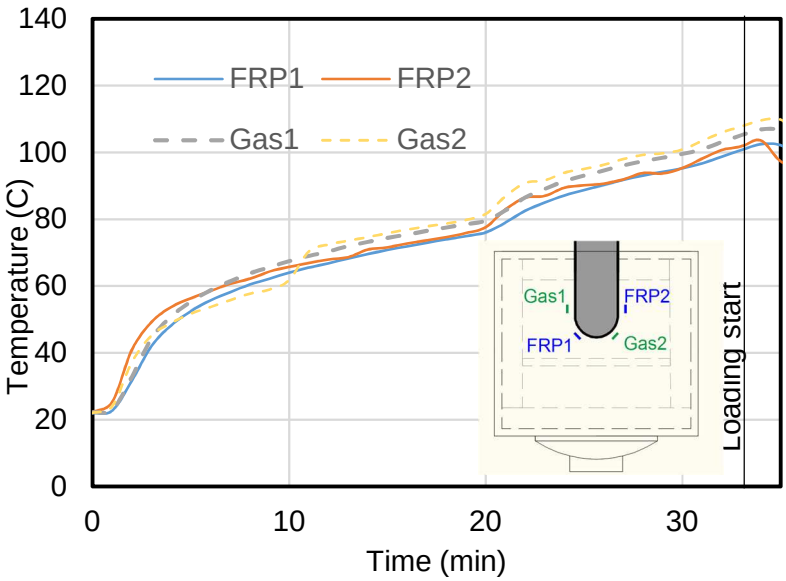

Figure B.1 Readings from thermocouples: control specimen AS3.

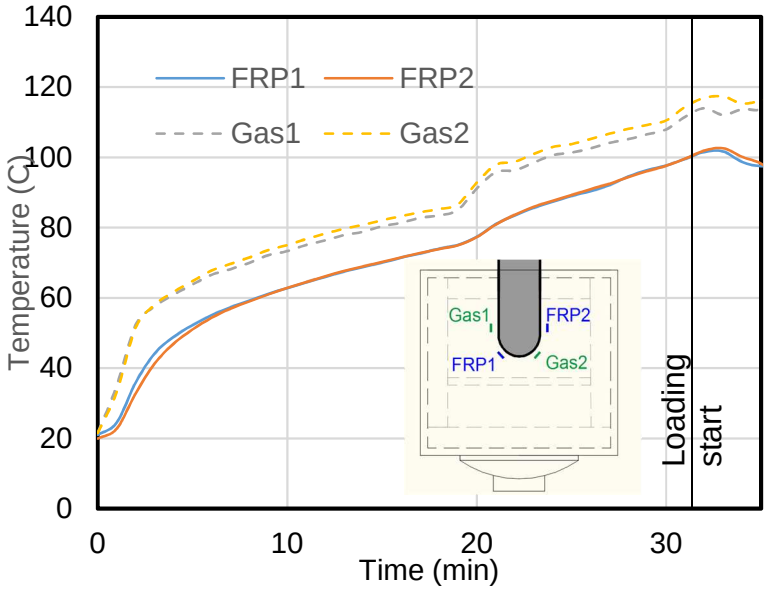

Figure B.2 Readings from thermocouples: control specimen AS4

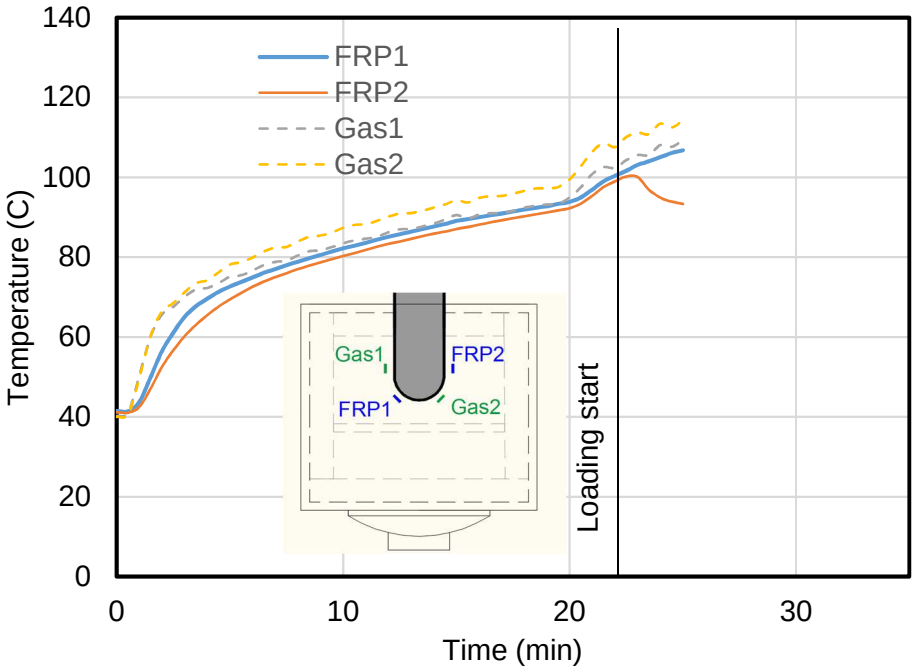

Figure B.3 Readings from thermocouples: Two concentric loops BS3.

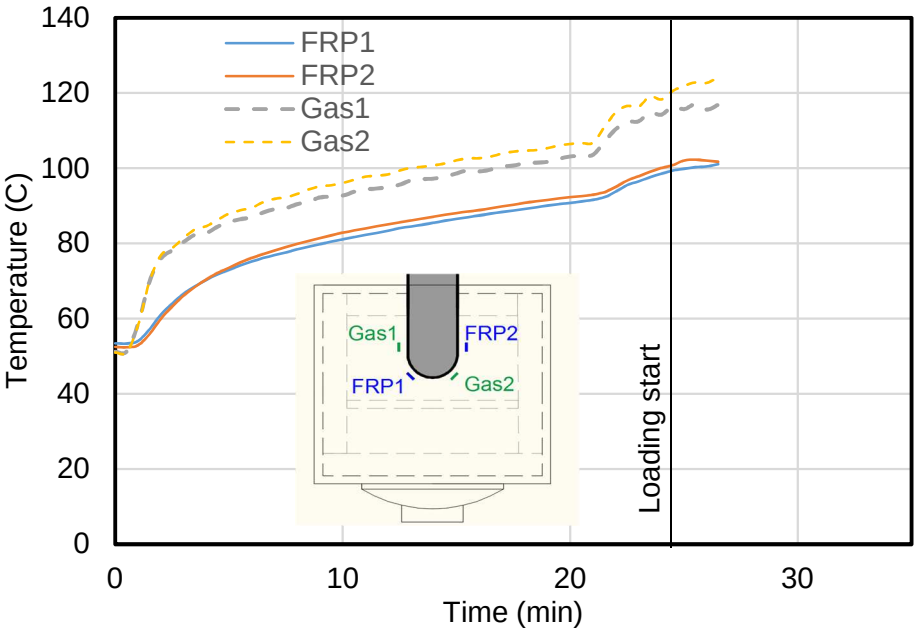

Figure B.4 Readings from thermocouples: Two concentric loops BS4.

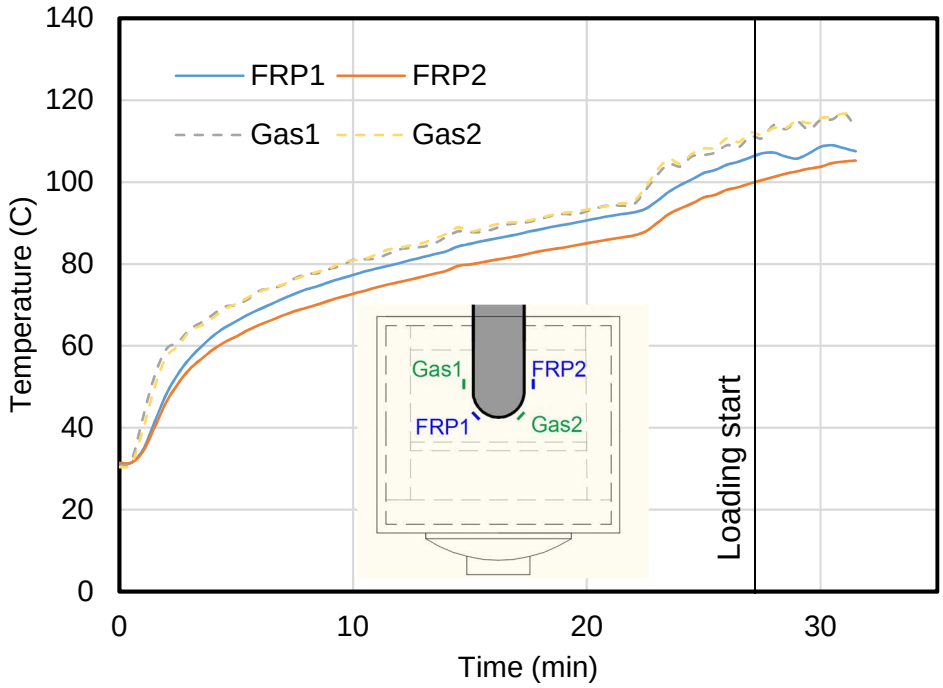

Figure B.5 Readings from thermocouples: Three concentric loops CS3.

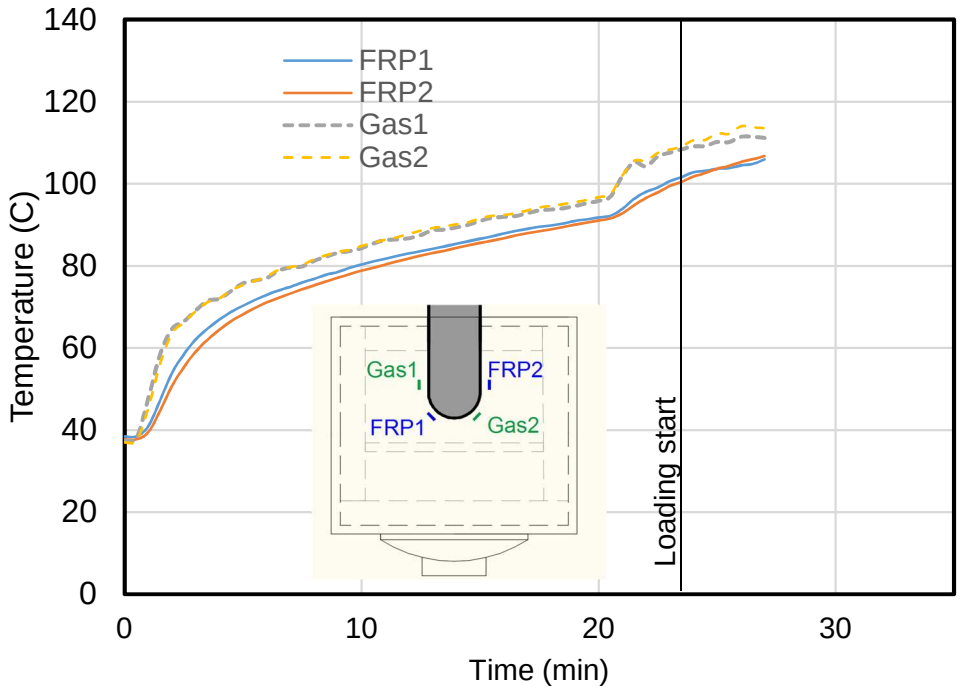

Figure B.6 Readings from thermocouples: Three concentric loops CS4

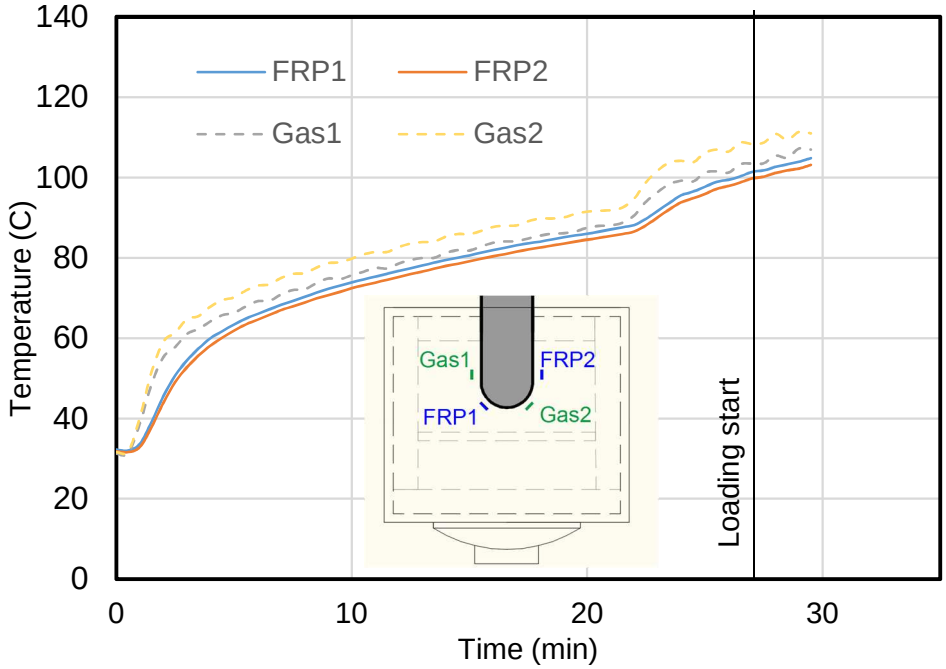

Figure B.7 Readings from thermocouples: Loops with high temperature resin DS3.

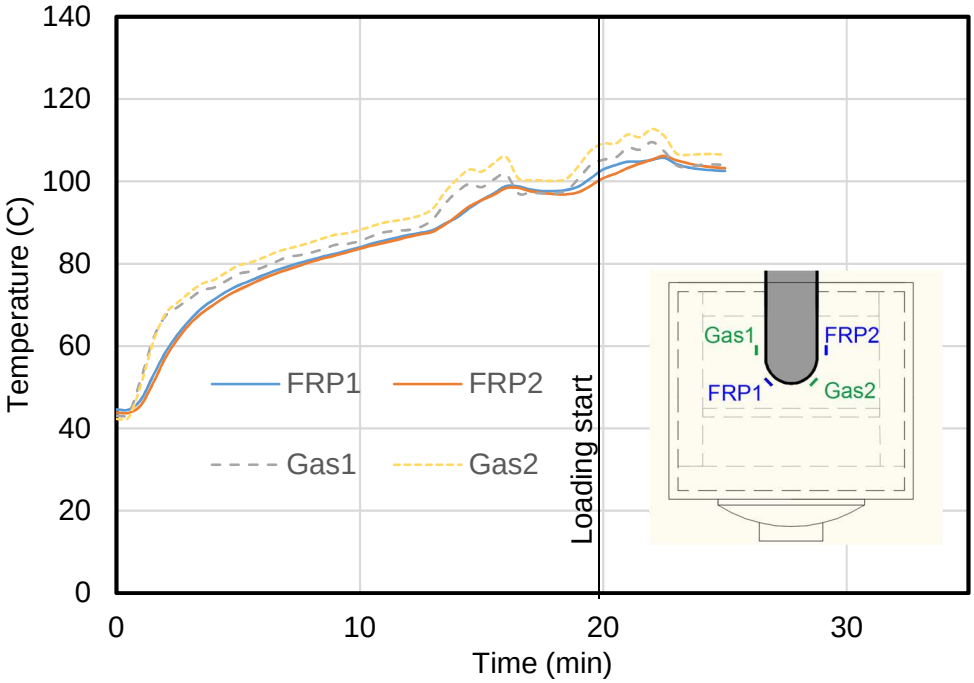

Figure B.8 Readings from thermocouples: Loops with high temperature resin DS4.

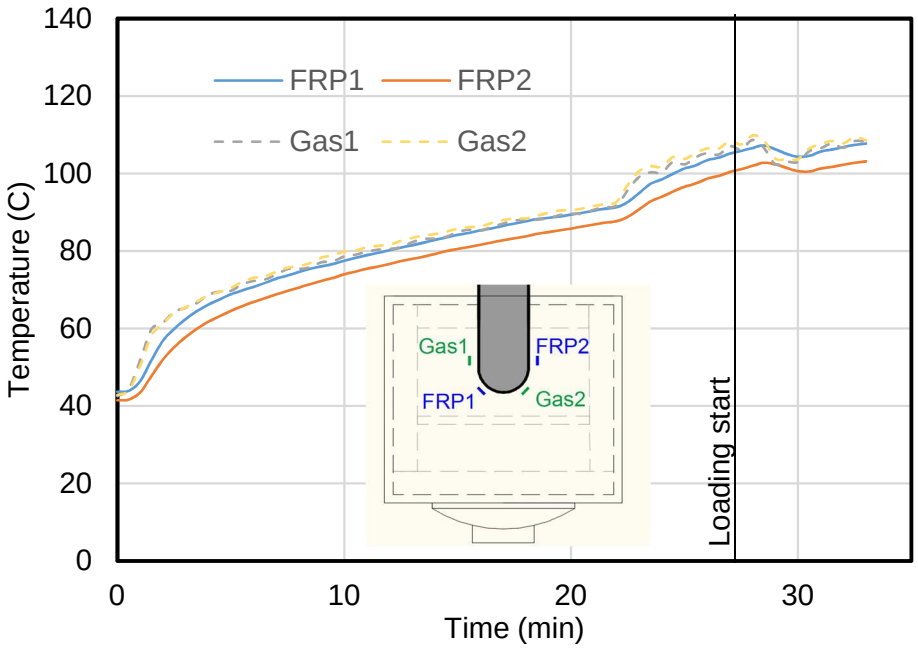

Figure B.9 Readings from thermocouples: Loop with reinforced end ES3.

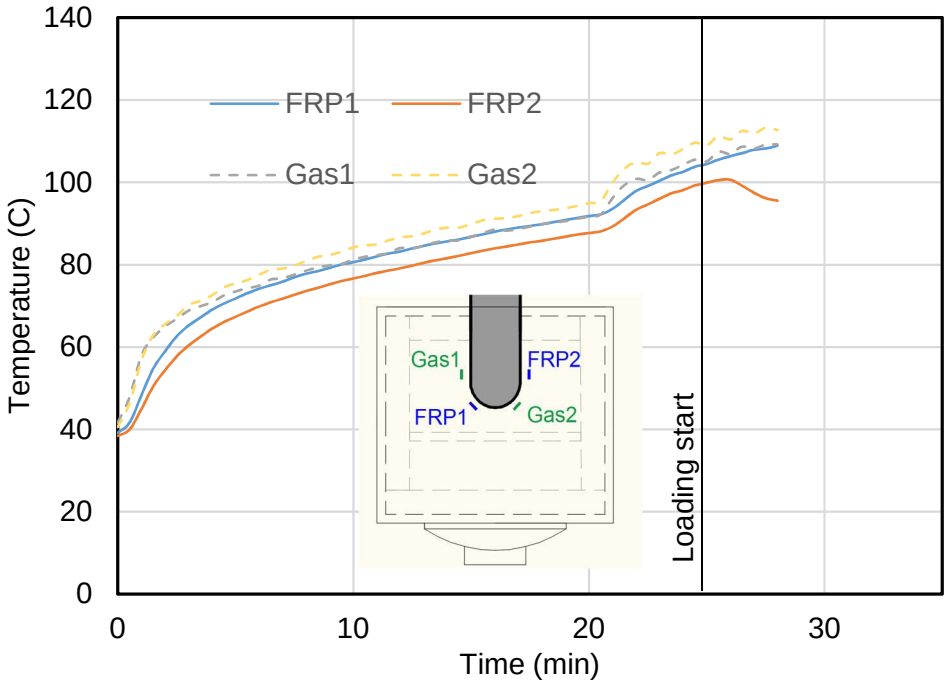

Figure B.10 Readings from thermocouples: Loop with reinforced end ES4.

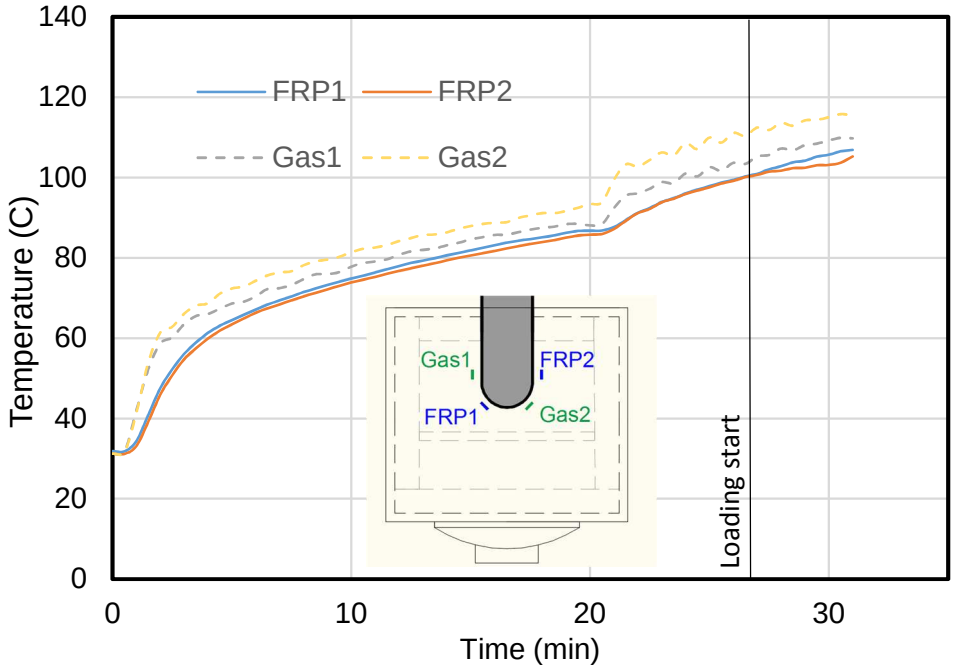

Figure B.11 Readings from thermocouples: Loop with flat ends FS3.

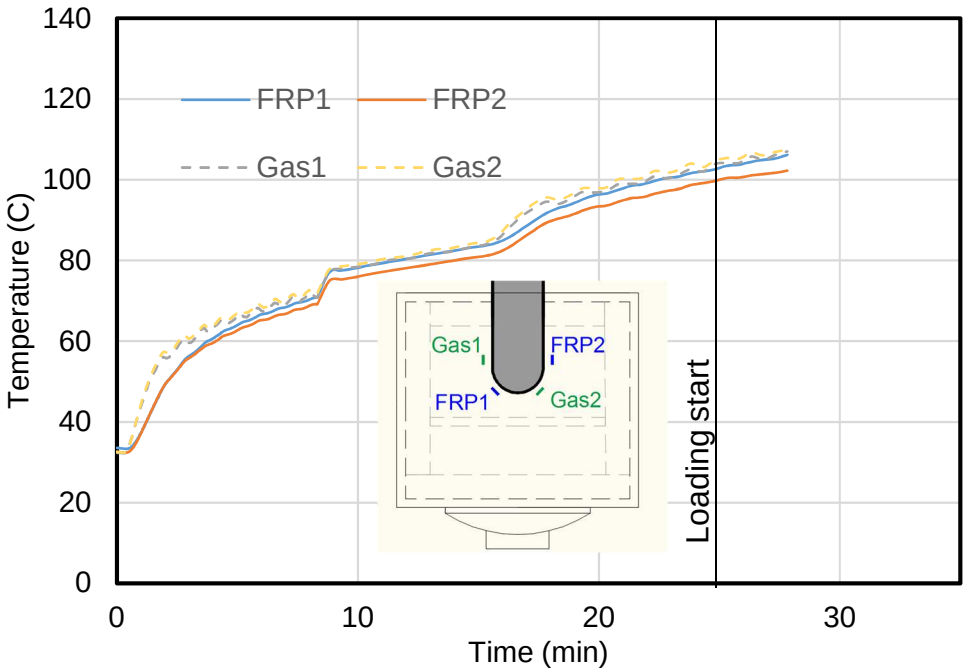

Figure B.12 Readings from thermocouples: Loop with flat ends FS4.

Appendix C – Theoretical Analysis of Beam Flexural and Shear Strength

This appendix contains theoretical analysis and design of phase I beam specimens. The flexural capacity of beams specimens of phase I (Figure 4.1) were calculated using strain compatibility analysis while cracking moment, development length, and shear capacity were calculated according to design guideline ACI (2015) and ISIS (2007). The summary of design data and assumptions are:

- The failure strain of concrete in compression is 0.0035
- The strain in concrete at any level is proportional to distance from neutral axis
- FPR reinforcement is linear elastic till failure
- Perfect bond exist between reinforcement and concrete
- Concrete compressive strength, f'_c = 40 MPa
- CFRP reinforcement ultimate strength f_{fu} = 2557 MPa based on average rupture load (56.76kN) of specimen in push-off test at ambient (Table 3.8), and actual areas of fibres (22.2 mm^2) in reinforcement. Each leg was made of 25 layers of 12K carbon tow (see section 3.6.3) and each layer of 12K tow has cross-section area of 0.444 mm^2 (see Table 3.1). f_{fu} = 1135 MPa based on nominal reinforcement are of 50 mm^2. Due to variation of section size resulted from manufacturing process, actual fibres area can be used as it's uniform.
- CFRP reinforcement elastic modulus, E_{frp} = 103.21 GPa based on nominal reinforcement area and 234.0 GPa (Table 3.1) based on fibre area only.
- Specimens geometry and reinforcement arrangement are shown in Figure 4.1

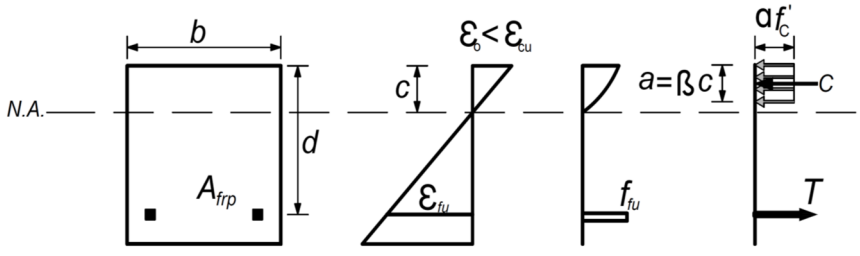

Figure C.1 Strain and stress distribution in the section (ISIS, 2007)

C.1 - The effective depth is measured from top of beam to the centre of reinforcement for straight reinforcement specimens (C and D). For specimens with loops overlapping (Type A and B) the reinforcement is staked (Figure 4.1) so centre of reinforcement was considered at the plane in between the overlapping loops.

- For Beams Type A and B

$$d_1 = h - cover - d_b \quad \text{(C.1)}$$
$$d_1 = 160 - 24 - 5 = 131\ mm$$

- For Beams Type C and D

$$d_2 = h - cover - \frac{d_b}{2} \quad \text{(C.2)}$$
$$d_2 = 160 - 24 - \frac{5}{2} = 133.5\ mm$$

Where d_1 effective depth beams Type A and B; *d_2* effective depth for beams Type C and D; *d_b* bar size.

C.2 - Calculating the FRP reinforcement ratio based on fibre area alone:

- For Beams Type A and B

$$\rho_{frp} = \frac{A_{frp}}{b\ d} \quad \text{(C.3)}$$

$$\rho_{frp1} = \frac{A_{frp}}{b\ d_1} = \frac{(2\times 11.1)}{150\times 131} = 0.0011$$

- For Beams Type C and D

$$\rho_{frp2} = \frac{A_{frp}}{b\ d_2} = \frac{(2\times 11.1)}{150\times 133.5} = 0.0011$$

Where ρ_{frp} reinforcement ratio; A_{frp} reinforcement area; b bean width.

C.3 - Calculation of balanced FRP reinforcement ratio: Same equation of balanced reinforcement ratio is used by design guidelines ACI (2015) [equation (7.2.1b)] and ISIS (2007) [equation 6.6]. As it is intended to calculate actual flexural strength the materials partial factors, Φ_c *and* Φ_{frp}, were set to 1.

$$\rho_{frpb} = \alpha_1\ \beta_1 \frac{f_c'}{f_{frpu}} \frac{\Phi_c}{\Phi_{frp}} \left(\frac{\varepsilon_{cu}}{\varepsilon_{cu} + \varepsilon_{frpu}}\right) \quad \text{(C.4)}$$

$$\alpha_1 = 0.85 - 0.0015\ f_c' \geq 0.67 \quad \text{(C.5)}$$

$$\alpha_1 = 0.79 \geq 0.64$$

$$\beta_1 = 0.97 - 0.0025\ f_c' \geq 0.67 \quad \text{(C.6)}$$

$$\beta_1 = 0.86 \geq 0.64$$

CFRP reinforcement ultimate strain

$$\varepsilon_{frpu} = \frac{f_{frpu}}{E_{frp}} \quad \text{(C.7)}$$

$$\varepsilon_{frpu} = \frac{f_{frpu}}{E_{frp}} = \frac{2557}{234000} = 0.011$$

$$\rho_{frpb} = 0.79\times 0.86\times \frac{40}{2557}\ \frac{1}{1} \left(\frac{0.0035}{0.0035 + 0.011}\right) = 0.0025$$

As ρ_{frp1} and $\rho_{frp2} < \rho_{frpb}$ the section is under reinforced.

Where Φ_c material partial factor for concrete, Φ_{frp} FRP material partial factor for FRP, ε_{cu} ultimate strain in concrete 0.0035, α_1 and β_1 parameters for concrete

stress block at ultimate strain, f_c' specified compressive strength of the concrete, f_{frpu} ultimate tensile strength of CFRP, ε_{frpu} ultimate strain of CFRP, E_{frp} Modulus of Elasticity of CFRP, ρ_{frpb} balance reinforcement ratio.

C.4 - Natural axis depth: As section fails by tension the strain in concrete is less than ultimate value ε_{cu}. Iteration strain-compatibly procedure is performed to calculate force in compression zone.

Assume the depth on neutral axis as 17.5 mm, using strain compatibility

$$\frac{\varepsilon_c}{c} = \frac{\varepsilon_{frpu}}{d-c} \tag{C.8}$$

- For Beams Type A and B

$$\varepsilon_c = 17.5 \times \frac{0.011}{131 - 17.5} = 0.0017$$

- For Beams Type C and D

$$\varepsilon_c = 17.5 \times \frac{0.011}{133.5 - 17.5} = 0.0017$$

- The tensile force in CFRP reinforcement at ultimate stress

$$T = \Phi_{frp}\, A_{frp}\, f_{frpu} \tag{C.9}$$
$$T = 1 \times 22.2 \times 2557 = 56.77\ kN$$

- The resultant of compressive force in concrete within compression zone C, is calculated as:

$$C = \alpha\ f_c'\ \beta\ c\ b \tag{C.10}$$

- The parameters of equivalent stress block α and β can be found using Figures 6.4 and 6.5 of ISIS (2007) and were found to be $\alpha = 0.8$ and $\beta = 0.67,$ Therefore:

$$C = 0.76\times40\times0.69\times17\times150 = 56.28\ kN$$

As C = 56.28 kN ≈ T = 56.77 kN, No further iteration is required.

Where ε_c strain in concrete, c depth of neutral axis, d effective depth, T tensile force in reinforcement, C compressive force in concrete, α & β parameters of concrete stress block.

C.5 - The nominal flexural strength of the section: The nominal flexural capacity of the section can be then calculated can be calculated as:

$$M_r = T\left(d - \frac{\beta\, c}{2}\right) \quad \text{(C.11)}$$

- For Beams Type A and B d_1=131mm

$$M_{r1} = 22.2\times2557\left(131 - \frac{0.71\times17}{2}\right) = 7.07\ kN.m$$

- For Beams Type C and D d_2=133.5mm

$$M_{r2} = 22.2\times2557\left(133.5 - \frac{0.69\times17}{2}\right) = 7.10\ kN.m$$

Therefore based on calculated bending moment capacity and test arrangement shown in Figure 4.1, Reaction in each load point is 15 kN and total failure load = 30 kN

Where M_r section bending moment capacity.

C.6 - Calculating the cracking moment:

According to equation 7.3.2.2d of ACI (2015) and equation 6.17 of (ISIS, 2007) the cracking moment can be calculated as following:

$$Mc_r = \frac{f_r\, I_t}{y_t} \tag{C.12}$$

$$f_r = 0.6\sqrt{f_c'} \tag{C.13}$$

$$f_r = 0.6\sqrt{40} = 3.79\ MPa$$

$$Mc_r = \frac{3.79\,\frac{150\times160^3}{12}}{\frac{160}{2}} = 2.24kN.m$$

The corresponding load of cracking moment can be calculated based on test arrangement shown in Figure 4.2

$$Fc_r = \frac{2\times2.24}{0.473} = 9.5kN \tag{C.14}$$

To avoid the failure of section directly after crack the ISIS (2007) guidelines require that cracking moment is at least 50% of ultimate bending moment.

$$M_{r1}\ and\ M_{r2} > 1.5\ M_{cr}\ O.K.$$

Where M_r section bending moment capacity, f_r modulus of rupture, I_t second moment of area of the transformed uncracked section about its centroidal axis, y_t distance from the centroid of uncraked section to extreme surface in tension.

C.7 - The development length: The development length is the shortest length of bar has to be embedded in concrete for the bar to develop its ultimate strength. The development length was calculated according to ACI (2015) and ISIS (2007)

According to equation (10.3a) of ACI (2015) development length can be calculated as following:

$$l_d = \frac{\propto \frac{f_{fr}}{0.083\sqrt{f_c'}} - 340}{13.6 + \frac{C}{d_b}}\, d_b \qquad \text{(C.15)}$$

Where: f_{fr} is stress level in bar and there the bar is assumed to develop its full capacity therefore stress level f_{fr} is considered to be f_{fu} = 1135 MPa (based on reinforcement nominal size), α is bar location modification factor and should be used as 1 because less 305 mm of concrete is cast below the reinforcement, *C* is the lesser of the cover to the centre of the bar (d_c) or one-half of the centre-on-centre spacing of the bars being developed.

$$C = \left(d_c\,, \frac{ctr - to - ctr\ spacing}{2}\right) \leq 3.5 d_b$$

$$C = \left(24 + \frac{5}{2}\,, \frac{105}{2}\right) \leq 3.5 d_b$$

$$C = \min(\,26.5, 52.5) \leq 17.5$$

$$Use\ C = 17.5\ mm$$

$$l_d = \frac{(1)\frac{1135}{0.083\sqrt{23.7}} - 340}{13.6 + \frac{17.5}{5}} 5$$

$$l_d \approx 535\ mm$$

Development length can also be calculated from equation (8-1) of design guideline ISIS (2007) as following:

$$l_d = 0.45\,\frac{k_1 k_4}{\left(d_{cs} + k_{tr}\frac{E_{frp}}{E_s}\right)}\left(\frac{f_{frp}}{f_{cr}}\right) A \qquad \text{(C.16)}$$

Where: k_1 is a bar location factor taken as 1.0 for horizontal reinforcement placed so that less than 300 mm of fresh concrete is cast below the bar, k_4 is a bar surface factor representing the ratio of bond strength of FRP to that of steel rebar having same cross-sectional area but not that 1.0 and value of 0.8 is used in absence of manufacturer test data, A bar cross section area mm^2, d_{cs} is the smaller of the distance from the closest concrete surface to the centre of the bar being developed or 2/3 of the centre-to-centre spacing of bars being developed (mm), k_{tr} is a transverse reinforcement index. = $(f_y A_{tr})/(10.5sn)$; A_{tr} = area of transverse reinforcement normal to the plane of splitting through the bars (mm^2); f_y=yield strength of transverse reinforcement (MPa); s = center to center spacing of the transverse reinforcement (mm); n = number of bars being developed along the plane of splitting; E_{FRP} = modulus of elasticity of FRP bar (MPa); E_s = modulus of elasticity of steel (MPa); f_F = specified tensile strength of FRP bar (MPa); f_{cr} cracking strength of concrete (MPa) = 0.4 $(f_c')^{0.5}$ for normal weight concrete. And $\left(d_{cs} + k_{tr}\frac{E_{frp}}{E_s}\right) > 2.5d_b$, d_b bar diameter.

In absence of shear reinforcement, bond strength of steel bar with same cross-sectional area, the values of k_{tr} and k_4 are set as zero and 0.8 respectively. Considering concrete and FRP materials properties and hence CFRP reinforcement has less than 300 mm of concrete cast below it (Figure 4.1), the development length of CFRP reinforcement can be calculated as:

$$l_d = 0.45\,\frac{1\times0.8}{(26.5+0)}\left(\frac{1135.3}{0.4\sqrt{40}}\right)\times(5\times5) \approx 155\,mm$$

C.8 - Tension Lap Splice: ISIS (2007) distinguishes between two types of tension splice based on stress level in reinforcement and fraction of bar spliced with a given length. For reinforcement with Class A the splice length is $1.0l_d$ while for Class B splice length is $1.3l_d$. Hence all reinforcement are spliced within same area and full reinforcement strength is required, splice length Class B ($1.3l_d$) was used. ACI (2015) consider previous classification is not appropriate for FRP reinforcement as its typical full tensile strength is not needed to be developed. However due to the limited data of FRP development length, splice length of $1.3l_d$ is recommended.

Based on developed length calculated from ACI (2015) equation (C.15):

$$\text{Splice length} = 1.3l_d \approx 700\ mm$$

Based on developed length calculated from ISIS (2007) equation (C.16):

$$\text{Splice length} = 1.3l_d \approx 205\ mm$$

The used splice length in specimens was 440 mm (see Figure 4.1) which longer than the required length by ISIS (2007) but less than the required by ACI (2015). The length 440mm was chosen so the bar splice fit within the heated region.

C.9 - Shear reinforcement: The required size and spacing for vertical shear reinforcement for the beam specimens were determined according to ACI (2015) and ISIS (2007).

The concrete contribution to shear resistance of member reinforced with FRP reinforcement can be calculated according to ACI (2015) equation (8.2b) as following:

$$V_c = \frac{2}{5}\sqrt{f_c'}\,b_w(kd) \qquad \text{(C.17)}$$

$$k = \sqrt{2\rho_f n_f + (\rho_f n_f)^2} - \rho_f n_f \quad \text{(C.18)}$$

$$n_f = \frac{E_f}{E_c} \quad \text{(C.19)}$$

$$E_c = 4750\sqrt{f_c'} \quad \text{(C.20)}$$

Where: V_c concrete shear strength MPa, f_c' concrete characteristic strength MPa, b_w width of web mm, d section depth mm, E_f FRP modulus of elasticity, E_c concrete modulus of elasticity, n_f ratio between FRP and concrete modulus of elasticity. ρ_f FRP reinforcement ratio.

$$E_c = 4750\sqrt{40} = 30.04\ GPa$$

$$n_f = \frac{103.21}{30.04} = 3.44$$

$$\rho_f = \frac{2\times25}{160\times150} = 0.0021$$

$$k = \sqrt{2\times0.0021\times3.44 + (0.0021\times3.44)^2} - 0.0021\times3.44$$

$$k = 0.113$$

$$V_c = \left(\frac{2}{5}\right)\sqrt{40}\times150\times0.113\times127 = 5.45\ kN$$

Concrete shear capacity using equation 10.4 of ISIS (2007)

$$V_c = 0.2\lambda\Phi_c\sqrt{f_c'}\ b_w\ d\ \sqrt{\frac{E_{frp}}{E_s}} \quad \text{(C.21)}$$

$$V_c = 0.2\sqrt{40}\times 122 \times 131\times \sqrt{\frac{103.21}{200}} = 14.52\ kN$$

Where: V_c concrete shear strength, λ modification factor for concrete density taken 1 for normal weight concrete, Φ_c resistance factor for concrete taken as 1, b_w minimum effective width (used 122 mm, see Figure 4.1), *d* effective depth, E_{frp} modulus of elasticity of FRP, E_s steel modulus of elasticity.

Hence the concrete shear resistance is less than shear forces generated at the ultimate flexural moment (15 kN) shear reinforcement is needed.

Calculation stirrup spacing using ACI (2015) equation (8.2e) for two legs steel stirrup perpendicular to beam axis of size Φ6mm and yield stress 550 MPa. The lower value of V_c (5.45 kN) was used.

$$s \leq \frac{A_{sv} f_{fv} d}{V_u - V_c} \qquad \text{(C.22)}$$

$$s \leq \frac{2\times\pi\frac{6^2}{4}\times 550\times 127}{(15-5.45)\times 10^3} \approx 415mm$$

Check maximum spacing: Maximum transverse reinforcement spacing recommended by ACI (2015) is *d*/2 (127/2 = 63.5mm)

Maximum transverse reinforcement spacing recommended by ISIS (2007) is *0.7d or 600mm* (0.7×127 = 89 mm)

The lower limit of transverse reinforcement spacing by ACI (2015) was considered and stirrups spacing were limited to 60 mm (see Figure 4.1).

Appendix D – Estimation of CFRP Rupture Stress and Section Cracking Moment Based on Beam Specimen Failure Load

D.1 Estimation of CFRP Reinforcement Rupture Stress

In the theoretical estimation of phase I beam specimen (Appendix C) the rupture stress of CFRP reinforcement was considered based on rupture load from push-off test specimens. The theoretical calculations showed tension failure at load of 30 kN (see Appendix C) while experimental data of four-point bending test showed tension failure occurred at average load of 39 kN (see Table 4.5), 30% over the theoretical failure load. As discussed in chapter 3 failure load from push-off test could been affected by eccentricity generated from specimen rotation under loading which caused the underestimate of beam specimens capacity.

Strain compatibility analysis was conducted to estimate the ultimate tensile strength of CFRP reinforcement based on the tension failure load of beam specimen D2 (Table 4.5).

The calculations are based on following experimental data and assumptions

- The failure strain of concrete in compression is 0.0035 (assumed)
- The strain in concrete at any level is proportional to distance from neutral axis (assumed)
- FPR reinforcement is linear elastic till failure (Figure 3.45)
- Perfect bond exist between reinforcement and concrete (assumed)
- Concrete Compressive Strength, f'_c = 42.37 MPa (Table 4.3)
- FRP Elastic Modulus, E_{frp} = 234.0 GPa (Table 3.1)
- Geometry and reinforcement details of beam specimen type D are shown in Figure 4.1

The ultimate bending moment based on failure load 37.5 kN and test arrangement shown in figure (4.20) can be calculated as:

$$M_r = \left(\frac{F}{2} \times L\right) \tag{D.1}$$

$$M_r = 9.0\ kN.m$$

The resultant of compressive force in concrete within compression zone F_c, is calculated as (Figure C.1):

$$F_c = \alpha\ f_c^{'}\ \beta\ c\ b \tag{D.2}$$

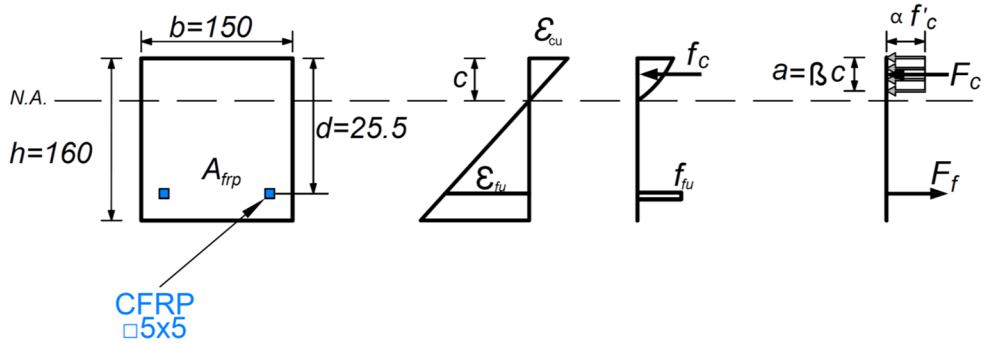

Figure D.1 Strain and stress distribution in the section (ISIS, 2007).

The parameters of equivalent stress block α and β at ε_{cu} (0.0035) can be found using Figures 6.4 and 6.5 of ISIS (2007) and were found to be $\alpha = 0.8$ and $\beta = 0.9$

$$F_c = 0.8 \times 42.37 \times 0.9 \times c \times 150 \tag{D.3}$$

$$F_c = 4576\ c$$

The tensile force in CFRP reinforcement at ultimate stress

$$F_f = \Phi_{frp}\ A_f\ f_{fu} \tag{D.4}$$

$$F_f = 1\times2\times25\times f_{fu} \tag{D.4a}$$

$$F_f = 50 f_{fu} \tag{D.4b}$$

The depth on neutral axis c, as a function of CFRP ultimate stress can be obtained from equating the compression force in concrete F_c (Eq C.3) and tensile force in CFRP reinforcement F_f $(Eq\ C.4)$leads to

$$c = \frac{50}{4576}\, f_{fu} \tag{D.5}$$

The sectional nominal flexural strength is calculated from couple of compression and tensile forces (Figure D.1)

$$M_r = F_F \left(d - \frac{\beta\, c}{2}\right) \tag{D.6}$$

$$9.0\times10^6 = f_{fu}\times50 \left(129.5 - \frac{0.9}{2}\,(\frac{50}{4576}\, f_{fu})\right) \tag{D.6a}$$

Solving the quadric equation C.6a for f_{fu} value yields

$$f_{fu} = 1322\ MPa \tag{D.6b}$$

Depth of Neutral axis c then can be calculated by subtitling value f_{fu} (Eq D. 6b) in equation (Eq D.5):

$$c = 14.4\ mm \tag{D.7}$$

D.2 Theoretical Calculation of the Cracking Moment Based on Experimental Data

According to equation 7.3.2.2d of ACI (2015) and equation 6.17 of (ISIS, 2007)

$$Mc_r = \frac{f_r\, I_t}{y_t} \tag{D.8}$$

$$f_r = 0.6\sqrt{f_c^{'}} \tag{D.9}$$

$$f_r = 0.6\sqrt{23.7} = 2.9 \text{ MPa} \tag{D.9a}$$

Using the averaged concrete cover of each beam specimen of phase I and II (Table 4.5 and 5.4)

$$Mc_r = \frac{2.90\,\frac{150\times160^3}{12}}{\frac{160}{2}} \tag{D.9a}$$

$$Mc_r = 1.70\ kN.m \tag{D.9a}$$

The corresponding load of cracking moment can be calculated based on test arrangement shown in Figure 4.2

$$Fc_r = \frac{2\times1.70}{0.473} = 7.2kN \tag{D.9a}$$

Appendix E – Estimation of Shear Force Caused by CFRP Loops on Concrete

Some beam specimens reinforced with overlapped CFRP loops failed due to concrete shear along overlap length. Analysis is made to estimate the parallel to CFRP reinforcement shear force that can be generated by CFRP loops and compare it with the shear resistance of concrete.

The ultimate (rupture) strain of CFRP reinforcement (f_{fu}) was estimated previously to be 1322 MPa (see Appendix D.1). The area of concrete affected by parallel to reinforcement shear force generated by CFRP loops for beam specimens type A and B is 7850 mm^2 (Figure E.1), and for specimen type E and F is 45050 mm^2 (Figure E.2).

Considering CFRP rupture stress (1322 MPa) and reinforcement cross sectional area (25 mm^2) for each of the two loop legs, the total force acting on concrete is 66.1 kN.

The theoretical shear resistance of concrete can be calculated based equation (10.4) of ISIS design guideline (2007).

$$V_c = 0.2\,\lambda\,\Phi_c\,\sqrt{f'_c}\,b_w\,d\,\sqrt{\frac{E_{frp}}{E_s}} \qquad \text{(E.1)}$$

Where: V_c is concrete shear resistance, λ is modification factor for density of concrete (1 is used for normal weight concrete), ϕ_c is resistance factor of concrete (used as 1), b_w is effective width of section, d is effective depth of section, E_{frp} is modulus of elasticity of FRP (here used as carbon fibres modulus of elasticity, Table 3.1), E_s is modulus of elasticity of steel.

The multiply of $b_w\,d$ was replaced with the area of affected concrete area (see Figures E.1 and E.2).

For Beams type A and B

$$V_c = 0.2\sqrt{42.4} \times 7850 \times \sqrt{\frac{103.21}{200}} = 7.34\ kN$$

For Beams type E and F

$$V_c = 0.2\sqrt{23.7} \times 45050 \times \sqrt{\frac{103.21}{200}} = 31.51\ kN$$

Based on above calculations the shear force that can be generated by CFRP loops exceeds the resistance of plain concrete within loops overlap zone for beam specimens A, B, E, and F. Therefore, concrete shear along loops overlap occurred in beam specimens type A, B, and E. To encounter such shear forces the loops overlap zone in beam specimens type F was provided with steel transverse reinforcement. The amount of steel stirrups needed to resist the horizontal shear force generated by CFRP loop against concrete within overlap zone was estimated using ACI (2015) equation (8.2e) for shear resistance of a concrete section. Two legged steel stirrups perpendicular to beam axis of size Φ6mm with yield stress 550 MPa were used. The effective depth *d* was replaced with the length of overlap zone 472mm.

$$s \leq \frac{A_{sv} f_{fv} d}{V_u - V_c} \qquad \text{(E.2)}$$

Where A_{sv} cross-sectional area of transverse reinforcement in mm^2, f_{fv} tensile yield stress of transverse reinforcement in MPa, d section effective depth (the length of overlap zone 472mm was used), V_u external shear force in N, V_c concrete shear resistance in N.

$$s \leq \frac{2 \times \pi \frac{6^2}{4} \times 550 \times 472}{(66.1 - 31.5) \times 10^3} \approx 424\ mm$$

A conservative amount of transverse reinforcement Φ6@60mm was used .

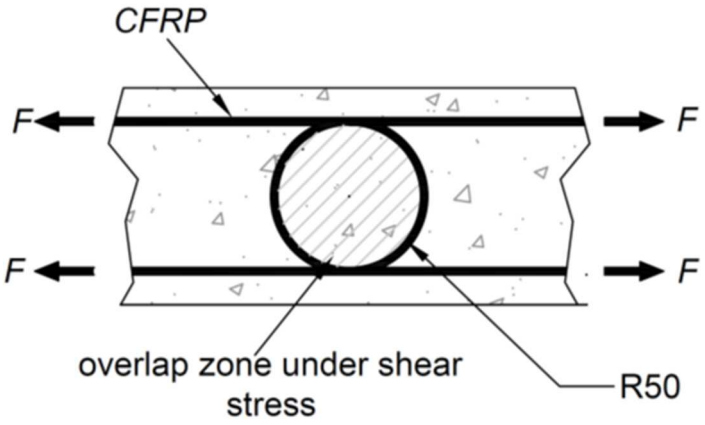

Figure E.1 Areas of concrete affected by along-reinforcement shear force caused by CFRP loop (Beam specimen type A and B).

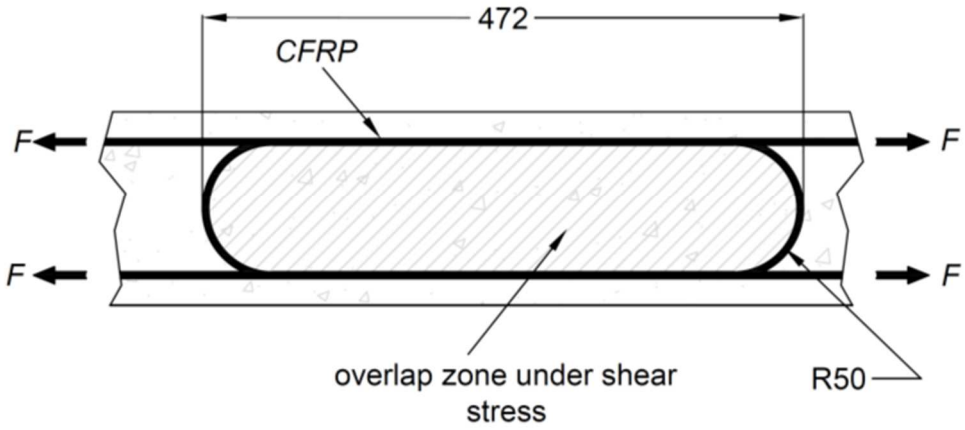

Figure E.2 Areas of concrete affected by along-reinforcement shear force caused by CFRP loop (Beam specimen type E and F).

Appendix F – Matlab Script for Bond Analysis

The following is the script of Matlab programme that was developed as a part of the current research to calculate slip, axial stress, and bond stress distribution along FRP reinforcement. Refer to Chapter 7 for more details.

```
clear
clc

tm=14.55; %maximum shear stress corresponds at maximum slip (N/mm2)
sm=0.28;  % maximum slip (mm)
sn=4.26;   % stiffness descending branch, slip at force equal zero
(mm)
p=13025; % total applied force (N)
pn=10;   % number of load increments
E=103210; % modlus of elasticity (N/mm2)
l=600;     % total length of rebar (mm)
n=600;     % number of bar segments
A=25;     % bar cross-section area (mm2)
pr=20;    % bar perimeter (mm)
D=5.642;  % bar diameter
tf=0; % residual bond in zone 3, fraction from ambient 0-1
s=1.01; % To avoid matrix singularity, fist element in matrix is
multiply by ss
fbc=0; % Fixed boundary condition if yes fbc=1 if no fbc=0
itr=10; % maximum number of iterations


display('**************************** PROGRAMME START
****************************')


tn=(tm/(sn-sm))*sn; %slop of descending part of bond model
px=p/pn;  % value of load increment (total load/number of load
increments)

lfa1=sqrt(4*tm/(sm*E*D));  % Yankevesky (1984) parameter

ln=l/n;  % bar segment length (mm)

as=pr*ln; % surface area of bar segments (mm2)

 x=0;
 y=0;
 q=0;
 v=0;

deltat=zeros(n+1,1); % 'deltat' is the nodal displacement matrix
```

```
k2=(tm-0)/(sn-sm);  % k2 is parameter for descend zone. Yankevesky
(1984)

lfa2=sqrt((4*k2)/(E*D)); % parameter for descend zone, Yankevesky
(1984)

zi=ones(n,1); % to indicate in what zone element was in previous
load step/iteration

z=ones(n,1);

for i=1:n % defining elements length
 ln(i)=l/n;
end

for i=1:n % Calculating stiffness matrix parameters ka & kb for each
element, assuming all element in zone 1
 ka(i,1)=(lfa1*E*A)/(tanh(lfa1*ln(i)));
 kb(i,1)=-1*(lfa1*E*A)/(sinh(lfa1*ln(i)));
end

fr(n+1,1)=p/pn; % fr force matrix for one load step.

for j=1:pn % Load increment loop. pn number of load increments
loop=0;
q=0;
force=zeros(n+1,1);

while loop <1 %start of iteration

v=v+1; % iteration counter

% Building force matrix. fr force matrix for current step
fr=zeros(n+1,1); % fr is load matrix for one load step
force=zeros(n+1,1);
fr(n+1,1)=fr(n+1,1)+p/pn;

% check if element still in same zone as previous step or fr to be
updated

for i=1:n

if zi(i)==2  %zi indicate what zone element in
 fr(i)=fr(i)+(lfa2*tn*E*A)*tan(lfa2*ln(i)/2)/k2;
 fr(i+1)=fr(i+1)+ 1*(lfa2*tn*E*A)*tan(lfa2*ln(i)/2)/k2;

elseif zi(i)==3
 fr(i)=fr(i)+(3.14*D*tf*ln(i))/2;
 fr(i+1)=fr(i+1)+-1*(3.14*D*tf*ln(i))/2;

end

end
```

```
% definig parameter of stiffness matrix depening on what zone each
element at.

for i=1:n

if zi(i)==1
 ka(i,1)=(lfa1*E*A)/(tanh(lfa1*ln(i)));
 kb(i,1)=-1*(lfa1*E*A)/(sinh(lfa1*ln(i)));

elseif z(i)==2
 ka(i)=(lfa2*E*A)/(tan(lfa2*ln(i)));
 kb(i)=-1*(lfa2*E*A)/(sin(lfa2*ln(i)));

elseif z(i)==3
 ka(i)=E*A/ln(i);
 kb(i)=-E*A/ln(i);
end

end

for i=1:n+1
 force(i,1)=fr(i,1);
end


%Building Stiffness Matrix
q=0;
xi=deltat;

ky(1,1)=ka(1,1)*ss; %ss to avoid matrix singularity
ky(n+1,n+1)=ka(n,1);

for i=2:n  %diagonal elements
 ky(i,i)=ka(i-1,1)+ka(i,1);
end

for i=1:n  % upper diagonal elements
 ky(i,i+1)=kb(i,1);
end

for i=2:n+1  % lower diagonal elements
 ky(i,i-1)=kb(i-1,1);
end

if fbc==0   % fbc=1 for fixed end, 0 for free end
 x=inv(ky)*force;
end

if fbc==1 % fbc=1 the bar has fixed end
 fyf1=ky;
 fyf1(:, 1) = []; % deleter the first column
 fyf1(1, :)= [];  % delete the first row
 fyf=inv(fyf1);
```

```
 forcef=force;
 forcef(1,:)=[];  % delete the first row of force matrix

 xf=fyf*forcef;
 x=[0;xf];
end

xi=xi+x;  %accumlative slip from current and previous steps

for i=1:n %cheking if elements in right region

  if xi(i)<=sm & xi(i+1) <=sm
   zz=1;
   z(i)=1;
  end

  if xi(i)<=sm & xi(i+1) >=sm
   zz=1;
   z(i)=1;
  end

  if xi(i)>=sm & xi(i+1)>=sm
   zz=2;
   z(i)=2;
  end

  if xi(i)<=sn & xi(i+1)>=sn
        zz=2;
        z(i)=2;
     end

      if xi(i)>=sn & xi(i+1)>=sn
        zz=3;
        z(i)=3;
     end

     if z(i)==zi(i) % this means element is still in the assumed
zone
       q=q+1;

     elseif z(i)==2 % this if whole element (both nodes) moved from
zone 1 to zone 2

        ka(i)=(lfa2*E*A)/(tan(lfa2*ln(i)));
        kb(i)=-1*(lfa2*E*A)/(sin(lfa2*ln(i)));
        fr(i)=fr(i)+(lfa2*tn*E*A)*tan(lfa2*ln(i)/2)/k2;
        fr(i+1)=fr(i+1)+-1*(lfa2*tn*E*A)*tan(lfa2*ln(i)/2)/k2;
        zi(i)=2;
     else % this if whole element (both nodes) moved to zone 3
        ka(i)=E*A/ln(i);
        kb(i)=-E*A/ln(i);
        fr(i)=fr(i)+(3.14*D*tf*ln(i))/2;
        fr(i+1)=fr(i+1)+-1*(3.14*D*tf*ln(i))/2;
        zi(i)=3;
```

```
   end

   if j==pn
       loop=2;
   end


  if q==n
      loop=2;
      v=0; % iteration counter
  end

 end

  if v==itr
  % this condition was added to exit the loop when maximum
  number of iteration (itr) is achieved.
       loop=2;
        display('Maximum number of iterations reached at load
increment')
        j
        v=0;
   end


 end % end of iteration

 for k=1:n
     zi(k)=z(k);
 end


   deltat=deltat+x;

 end  % End of load increment loop

 strain=zeros(n,1);
 straint=zeros(n,1);
 stress=zeros(n,1);
 stresst=zeros(n,1);
 bondt=zeros(n,1);

 for t=1:n

     % strain for current increment
     strain(t,1)=(deltat(t+1,1)-deltat(t,1))/(ln(t));

     if fbc==1 & t==1

     % to avoid high strain and stress concentration resulted
     from zero slip at fixed end and slip at next node
     strain(1,1)=0;
```

```
    end

    % total segments strain
    straint(t,1)=straint(t,1)+strain(t,1);

    %stress for current increment
    stress(t,1)=strain(t,1)*E;

    % total element normal stress
    stresst(t,1)=stresst(t,1)+stress(t,1);

 end

slope=(0-tm)/(sn-sm);

 for w=1:n
   if (deltat(w+1,1)<=sm)    % bond stress for current increment
          bondt(w,1)=((tm/sm)*deltat(w+1,1));
   elseif (deltat(w+1,1)>=sn)
       bondt(w,1)=tf*tm;
   else
       bondt(w,1)=-1*slope*(sn-deltat(w+1,1));

   end

 end

    deltatplot=zeros(n,1);
    lx=0;
    xaxis=zeros(n,1);

 for w=1:n
     lx=lx+ln(w);
     xaxis(w)=lx; % create vector to bar lenght
     deltatplot(w)=deltat(w+1,1);  % create vector for slip
 end

 figure
 subplot(2,2,1)
 plot(xaxis,deltatplot),
 xlabel('Bar length mm')
 ylabel('Bar slip mm')


 subplot(2,2,2)
 plot(xaxis,straint),
 xlabel('Bar length mm')
 ylabel('Strain')


subplot(2,2,3)
plot(xaxis,stresst),
xlabel('Bar length mm')
ylabel('Stress N/mm2')
```

```
subplot(2,2,4)
plot(xaxis,bondt)
xlabel('Bar length mm')
ylabel('Bond stress N/mm2')

% To print results into text files
dlmwrite('bondstress.txt',bondt)
dlmwrite('axialstress.txt',stresst)
dlmwrite('strain.txt',straint)
dlmwrite('slip.txt',deltat)
```

Appendix G – Convergence Analysis

This appendix includes a converge analysis for the numerical solution for bond stress discussed in Chapter 6. The converge analysis investigates the influence of element size and load step size on the obtained results of slip, axial stress, and bond stress.

The analysis was conducted as a 1D finite element problem; therefore, element and load step sizes can affect the obtained results. The influence of element and load step size was investigated by conducting an analysis to calculated the development length of a straight bar using different sizes of elements and load steps, as discussed below. The applied stress on the bar is 1322 MPa and maximum bond stress is 16.44 MPa. Refer to section 7.4.1 for more details.

G.1 Effect of Element Size

Table G.1 below lists the change of development length of a CFRP straight bar due to a change of element size. The effect of element size on slip, axial stress, and bond stress responses is shown in Figures G.1 to G.3.

Table G.1 Effect of element size of development length.

Element size (mm)	Load increments	Development length (mm)	Difference (%)
0.5	10	391	3.5
1	10	405	0
2	10	416	2.7
3	10	417	3.0

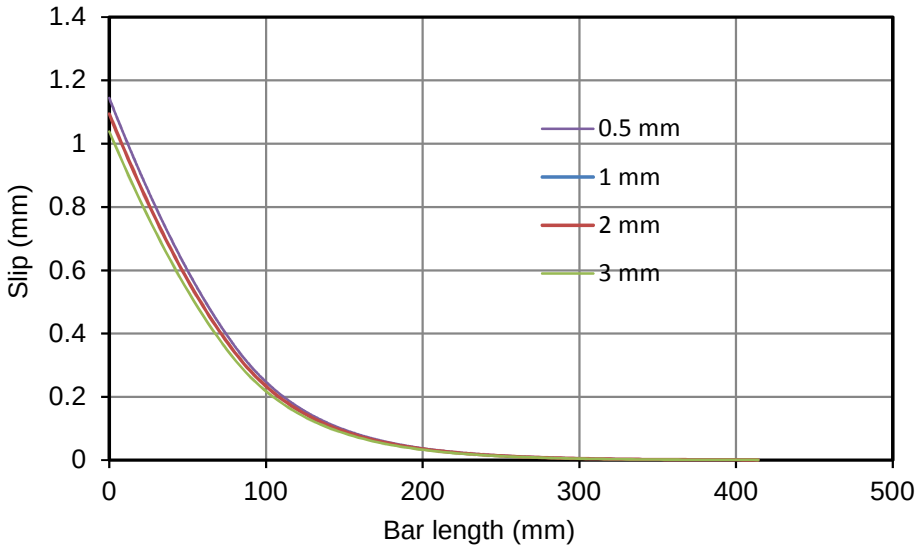

Figure G.1 Effect of element size of slip response of straight bar.

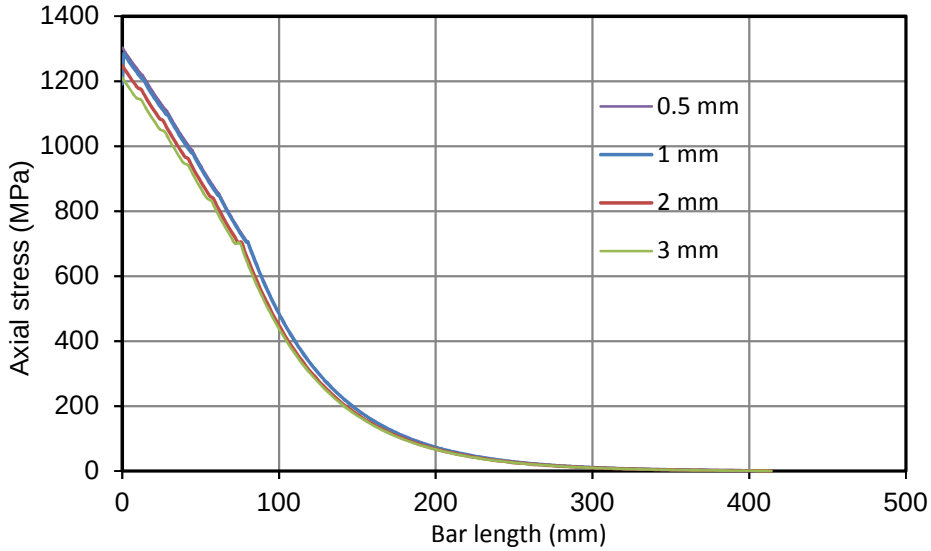

Figure G.2 Effect of element size on axial stress response of straight CFRP bar.

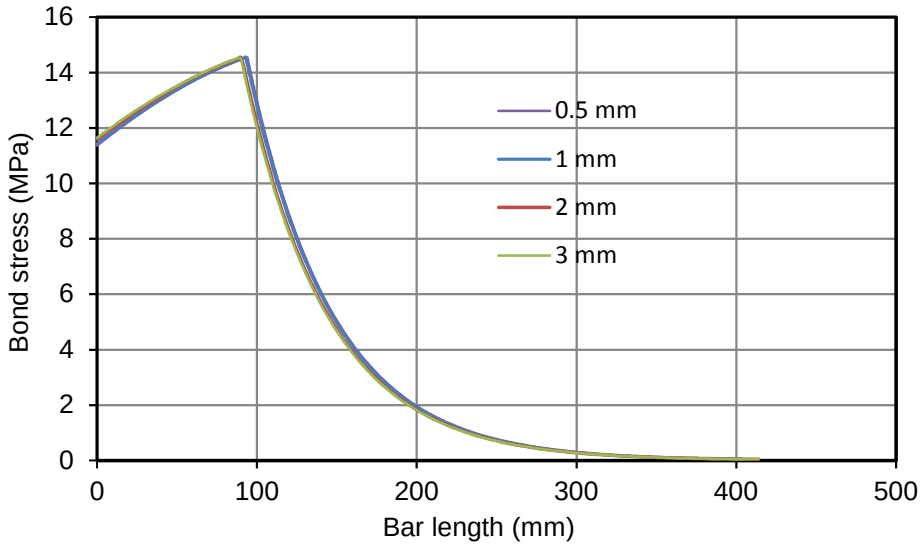

Figure G.3 Effect of element size on bond stress response of straight CFRP bar

G.2 Effect of Load Step Size

Table G.2 below lists the development length of CFRP straight bar using different element sizes. The effect of element size on slip, axial stress, and bond stress responses is shown in Figures G.4 to G.6.

Table G.2 Effect of load step size on development length

Load increments	Element size (mm)	Development length (mm)	Difference (%)
10	1	405	0
20	1	400	1.2
30	1	399	1.5

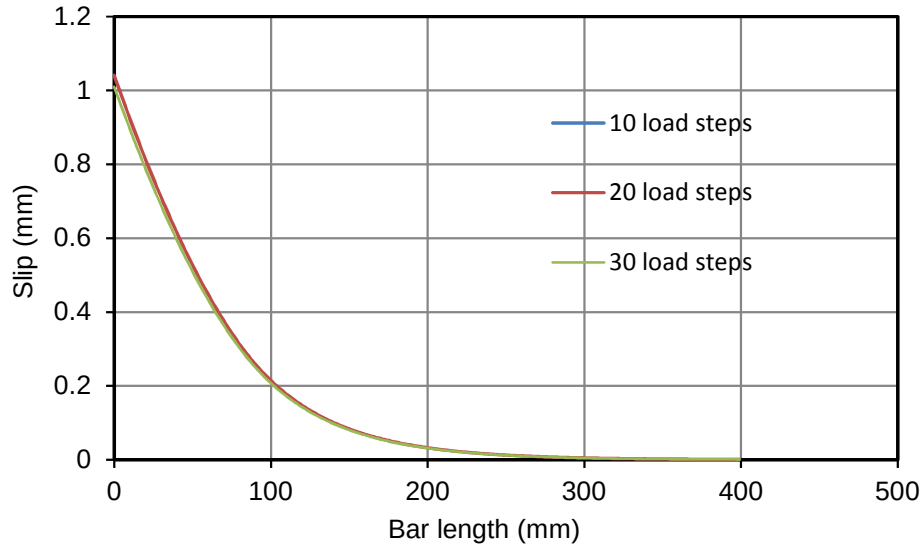

Figure G.4 Effect of load step size on slip response of straight CFRP bar.

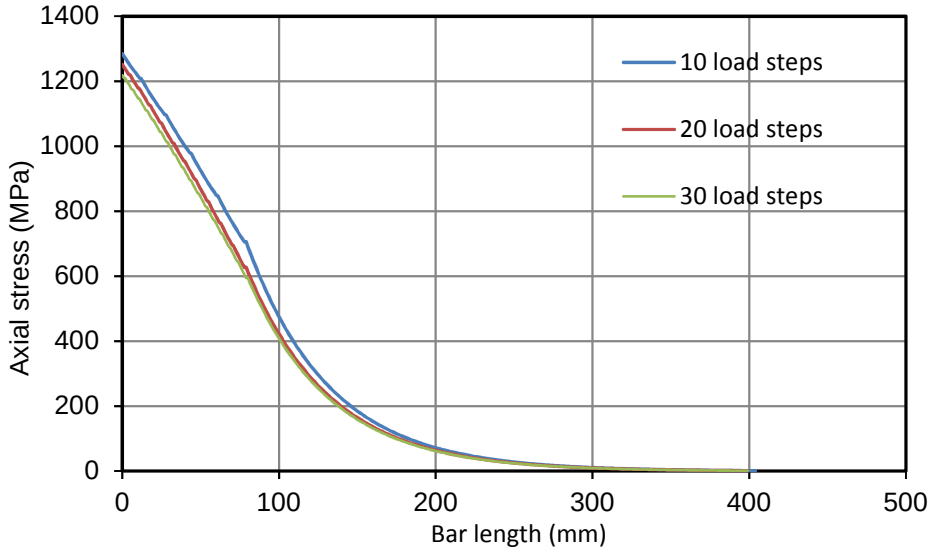

Figure G.5 Effect of load step size on axial stress response of straight CFRP bar.

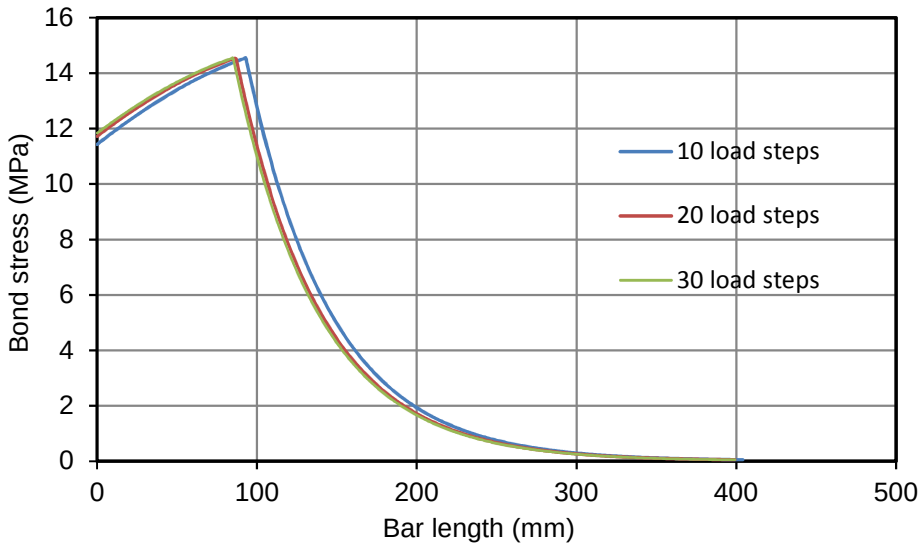

Figure G.6 Effect of load step size on axial stress response of straight CFRP bar.

G.3 Discussion

The converge analysis was conducted to investigate the influence of element size and load step size on the results of slip, axial stress, and bond stress. Different element sizes, 0.5, 1, 2, and 3 mm, were used in the calculation of development length and variation of up to 3.5% was observed. Different load steps, 10, 20, and 30, were also used which caused a variation in results up to 1.5%. For the purpose of the current work the variation in results is considered not to be significant and element size of 1 mm and 10 equal load steps were decided to be used for the rest of analysis within Chapter 6.

Appendix H – Theoretical Estimation of Stress in Beam Reinforcement

The stress level in reinforcement is needed for the calculation of reinforcement bond-slip response. Analysis of a cracked section was done using a triangular stress block to estimate axial stress in FRP reinforcement. The triangular stress block applied when materials still within the elastic region which is typically the case under the service loads. A cracked section is shown in Figure H.1 with a CFRP stress resultant acting through the centroid of CFRP reinforcement, and F_s through the centroid of steel bars, and F_c through the centroid of triangular stress block.

$$F_c+F_s=F_{frp} \tag{H.1}$$

$$0.5bxf_c+ A_sf_s =A_{frp}f_{frp} \tag{H.2}$$

$$M= 0.5bxf_c(d-x/3)+f_sA_s(d-d_s) \tag{H.3}$$

The depth of the neutral axis, x, can be determined by converting the section into equivalent area of concrete as shown in Figure H.1.

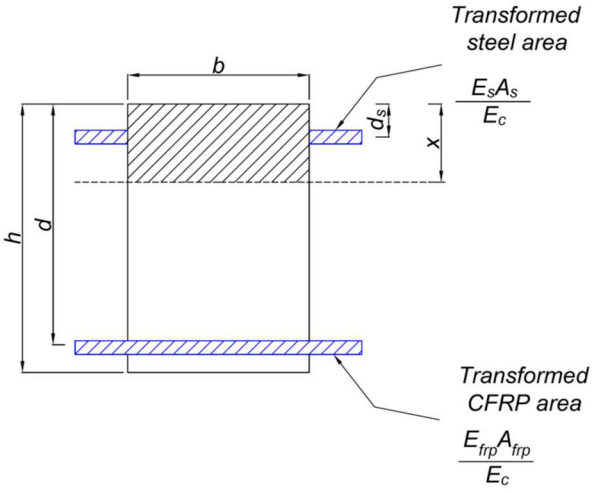

Figure H.1 Beam cross section with transformed area (Mosley et al., 2007).

Taking the area moments about the upper edge (Mosley et al., 2007).

$$x = \frac{\sum(Al_a)}{\sum A} \quad \text{(H.4)}$$

Therefore

$$x = \frac{bx\times\frac{x}{2} + \frac{E_s}{E_c}A_s\times d_s + \frac{E_{frp}}{E_c}A_{frp}\times d}{bx + \frac{E_s}{E_c}A_s + \frac{E_{frp}}{E_c}A_{frp}} \quad \text{(H.5)}$$

Or

$$\frac{1}{2}\,bx^2 + x\left(\alpha_s A_s + \alpha_{frp}A_{frp}\right) - \left(\alpha_s A_s d_s + \alpha_{frp}A_{frp}d\right) = 0 \quad \text{(H.6)}$$

Where $\alpha_s = \frac{E_s}{E_c}\ and\ \alpha_{frp} = \frac{E_{frp}}{E_c}$

$$x = \frac{-\left(\alpha_s A_s + \alpha_{frp}A_{frp}\right) \pm \sqrt{\left[\left(\alpha_s A_s + \alpha_{frp}A_{frp}\right) + 2b\left(\alpha_s A_s d_s + \alpha_{frp}A_{frp}d\right)\right]}}{b} \quad \text{(H.7)}$$

Based on above equations the stress level in FRP reinforcement of beam specimens of phase I and II caused by the sustained load in heated tests can be estimated using the materials mechanical properties and the applied bending moment. The area of steel reinforcement within concrete compression area of phase II beam specimens were ignored as a simplification.

For phase I beam specimens:

$n_f = 3.44$ (see appendix C.9), A_{frp} = 50 mm^2, b = 150 mm, As = 0, *d*: varies depending on average measured concrete cover after failure (Table 4.6).

Table H.1 Stress level in FRP reinforcement of phase I beam specimens.

Specimen	d (mm)[1]	Applied bending moment (kN.m)	x (mm)[2]	Stress in FRP reinforcement (MPa)
A3	131.5	3.31	16.3	525
A4	125.5		15.9	551
B3	131		16.2	527
B4	135.5		16.5	509
C3	134		16.4	515
C4	132.5		16.3	521
D3	129.5		16.1	534
D4	131.5		16.3	525

[1]d: effective depth, [2]x: depth of neutral axis

For phase II beam specimens:

Concrete modular ratio n_f and Young's modulus according to ACI (2015) can be calculated as following:

$$E_c = 4750\sqrt{f_c'} \quad \text{(H.8)}$$

$$n_f = \frac{E_f}{E_c} \quad \text{(H.9)}$$

For beam specimen of phase *fc'* 23.7 MPa (Table 5.2), and E_f 103.21 GPa (Appendix C)

$$E_c = 4750\sqrt{23.7} = 23.12\ GPa \quad \text{(H.10)}$$

$$n_f = \frac{103.21}{23.12} = 4.46 \quad \text{(H.11)}$$

Table H.2 Stress level in FRP reinforcement of phase II beam specimens.

Specimen	d (mm)[1]	Applied bending moment (kN.m)	x (mm)[2]	Stress in FRP reinforcement (MPa)
E3	128	8.74	18.1	717
E4	128	5.48	18.1	450
F3	128		18.1	450
F4	126		17.9	457
G3	131.5		18.3	437
G4	126.5		18.0	455